Vol. 202, November 16, 1987
Complete in one issue

ISSN 0003-2670

ANALYTICA CHIMICA ACTA

International journal devoted to all branches of analytical chemistry

ELSEVIER

ANALYTICA CHIMICA ACTA

International journal devoted to all branches of analytical chemistry
Revue internationale consacrée à tous les domaines de la chimie analytique
Internationale Zeitschrift für alle Gebiete der analytischen Chemie

PUBLICATION SCHEDULE FOR 1988

	J	F	M	A	M	J	J	A	S	O	N	D
Analytica Chimica Acta	204	205	206	207	208	209	210/1 210/2	211	212	213	214	215

Scope. *Analytica Chimica Acta* publishes original papers, short communications, and reviews dealing with every aspect of modern chemical analysis both fundamental and applied.
Submission of Papers. Manuscripts (three copies) should be submitted as designated below for rapid and efficient handling:
Papers from the Americas to: Professor Harry L. Pardue, Department of Chemistry, Purdue University, West Lafayette, IN 47907, U.S.A.
Papers from all other countries to: Dr. A.M.G. Macdonald, Department of Chemistry, The University, P.O. Box 363, Birmingham B15 2TT, England. Papers dealing particularly with computer techniques to: Professor J.T. Clerc, Universität Bern, Pharmazeutisches Institut, Baltzerstrasse 5, CH-3012 Bern, Switzerland.
Submission of an article is understood to imply that the article is original and unpublished and is not being considered for publication elsewhere. Papers in English, French and German are published. There are no page charges. Manuscripts should conform in layout and style to the papers published in this Volume. See inside back cover for "Information for Authors".
Reprints. Fifty reprints will be supplied free of charge. Additional reprints (minimum 100) can be ordered. An order form containing price quotations will be sent to the authors together with the proofs of their article.
Publication. *Analytica Chimica Acta appears* in 12 volumes in 1988. The subscription for 1988 (Vols. 204-215) is Dfl. 2820.00 plus Dfl. 312.00 (p.p.h.) (total approx. US $1566.00). All earlier volumes (Vols. 1–203) except Vols. 23 and 28 are available at Dfl. 243.00 (US $121.50), plus Dfl. 18.00 (US $9.00) p.p.h., per volume.
Our p.p.h. (postage, packing and handling) charge includes surface delivery of all issues, except to subscribers in the U.S.A., Canada, Australia, New Zealand, P.R. China, India, Israel, South Africa, Malaysia, Thailand, Singapore, South Korea, Taiwan, Pakistan, Hong Kong, Brazil, Argentina and Mexico, who receive all issues by air delivery (S.A.L.–Surface Air Lifted) at no extra cost. For Japan, air delivery requires 50% additional charge; for all other countries airmail and S.A.L. charges are available upon request.
Subscription. Subscription should be sent to: Elsevier Science Publishers B.V., Journals Department, P.O. Box 211, 1000 AE Amsterdam, The Netherlands. Tel: 5803 911, Telex: 18582, to which requests for sample copies can also be sent. Claims for issues not received should be made within three months of publication of the issues. If not they cannot be honoured free of charge. Readers in the U.S.A. and Canada can contact the following address: Elsevier Science Publishing Co. Inc., Journal Information Center, 52 Vanderbilt Avenue, New York, NY 10017, U.S.A., Tel: (212) 916-1250, for further information, or a free sample copy of this or any other Elsevier Science Publishers journal.
Advertisements. Advertisement rates are available from the publisher on request.

0003-2670/87/$03.50

PRINTED IN THE NETHERLANDS

ANALYTICA CHIMICA ACTA

International journal devoted to all branches of analytical chemistry

(Abstracted, Indexed in: Anal. Abstr.; Biol. Abstr.; Chem. Abstr.; Curr. Contents Phys. Chem. Earth Sci.; Life Sci.; Index Med.; Mass Spectrom. Bull.; Sci. Citation Index; Excerpta Med.)

VOL. 202 CONTENTS NOVEMBER 16, 1987

(Continued overleaf)

(*Contents continued*)

ANALYTICA CHIMICA ACTA
VOL. 202 (1987)

ANALYTICA CHIMICA ACTA

International journal devoted to all branches of analytical chemistry

---

Anal. Chim. Acta, Vol. 202 (1987)

ELSEVIER, Amsterdam – Oxford – New York – Tokyo

0003-2670/87/$03.50

PRINTED IN THE NETHERLANDS

Analytica Chimica Acta, 202 (1987) 1-24
Elsevier Science Publishers B.V., Amsterdam — Printed in The Netherlands

Review

CATALYTIC END-POINT DETECTION IN TITRIMETRIC ANALYSIS

SIEGBERT PANTEL and HERBERT WEISZ*

Institut für Anorganische und Analytische Chemie, Albert Ludwigs Universität Freiburg, Albertstr. 21, D-7800 Freiburg i.Br. (Federal Republic of Germany)

(Received 5th March 1987)

SUMMARY

In catalytic end-point detection, the first drop of titrant in excess is not used for a stoichiometric reaction with the indicator (as in conventional titrations) but acts as, or liberates, a catalyst for the indicator reaction. A very small excess of titrant thus suffices to catalyze large amounts of the indicator reaction mixture. Such catalytic end-points are therefore very sensitive. Terminology is discussed briefly. The various types of titration (direct, with a "brake", reversed, indirect and substitution) and of end-point detection (visual, olfactory, photometric, thermometric and electrometric) are described. Applications of these techniques are summarized.

Catalyzed reactions can be applied in different ways in quantitative analytical chemistry. In kinetic methods, the catalyst concentration is determined via the reaction rate (expressed as the dependence of the measured property on time) using a calibration graph (see, e.g. [1,2]). The so-called "catalymetric titrations", which were first described by Yatsimirskii and Fedorova [1,3-5], can be regarded as simulated titrations. For example, in the determination of silver(I), the course of the indicator reaction [the iodide-catalyzed oxidation of arsenic(III) by cerium(IV)] is followed photometrically in several samples containing equal amounts of the indicator-reaction mixture and the inhibitor to be determined, Ag(I), and increasing amounts of catalyst (iodide standard solution, up to about 100% in excess). Plots of logarithmic absorbance vs. time yield straight lines with slopes (tan α) directly proportional to the concentration of the catalyst as soon as the stoichiometric amount needed for the formation of the silver iodide precipitate is exceeded. Before this point, only a very small and constant reaction rate is observed, which is due to the iodide concentration equivalent to the solubility product of the silver iodide formed. A calibration graph is drawn by plotting tan α vs. catalyst concentration; the intersection point of the two straight lines gives the amount of iodide necessary to precipitate the amount of silver(I) in the sample solution. This "catalymetric titration" can also be done by using a "simultaneous comparison" method [6], which has then been called "simultaneous indication" [7].

0003-2670/87/$03.50

The method described above is a kind of kinetic analysis, but certainly not a real titration in the conventional definition of the term. Nevertheless, several authors have used the term "catalymetric titration" for catalytic end-point detection. Therefore, it is necessary to distinguish quite clearly between the "catalymetric titration" and the "catalytic titration" which is described below.

Kinetic titrations (comparative titrations), which were described by Sájo [8], are also not titrations in the conventional sense. A reference solution, identical with the sample solution except for the catalyst, is titrated with a standard solution of the catalyst until the rates of reaction become identical in both vessels as shown by a zero deflection of the galvanometer connected via a bridge circuit to two thermistors placed in the two solutions.

Another type is the accelerated titration, in which catalysts are used to accelerate classical titrations in order to simplify their application. For example, molybdenum(VI) catalyzes the oxidation of iodide by hydrogen peroxide in the iodimetric titration of the latter [9]; several other examples could be mentioned.

CATALYTIC END-POINT DETECTION IN TITRIMETRIC ANALYSIS (CATALYTIC TITRATION)

Catalytic end-point detection in titrimetric analysis is based on the fact that the first drop of titrant in excess is not used for a stoichiometric reaction with the indicator (titration in the conventional sense), but acts as a catalyst for the indicator reaction (Table 1). Consequently, a very small excess of titrant suffices to catalyze large amounts of the indicator-reaction mixture. Such catalytic end-points are therefore markedly sensitive and very easily detectable [10]. Mathematical treatments of catalytic titration curves have been described by Mottola [11], Goizman [12], Simpson [13] and Gaal and Abramovic [14]. For redox and precipitation titrations, the theory was discussed by Abramovic et al. [15] and for acid-base titrations by Gaal and Abramovic [16]. The first application of the theoretical treatment to practical titrations was described for the complexiметric determination of metal ions with the periodate/triethanolamine indicator reaction, catalyzed by manganese(II) [17].

The general interest in catalytic methods of analysis is demonstrated by the number of books and reviews on this subject [1,2,18–33] as well as by the increasing number of original publications dealing with various possibilities for the application of such methods in routine analysis. In this review, only those methods in which catalytic end-point detection is applied in titrimetric analysis will be considered.

The first titration based on this principle (but surprisingly without mentioning the fact that it was a new method of end-point indication, namely "catalytic titration") was published in 1960 by Erdey and Buzas [34]. EDTA was

TABLE 1

Catalytic end-point indication methods in which catalyst K is added to a solution containing the inhibitor I to be determined and the components A and B of the reaction to be catalyzed

EXAMPLES
Precipitation: K, I^-; A, Ce(IV); B, As(III); I, Ag^+.
Complexing: K, Co; A, Tiron; B, H_2O_2; I, EDTA.
STOICHIOMETRIC REACTION (titration reaction)
I+K→(IK) where (IK) is the inhibited catalyst.
CATALYZED REACTION (indicator reaction)
$A+B \xrightarrow{K} C$
INHIBITION OF CATALYST
Precipitation, complexing, oxidation/reduction.
MONITORING OF CATALYZED INDICATOR REACTION (disappearance of A or B or appearance of C)
Visual, photometric.
Potentiometric, biamperometric, conductometric.
Thermometric, olfactory.
TITRATION METHODS
Direct, indirect (back), reversed, substitution, non-aqueous, automated.

determined with copper(II) standard solution in the presence of luminol and hydrogen peroxide. In 1965, Vaughan and Swithenbank [35] reported a method for acid-base titrations with the application of the base-catalyzed dimerization of acetone (solvent) for end-point detection with thermometric indication. But Weisz and Muschelknautz [10] were the first to recognize in 1966 the universal applicability of this principle for end-point detection in titrimetric analysis. They determined several metal ions and inorganic anions with various catalyzable indicator reactions.

The principle of catalytic end-point indication can be described by two correlations:

I+K→(IK) (stoichiometric titration reaction)

$A+B \xrightarrow{K} C$ (non-stoichiometric indicator reaction)

The second reaction starts at the moment the first one stops.

The general method can be illustrated by the precipitation titration of silver(I) (I) with a standard iodide solution (the catalyst, K). To the silver sample solution are added solutions of yellow cerium(IV) sulphate (A) and colourless arsenic(III) (B); titration with 0.1 M iodide is then begun with vigorous stirring. Iodide ion is precipitated as catalytically inactive silver iodide (IK). The first excess of iodide catalyzes the cerium/arsenic indicator reaction and the yellow cerium(IV) solution is immediately decolorized with the formation of cerium(III) (C).

For the application of catalyzed reactions in titrimetric end-point indication, five conditions must be fulfilled. First, the catalyzable reaction must be very slow in the absence of the catalyst and considerably faster in its presence. Secondly, the catalytic activity must be reduced so effectively by inhibition that the indicator reaction is very slow in the presence of the inhibited catalyst. Thirdly, the inhibitors used must not react with the reactants of the indicator reaction. Fourthly, the catalyzable reaction must proceed under the same conditions as the stoichiometric titration reaction (e.g., pH value). Finally, it must be possible to follow the indicator reaction in some way, visually or by physical properties.

Numerous catalyzable reactions fulfil the first and fourth conditions, but for the second condition it is often impossible to find a suitable inhibitor. The third condition is fulfilled for precipitation and complexation reactions; for redox reactions, only one example has so far been reported [36].

The catalyzable reactions used for end-point indication can be divided into three groups: (1) reactions of inorganic substances; (2) reaction of organic substances with inorganic oxidants (H_2O_2, IO_3^-, IO_4^-, $S_2O_8^{2-}$, O_2); and (3) reactions involving polymerization, hydrolysis, addition or condensation.

Titration techniques

The following titration techniques are possible (Table 1).

Direct titration. The inhibitor (e.g., silver ion) is titrated with the catalyst (iodide); the indicator-reaction mixture, here As(III)/Ce(IV), is in the titration vessel.

Titration with a "brake". Whenever a catalyst (e.g., iodide) is titrated with an inhibitor [e.g., mercury(II)], "titration with a brake" becomes essential [21,34, 37–39]. In this case, one of the reactants in the indicator reaction, As(III)/Ce(IV), must be added to the catalyst solution [here As(III)], and the other to the inhibitor titrant solution [here Ce(IV)].

Reversed (inverse) titration. A known amount of the standard solution of a suitable inhibitor (e.g., silver ion) is titrated with the solution of the sample (catalyst) (e.g., iodide with the As(III)/Ce(IV) indicator reaction).

Indirect (back-) titration. To the metal sample solution (Co, Cu, Pb, Cd. . .) a known excess of an inhibitor standard solution (e.g., EDTA) is added; the unconsumed part of the inhibitor is back-titrated with a standard solution of the catalyst (e.g., cobalt in the Tiron/perborate indicator reaction).

In this way, it is possible to determine even ions which are not active either as catalyst or inhibitor in the relevant indicator reaction. The only prerequisite is that the ion to be determined forms a more stable compound with the inhibitor than does the catalyst (titrant).

Species that can be determined by reversed titration can also be determined by back-titration; for example, an excess of EDTA is added to copper(II) (sample) and then back-titrated with a standard copper(II) solution. This

has a special advantage. In the reversed titration, the excess of catalyst after the end-point is quite different for the same volume increment because of the various concentrations of the catalyst (sample) solution, so that the reaction rates for the indicator reaction are always different. When the back-titration is used, the same excess of catalyst is always present in the titration solution after the end-point for a certain volume increment; thus the reaction rate is always the same, and a higher precision can be achieved for the end-point detection. For the back-titration, however, two standard solutions are required (EDTA and catalyst solution), whereas in the indirect titration only one standard solution is necessary (EDTA).

Substitution (displacement-) titration. The sample solution (e.g., the metal ion to be determined and a known excess of EDTA) contains the components of the catalyzed indicator reaction (e.g., resorcinol/hydrogen peroxide) as well as the catalyst in a blocked, inactive form (e.g., MnEDTA). At the end-point of the titration with a standard solution of a metal ion which forms more stable complexes than Mn(II) with EDTA, the first drop in excess of the titrant causes the release of the catalyst and consequently the start of the indicator reaction [40]. This method is of special interest when it is necessary to determine a metal (e.g., calcium) which has itself no catalytic activity.

METHODS FOR THE END-POINT DETECTION IN CATALYTIC TITRIMETRIC ANALYSIS

Visual and photometric observation of the indicator reaction

Most of the catalyzable indicator reactions are redox reactions with a colour effect; they can therefore be followed visually or photometrically. The visual variant, however, is only possible if the titration end-point is very sharp, i.e., when a very small portion of the titrant suffices to start the indicator reaction. This will happen only when a very strong complex or a precipitate with a very low solubility product is formed; in all other cases, the catalyzed reaction starts before the end-point is reached and the end-point tends to creep; evaluation must then be done from plots of observed absorbance vs. volume of titrant. Here, and in all other methods based on physical properties of the system for observation of the end-point, motor-driven micrometer syringes are used for continuous addition of the titrant. The end-point of the titration is obtained graphically by extrapolating the linear parts of the titration curve before and after the titration end-point to their intersect. Evaluation is usually done with the aid of a standard graph.

The indicator reactions used have been based on metal ion-catalyzed oxidation of iodide and numerous organic substrates (substituted anilines, phenols, hydrazones, thiosemicarbazones) with suitable oxidants (atmospheric oxygen, hydrogen peroxide, perborate, iodate, periodate, peroxodisulphate) to form coloured oxidation products. Such reactions have been applied in direct

titrations of aminopolycarboxylic acids (EDTA, EGTA, DCTA and NTA) or other inhibitors (fluoride, hexafluorosilicate and cyanide), in reversed titrations of the catalyst, e.g., Cr(VI), Mn, Fe(III), Co, Ni, Cu and Th(IV), in back-titrations with standard catalyst solution, and in substitution titrations with standard metal solution using, for example, MnEDTA as the inhibited catalyst. Decolorization reactions, chemiluminescence reactions and fluorescence reactions have also been used for visual or photometric end-point indication in catalytic titrations. The iodide-catalyzed oxidation of arsenic(III) with cerium(IV) can be monitored photometrically [41,42] for the determination of very low catalyst concentrations.

Numerous examples are summarized in Table 2, which is based in part on the literature searches of Schlipf [45].

Gas evolution can also be used for visual end-point detection in titrimetric analysis [10] by the addition of a detergent (e.g., iodide-catalyzed decomposition of hydrogen peroxide in presence of a detergent for the determination of silver).

Potentiometric observation of the indicator reaction

Potentiometric observation of the indicator reaction in catalytic titrations has been used widely for the determination of catalysts and inhibitors by direct or reversed titration and for the determination of many ions by back-titration. The advantage offered here is the possibility of titrating turbid or coloured solutions.

As indicator reaction, the iodide-catalyzed oxidation of arsenic(III) with cerium(IV) has been used for the determination of Ag, Hg(II), Pd(II), Au(III), iodide and thioacetamide; the copper(II)-catalyzed oxidation of thiosulphate [85] or the manganese(II)-catalyzed oxidation of triethanolamine [17,87] with periodate was used to determine microgram amounts of aminopolycarboxylic acids and metal ions, by using a platinum electrode or a perchlorate ion-selective electrode, respectively. The iodide-catalyzed oxidation of arsenite or hydrogen peroxide by chloramine-T was followed by using a chloramine-T-selective electrode to determine silver and mercury(II) [95].

The urea/urease (EC 3.5.1.5) system is an example of a titration with a standard enzyme solution. A glass electrode was used to monitor the indicator reaction. Mercury(II) and silver (0.1–1 μg) were determined by titrating with a standard urease solution (3.6 IU ml^{-1} enzymatic activity); 0.01–0.1 μg of sulphide, as "inhibitor" for the silver inhibitor, could be determined with good reproducibility [96].

Other electrometric techniques for observation of the indicator reaction

Conductometric and high-frequency conductometric observation of the indicator reaction can be used for end-point detection in titrations of organic bases with strong acids; the methods were based on acylation of aliphatic or

aromatic hydroxy compounds with acetic anhydride or dehydration of formic acid [140] in nonaqueous medium.

The acetic anhydride/acetic acid indicator reaction in acid-base titrations [135], the decomposition of hydrogen peroxide [37,62,59,61], the reaction of arsenic(III) or antimony(III) with cerium(IV) or permanganate [59,47], and the iodide/hydrogen peroxide reaction [67] have been followed biamperometrically, amperometrically and by constant-current potentiometry in catalytic titrations. In the special case of biamperometry, titrations are possible on the micro-scale, because the electrodes can be made very small [59].

Thermometric observation of the indicator reaction

The most universally applicable indication method in titrimetric analysis is the thermometric technique [18,22,24,28], which is applicable in homogeneous and in turbid media, and in colourless or coloured solutions. Here, catalytic end-point detection is of special interest, because it is not the calorific effect of the stoichiometric titration reaction which is observed, but the much higher effect of the catalyzed indicator reaction. For example, in organic polymerization reactions, the temperature rise can be 10°C or more. In inorganic redox reactions, the differences may be only a few millidegrees; the most exothermal reaction in this class is the oxidation of hydrazine with hydrogen peroxide [62].

If the calorific effect of the catalytic indicator reaction is high, the titration can be done in a simple polyethylene or glass beaker, fitted into a block of polystyrene or even filter paper. For more sensitive work, a Dewar vessel is needed.

The titrant should be ten times more concentrated than the analyte solution. By using catalytic titrations, down to 10^{-5} M concentrations can be determined with errors of about 1%.

When the calorific effects are high, the temperature can be measured even with a simple thermometer. In most cases, however, it is necessary to use a thermistor, which is attached to a Wheatstone bridge, with or without amplifier, and connected to a strip-chart recorder. The temperature/volume curve is plotted either directly or as the first or second derivative. The differential technique, in which the temperature is measured with two thermistors having the same resistance but different response times, improves the sensitivity of this method [132].

Catalytic thermometric end-points have been used in organic analysis for the titration of acids and bases in non-aqueous medium, mainly by using polymerization reactions, acylation reactions, esterification and hydrolysis of anhydrides. Polymerizations catalyzed by iodonium ions can be used in the titration of organic compounds with iodine in a suitable organic solvent.

Thermometric end-point detection has also been used in precipitation titrations, with cerium(IV)/arsenic(III), cerium(IV)/antimony(III) or manga-

TABLE 2

Titrimetric determinations with catalytic end-point detection

[EP, end-point detection method: vis, visual; phot, photometric; pot, potentiometric; ISE, potentiometric with ion-selective electrode; amp, amperometric; biamp, biamperometric; therm, thermometric; cond, conductometric; fluor, fluorimetric; olf, olfactory.
Tech, titration technique: dir, direct titration; back, indirect (back-) titration; brake, titration with brake; rev, reversed (inverse) titration; subst, substitution titration; simlt, simultaneous determination.
EDTA, ethylenediamine-*N*,*N*,*N*',*N*' -tetraacetic acid; DCTA, 1,2-diaminocyclohexane-*N*,*N*,*N*',*N*'-tetraacetic acid; EGTA, ethyleneglycol-bis(2-aminoethylether)-*N*,*N*,*N*',*N*' -tetraacetic acid; DTPA, diethylenetriamine-pentaacetic acid; DBPT, 4,4'-dihydroxybentophenone thiosemicarbazone.]

Indicator reaction	EP	Tech	Titrant	Analyte	Notes	References
As(III)/Ce(IV)	Vis	Dir	I^-	Ag		10, 43
		Back	I^-	Cl^-, Br^-, SCN^-	Excess Ag	10
		Dir	BrO_3^-	Sb, As	Direct titn. in acid soln., indicn. in separate vessel; Br_2 swept to liberate I_2	44
		Dir	I^-	Ag	Indicn. by spotting	45
		Dir, brake	Ag	$I^- + Cl^-$	Detn. of I^- with Ce/As, then Cl^- with Ag-catalyzed oxidn. of leucomalachite green with $S_2O_8^{2-}$	38
	Phot	Dir	I^-	Ag, Hg		41, 42
		Back	I^-	I^-	Excess Hg	42
	Pot	Dir	I^-	Ag		46, 37, 41, 47
		Dir	I^-	Hg or org. Hg comp.		46, 37, 42, 47, 48
		Dir	I^-	Pd		49, 47
		Dir	I^-	Au		49
		Brake	Hg	I^-		37
		Rev	Ag	I^-		46
		Back	I^-	I^-	Excess Ag	46, 42
		Back	I^-	Thioacetamide	Addn. of NaOH→sulphide; excess Hg	42
		Back	I^-	I^-	Addn. of excess Hg	50

	Amp	Dir	I^-	Ag, Hg, Pd		47
	Therm	Dir	I^-	Hg, Ag, Pd		51–54
		Dir	I^-	Amines	Formn. of dithiocarbamate; +Ag, extn.; liberate Ag with HNO_3	55
		Back	I^-	Cl^-, Br^-, I^-, SCN^-, $Fe(CN)_6^{4-}$, S^{2-}, CN^-	Excess Ag, Hg or Pd	51
		Subst	SCN^-	Ag, Hg, Pd	Add AgI, HgI_2 or PdI_2	56
As(III)/Mn(III)	Therm	Dir	I^-	Ag, Hg, Pd		57
As(III)/MnO_4^-	Vis	Dir	I^-	Ag		58
	Biamp	Dir	I^-	Ag, Hg		59
I_2/MnO_4^-	Vis	Dir	BrO_3^-	As(III)	Dir. titn. in acid soln., indicn. in separate vessel; Br_2 swept and reduced to Br^- to catalyze indic. reaction	44
Sb(III)/Ce(IV)	Pot, amp	Dir	I^-	Ag, Hg, Pd		47
	Therm	Dir	I^-	Ag		53
		Back	I^-	I^-, Br^-, SCN^-	Excess Ag	53
$[Fe(CN)_6]^{4-}$	Vis	Dir	Ag	I^-	Formn. of Prussian blue	58
N_3^-/I_2	Vis	Dir	Ag	$S_2O_3^{2-}$	Spots on I^-/N_3^- paper	58
			$S_2O_3^{2-}$	Ag		
		Dir	Na_2S	Sb(III)	Direct titn. in acid soln, indicn. in a separate vessel; H_2S swept	60
		Back	Na_2S	Ni	Addn. of excess S^{2-} and def. amt. of Cu; back-titn. with Na_2S	60
		Dir	Na_2S	Fe(III)	Addn. of CuEDTA; titn. of demasked Cu	60

TABLE 2 (continued)

Indicator reaction	EP	Tech	Titrant	Analyte	Notes	References
N_3^-/I_2		Dir, simlt	Na_2S	Hg+Cd	Titn. of Hg in strongly acid soln and of Cd at pH 4.6	60
		Dir, simlt	Na_2S	Cu+Pb	Titn. of Cu in 0.5 M HNO_3 and Pb at pH 4.6	60
		Dir, simlt	Na_2S	Ag+Cu	Titn. of Ag after addn. of excess EDTA; titn. of Cu after addn. of Fe(III)	60
		Dir	Na_2S	MnO_4^-	Redox titn.	60
		Dir	H^+	OH^-	Acid-base titn. with Na_2S as indicator	60
H_2O_2	Vis	Dir	I^-	Ag	Addn. of detergent; formn. of foam	10
		Dir	Cu	EDTA	Displacement of soln. from the titn. vessel by O_2; spotting technique	45
	Lum	Dir	Cu	EDTA	Addn. of lucigenin	34
		Brake	EDTA	Cu		34
		Back	Cu	Pb, Hg	Excess EDTA	34
	Pot, amp	Dir	Cu	EDTA		61
	Biamp	Brake	EDTA	Cu		37
		Brake	Cu	Salicylaldoxime, EDTA		59
		Rev	EDTA	Mn		62, 21
		Back	Cu	Cu	Excess salicylaldoxime or EDTA	59
		Back	Mn	Mn, Ni, Zn	Excess EDTA	59

	Therm	Dir	Cu	EDTA, DCTA, NTA		63
		Rev	EDTA	Cu, Pb		63
		Back	Cu	Zn, Cd, Cu, Pb, Ga, In, Ni, Bi, Th	Excess EDTA	63
		Dir	Mn	EDTA, DCTA, NTA	In DMSO	64, 56
		Back	Mn	Zn, Cu, Ni, Pb, Hg, Sn, In, Ga, Th, Tl	Excess EDTA in water, DMSO or ethanolamine	64, 56, 65
				Cd, Mn, Al, Mg, Ca, Sr, Ba, Co, Bi, Pd		64, 56
		Rev, subst	EDTA	Zn, Cd, Cu, Ni, In, Hg, Pb	Excess EDTA; addn. of MnEDTA	56
N_2H_4/H_2O_2	Therm	Rev	EDTA	Cu		62, 21
		Back, simlt	Cu	Cu + Ni	Excess EDTA; (1) detn. of Cu + Ni; (2) extn. of Ni with DMG into amyl alc.; detn. of Cu in H_2O	45
		Back, simlt	Cu	Cu + Zn	Excess EDTA; (1) detn. of Cu + Zn; (2) extn. of Cu-α-benzoinoxime into amyl alc.; detn. of Zn in H_2O	45
Iodide/H_2O_2	Phot	Dir	Th, Zr, Fe	F^-, SiF_6^{2-}		66, 67
	Pot, amp	Dir	Th	F^-, SiF_6^{2-}		67
Catechol/H_2O_2	Vis	Rev	EDTA	Ni		68
Resorcinol or catechol/H_2O_2	Therm	Dir	Cu, Fe	EDTA, DCTA, NTA		69
		Rev	EDTA	Cu, Fe		69
		Back	Cu	Mg, Ca, Sr, Ba, Cu, Ni, Co, Zn, Sn, Fe, Al, Cr, Sb, Bi, In, Ga, Th	Excess EDTA	69

TABLE 2 (continued)

Indicator reaction	EP	Tech	Titrant	Analyte	Notes	References
Resorcinol/H_2O_2	Vis	Rev	EDTA	Co, Mn, Fe		68
		Back	Mn	Pb, Cd, Ni, Zn, In	Excess EDTA	68
		Subst	Zn	Zn	Excess EDTA; addn. of MnEDTA	40
		Subst	Zn	Eu	Excess EDTA; addn. of MnEDTA	40
		Subst	Pb	Mg, Ca, Sr, Ba	Excess EDTA; addn. of MnEDTA	40
	Therm	Dir	Mn	EDTA, DCTA, NTA		64, 56
		Back	Mn	Zn, Cu, Ni, Pb, Hg, Sn, In, Ga, Th, Cd, Mn, Al, Mg, Ca, Sr, Ba, Co, Bi, Pd	Excess EDTA	64, 56
		Rev, subst	EDTA	Zn, Cd, Cu, Ni, In, Hg, Pb	Addn. of MnEDTA	56
Hydroquinone/H_2O_2	Vis	Dir	Cu	oxine		70
		Rev	EDTA	Fe		68
		Rev	Oxine	Cu		70
		Back	Cu	Zn, Fe	Excess oxine	70
		Brake	EDTA	Cu	Spotting techn.	38
		Dir	Cu	EDTA	Spotting techn.	38
Hydroquinone or dimethyl-*p*-phenylene-diamine/H_2O_2	Therm	Dir	Fe	EDTA, DCTA, NTA		69
		Rev	EDTA	Fe		69
		Back	Fe	Mg, Ca, Sr, Ba, Cu, Ni, Co, Zn, Sn, Fe, Al, Cr, Sb, Bi, In, Ga, Th	Excess EDTA	69
		Subst	Cu	As above	Addn. of FeEDTA	69

Tiron/H_2O_2	Vis	Brake	EDTA	Co	Spotting techn.	38
		Brake	EDTA	Ni, Zn	Addn. of known amount of Co; spotting techn.	38
		Dir	EDTA	Al	Addn. of equiv. amounts of EDTA and Co; spotting techn.	38
		Dir	EDTA	Fe+Ni	(1) Titn.: Fe with EDTA, SCN^- as indic. (2) Titn.: detn. of sum as for Al	38
		Dir	EDTA	Fe+Al	(1) Titn.: Al masked with F^-; detn. of Fe as for Al. (2) Titn.: detn. of Fe+Al as for Al	38
Tiron/perborate	Vis, phot	Rev	EDTA	Co		10
		Rev	EDTA	Mn		43, 71
		Back	Co	Hg, Cu, Cd, Pb, Mn, Ni, V, Bi, Th, Al, Ga, In, Y, La, Ce, Zr	Excess EDTA	10, 68
		Back	Mn	Zn, Cd, Pb, Hg	Excess EDTA	43, 71
α-Naphthol/H_2O_2	Vis	Rev	EDTA	Cu		68
		Back	Cu	Hg, Pb, Cd, Al, In, Ni, Zn	Excess EDTA	68
m-Aminophenol/ H_2O_2	Vis	Rev	EDTA	Mn		72, 73
		Back	Mn	Zn, Cd, Pb, Hg	Excess EDTA	72, 73
p-Methylaminophenol/ H_2O_2	Vis	Rev	EDTA	Cu		68
		Back	Cu	Pb, Cd, Al, In, Ni, Zn	Excess EDTA	68
p-Dimethylaminophenol or *p*-diethylaminophenol/H_2O_2	Vis	Rev	EDTA	Mn		73
		Back	Mn	Cd, Hg, Pb	Excess EDTA	73
p-Anisidine or *p*-phenetidine/ H_2O_2	Vis	Rev	EDTA	Mn		73
		Back	Mn	Cd, Hg, Pb, Mn, Zn	Excess EDTA	74, 73
		Brake	EDTA	Fe	Spotting technique	45

TABLE 2 (continued)

Indicator reaction	EP	Tech	Titrant	Analyte	Notes	References
p-Toluidine/H_2O_2	Olf	Rev	DCTA	Mn		73, 75
		Back	Mn	Cd, Hg, Pb, Zn	Excess EDTA	73, 75
p-Dimethylaminobenzaldehyde/ H_2O_2	Vis	Rev	EDTA	Mn		73, 75
		Back	Mn	Cd, Hg, Pb	Excess EDTA	73
2-Hydroxybenzaldehyde thiosemicarbazone/H_2O_2	Fluor	Dir	Fe	EDTA		76, 77
		Back	Fe	Fe, Mg, Ca, Sr, Ba	Excess EDTA	76, 77
		Dir	Mn	DCTA		77
		Back	Mn	Mn, Ni	Excess DCTA	77
4,4′-Dihydroxy-benzophenone thio-semicarbazone (DBPT) H_2O_2	Phot	Dir	Cu	EDTA, EGTA		78, 79
		Back	Cu	Cu, Ni, Mn, Co, Fe, Zn,	Excess EDTA or EGTA	78, 79
		Back, simlt	Cu	Cd Fe + Cu, Ni or Mn	(1) Titn., both detd. with EDTA. (2) Titn., Fe masked with triethanolamine or F^-	78, 79
		Dir	DBPT	Hg	Known amount of Cu added	39
		Brake, simlt	EDTA + DBPT	Hg + Cu; Cu	Hg as inhib. for DBPT; Cu as catal. for indic. reaction.	39
		Brake, simlt	EDTA + DBPT	Hg + Cd	Addn. of known amount of Cu; further as above	39
		Dir	EDTA + DBPT	Cd	Known amount of Cu added to sample	39
p-Dimethylphenylenediamine/ H_2O_2	Vis	Rev	EDTA	Cu		68
o-Dianisidine/H_2O_2	Phot	Dir	$Cr_2O_7^{2-}$	Ascorbic acid		36
		Back	$Cr_2O_7^{2-}$	V(V), Tl(III), Ce(IV)	Excess of ascorbic acid	36
Luminol/H_2O_2	Lum	Dir	Cu	EDTA		34
		Brake	EDTA	Cu		34
		Back	Cu	Pb, Hg	Excess EDTA	34
		Back	Mn	Mn	Excess EDTA	59

		Back	Cu	Ca	Excess EGTA; detn. of Ca in presence of Mg	80
		Subst	Zn	Zn	Excess EDTA; addn. of MnEDTA	59
Alizarin S/H_2O_2	Vis	Rev	EDTA	Mn, Co		68
Carminic acid/H_2O_2	Phot	Rev	EDTA	Mn		62, 21
Acid blue 45/H_2O_2	Vis	Rev	EDTA	Mn		81
		Back	Mn	Zn, Cd, Pb, Hg	Excess EDTA	81
	Phot	Rev	EDTA	Mn		82
		Back	Mn	Co, Ni, Cu, Zn, Cd	Excess EDTA	82
Acid violet 6B/H_2O_2	Vis	Rev	EDTA	Mn		83
Phenolphthalein/H_2O_2	Vis	Rev	EDTA	Mn, Cu		84
		Back	Cu	Zn, Cd, Pb	Excess EDTA	84
Thorin/H_2O_2	Phot	Rev	EDTA	Mn		37, 62, 21
$S_2O_3^{2-}$/IO_4^-	Pot	Dir	Cu	EDTA, DCTA, EGTA, DTPA		85
		Back	EDTA	Cu		85
Indigo carmine/H_2O_2	Vis	Brake	EDTA	Fe	Spotting technique	38
Malachite green/IO_4^-	Vis	Brake	EDTA	Mn	Spotting technique	45
Triethanolamine/IO_4^-	ISE	Dir	Mn	EDTA, DCTA, DTPA		14, 17
Diethylaniline/IO_4^-	Phot	Dir	Mn	EDTA, DCTA		86
		Back	Mn	Ga, Pd, Cu, Cd, Pb, Zn, Hg, Co, Ni	Excess EDTA	86
		Back, simlt	Mn	Ni+Co	(1) Sum by back-titn.	86
				Hg+Zn	(2) Separate Ni with DMG; addn. of	86
				Hg+Pb	CN^- to mask Hg	86
				Hg+Cu		
				Hg+Cd		

TABLE 2 (continued)

Indicator reaction	Pot	Dir Back	Mn Mn	EDTA Cu, Zn, Hg, Pb	Excess EDTA	87 87
	EP	Tech	Titrant	Analyte	Notes	References
Leucomalachite green/$S_2O_8^{2-}$	Vis	Dir	Ag	Cl^-, Br^-, I^-		62, 21
Methyl orange/$S_2O_8^{2-}$	Vis	Dir	Ag	SCN^-, Br^-, Cl^-		10
Phloxine/$S_2O_8^{2-}$	Phot	Dir	Ag	Br^-, I^-, SCN^-	2,2′-Bipyridine as activator	88
Carminic acid/$S_2O_8^{2-}$	Phot	Rev Back	EDTA Cu	Cu Cd, Hg, Pb, Zn	Excess EDTA	71 71
1,4-Dihydroxyphthalimide-dioxime/IO_3^-	Phot	Dir Back	Ni Ni	EDTA, DCTA Ni, Hg, Fe	Excess EDTA or DCTA	89 89
Ascorbic acid/O_2	Phot	Dir	Cu	CN^-		90
1,4-Dihydroxyphthalimidedithio-semicarbazone/O_2	Phot	Dir Back	Mn Mn	EDTA, EGTA Mn, Ni, Mg, Ca, Sr, Ba	Excess EDTA	91 91, 92
Dimedonediphenylhydrazone/O_2	Phot	Dir Back	Cu Cu	EDTA Cu, Ni, Co, Zn	Excess EDTA	93 93
p-Phenylenediamine or *o*-toluylenediamine/*m*-aminophenol	Phot	Dir Rev Subst	Mn EDTA	EDTA Mn Zn, Cd, Pb	Coupling reaction Excess EDTA; addn. of MnEDTA	94 94 94
p-Phenylenediamine/*m*-phenylenediamine	Phot	Rev Dir	I^- Ag	Ag Cl^-, Br^-, I^-	Coupling reaction	94 94
As(III) or H_2O_2/chloramine-T	ISE	Dir	I^-	Ag, Hg		95
Urea (enzym. degradation)	ISE	Dir Back	Urease Urease	Hg, Ag S^{2-}	pH electrode Addn. of excess Ag	96 96

Acetone	Therm	Dir	KOH or alkoxide, OH^- coul.	Carboxylic acids, phenols, imides, thiols, barbituric acid, sulphonamides, etc.	Dimerization	35, 97–100, 22, 101–105
Diacetyl	Therm	Dir	KOH	Carboxylic acids	Condensation	106
Cyclohexanone, propanone, cyclohexanedione, 1-phenylpropan-1-one	Therm	Dir	KOH	Carboxylic acids, phenols, etc.	Aldol condensation	107, 108, 106
Formaldehyde	Therm	Dir	Alkoxide	Carboxylic acids		109
Benzaldehyde/acetophenone	Therm	Dir	Alkoxide	Maleic anhydride		109
Acetaldehyde	Therm	Dir	KOH	Boric acid, phosphoric acid, amino acids, etc.		110
Acrylonitrile	Therm	Dir	KOH or alkoxide	Carboxylic acids, phenols, thiols, sulphonamides, catecholamines, etc.	Anionic polymerization, cyanomethylation	101–103, 111–124
Acetic anhydride/H_2O_2	Therm	Dir	$HClO_4$ or H_+ coul.	Tert. amines, carboxylates, F^-, etc.	Hydrolysis	125–130, 54
Acetic anhydride/alcohols, phenols, formic acid	Therm	Dir Dir	$HClO_4$, HCL, H^+ coul.	Tert. amines, carboxylates, steroids, etc.	Acylation, dehydrogenation	53, 129–139
	Cond	Dir	$HClO_4$	Na acetate, org. bases		140
α-Methylstyrene	Therm	Dir	$HClO_4$	Amines, heterocyclic amines, amides, amino acids, catecholamine, alkaloids, etc.		141–143, 112, 138

TABLE 2 (continued)

Indicator reaction	EP	Tech	Titrant	Analyte	Notes	References
Isobutyl vinyl ether	Therm	Dir	BF_3	Amines, heterocyclic amines, etc.		142
Ethyl vinyl ether	Therm	Dir	I_2, ICl, IBr, ICl_3	Amines, heterocyclic amines, dithiocarbonates, dithiocarbamates, thiols, hydrazine, metal iodides, etc.	Addn. of 1,3-dioxolane increases EP sharpness	144–149, 15
Cyclic acetals	Therm	Dir	$HClO_4$	Weak bases	Cationic polymerization	150

nese(III)/arsenic(III) as indicator reaction, and for complexiметric titrations with catalyzable redox reactions as indicator systems.

Olfactory detection of the indicator reaction and gaseous catalysts

The odour of an indicator reaction sometimes served for end-point detection in classical titrimetry [151]. It can also be used in catalytic end-point detection, as was shown [73,75] for the manganese(II)-catalyzed oxidation of *p*-toluidine with hydrogen peroxide.

The applicability of catalyzed reactions for end-point detection is often limited by interactions between the titration reaction and the indicator reaction. These difficulties can be overcome by separating the titration vessel from the indicator vessel if the catalyst is a gas. For example, it is possible to titrate metal ions with a standard sulphide solution by using the sulphide-catalyzed oxidation of sodium azide by iodine [60]. Another example is the titration of reductants with bromate solution [44]. When the iodide-catalyzed oxidation of arsenic(III) with cerium(IV) is used for end-point detection, the first drop of titrant in excess causes evolution of bromine, which is swept by nitrogen into a layer of potassium iodide from which iodine is liberated; this iodine is swept into the indicator vessel and catalyzes the indicator reaction. Another possibility is to reduce the liberated bromine to bromide, which then catalyzes the permanganate/iodine indicator reaction [44].

Catalytic end-point detection with a spotting technique

This method is appropriate when the indicator reaction and the titration reaction cannot proceed under the same conditions (e.g., of pH) and no volatile reaction product is formed. The titration is done in a closed vessel without any air in it; when the motor-driven syringe is started, a small amount of the sample solution is displaced continuously into a mixing chamber, where it reacts with a suitable indicator solution and then drops onto a moving teflon band, on which the end-point can be recognized by a colour change in successive drops [38]. This technique was used in the titration of various metal ions (Cu, Fe, Co, Ni, Zn, Al) with EDTA and in titrations of mixtures of iodide and chloride with silver nitrate. Two or more indicator reactions can be used with the same batch. Calibration graphs are essential.

DETERMINATION OF TWO COMPONENTS IN THE SAME SOLUTION

Water-soluble metal salts and strong mineral acids can be determined sequentially by titration with aqueous potassium hydroxide solution in acetaldehyde/H_2O (1:1) media. The non-catalyzed end-point corresponding to the neutralization of the free acid is detected by the onset of turbidity caused by the precipitation of the metal hydroxide with the first excess of hydroxide. The titration is continued and, when all the metal hydroxide has precipitated,

the final excess of titrant initiates the catalytic-thermometric indicator reaction of hydroxide with acetaldehyde [110,152].

For the determination of binary mixtures of metal ions, two sample aliquots are usually necessary. In one, both metals are titrated with a suitable titrant, giving the total concentration; in the second, one of the ions is masked with a suitable reagent and the other metal is titrated. Binary mixtures of iron(III) with Cu, Ni or Mn can be analyzed by masking iron(III) with triethanolamine or fluoride [79].

Binary mixtures of mercury(II) and copper(II) have been analyzed simultaneously by titration with a mixture of 4,4′-dihydroxybenzophenone thiosemicarbazone (DBPT) and EDTA as titrant; the indicator reaction involves the oxidation of DBPT with hydrogen peroxide, which is catalyzed by copper(II) and inhibited by mercury(II). This catalytic titration is based on the inactivation of one of the components of the indicator reaction (DBPT) with one of the analytes (Hg); as soon as all the mercury has been consumed, the indicator reaction proceeds to form a coloured product and stops doing so as soon as all the Cu(II) in the titrated solution has been complexed by the EDTA [39]; this is another example of titration with a "brake" [21,34,37]). A mixture of mercury(II) and cadmium(II) can be determined similarly by first adding a known amount of standard copper(II) solution to the sample solution [39]. This kind of catalytic end-point detection has the advantage that it is possible to determine "inhibitors" for one reactant of the indicator reaction, but the disadvantage that, at the titration end-point, only a small concentration of one component of the indicator reaction is present.

Liquid-liquid extraction is commonly used for the separation of ions, and can also be applied in catalytic end-point detection [45]. Such titrations are possible without prior separation of the organic phase. In the first step, the ions to be determined (e.g., Cu and Zn or Cu and Ni) are determined simultaneously by adding an excess of EDTA and back-titrating with standard copper(II) solution. In the second step, one of the two ions is extracted with a suitable reagent, e.g., dimethylglyoxime (DMG) for nickel or α-benzoinoxime for copper, and amyl alcohol as the solvent. The other metal is then determined, without separation of the organic phase, by adding excess of EDTA and back-titrating with copper(II) solution [45]. The hydrazine/hydrogen peroxide reaction was used for end-point detection in both cases.

Mixtures of iron(III) and nickel(II) or aluminium, and of chloride and iodide can be determined by using the spotting technique for catalytic end-point detection [38]. Mixtures of Hg(II) and Cd(II), Pb(II) and Cu(II), and Ag and Cu(II) can be determined with the gaseous technique for catalytic end-point detection [60] without previous separation.

TITRATION IN NON-AQUEOUS MEDIUM, AUTOMATION AND COULOMETRIC GENERATION

Acid-base titrations with thermometric end-point detection are always conducted in non-aqueous medium, as was pointed out above. It is also often helpful to use mixtures of an organic solvent with water in the determination of inorganic cations and anions; this has been demonstrated in several papers [56,65,67,94,152]. The advantages are that many metal complexes are more stable and many precipitates less soluble in the presence of organic solvents. Some solvents can also serve as activators for the indicator reaction.

When physical methods are used to monitor the catalyzed indicator reaction, the signal can be applied after suitable amplification of the electric output to regulate an automatic burette; many titrations with catalytic end-point indication have been made semi-automatic in this way [37,41,71,153]. The second-derivative technique has proved best for this purpose [41]. Instead of using a standard solution as the titrant, coulometric generation of the titrant is possible [14,16,53,54,105,128–130,132,135,140].

REFERENCES

1 K.B. Yatsimirskii, Kinetic Methods of Analysis, Pergamon, Oxford, 1966.
2 H. Müller, M. Otto and G. Werner, Katalytische Methoden in der Spurenanalyse, Akadem. Verlagsgesellschaft Geest und Portig, Leipzig, 1980.
3 K.B. Yatsimirskii and T.I. Fedorova, Dokl. Akad. Nauk SSSR, 143 (1962) 143.
4 K.B. Yatsimirskii and T.I. Fedorova, Zh. Anal. Khim., 18 (1963) 1300.
5 T.I. Fedorova and K.B. Yatsimirskii, Zh. Anal. Khim., 22 (1967) 283.
6 J. Bognar, Mikrochim. Acta, (1963) 397, 801.
7 J. Bognar and S. Sarosi, Mikrochim. Acta, (1963) 1072.
8 J. Sájo, Talanta, 15 (1968) 578.
9 I.M. Kolthoff, Z. Anal. Chem., 60 (1921) 393.
10 H. Weisz and U. Muschelknautz, Fresenius' Z. Anal. Chem., 215 (1966) 17.
11 H.A. Mottola, Anal. Chem., 42 (1970) 630.
12 M.S. Goizman, Zavod. Lab., 10 (1971) 1164.
13 B.E. Simpson, M.Sc. Thesis, Oklahoma State University, 1973.
14 F.F. Gaal and B.F. Abramovic, Talanta, 31 (1984) 987.
15 B.F. Abramovic, F.F. Gaal and D.Z. Paunic, Talanta, 32 (1985) 549.
16 F.F. Gaal and B.F. Abramovic, Talanta, 32 (1985) 559.
17 B.F. Abramovic and F.F. Gaal, Microchem. J., 32 (1985) 226.
18 H.J.V. Tyrrell and A.E. Beezer, Thermometric Titrimetry, Chapman and Hall, London, 1968.
19 H.A. Mottola, Talanta, 16 (1969) 1267.
20 H. Weisz, Allg. Prakt. Chem., 22 (1971) 98.
21 H. Weisz and S. Pantel, Fresenius' Z. Anal. Chem., 264 (1973) 389.
22 G.A. Vaughan, Thermometric and Enthalpimetric Titrimetry, Van Nostrand, London, 1973.
23 H.A. Mottola, Anal. Chim. Acta, 71 (1974) 443.
24 J. Barthel, Thermometric Titrations, Wiley, New York, 1975.

25 H.A. Mottola, Crit. Rev. Anal. Chem., 4 (1975) 229.
26 H. Weisz, Angew. Chem. Int. Ed. Engl., 15 (1976) 150.
27 T.P. Hadjiioannou, Rev. Anal. Chem. Isr., 3 (1976) 82.
28 E.J. Greenhow, Chem. Rev., 77 (1977) 835.
29 R. Yu, Clin. J. Pharm. Anal., 1 (1981) 54.
30 H. Müller, Crit. Rev. Anal. Chem., 13 (1982) 313.
31 T.F.A. Kiss, Talanta, 30 (1983) 771.
32 G.A. Milovanovic, Microchem. J., 28 (1983) 437.
33 M. Kopanica and V. Stara, in G. Svehla (Ed.), Comprehensive Analytical Chemistry, Vol. XVIII, Elsevier, Amsterdam, 1983.
34 L. Erdey and I. Buzas, Anal. Chim. Acta, 22 (1960) 524.
35 G.A. Vaughan and J.J. Swithenbank, Analyst, 90 (1965) 594.
36 S. Pantel and H. Weisz, Anal. Chim. Acta, 116 (1980) 421.
37 H. Weisz, S. Pantel and H. Ludwig, Fresenius' Z. Anal. Chem., 262 (1972) 269.
38 H. Weisz and J. Schlipf, Anal. Chim. Acta, 147 (1983) 247.
39 T. Raya Saro and D. Perez Bendito, Anal. Chim. Acta, 182 (1986) 163.
40 D. Klockow and L. Garcia-Beltran, Fresenius' Z. Anal. Chem., 249 (1970) 304.
41 T.P. Hadjiioannou, E.A. Piperaki and D.S. Papastathopoulos, Anal. Chem. Acta, 68 (1974) 447.
42 T.P. Hadjiioannou and E.A. Piperaki, Anal. Chim. Acta, 90 (1977) 329.
43 N. Hotta, Toyama Kogyo Koto Semmon Gakko Kiyo, 11 (1977) 83.
44 H. Weisz and J. Schlipf, Anal. Chim. Acta, 134 (1982) 349.
45 J. Schlipf, Ph.D. Thesis, University of Freiburg i. Br., 1982.
46 H. Weisz and D. Klockow, Fresenius' Z. Anal. Chem., 232 (1967) 321.
47 F.F. Gaal and B.F. Abramovic, Talanta, 27 (1980) 733.
48 F.F. Gaal and B.F. Abramovic, Mikrochim. Acta, Part I, (1982) 465.
49 T.P. Hadjiioannou and M.M. Timotheou, Mikrochim. Acta, Part I, (1977) 61.
50 M.M. Timotheou-Potamia and T.P. Hadjiioannou, Mikrochim. Acta, Part II, (1983) 59.
51 H. Weisz, T. Kiss and D. Klockow, Fresenius' Z. Anal. Chem., 247 (1969) 248.
52 K.C. Burton and H.M.N.H. Irving, Anal. Chim. Acta, 52 (1970) 441.
53 V.J. Vajgand, F.F. Gaal, L.P. Zrnic-Zeremski and V.I. Soros, 3rd Therm. Anal. Proc. Int. Conf., 2 (1971) 437.
54 F.F. Gaal and L. Bjelica, Chem. Anal. (Warsaw), 21 (1976) 227.
55 N. Kiba, Y. Suzuki and M. Furusawa, Talanta, 28 (1981) 691.
56 T. Kiss, Fresenius' Z. Anal. Chem., 252 (1970) 12.
57 N. Kiba and M. Furusawa, Anal. Chim. Acta, 98 (1978) 343.
58 U. Muschelknautz, Ph.D. Thesis, University of Freiburg i. Br., 1966.
59 S. Pantel and H. Weisz, Fresenius' Z. Anal. Chem., 281 (1976) 211.
60 H. Weisz and J. Schlipf, Anal. Chim. Acta, 121 (1980) 257.
61 F.F. Gaal, B.F. Abramovic, F.B. Szebenyi and V.D. Canic, Fresenius' Z. Anal. Chem., 286 (1977) 222.
62 H. Weisz and S. Pantel, Anal. Chim. Acta, 62 (1972) 361.
63 T.F.A. Kiss, Mikrochim. Acta, (1972) 420.
64 H. Weisz and T. Kiss, Fresenius' Z. Anal. Chem., 249 (1970) 302.
65 T.F.A. Kiss, Mikrochim. Acta, Part II, (1975) 471.
66 J. Schlipf, Diploma Thesis, University of Freiburg i. Br., 1978.
67 F.F. Gaal, B.F. Abramovic and V.D. Canic, Talanta, 25 (1978) 113.
68 H. Weisz and T. Janjic, Fresenius' Z. Anal. Chem., 227 (1967) 1.
69 T. Kiss, Mikrochim. Acta, (1973) 847.
70 A. Brock, Diploma Thesis, University of Freiburg i. Br., 1967.
71 N. Hotta, Toyama Kogyo Koto Semmon Gakko Kiyo, 15 (1981) 119.

72 S. Abe and S. Kon, Bunseki Kagaku, 25 (1976) 846.
73 S. Abe, S. Kon and A. Yamagata, Asahi Garasu Kogyo Gijutsu Shoreikai Kenkyu Hokoku, 30 (1977) 225.
74 S. Abe, K. Takahashi and M. Matsuo, Nippon Kagaku Kaishi, 5 (1973) 963.
75 S. Abe, S. Kon and T. Matsuo, Anal. Chim. Acta, 96 (1978) 429.
76 D. Perez Bendito, M Valcárcel and M. Silva, SAC 1983 Edinburgh, Anal. Proc., (1983) 325.
77 A. Moreno, M. Silva, D. Perez-Bendito and M. Valcárcel, Analyst, 109 (1984) 249; Quim. Anal., 4 (1985) 39.
78 T. Raya-Saro and D. Perez-Bendito, Analyst, 108 (1983) 857.
79 T. Raya-Saro and D. Perez-Bendito, Anal. Chim. Acta, 172 (1985) 273.
80 D.L. Duewer and G.D. Christian, Chem. Biomed. Environ. Instrum., 9 (1979) 373.
81 S. Abe and K. Takahashi, Bunseki Kagaku, 23 (1974) 1326.
82 S. Abe, N. Nakamura and T. Matsuo, Bunseki Kagaku, 30 (1981) 809.
83 N. Hotta, Toyama Kogyo Semmon Gakko Kiyo, 10 (1976) 1.
84 S. Abe and T. Matsuo, Bunseki Kagaku, 20 (1981) 1168.
85 M.M. Timotheou-Potamia, M.A. Koupparis and T.P. Hadjiioannou, Mikrochim. Acta, Part II, (1982) 433.
86 E.A. Piperaki and T.P. Hadjiioannou, Chim. Chron., 6 (1977) 375.
87 T.P. Hadjiioannou, M.A. Koupparis and C.E. Efstathiou, Anal. Chim. Acta, 88 (1977) 281.
88 C. Sanchez-Pedreno, M. Hernandez-Cordoba and P. Vinas, Talanta, 32 (1985) 218.
89 A. Gomez-Hens, M. Ternero, D. Perez-Bendito and M. Valcárcel, Mikrochim. Acta, Part I, (1979) 375.
90 H.A. Mottola and H. Freiser, Anal. Chem., 40 (1968) 1266.
91 M. Ternero, F. Pino, D. Perez-Bendito and M. Valcárcel, Anal. Chim. Acta, 109 (1979) 401.
92 M. Ternero, D. Perez-Bendito and M. Valcárcel, Microchem. J., 26 (1981) 61.
93 F. Salinas-Lopez, J.J. Berzas Nevado and A. Espinosa Mansilla, Ann. Quim. B, 80 (1984) 125.
94 S. Abe, K. Watanabe and T. Sugai, Bunseki Kagaku, 32 (1983) 398.
95 M.M. Timotheou-Potamia, M.A. Koupparis and T.P. Hadjiioannou, Microchem. J., 28 (1983) 392.
96 W. Gerlach, Diploma Thesis, University of Freiburg i. Br., 1983.
97 G.A. Vaughan, British Wood Preserving Association, Cambridge Meeting, 1967, p. 16.
98 Standardisation of Tar Products Tests Committee, Standard Methods of Testing Tar and its Products, 6th edn., Gomersal, Yorkshire, U.K., 1967, p. 454.
99 G.A. Vaughan and J.J. Swithenbank, Analyst, 95 (1970) 890.
100 British Standards Institution, Specification for Preservative in Textile Treatments, BS 2087: 1971, London, 1971, p. 38.
101 E.J. Greenhow and L.E. Spencer, Analyst, 98 (1973) 90.
102 E.J. Greenhow and L.H. Loo, Analyst, 99 (1974) 360.
103 L.S. Bark and O. Ladipo, Analyst, 101 (1976) 203.
104 N. Kiba, Y. Sawada and M. Furusawa, Talanta, 29 (1982) 416.
105 F.F. Gaal, A.S. Topalov and Zs. J. Vitez, Microchem. J., 33 (1986) 71.
106 D. Marrero-Ardila and E.J. Greenhow, Anal. Proc., 20 (1983) 130.
107 E.J. Greenhow, Chem. Ind. (London), (1974) 456.
108 R.L. Parry-Jones, Educ. Chem., 13 (1976) 76.
109 F.F. Gaal, B.D. Abramovic and V.J. Vajgand, Microchem. J., 27 (1982) 231.
110 E.J. Greenhow and L.E. Spencer, Talanta, 24 (1977) 201.
111 E.J. Greenhow, Chem. Ind. (London), (1972) 422.
112 E.J. Greenhow and L.E. Spencer, Analyst, 98 (1973) 485.
113 E.J. Greenhow and R. Hargitt, Proc. Soc. Anal. Chem., 10 (1973) 276.
114 R. Parry-Jones, Chem. Ind. (London), (1974) 770.
115 E.J. Greenhow and L.E. Spencer, Anal. Chem., 47 (1975) 1384.

116 E.J. Greenhow and A.A. Shafi, Proc. Anal. Div. Chem. Soc., 12 (1975) 286.
117 E.J. Greenhow, R. Hargitt and A.A. Shafi, Angew. Makromol. Chem., 48 (1975) 55.
118 E.J. Greenhow and A.A. Shafi, Talanta, 23 (1976) 73.
119 E.J. Greenhow and A.A. Shafi, Analyst, 101 (1976) 421.
120 E.J. Greenhow and A.A. Shafi, Angew. Makromol. Chem., 53 (1976) 187.
121 E.J. Greenhow, A. Nadjafi and L.A. Dajer de Torrijos, Analyst, 103 (1978) 411.
122 E.J. Greenhow and L.A. Dajer de Torrijos, Analyst, 104 (1979) 801.
123 E.J. Greenhow and A. Nadjafi, Anal. Chim. Acta, 109 (1979) 129.
124 O.E.S. Godhino and E.J. Greenhow, Anal. Chem., 57 (1985) 1725.
125 V.J. Vajgand and F.F. Gaal, Glas. Hem. Drus., Beograd, 31 (1966) 103.
126 V.J. Vajgand, T.J. Pastor, F.F. Gaal and M. Todorovic, Proc. Conf. Appl. Phys.-Chem. Methods Chem. Anal. (Budapest), 1 (1966) 152.
127 V.J. Vajgand and F.F. Gaal, Talanta, 14 (1967) 345.
128 V.J. Vajgand, T.A. Kiss, F.F. Gaal and I.J. Zsigrai, Talanta, 15 (1968) 699.
129 V.J. Vajgand, F.F. Gaal, L. Zrnic, S.S. Brusin and D. Velimirovic, Proc. 3rd Anal. Chem. Conf., 2 (1970) 443.
130 V.J. Vajgand, F.F. Gaal and S.S. Brusin, Talanta, 17 (1970) 415.
131 M.S. Goizman, Dokl. Akad. Nauk SSSR, 184 (1969) 599.
132 V.J. Vajgand and F.F. Gaal, Proc. 2nd Conf. Appl. Phys.-Chem., 1 (1971) 683.
133 E.J. Greenhow, Analyst, 102 (1977) 584.
134 E.J. Greenhow, J. Chem. Soc. Perkin Trans. 2, (1978) 1248.
135 F.F. Gaal, D.L. Kuzmic and R.I. Horvat, Microchem. J., 23 (1978) 417.
136 F.F. Gaal, D.A. Miljkovic, K.M. Gasi and D.Lj. Kuzmic, Fresenius' Z. Anal. Chem., 312 (1982) 618.
137 K. Ni, Q. Yang and R. Yu, Yaowu Fenxi Zazhi, 3 (1983) 326.
138 E.J. Greenhow and P. Vinas, Talanta, 31 (1984) 611.
139 E.J. Greenhow and O. Ladipo, Anal. Chim. Acta, 172 (1985) 387.
140 F.F. Gaal, B.F. Abramovic and R.I. Cservenak, Microchem. J., 34 (1986) 295.
141 E.J. Greenhow, Chem. Ind. (London), (1972) 466.
142 E.J. Greenhow and L.E. Spencer, Analyst, 98 (1973) 81.
143 E.J. Greenhow and L.E. Spencer, Analyst, 98 (1973) 98.
144 E.J. Greenhow, Chem. Ind. (London), (1973) 697.
145 E.J. Greenhow and L.E. Spencer, Analyst, 99 (1974) 82.
146 E.J. Greenhow and L.E. Spencer, Analyst, 100 (1975) 747.
147 E.J. Greenhow and L.E. Spencer, Analyst, 101 (1976) 777.
148 G.L. Jeyaraj and E.J. Greenhow, Proc. Anal. Div. Chem. Soc., 19 (1982) 326.
149 E.J. Greenhow and G.L. Jeyaraj, Analyst, 108 (1983) 991.
150 E.J. Greenhow and M. Kashanipour, Analyst, 110 (1985) 1209.
151 E. Rancke Madsen, The Development of Titrimetric Analysis Till 1806, G.E.C. Gad, Copenhagen, 1958.
152 E.J. Greenhow and M. Kashanipour, Analyst, 109 (1984) 931.
153 K. Mangold, H. Schweers and B. Dörenkämper, Fresenius' Z. Anal. Chem., 309 (1981) 193.

Analytica Chimica Acta, 202 (1987) 25-34
Elsevier Science Publishers B.V., Amsterdam — Printed in The Netherlands

RECENT APPLICATIONS OF THE RING-OVEN TECHNIQUE
A brief review

HERBERT WEISZ

Institut für Anorganische und Analytische Chemie, Albert Ludwigs Universität Freiburg, Albertstr. 21, D-7800 Freiburg i.Br. (Federal Republic of Germany)

(Received 21st March 1987)

SUMMARY

The ring-oven technique is a special type of spot analysis. In this review, papers published since 1976 are discussed. The aspects dealt with include developments in the technique and its use, the identification and determination of inorganic ions, organic substances, enzymatic analysis, applications to air and water samples, and combinations with other techniques.

The first paper on the ring-oven technique, was published in 1954 [1]. This technique, basically a special type of spot analysis on filter paper, was originally proposed for separations of extremely small samples in investigations of works of art. In contrast to conventional spot tests, the substances to be separated, identified or determined are concentrated in the form of sharply outlined circular lines. The main features are the concentration of substances on filter paper in the form of narrow lines with simple equipment and the possibility of obtaining separations in a single 1-μl drop of sample solution. Numerous applications of the technique in many fields have been published in more than 400 papers. A second edition of "Microanalysis by the Ring-Oven Technique" appeared in 1970 [2] and the then-recent advances in this technique were reviewed in 1976 [3]. Two Chinese reviews on various applications of the ring-oven should be mentioned [4,5] and also the Chinese translation of the monograph [6]. An extensive review of the technique was published by Grdinic in 1975 [7].

Since then, about 90 further publications on the ring-oven method have appeared. Most of these papers, and some earlier ones which only later became known to the present reviewer, are discussed below.

0003-2670/87/$03.50

The original form of the ring-oven has still not been altered. A portable glass ring-oven monitoring box has been described for the use in air-pollution studies [8], and ring-ovens with several holes (e.g., a three-hole ring-oven) have been proposed [9]. This type serves to prepare several rings on one filter paper, thus allowing simultaneous comparisons of sample with standard ring segments [10]. It is to be regretted that a number of papers in Chinese, obviously of interest, are not completely understood (and consequently cannot be evaluated properly), because they often have only a short summary in English or none at all.

The segment technique, in which standard and sample drops are placed on concentric points around the centre of a round filter paper and washed to the ring zone, thus forming sharply outlined circular segments has been extended from three to five segments [11]. This procedure simplifies simultaneous comparisons and has been applied to the determination of organic and inorganic substances in the nanogram–microgram range by means of fluorescence reactions; self-fluorescence, or fluorescence as a result of a chemical reaction, or fluorescence quenching has been used [12]. This technique has often been applied as an alternative to the usual standard-scale method; some of these uses will be indicated below.

A rotating ring-oven has been described, as a sort of fraction collector in combination with column chromatography [13].

The use of a stream of hot air as an alternative to the hot edge of the ring-oven was mentioned in the previous review [3,14,15]. A similar ring-air technique has been proposed for circular thin-layer chromatography, to enhance the local sample concentration [16]. "Enrichment and focussing of traces from a maximum volume of solution in a ring similar to the ring-oven technique" by using a heated ring in high-performance thin-layer chromatography has been proposed by Kaiser and Rieder [17] (see also Zlatkis and Kaiser [18]).

Semiquantitative analysis by comparing the speed of decolorization on filter paper has advantages; three ring segments of sample and standards have been applied for both inorganic and organic substances [19].

Grdinic, Gertner and co-workers have continued their theoretical studies on the process of fixation, elution and complexing ions on filter paper in connection with the ring-oven method [20–23]. An interesting study on the sorption capacity of filters [24] and a comparative study of the detection limits attainable with several techniques should be mentioned [25]. In some of these investigations, autoradiography was applied [20,22,24].

A method for the simultaneous determination of two or three ions in one ring zone without weighing the sample has been used for the analysis of inorganic pigments in paintings. Instead of using three different drop numbers of sample solution, three different grains of the sample (about 1–2 μg each) are

dissolved, or fused on a platinum foil with a suitable decomposition reagent [2], and transferred to the ring zone. In one half of the ring, one of the two ions in question is determined and so the ratio of the two components is evaluated; this can serve as a means of identifying a suspected compound [26]. It has also been used for tiny particles of minerals and inclusions in mineral samples [27].

IDENTIFICATION AND DETERMINATION OF INORGANIC IONS

For practically all metal ions, identification reactions have already been adapted for the ring-oven method [2], therefore only some special qualitative applications are mentioned below. An interesting scheme for traces of eleven metals by precipitating them all as sulphides has been described; they can be separated into six groups based on differences in their solubility in different concentrations of hydrochloric acid [28].

An unclear method for separation and detection of thorium and zirconium has been published [29]. A systematic separation scheme for platinum metals (Ir, Pd, Pt, Rh, Ru) and gold was recently reported [30].

The detection of contamination of pharmaceutical materials with heavy metals (Fe, Cu, Pb, Zn, Ni and Co) [31] and a rapid microtechnique for the identification of trace metals (Cu, Sb, Pb, Ba) from gunshot residues [32] are two examples of practical applications of the method.

In ring colorimetry, the colour intensities of unknown rings are compared with those of standard rings; for many cations and anions, suitable methods are available [2,3]. More recently, several papers on the analysis of minerals have appeared: lithium has been quantified with 8-quinolinol by means of its fluorescence (0.02–1.5 μg) [33]; barium, lead and strontium have been determined with rhodizonic acid (0.15–1.5 μg each) [34] and beryllium with chromazurol S (1–10 μg in epididymite) [35,36]. The simultaneous comparison (segment) technique was used instead of the usual standard-scale technique in the lithium determination. Palladium (with rubeanic acid) [37] and cadmium (with cadion) [38] have been estimated with both methods.

Some more organic reagents have been proposed for the determination of metal ions. 2,2-Pyridinediol has been applied for submicrogram amounts of iron(III) [39], and glyoxal-bis(*o*-hydroxyanil) for cadmium (0.025–1.25 μg) in alloys [40], and for nickel(II) and uranium(VI) combined with liquid–liquid extraction [41]. Uranium has also been estimated with a Schiff base of *N,N'*-dimethyl-*p*-phenylenediamine and salicylaldehyde in the presence of sodium arsenate; arsenic in tobacco samples was determined indirectly with this procedure [42]. Other reagents suggested are 3-mercapto-4-amino-5-methyl-1,2,4-triazole for platinum and gold [43] and for gold, thallium(I) and silver [44], glyoxal-bis(2-mercaptoanil) for submicrogram amounts of mercury [45], 3-hydroxypyridine-2-thiol for iron in alloys [46] and several di-

azolyl dyes for the determination of copper [47]. Ethyl 4-(4-hydroxy-6-methyl-2-oxopyran-3-yl)-2,4-dioxobutyrate gives coloured and fluorescent chelates with a number of metal ions; determinations of aluminium, chromium(III) and iron(III) in mixtures were described [48].

A sensitive microdetermination for aluminium and beryllium based on precipitate exchange with calcium fluoride has been reported; the liberated calcium was determined on the ring oven with glyoxal-bis(*o*-hydroxyanil) [49]. The possibilities offered by precipitate exchange have been little exploited. Other examples are the determination of copper by reaction with lead sulphide [50] and a method for lead based on tetrahydroxy-*p*-benzoquinone [51].

Fluorescence quenching has been proposed [12] for determinations of titanium (salicylic acid), nickel (salicylic acid and 8-quinolinol) and copper and cobalt (rhodamine B), and formation of fluorescence for estimating aluminium and thorium (morin), calcium, magnesium and zinc (8-quinolinol) and lithium (quercetin). The segment technique was used in these procedures.

Little has been reported about new methods for anions. Nanogram amounts of sulphate have been determined based on the conversion of 2-aminoperimidine (bound to the sulphate) to 2-amino-4,6,9-trinitroperimidine; a glass-fibre filter is essential for this procedure [52]. Fluorescence quenching and indirect fluorescence determination have been used for estimating sulphide (with copper and rhodamine B), fluoride (with titanium(IV) salicylate), sulphate (with thorium and morin) and oxalic acid (with calcium and 8-quinolinol); borate was determined by a fluorescence reaction with alizarin S [12].

Sulphate and sulphide (after oxidation to sulphate) can be estimated through the reproducible coprecipitation of barium ions with the precipitate of barium sulphate; the coprecipitated barium is made visible with rhodizonate. A modified procedure makes it possible to estimate sulphide and sulphate in one sample [26].

ORGANIC SUBSTANCES

Several interesting applications of the ring-oven method for the determination of various organic substances have been reported. The combination of the Schöniger oxygen flask method for 14 hetero-elements in organic compounds and the determination of common organic functional groups have been reviewed [53].

Some more amino acids have been determined with the segment technique [54]. In a combination of column chromatography with the ring-oven technique, several amino acids (β-alanine, valine, leucine and glutamic acid) were separated [13]. Salicylic acid was determined in Japanese sake with iron(III) chloride as the reagent [55].

Apart from method already discussed [2] for the determination of phenols, some others have been proposed. Thus 4-aminoantipyrine and potassium hexa-

cyanoferrate(III) have been used to estimate phenol, resorcinol, pyrogallol, hydroquinone, phloroglucinol and cresol [56,57] as well as a number of mono-, di-, tri-, tetra- and penta-chlorophenols [58]. The same group of substituted phenols could also be estimated with methylbenzothiazolinone hydrazone [59].

As interest in estimating traces of pesticides has increased, the ring-oven technique has found further applications. An IUPAC report has mentioned its use [60]; organochlorine agrochemicals have been determined via silver chloride and silver sulphide [61]. In a continuation of earlier work [62], some more organophosphorous insecticides (Malathion, Diazinon, Baytex, Guthion) have been estimated, after thin-layer chromatographic separation, with palladium(II) chloride and ammonium sulphide; residues on wheat, corn and potatoes were determined [63].

The determination of nicotine with Dragendorf reagent [64] and of brucine in strychnine [65] are additional examples of estimations of alkaloids. The carcinogens 1,12-benzperylene, 1,2-benzpyrene and 3,4-benzpyrene have been estimated by their blue-green fluorescence compared with standard quinine sulphate rings [66].

Ring-oven methods had been described for a number of substances of pharmaceutical interest: isonicotinic acid hydrazide (isoniazid) with vanillin [67], salicylamide with 4-aminoantipyrine and hexacyanoferrate(III) [68] and barbituric acid with sodium nitrite [69]. Nitrazepam [70], quinine, riboflavin and esculin have been estimated by their fluorescence, and acetylsalicylic acid, thiamine, etc. by suitable reactions to produce fluorescence [12]. An application of the ring-oven technique in preliminary tests for components in traditional Chinese drugs should be mentioned [71].

ENZYMATIC ANALYSIS

Two basic difficulties had to be overcome before enzymatic methods could be used in ring-oven procedures. In such methods, the reaction time plays a decisive role, but this problem had already been solved for inorganic catalysts with the segment technique [3,10]. The other difficulty is, of course, that enzymes cannot be transferred to the ring zone on the hot ring oven. Three techniques were developed to solve this problem for determining various enzymes (e.g., phosphatase, hyaluronidase, acetylcholinesterase, lipase and alcohol dehydrogenase) as well as inhibitors (metals, herbicides and fungicides) and substrates (ethanol or glucose). In one technique, the known adsorption-barrier ($BaSO_4$) was applied [3,72]. In the two other techniques, either the enzymatic reaction is allowed to proceed inside the ring zone and the products are transported to the ring zone, or the enzyme is applied directly to the segments [73,74].

Immobilized enzymes have also been used for the determination of sub-

strates. Both a microcolumn containing an enzyme (alkaline phosphatase) immobilized on Sepharose 4B and direct fixation of the enzyme on filter paper activated with triazine have been applied. In the determination of β-glycerophosphate, the enzyme cleaves the substrate to liberate phosphate, which can be estimated with the well known *o*-dianisidine/molybdate reaction (segment technique) [75]. Only a little experience has been gained so far.

APPLICATION TO AIR AND WATER SAMPLES

For the analysis of gases, mainly in air pollution studies, the samples are usually collected by impaction and the resulting solution is examined by ring colorimetry, or the gas sample is sucked through an impregnated filter [2]. A later example of this procedure is the determination of ammonia with *o*-phthalic dicarboxaldehyde [76].

In a recent method, filter papers impregnated in the centre with a suitable absorbent, are simply exposed to the gas, which is not sucked through the paper. The amount of gas absorbed is then determined directly on the paper itself. Varying the exposure time replaces varying the drop numbers, so that three rings are obtained finally for comparison with the calibration scale; hydrogen sulphide, sulphur dioxide and formaldehyde were determined [77].

The ring-oven method has been applied frequently in studies of air and water pollution [2,3]. This technique has been particularly recommended for air pollution work involving the determination of metals, on the basis of a 3-year research project in which results were compared with those obtained by "recognized methods" [78]. The composition of aerosols collected on flights has been investigated (sulphate, Mg, Ca, Cu, Al) [79]. A field test kit has been described for determinations of metals in environmental samples; it was tested for eleven metals [80].

In several applications, the reactions used are known, so that only brief listing is necessary. Thus cadmium, calcium and copper [81], iron and tetraethyl lead in a car plant [82], lead with rhodizonate (the intensity of the rings is measured with a microphotometer system) [83] and mercury [84] have been estimated in air pollution studies. Nitrogen oxides have been estimated on a three-hole ring oven [9]. In other work, hydrogen fluoride has been determined by using an adsorption ring technique and chromazurol S [85], hydrogen chloride via silver chloride to yield silver sulphide [8,86], nicotine in air from a tobacco factory [64], and three polynuclear aromatic hydrocarbons in smoke samples [66].

In the field of water pollution, the ring-oven technique has been evaluated for Fe, Pb, Mg, Zn, Cu, Cd, Mn, Cr, Ca, chloride, fluoride, nitrate and cyanide [87–90], sulphate in potable waters [52], lead in sewage [91] and phosphate [92].

COMBINATIONS WITH OTHER ANALYTICAL TECHNIQUES

Electrographic sampling by anodic dissolution of metals as originally described [2,93] has again been used for the determination of silver [94] and for non-destructive analysis of art objects [95] and of ancient punch-marked silver coins from India [96]. In the latter two methods, a rather unusual procedure is followed: the electrographed metal ions are extracted from the paper and this solution is used for further work.

Combinations with thin-layer chromatography (TLC) have found numerous applications [2,3]. Later papers have dealt with separation by TLC and determination by ring colorimetry of platinum metals and gold [43], of iron, mercury, thallium and antimony [97] and of various other mixtures of metal ions [98–100]. The combination of these two techniques has also been used for the separation and determination of organophosphorus insecticides [62,63].

Decreasing the area of spots with the heat barrier of a rectangular oven and application of ring colorimetry has been described for various metals [101,102]. A "rotating ring-oven" (see above) had been used for column-chromatographic separation and ring-oven detection of four amino acids [13].

Combination with photoacoustic spectroscopy (PAS) has been suggested for determinations of palladium and nickel [103] and copper [104]; the ring-oven served to separate the species of interest and PAS served to quantify them.

Conclusion

Because of the simplicity, sensitivity and portability of the ring-oven method, many practical applications were proposed soon after its first introduction [2,3]. Air and water pollution is a major field of application. Applications during the last ten years have included the detection of trace metals from gunshot residues [32] and determinations of salicylic acid in Japanese sake [55], arsenic in tobacco [42] and organochlorine pesticides [61] as well as the analysis of pharmaceutical compounds [31,68,71].

In the field of art investigation, the analysis of ancient Indian coins [96] and the method for analyzing pigments of paintings [26] emphasize the value of the technique.

The reviewer would be grateful to receive information from colleagues who use any of these ring-oven methods in whatever field of application.

REFERENCES

1 H. Weisz, Mikrochim. Acta, (1954) 140.
2 H. Weisz, Microanalysis by the Ring-Oven Technique, 2nd edn., Pergamon, Oxford, 1970.
3 H. Weisz, Analyst, 101 (1976) 152.

4 Xin-Du Geng and Shu-Ren Liu, Huaxue Tongbao, (1976) 38 (Anal. Abstr., 31 (1976) 3J21).
5 Xin-Du Geng, Xibeidaxue Xuebao, 1 (1979) 77.
6 H. Weisz, Microanalysis by the Ring-Oven Technique (in Chinese), translated by Shih-Nien Shen, Shanghai Science and Technology Publisher, 1965.
7 V. Grdinic, Acta Pharm. Jugosl., 25 (1975) 195.
8 Xin-Du Geng, Huanjing Kexue, 2 (1979) 28.
9 Xin-Du Geng, Rui Chao and Xiurong Dang, Hua Hsueh Tung Pao, 4 (1981) 22 (Anal. Abstr., 42 (1982) 1H13).
10 H. Weisz, S. Pantel and I. Vereno, Mikrochim. Acta, Part II, (1975) 287.
11 H. Weisz, S. Pantel and E. Räpple, Mikrochim. Acta, Part II, (1982) 289.
12 H. Weisz, S. Pantel, C.M. Dilger and U. Glatz, Mikrochim. Acta, Part I, (1984) 69.
13 H. Weisz, I. Vereno and W. Meiners, Anal. Chim. Acta, 100 (1978) 571.
14 K. Moskaliuk, V. Marjanovic, K. Mazuranic, A. Golubovic and I. Eskinja, Mikrochim. Acta, (1970) 29.
15 C.J.M. Ronneau, N.M. Jacob and D.J. Apers, Anal. Chem., 45 (1973) 2152.
16 R.D. Davies and V. Pretorius, Talanta, 26 (1979) 137.
17 R.E. Kaiser and R. Rieder, J. Chromatogr., 142 (1977) 411.
18 A. Zlatkis and R.E. Kaiser, High-Performance Thin-Layer Chromatography, Elsevier, Amsterdam, 1977.
19 H. Weisz, S. Pantel and R. Giesin, Anal. Chim. Acta, 101 (1978) 187.
20 V. Grdinic and A. Gertner, Acta Pharm. Jugosl., 25 (1975) 89.
21 V. Grdinic and A. Gertner, Acta Pharm. Jugosl., 27 (1977) 235.
22 V. Grdinic and A. Gertner, Acta Pharm. Jugosl., 27 (1977) 241.
23 D. Pavisic, D. Kodrnja and A. Gertner, Acta Pharm. Jugosl., 27 (1977) 253.
24 V. Grdinic, Mikrochim. Acta, Part II, (1979) 493.
25 V. Grdinic, S. Luterotti and L. Stefanini-Oresic, Microchem. J., 28 (1983) 107.
26 W. Köhler and H. Weisz, Berl. Beiträge zur Archäometrie, 9 (1984) 147.
27 W. Köhler, Ph.D. Thesis, University of Freiburg i.Br., 1982.
28 A. Chiba, Bunseki Kagaku, 29 (1980) 489 (Anal. Abstr., 40 (1981) 2B14).
29 Xin-Du Geng, Huaxue Tongbao, 3 (1965) 59 (Chem. Abstr., 63 (1965) 10677).
30 A. Chiba, S. Suyama and T. Ogawa, Bunseki Kagaku, 35 (1986) 946.
31 J. Pawlaczyk and D. Nowacka, Farm. Pol., 34 (1978) 175 (Anal. Abstr., 35 (1978) 3E7).
32 S.F. Bosen and D.R. Scheuing, J. Forensic Sci., 21 (1976) 163.
33 N.B. Hansen, Mikrochim Acta, Part II, (1983) 277.
34 N.B. Hansen, Kem. Anal. Miner. Bjergarter, 6 (1978) (Chem. Abstr., 92 (1980) 5609).
35 N.B. Hansen, Kem. Anal. Miner. Bjergarter, 9 (1980).
36 N.B. Hanse, Mikrochim. Acta, Part II, (1982) 133.
37 M. Hanif, M.A. Chaudhry and Sh. Hamdani, Anal. Chim. Acta, 98 (1978) 145.
38 M. Hanif, M.S. Chaudhry and T.A. Qureshi, Anal. Chim. Acta, 90 (1977) 307.
39 H.C. Mehra and G.R. Chhatwal, Anal. Chim. Acta, 72 (1974) 194.
40 H.C. Mehra, Fresenius Z. Anal. Chem., 282 (1976) 219.
41 H.C. Mehra, Fresenius Z. Anal. Chem., 296 (1979) 413.
42 A.C. Handa and K.N. Johri, Indian J. Chem., Sect. A, 14 (1976) 294 (Anal. Abstr., 32 (1977) 1D9).
43 K.N. Johri, N.K. Gautam and S. Saxena, Chromatographia, 9 (1976) 175.
44 K.N. Johri and S. Saxena, Microchem. J., 23 (1978) 453.
45 H.C. Mehra, Fresenius, Z. Anal. Chem., 285 (1977) 262.
46 M. Katyal, N.K. Kaushik and B. Bhushan, J. Inst. Chem., Calcutta, 50 (1978) 192 (Chem. Abstr., 91 (1979) 13129).

47 M.H. Gandhi and K.C. Pathak, Indian J. Chem., Sect. A, 25 (1986) 499 (Chem. Abstr., 105 (1986) 71655).
48 A. Gertner and D. Pavisic, Microchem. J., 23 (1978) 336.
49 K.N. Johri and A.C. Handa, Mikrochim. Acta, Part II, (1975) 683.
50 Ngo Huy Du, Tap San and Hoa-Hoc, 17 (1979) 18 (Chem. Abstr., 92 (1980) 226000).
51 A. Llacer, DNQ, 5 (1978) 197 (Chem. Abstr., 91 (1979) 32299).
52 P.K. Dasgupta and P.W. West, Mikrochim. Acta, Part II, (1978) 505.
53 Yao-Zu Chen, Mikrochim. Acta, Part I, (1981) 343.
54 H. Weisz and I. Vereno, Mikrochim. Acta, Part I, (1979) 113.
55 A. Chiba, Ansen Kagaku, 13 (1974) 380.
56 M. Hanif, F. Jamshaid, T. Aman and M.H. Hashmi, Pak. J. Sci. Ind. Res., 19 (1976) 204 (Chem. Abstr., 89 (1978) 70344).
57 M. Hanif, F. Jamshaid and T. Aman, Pak. J. Sci. Ind. Res., 20 (1977) 215 (Chem. Abstr., 90 (1979) 97120).
58 N.G. Buckman, J.O. Hill and R.J. Magee, Microchem. J., 28 (1983) 470.
59 N.G. Buckman, J.O. Hill and R.J. Magee, Analyst, 108 (1983) 573.
60 International Union of Pure and Applied Chemistry, Applied Chemistry Division, Commission on Pesticide Chemistry, Pure Appl. Chem., 53 (1981) 1039.
61 Zhenjie Zhang, Jiequan Hu and Jumie Jian, Huanjing Kexue, 3 (1982) 79 (Anal. Abstr., 46 (1983) 6G29; Chem. Abstr., 98 (1983) 102491).
62 I. Pejkovic-Tadic, M.B. Celap, T.J. Janjic and S.L. Vitorovic, Analyst, 91 (1966) 595.
63 I. Pejkovic-Tadic and S. Vitorovic, Hrana Ishrana, 9 (1968) 29 (Chem. Abstr., 69 (1968) 58436).
64 W. Szczepaniak and W. Walkowski, Ochr. Powietrza, 5 (1971) 20.
65 A. Chiba, Bull. Chem. Soc. Jpn., 49 (1976) 2323.
66 M. Cigula, M. Fugas and F. Valic, Arh. Hig. Rada Toksikol., 23 (1972) 199.
67 M. Hanif, F. Jamshaid and S. Parveen, Anal. Chim. Acta, 110 (1979) 171.
68 M. Hanif, S. Parveen, F. Jamshaid, S. Shahnawaz and Z. Sheikh, J. Chem. Soc. Pak., 2 (1980) 67 (Chem. Abstr., 94 (1981) 71629).
69 M. Hanif, S. Parveen and S. Qureshi, J. Chem. Soc. Pak., 5 (1983) 15 (Chem. Abstr., 99 (1983) 146206).
70 M. Hanif, S. Naeem, B. Chandhry and S. Ali, Pak. J. Sci. Ind. Res., 26 (1983) 210 (Chem. Abstr., 100 (1984) 74073).
71 Zhen-Jie Zang and Chi-Chua Hu, Chung Tsao Yao, 11 (1980) 533 (Chem. Abstr., 94 (1981) 214666).
72 H. Weisz and S. Abe, Mikrochim. Acta, (1970) 1054.
73 H. Weisz and I. Vereno, Anal. Chim. Acta, 91 (1977) 229.
74 H. Weisz and I. Vereno, Proc. Anal. Div. Chem. Soc., 15 (1978) 43.
75 M.L. Danailov, Diploma Thesis, University of Freiburg i.Br., 1980.
76 A.D. Shendrikar and J.P. Lodge, Jr., Atmos. Environ., 9 (1975) 431.
77 H. Weisz and H.J. Kölsch, Mikrochim. Acta, Part I, (1985) 45.
78 World Health Organization Chronicle, March 1970, p. 115.
79 F.C.R. Cattell, W.D. Scott and D. Du Cros, J. Geophys. Res., 82 (1977) 3457.
80 G. Lövblad and K. Anderson, Inst. Vatten. Luftvardsforsk., (1979) B515 (Chem. Abstr., 92 (1980) 51275).
81 A. Chiba, Nippon Kagaku Kaishi (1975) 1193 (Anal. Abstr., 31 (1976) 3H9).
82 W. Szczepaniak and W. Chalcarz, Ochr. Powietrza, 8 (1974) 116 (Chem. Abstr., 88 (1978) 11273).
83 Y.P. Grover, Anal. Chim. Acta, 101 (1978) 225.
84 Xin-Du Geng, Man-Jun Zhou, Xiu-Jun Zhang and Ran Liu, Fenxi Huaxue, 8 (1980) 140 (Chem. Abstr., 93 (1980) 154962).

85 Xin-Du Geng, Dehui Dong and Shujun Bai, Fen Hsi Hua Hsueh, 9 (1981) 428 (Anal. Abstr., 42 (1982) 3H26).
86 Shengru Zhou, Fenxi Huaxue, 11 (1983) 79 (Anal. Abstr., 45 (1983) 5H22).
87 R. Snyder, M. Tonkin, A. McKissick and J. Kitchens, Gov. Rep. Announce (U.S.), 74 (1974) 76 (Chem. Abstr., 82 (1975) 102950).
88 R. Snyder, M. Tonkin and A. McKissick, Gov. Rep. Announce (U.S.), 76 (1976) 86 (Chem. Abstr., 85 (1976) 68045).
89 R. Snyder, M. Tonkin and A. McKissick, Gov. Rep. Announce (U.S.), 76 (1976) 86 (Chem. Abstr., 85 (1976) 68047).
90 R. Snyder, M. Tonkin, A. McKissick and R. Valentine, Gov. Rep. Announce (U.S.), 78 (1978) 108 (Chem. Abstr., 90 (1979) 209824).
91 Xu Huimin, Xiao Ruiying and Qin Suying, Huanjing Kexue, 3 (1982) 57 (Chem. Abstr., 96 (1982) 222921).
92 N. Buckman, E. Kaiser, R.J. Magee and J.O. Hill, Anal. Proc., 19 (1982) 394.
93 W.I. Stephen, Mikrochim. Acta, (1956) 1531.
94 K.N. Johri, S. Saxena and N.K. Gautam, Sep. Sci., 11 (1976) 177.
95 A.K. Dey, A.K. Ghose and D.K. Shukla, Mikrochim. Acta, Part II, (1981) 175.
96 D.K. Shukla, A.K. Ghose and A.K. Dey, Microchem. J., 29 (1984) 391.
97 K.N. Johri and H.C. Mehra, Chromatographia, 4 (1971) 80.
98 H.C. Mehra, Curr. Sci., 46 (1977) 518.
99 K.N. Johri and M. Johri, Chromatographia, 13 (1980) 619.
100 M. Dey, A. Ghose and A. Dey, J. Liq. Chromatogr., 4 (1981) 1577.
101 T. Janjic, M. Celap and L.J. Stojkovic, Bull. Chem. Soc. Belgrade, 27 (1962) 83.
102 T. Janjic, M. Celap, L. Zarubica and L. Radnovic, Bull. Chem. Soc. Belgrade, 28 (1963) 201.
103 A. Chiba, K. Sugano and T. Ogawa, Nippon Kagaku Kaishi, (1981) 1106.
104 A. Chiba and T. Ogawa, Nippon Kagaku Kaishi, 8 (1982) 1422.

Analytica Chimica Acta, 202 (1987) 35–47
Elsevier Science Publishers B.V., Amsterdam — Printed in The Netherlands

ON-LINE ELECTROCHEMICAL DERIVATIZATION COMBINED WITH DIODE-ARRAY DETECTION IN FLOW-INJECTION ANALYSIS

Rapid Determination of Etoposide and Teniposide in Blood Plasma

M.A.J. VAN OPSTAL*, J.S. BLAUW, J.J.M. HOLTHUIS, W.P. VAN BENNEKOM and A. BULT

Faculty of Pharmacy, Department of Pharmaceutical Analysis, Catharijnesingel 60, 3511 GH Utrecht (The Netherlands)

(Received 6th May 1987)

SUMMARY

On-line electrochemical derivatization combined with diode-array u.v./visible detection in flow-injection systems greatly enhances the selectivity. The system is applied for the determination of the antineoplastic agents etoposide (VP 16-213) and teniposide (VM 26) in blood plasma. The optimum oxidation potential, detection wavelength, solvent composition, pH and flow rate are established. Calibration graphs for spiked plasma are linear in the range 1–50 $\mu g\ ml^{-1}$ for both etoposide and teniposide. The detection limit in absolute amount is 6 ng for each compound at a signal-to-noise ratio of 3. The injection frequency can be as high as 40 h^{-1}. The method is validated by quantifying teniposide in plasma of a patient treated with teniposide.

Since its introduction [1,2], flow injection analysis (f.i.a.) has become widely applied in many fields of analysis. Its benefits of speed and flexibility and the possibility for full automation have stimulated its widespread use, especially in routine analysis. In pharmaceutical quality control, its use has grown increasingly during recent years [3,4].

The determination of drugs and metabolites in biological fluids (bioanalysis) is an important area within the general field of pharmaceutical and biomedical analysis. Chromatographic and immunochemical techniques are well established [5] but f.i.a. is rarely applied. To play a more important role in bioanalysis, the selectivity of f.i.a. must be improved. Most reported applications of flow-injection techniques involve simple chemical derivatization reactions and one-channel detection methods, but more selective derivatization reactions, e.g., enzymatic or photochemical conversions, have also been applied. Krull et al. [6] published a survey of these derivatization methods for high-performance liquid chromatography (h.p.l.c.); these post-column reac-

0003-2670/87/$03.50

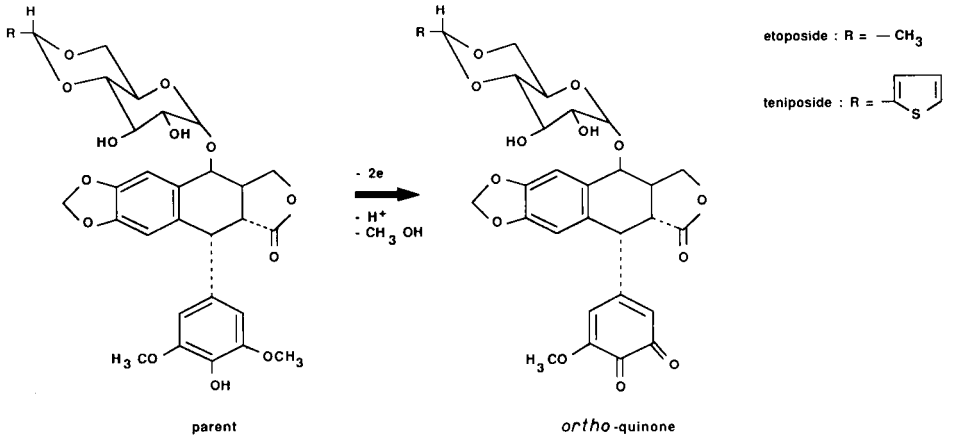

Fig. 1. Structures and oxidation reactions of etoposide and teniposide to their corresponding *o*-quinones.

tion techniques can also be used in f.i.a. Electrochemical conversion followed by electrochemical detection by using dual electrodes in h.p.l.c. has been described by several authors [7–13]. Only a few papers, however, in the field of h.p.l.c. [14,15] or f.i.a. [16] combine electrochemical derivatization with spectrophotometric detection. The flow-injection method reported here uses two advanced techniques, on-line electrochemical derivatization and multichannel ultraviolet/visible detection, to improve selectivity and to increase the amount of information attainable from one injection.

The aim of the present investigations was to develop a flow-injection method suitable for bioanalysis. The antineoplastic agents etoposide (VP 16-213) and teniposide (VM 26) were selected as model compounds. Several methods of analysis for these substances are known [17]. Very recently, an improved radioimmunoassay was described for the measurement of etoposide in plasma [18]. H.p.l.c. methods for the determination of etoposide and teniposide in plasma with either u.v. detection [19] or electrochemical detection [20] were developed earlier in this laboratory by Holthuis and co-workers. The electrochemical behaviour of both compounds has been studied in detail [21,22] and it was shown that they can be converted to their corresponding *o*-quinones by electrochemical oxidation (Fig. 1). The present study describes a flow-injection method for both etoposide and teniposide based on the electrochemical oxidation reaction. The ultraviolet absorbance of the produced *o*-quinones is exploited for detection.

EXPERIMENTAL

Chemicals and solutions

Etoposide (VP 16-213) and teniposide (VM 26) were kindly supplied by Bristol Myers B.V. (Bussum, The Netherlands). 1,2-Dichloroethane was

freshly distilled before use. Other solvents and chemicals were of analytical grade and were used without further purification. All aqueous solutions were prepared with Millipore-Q water. Britton–Robinson buffers were prepared by mixing 100 ml of 0.04 M acetic acid, 100 ml of 0.04 M phosphoric acid and 100 ml of 0.04 M boric acid. The pH (2–8) was adjusted with 1 M sodium hydroxide and water was added to a final volume of 500 ml [23]. Carrier solution and the solvent for standard solutions and plasma extracts were prepared by mixing equal volumes of the buffer and methanol. Stock solutions (1.0 mg ml^{-1}) of etoposide and teniposide were prepared in methanol and stored at 4°C. The stock solutions were diluted to 0.10 mg ml^{-1} with methanol. These methanolic solutions were used for spiking. Standard solutions in the range 0.25–100 μg ml^{-1} were prepared by diluting with appropriate volumes of the buffer/methanol mixture and were used for optimization and calibration.

Plasma sample treatment and calibration

Blank plasma was obtained from healthy volunteers and stored in a freezer at −15°C. Plasma samples were spiked in the range of 1–50 μg ml^{-1} with appropriate quantities of the methanolic solutions of etoposide or teniposide.

After 1.0 ml of spiked plasma had been pipetted into a polypropylene tube (4.0 ml), 2.0 ml of 1,2-dichloroethane was added. The plasma was extracted by vortexing for 2 min. After centrifugation for 2 min at 2500 *g*, 1.0 ml of the organic layer was transferred to a polypropylene tube (1.5 ml) and evaporated under nitrogen at room temperature. The residue was dissolved in 100–200 μl of the carrier solvent and sonicated for 6 min.

Amounts of 25 μl of the plasma extracts were introduced into the carrier stream by fixed-loop injection. The extracts were analyzed under optimized conditions (see Apparatus); peak heights were measured and the calibration was performed.

Apparatus

Flow system . A diagram of the flow-injection manifold is shown in Fig. 2. The carrier solvent was delivered by an h.p.l.c. pump (Waters, model M-45). The sample was injected into the carrier stream by means of an injector (Rheodyne, model 7125) provided with a 25-μl sample loop. A dual-electrode detector (ESA, model 5010, Coulochem) with a potentiostat (ESA, model 5100A) was used as the electrochemical reactor. It consists of a low volume (5 μl) flow-through cell which contains two porous graphite working electrodes. Each electrode is connected to an auxiliary and to a reference electrode up stream and down stream as well. One of the two working electrodes with its two reference/auxiliary electrode systems is marked schematically in Fig. 2. The reference electrodes are constructed of a proprietary material and are typically placed within a millimeter of the working electrode. All subsequently indicated poten-

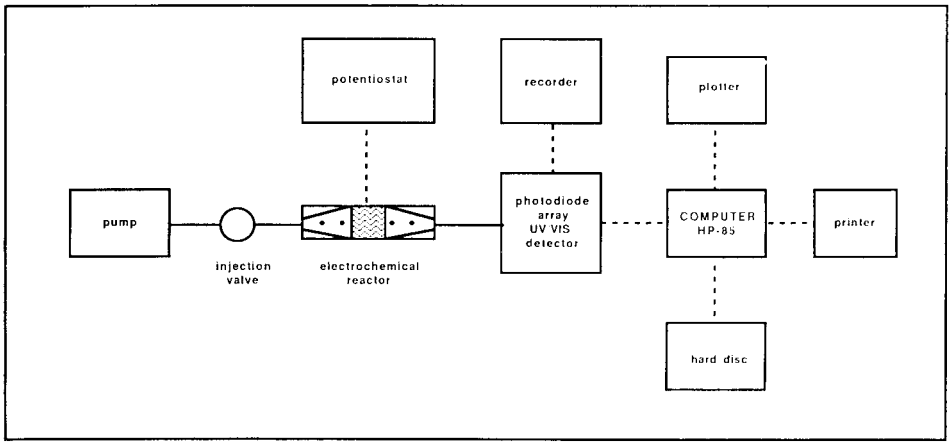

Fig. 2. Diagram of the instrumental setup of the flow-injection system. One working electrode is shown with its two reference/auxiliary electrode systems (• •).

tials in this text are measured vs. this electrode. The potential of this reference electrode vs. H_2/H^+ is about 200 mV higher than the potential of the frequently used Ag/AgCl reference electrode vs. H_2/H^+. The absorbance was measured with a u.v./visible photodiode-array detector (Hewlett-Packard model 1040A) which was connected by a HP interface to the computer (HP model 85). Data were measured on-line and stored on a hard disk (HP model 9133), and evaluated off-line. Hard copies of the spectra and of the flow-injection output were obtained by plotting the stored data on a plotter (HP model 7470A).

Optimized conditions

For the determination of etoposide and teniposide, the oxidation potential was adjusted to +500 mV and +450 mV, respectively. The absorbance of the oxidized product was measured at 365 nm. A buffer (pH 4)/methanol mixture (1+1, v/v) was used as carrier solvent at a flow rate of 0.2 ml min^{-1}. Samples (25 μl) were injected into the carrier stream by using the fixed-loop injection valve.

RESULTS AND DISCUSSION

Electrospectrophotometric properties

Only electro-active substances which provide reaction products with unique absorption properties, are suitable for selective determination by the proposed method. A rapid screening procedure for acquisition of data concerning such electrospectrophotometric activity was applied for etoposide and teniposide. Six repeated injections of standard solutions of etoposide and teniposide (25

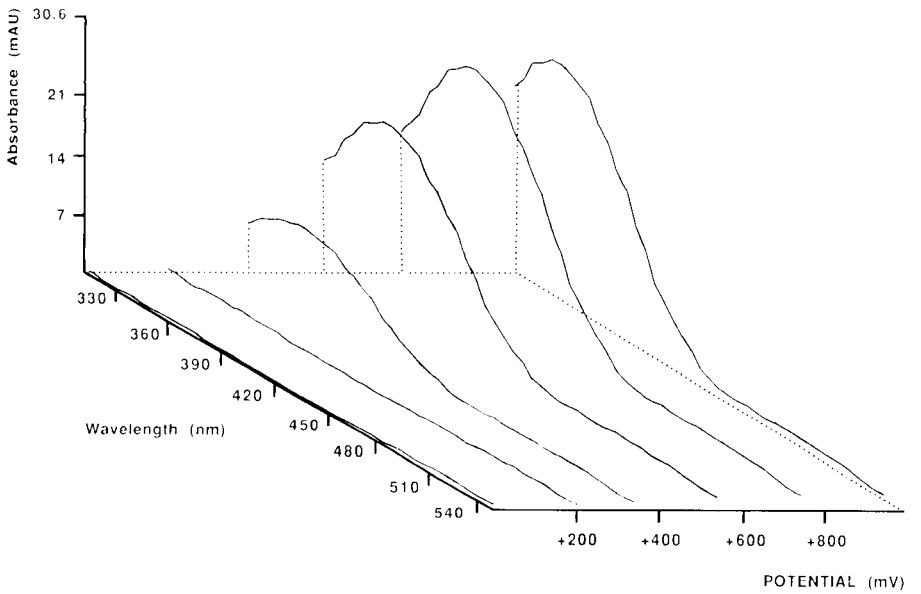

Fig. 3. Three-dimensional plot demonstrating the dependence of the absorbance on the wavelength and the applied potential in the reactor. The spectra were obtained by repeated injections of 25 μl of a standard solution (25 μg ml^{-1}) of teniposide at 0, +200, +400, +600, +800 and +1000 mV. The buffer (pH 4)/methanol mixture was used as carrier solvent at a flow rate of 0.2 ml min^{-1}.

μg ml^{-1}) were tested at reactor potentials of 0, +200, +400, +600, +800 and +1000 mV, respectively. Because the absorbance of substances between 200 and 300 nm is not at all selective, spectra of the oxidized products were recorded on-line from 300 to 550 nm. The spectra of the reaction products of teniposide vs. the applied reactor potentials are presented in Fig. 3. It is clearly shown that the absorbance varies with potential. An absorbance band between 320 and 400 nm appears at 200 mV; its intensity increases and reaches a plateau at +800 mV. The same results were obtained with etoposide. Both compounds were found to be suitable for determination by the proposed flow-injection method. Selection of the optimal detection wavelength (λ_{max}) and the optimal reactor potential is described in the next section. Maximum response and minimum interference were the optimizing criteria. Additionally, the influence of the pH and the flow rate on the response was studied.

Optimization of conditions

Detection wavelength . Standard solutions of etoposide and teniposide (100 μg ml^{-1}) were injected with the potential of the electrochemical reactor switched off. The spectrum of the parent compound in the range 260–550 nm was recorded on-line. Subsequently, the electrochemical reactor was switched

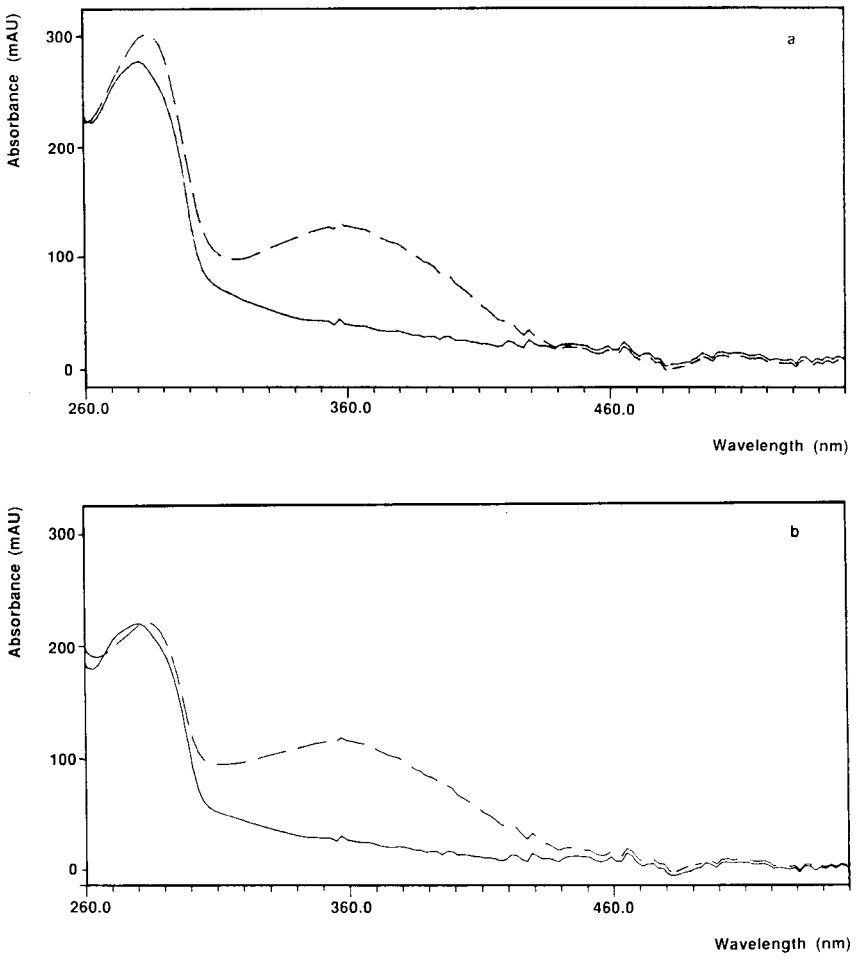

Fig. 4. The spectrum of the oxidized product (---) and the spectrum of the parent compound (——). Reactor potential: (a) +800 mV for etoposide; (b) +800 mV for teniposide. The buffer (pH 4)/methanol mixture was used as carrier stream at a flow rate of 0.2 ml min^{-1}.

on and adjusted to an oxidation potential of +800 mV, and the spectrum of the oxidation product was measured. Figure 4 shows the recorded spectra. The oxidation product shows two absorption bands with maxima at 280 and 365 nm, whereas the parent compound only shows one absorption band with $\lambda_{max} = 280$ nm. The appearance of the 365-nm band caused by the oxidation is obvious and therefore 365 nm was selected as detection wavelength.

Oxidation potential. For selection of the optimal oxidation potential, 25-μl portions of standard solutions (25 μg ml^{-1}) of etoposide or teniposide were injected. The potential was varied from 0 to +900 mV in steps of 50 mV. The

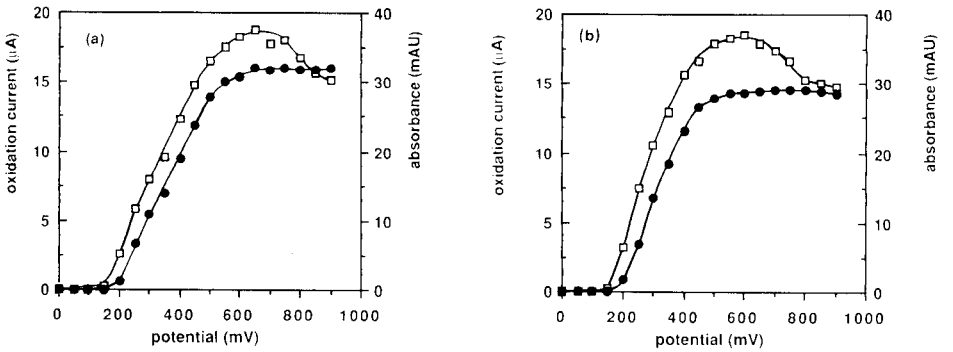

Fig. 5. The hydrodynamic I/E relation (□) and the hydrodynamic I/A relation (●), obtained by repeated injections of 25 μl of standard solution (25 μg ml^{-1}) of (a) etoposide or (b) teniposide. The absorbance was measured at 365 nm. The buffer (pH 4)/methanol mixture was used as the carrier stream at a flow rate of 0.2 ml min^{-1}.

oxidation current and the absorbance at 365 nm were measured. The hydrodynamic current/potential (I/E) relation and the hydrodynamic absorbance/potential (A/E) relation were constructed. These relations are shown in Fig. 5 for both etoposide and teniposide. Only one oxidation wave with a half-wave potential ($E_{1/2}$) of approximately +300 mV was observed for both compounds. This $E_{1/2}$ is shifted about 200 mV to lower potential compared with earlier measurements [21,22], because of the kind of reference electrode used in this study (see Experimental); a Ag/AgCl reference electrode was used in the earlier studies. The shapes of the I/E and A/E curves differ significantly from each other. The oxidation current reaches a maximum at +650 mV and +600 mV for etoposide and teniposide, respectively, and decreases at higher potentials, while the absorbance reaches a plateau. No satisfying explanation can be given for this phenomenon, but probably various oxidation processes will take place, while only one of these results in the production of *o*-quinones. The A/E relations are unambiguous and show the expected plateau. Oxidation potentials of +500 mV and +450 mV for etoposide and teniposide, respectively, were selected.

pH dependence . The influence of the pH on the electrochemical oxidation was studied by varying the carrier solvent. The pH of the buffer was changed from 2 to 8 in steps of 1 pH. With each of these buffers, a carrier solvent was prepared and a standard solution of 25 μg ml^{-1} of teniposide was prepared in each of these solvents. In the same way as described in the previous section, hydrodynamic I/E and A/E relations were measured by repeated injections of the standard solution. In the investigated pH range, all I/E and A/E relations exhibited the same shapes as presented in Fig. 5, i.e., the oxidation current reached a maximum and decreased at further increasing potentials, while the

TABLE 1

The absorbance at 365 nm of teniposide at an oxidation potential of +450 mV and different pH values

pH[a]	2	3	4	5	6	7	8
Absorbance ($\times 10^{-3}$)	19.8	21.3	21.3	22.4	22.3	21.3	21.5

Mean absorbance ± r.s.d. = 0.0214 ± 4%

[a]The pH of the buffer before mixing with methanol (1+1, v/v).

absorbance reached a plateau. No shift of the oxidation half-wave potential of etoposide or teniposide was observed as a function of pH. The height of the absorbance plateau varied only negligibly in the investigated pH range (Table 1). A pH of 4 was chosen for reasons of chemical stability of etoposide and teniposide [17].

Flow-rate dependence . The relationship between the flow rate and the absorbance at 365 nm is shown in Fig. 6 for teniposide. A standard solution (25

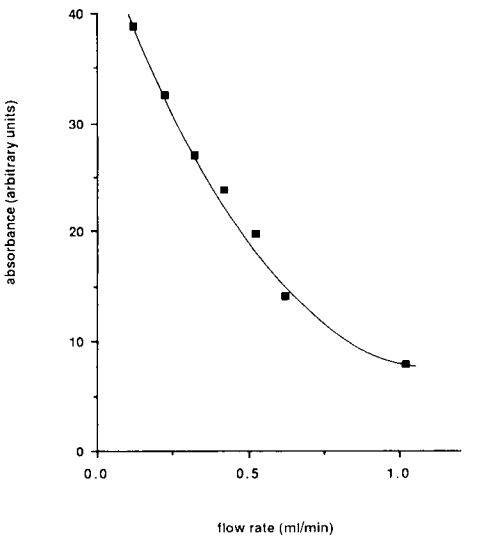

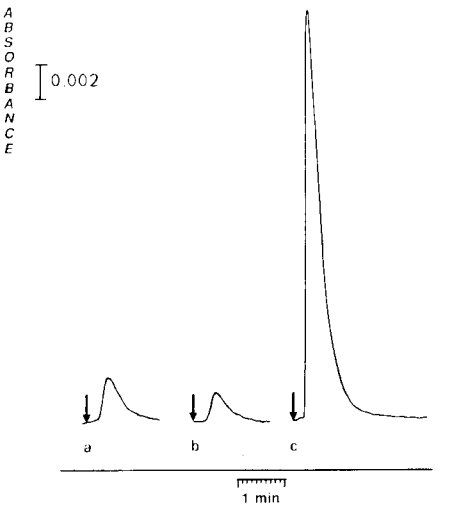

Fig. 6. Relationship between absorbance and flow rate for teniposide. A standard solution (25 μl, 25 μg ml^{-1}) was injected at flow rates of 0.1, 0.2, 0.3, 0.4, 0.5 and 1.0 ml min^{-1}. The oxidation potential was +450 mV and the absorbance was measured at 365 nm. The carrier solution was the buffer (pH 4)/methanol mixture.

Fig. 7. Recorded outputs: (a) blank patient plasma; (b) residue of evaporated 1,2-dichloroethane, dissolved in the carrier solution; (c) the plasma of a patient treated with teniposide. The sample was concentrated by a factor of 5 during the sample treatment. Reactor potential, +450 mV; detection wavelength, 365 nm; carrier solution, buffer (pH 4)/methanol mixture at 0.2 ml min^{-1}.

$\mu g\ ml^{-1}$) was injected at several flow rates between 0.1 and 1.0 ml min^{-1}. The peak height varies with the flow rate because of the varying dispersion of the sample plug, therefore the absorbance was quantified by measuring the peak area. However, because the peak area is inversely proportional to the flow rate in a concentration-sensitive detector, the peak area was multiplied by the corresponding flow rate. It was demonstrated that the absorbance increased as the flow rate decreased (Fig. 6). This indicates that the oxidation current and consequently the intensity of the absorbance depend on the residence time. The manufacturer claims that the electrochemical cell converts coulometrically. From this experiment, however, it was obvious that the studied reaction did not occur coulometrically. The reason for this disagreement may be the limited overall reaction rate caused by mass-transfer resistance. The yield increases at increasing residence time, but the peak broadens because of dispersion, resulting in decreased peak heights. A compromise between these two competing effects had to be found and therefore a flow rate of 0.2 ml min^{-1} was selected.

Calibration, linearity and reproducibility

Calibration graphs for both etoposide and teniposide were measured by injecting standard solutions under the optimized conditions. The calibration graphs were found to be linear in the range 1–50 $\mu g\ ml^{-1}$. The intercepts were not significantly different from zero ($\alpha = 0.05$). The correlation coefficients were 0.995 and 0.997 for etoposide and teniposide, respectively. The relative standard deviation (r.s.d.) of repeated injections ($n = 6$) was 2% at the 5 $\mu g\ ml^{-1}$ level and 1% at the 50 $\mu g\ ml^{-1}$ level. The detection limit in absolute amounts of both compounds was 6 ng (picomolar range) at a signal-to-noise ratio of 3. The linear range and detection limits were measured at the optimum flow rate of 0.2 ml min^{-1}. It was found, however, that both parameters vary with the flow rate: the linear range and detection limit increase as the flow rate increases. These effects can be explained by the dependence of the degree of conversion on the flow rate.

Analysis of plasma

A blank plasma sample from a patient before treatment was analyzed. The result is shown in Fig. 7(a); an absorbance of 0.0024 at 365 nm was measured. This relative high blank response was found to be caused by the undistilled solvent, dichloroethane. When 2 ml of this solvent was evaporated and the residue was dissolved in the carrier solution and injected, an absorbance of 0.0017 was measured (Fig. 7b). After distillation of the dichloroethane, the blank response was strongly reduced. Figure 8 shows the on-line recorded spectrum of blank plasma obtained by extracting the plasma with freshly distilled dichloroethane; the background absorbance at 365 nm was about 0.001.

The recovery of the extraction was measured by analyzing plasma samples

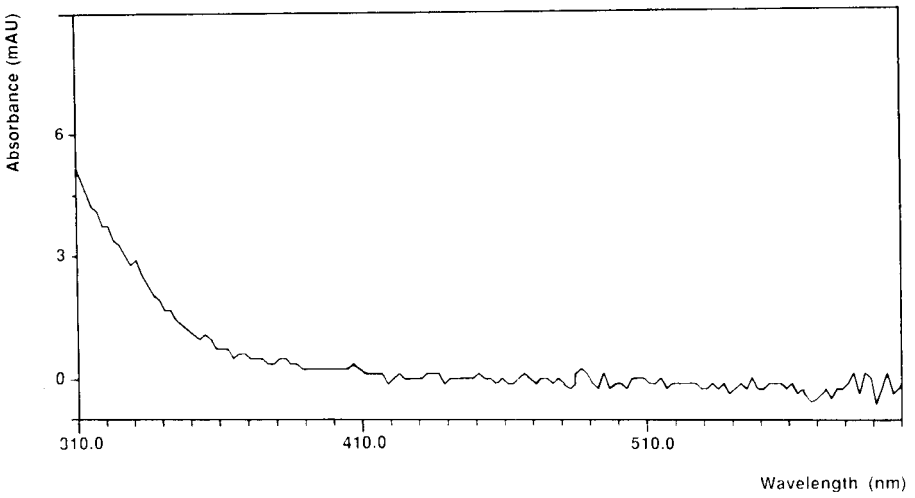

Fig. 8. The spectrum of a blank plasma sample extracted by using freshly distilled 1,2-dichloroethane. The spectrum was recorded on-line. Reactor potential, +450 mV; carrier solution, buffer (pH 4)/methanol mixture at 0.2 ml min^{-1}.

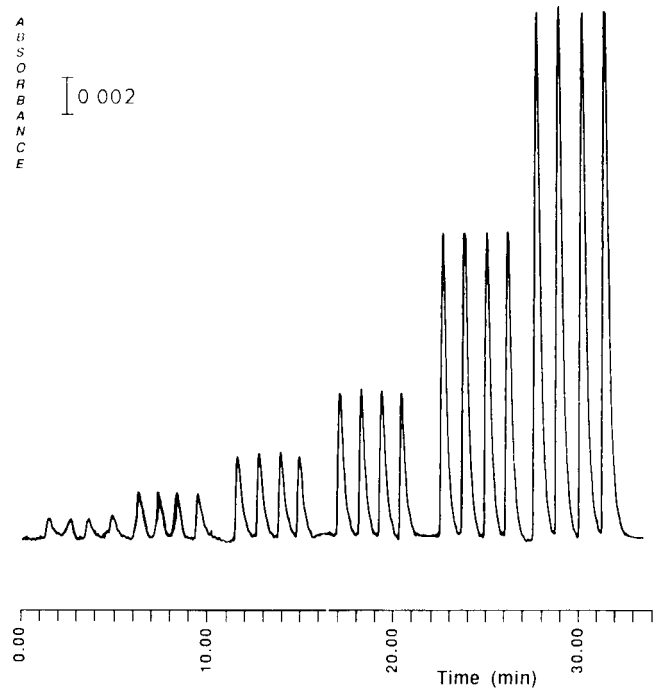

Fig. 9. The recorded output for quadruplicate injections of plasma spiked with teniposide. Peaks: 0, 2, 5, 10, 25 and 50 μg ml^{-1} teniposide. Reactor potential, +450 mV; absorbance measured at 365 nm; carrier solution, buffer (pH 4)/methanol mixture at 0.2 ml min^{-1}.

spiked with standard solutions of etoposide or teniposide to a concentration of 10 μg ml^{-1}. The recovery (with standard deviation) was found to be 95.7 $\pm$ 2.7% (n=6).

For calibration, blank plasma samples were spiked with known amounts of methanolic solutions of etoposide or teniposide. The calibration curves (n=6) were measured under the optimized conditions. The linear range was found to be 1–50 μg ml^{-1} with correlation coefficients of 0.997 and 0.996 for etoposide and teniposide, respectively. The intercepts (with standard deviation) were +0.76 $\pm$ 0.12 and +0.78 $\pm$ 0.11, which were shown to differ significantly from zero (α=0.05). These intercept values can be attributed to the response to a plasma blank at 365 nm. This blank response corresponds approximately to the response for 1 μg ml^{-1}. Based on these results, the determination limit was fixed at 1.0 μg ml^{-1}. Figure 9 shows the output from the flow-injection system for injections of extracts of spiked plasma; the high injection frequency is demonstrated.

Endogenous compounds with a comparable structure to etoposide and teniposide may interfere. Only the catecholamines can cause interfering signals in plasma samples [24]. However, because of their relatively low levels (ng ml^{-1} range), they will not interfere with etoposide or teniposide which are usually at levels in the μg ml^{-1} range [17]. Metabolites can also give rise to false positive responses. The metabolites of etoposide and teniposide, however, differ significantly from their parent compounds with respect to their physicochemical properties [17]. The main metabolites are strongly hydrophilic and are therefore not extractable with dichloroethane [17].

A portion of blank plasma was spiked at a concentration of 2.5 μg ml^{-1} and another at 25 μg ml^{-1}. The spiked plasma was divided into parts of 1.0 ml and stored at −15 °C. A single analysis of each concentration was obtained after 1, 2, 3, 4 and 7 days. The r.s.d. was 6.5% for the concentration of 2.5 μg ml^{-1} and 3.2% for 25 μg ml^{-1}. The system needed daily calibration because the slope of the calibration graph decreased, presumably because of poisoning of the electrode surface by the plasma extracts. When the cell was flushed overnight at a potential of −600 mV with the carrier solution at a flow rate of 0.1 ml min^{-1}, the electrode appeared to be self-regenerating.

Finally, the proposed method of analysis was evaluated by applying it to quantify teniposide in blood plasma from a treated patient. The teniposide concentration was calculated by using a calibration graph prepared with spiked plasma. Figure 7(c) shows the response; the concentration of teniposide in the plasma was found to be 5 μg ml^{-1}.

Conclusions

The proposed flow-injection method proved to be useful for the bioanalysis of both etoposide and teniposide. The combination of electrochemical derivatization and spectrophotometric detection increases the selectivity of the sys-

tem. Only compounds which possess electrochemical activity at the set reactor potential are converted, and selectivity is further improved by a proper choice of detection wavelength. The present investigation has demonstrated that direct injection of plasma extracts is possible, and that no column separation step is necessary. The high injection frequency and rapid system stabilization are further advantages.

The diode-array detector is not strictly necessary for the proposed method, but it proved to be very useful during the development of the method. The on-line availability of the spectra enhances considerably the information obtained from one injection. The spectra are very helpful, e.g., for rapid screening of the electrospectrophotometric properties of the investigated compounds, for choice of the optimum detection wavelength and for confirmation of the identity of the reaction product.

Although the applied reactor could not be used coulometrically, the cell proved to be adaptable as an electrochemical reactor. A disadvantage was the poisoning of the electrode surface by the plasma samples, but regeneration of the cell overnight was simple.

Etoposide and teniposide were suitable model compounds and the method was successfully applied to determine teniposide in plasma from treated patients. Drug levels in treated patients must be monitored; the proposed system provides a rapid and reliable technique for such work, provided that the drug possesses electrospectrophotometric activity and that endogenous compounds or metabolites do not interfere.

Work is in progress on a systematic comparison of the proposed method with the h.p.l.c. method, and on the application of the technique to other therapeutically interesting drugs. Further attempts will be made to increase selectivity and sensitivity, e.g., by applying enzymatic reactions and multichannel detection, with the goal of extending the role of f.i.a. in bioanalysis.

The authors are grateful to ESA (Bedford, MA) and Kipp & Zonen (Delft, The Netherlands) for the loan of the Coulochem.

REFERENCES

1 J. Růžička and E.H. Hansen, Anal. Chim. Acta, 78 (1975) 145.
2 K.K. Stewart, G.R. Beecher and P.E. Hare, Anal. Biochem., 70 (1976) 167.
3 A. Rios, J. Pharm. Biomed. Anal., 3 (1985) 105.
4 J.M. Calatayud, Pharmazie, 41 (1986) 92.
5 R.V. Smith, Trends Anal. Chem., 3 (1984) 178.
6 I.S. Krull, C.M. Selavka, C. Duda and W. Jacobs, J. Liq. Chromatogr., 8 (1985) 2845.
7 Y. Haroon, C.A.W. Schulbert and P.V. Hauschka, J. Chromatogr. Sci., 22 (1984) 89.
8 G.S. Mayer and R.E. Shoup, J. Chromatogr., 255 (1983) 253.

9 R. Eggli and R. Asper, Anal. Chim. Acta, 101 (1978) 253.
10 M. Goto, E. Sakuri and D. Ishi, J. Liq. Chromatogr., 6 (1983) 1907.
11 D.A. Roston and P.T. Kissinger, Anal. Chem., 54 (1982) 429.
12 W.A. MacCrehan and R.A. Durst, Anal. Chem., 53 (1981) 1700.
13 C.E. Lunte and P.T. Kissinger, Anal. Chem., 56 (1984) 658.
14 G.W. Schieffer, Anal. Chem., 53 (1981) 126.
15 J.P. Langenberg, Ph.D. Thesis, University of Leiden, The Netherlands, 1985.
16 K. Kusube, K. Abe, O. Hiroshima, Y. Ishiguro and S. Ishikawa, Chem. Pharm. Bull., 10 (1983) 3589.
17 J.J.M. Holthuis, Ph.D. Thesis, University of Utrecht, The Netherlands, 1985.
18 K. Yamashita, K. Watanabe, H. Takayama, M. Ishibashi and H. Miyazaki, J. Pharm. Biomed. Anal., 5 (1987) 11.
19 J.J.M. Holthuis, W.J. Van Oort and H.M. Pinedo, Anal. Chim. Acta, 130 (1981) 23.
20 J.J.M. Holthuis, F.M.G.M. Römkens, H.M. Pinedo and W.J. Van Oort, J. Pharm. Biomed. Anal., 1 (1983) 83.
21 J.J.M. Holthuis, W.J. Van Oort, F.M.G.M. Römkens, J. Renema and P. Zuman, J. Electroanal. Chem., 184 (1985) 317.
22 J.J.M. Holthuis, D.E.M.M. Vendrig, W.J. Van Oort and P. Zuman, J. Electroanal. Chem., 220 (1987) 101.
23 M. Brezina and P. Zuman, Die Polarographie in der Medizin, Biochemie und Pharmazie, Geest & Portig, Leipzig, 1956, p. 692.
24 W. Sadee and G.C.M. Beelen, Drug Level Monitoring, Wiley, New York, 1980.

Analytica Chimica Acta, 202 (1987) 49–59
Elsevier Science Publishers B.V., Amsterdam — Printed in The Netherlands

THE DETERMINATION OF HYDROGEN CHLORIDE IN AMBIENT AIR WITH DIFFUSION/DENUDER TUBES

N.A. DIMMOCK and G.B. MARSHALL*

Central Electricity Generating Board, Central Electricity Research Laboratories, Kelvin Avenue, Leatherhead, Surrey KT22 7SE (Great Britain)

(Received 9th April 1987)

SUMMARY

A manual method for the determination of hydrogen chloride in air, based on diffusion/denuder tube separation from particulate chloride aerosol is described. When air is drawn through a tube coated with a selective absorbent (sodium fluoride), separation is achieved because gaseous hydrogen chloride diffuses much more rapidly to the tube walls than particulate chloride aerosol, which passes through virtually unabsorbed. After the sampling period (the length of which depends on the concentration of gaseous hydrogen chloride expected), the sorbed hydrogen chloride is washed from the tube and measured with a highly sensitive chloride ion-selective electrode with a mercury(I) chloride membrane. The method is examined theoretically and experimentally. The experimentally derived absorption efficiencies of the diffusion/denuder tubes were > 90% and the standard deviation of the method was 0.023 $\mu g\ m^{-3}$ for hydrogen chloride concentrations of 0.16–0.55 $\mu g\ m^{-3}$. Interference from particulate chloride salts was negligible; this was confirmed by tests with artificially generated aerosol particles from an aerosol generator. The diffusion/denuder tubes have high capacity; levels as high as 330 $\mu g\ m^{-3}$ hydrogen chloride can be sampled for 60 min without affecting performance. A detection limit of $(50/t)\ \mu g\ m^{-3}$ can be achieved, where t is the sampling time (min); e.g., 1 $\mu g\ m^{-3}$ hydrogen chloride can be detected with a sampling period of 50 min.

There are small amounts of chlorine in British coals, ranging from 0.1 to 0.6% by weight, which on combustion are released to the atmosphere mostly as gaseous hydrogen chloride. Hydrogen chloride can also be released to the atmosphere from municipal refuse-incineration plants. In addition, hydrogen chloride is present in the atmosphere from natural sources, arising from the reaction of sea-salt aerosol with atmospheric sulphuric acid and nitric acid [1], or from volcanic emissions [2]. Vierkorn-Rudolph et al. [3] used diffusion-/denuder tubes to collect tropospheric hydrogen chloride, which was later determined in the laboratory by derivatization with 7-oxabicyclo-(4.1.0)-heptane and by gas chromatographic separation and detection. In an earlier paper from this laboratory, Dimmock and Marshall [4] described a manual method for

the determination of free ammonia in ambient air, based on separation from concomitant ammonium salt aerosol with diffusion/denuder tubes.

This paper describes a manual method for the determination of hydrogen chloride in air with diffusion/denuder tube separation from particulate chloride aerosol. The method was tested for its effectiveness in separating hydrogen chloride from sodium chloride aerosol with a laboratory-constructed aerosol generator, and was also applied in fieldwork.

The theory of diffusion/denuder tubes has been fully discussed by Ferm [5] and in our previous paper [4]. In brief, the air sample is drawn through a cylindrical tube coated with a selective absorbent, and the molecules of hydrogen chloride diffuse to the walls according to the mathematical model first developed by Gormley and Kennedy [6]:

$$C/C_0 = 0.819 \exp[-14.6272\, \pi DL/4F] \quad (1)$$

where C is the mean concentration of hydrogen chloride in the air leaving the tube, C_0 is the concentration of hydrogen chloride in the incoming air, D is the diffusion coefficient of hydrogen chloride in air, L is the length of the coated tube, and F is the flow rate of air.

Separation of gaseous hydrogen chloride from particulate chloride salt aerosol is achieved because of the much faster diffusion of gaseous hydrogen chloride to the walls of the tube than particulate chloride; the latter passes through the tube unabsorbed.

EXPERIMENTAL

Equipment and reagents

The glass diffusion/denuder tubes were 95 cm long (i.d. 3 mm). An etch mark was made 15 cm from one end. The remaining 80-cm length was coated with the selective absorbent (see Procedures). Before coating, the tubes were soaked overnight in a chromic acid cleaning solution, washed with deionized/distilled water and stored completely submerged under water. The air-sampling apparatus was the same as described previously [4].

All chemicals were of the highest available purity, i.e., AnalaR, AristaR or Spectrosol grade (BDH). Deionized/distilled water was used unless stated otherwise.

Chloride measurements

Chloride measurements were made on the aqueous extracts from the diffusion/denuder tube using a chloride ion-selective electrode with a mercury(I) chloride membrane (Graphic Controls, now obtainable from Serck Glocon) and a mercury/mercury(I) sulphate reference electrode (EIL). The characteristics and performance of this system have been described [7,8]. In order that measurements could be made in the minimum volume of aqueous solution,

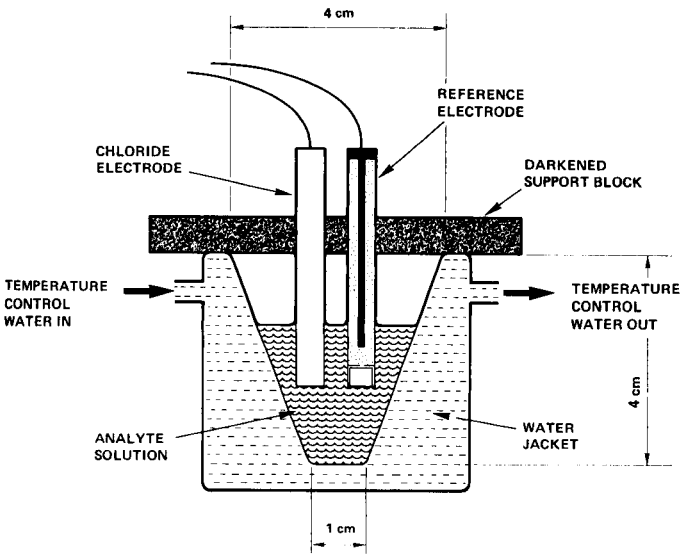

Fig. 1. Apparatus for chloride measurements.

a specially designed vessel was used; this was conical in shape and water-jacketed (Fig. 1). It was painted black to exclude light. Tap water was circulated around the measurement cell via a temperature-controlled circulator (Churchill Instruments) and maintained at $25 \pm 0.5\,^{\circ}C$. The chloride electrode and reference electrode were supported in a block of perspex that was also painted black to exclude light. E.m.f. measurements were taken with a pH meter (Orion 801) and recorded on a chart recorder (Servoscribe 1S).

Procedures

The coating solution was prepared fresh every day by diluting 0.5 ml of a 40 $g\,l^{-1}$ sodium fluoride stock solution to 10 ml with ethanol. Before coating, the diffusion/denuder tube was washed successively with water, methanol and ethanol. The end of the section of tube to be coated (i.e., the 80-cm section) was then placed in the ethanolic sodium fluoride coating solution and, with the aid of a pipette filler, was filled to the etch mark and then allowed to drain back into the sodium fluoride container. This operation was repeated five times. The coated tube was then allowed to drain for 20 s and dried by pumping dry air through it for 20 s with a diaphragm pump. (If the tube was to be stored, both ends were sealed immediately with Parafilm.) The unsealed diffusion-/denuder tube was placed in position in the sampling apparatus and sampling commenced at about $2\,l\,min^{-1}$. At the end of the sampling period, the tube was removed and sealed at both ends with Parafilm, and the volume sampled was recorded.

Immediately before the potentiometric measurements, the Parafilm was re-

moved from both ends with a scalpel, care being taken to avoid contamination. The open end of the coated section of the exposed diffusion/denuder tube was then placed in 5 ml of water contained in a small sample vial, and the water was drawn into the tube to the etch mark and then allowed to drain out. This operation was repeated five times.

To the 5 ml of solution, 0.5 ml of 0.1 mol l^{-1} nitric acid was added and the solution was transferred to the measurement vessel. The e.m.f. of the stirred solution was recorded after equilibrium had been reached. In all cases, the electrode assembly was previously immersed in 0.01 mol l^{-1} nitric acid so that on presentation of a sample (or standard) solution the electrode responded to an increasing chloride concentration. The e.m.f. was compared with a previously prepared calibration curve of chloride standard solutions.

The concentration of hydrogen chloride in air (assuming 100% efficiency of absorption) is given by $C_0 = a \times 5/V$, where C_0 is the concentration of hydrogen chloride in air ($\mu g\ m^{-3}$), a is the concentration of hydrogen chloride in the 5 ml of washing solution ($\mu g\ l^{-1}$), and V is the volume of air sampled in litres.

RESULTS

Method development

The method was developed and tested by sampling laboratory air. Because levels of hydrogen chloride were so low in the normal laboratory atmosphere, they were artificially increased by passing air from a peristaltic pump at approximately 4 ml min^{-1} through a solution of 20% (v/v) hydrochloric acid in a Dreschsel bottle fitted with a coarse frit.

The appropriate tube length and flow rate were selected by reference to Eqn. 1. For a 99% absorption efficiency (i.e., $C/C_0 = 0.01$), the required length of coated tube can be calculated (given a flow rate of 2 l min^{-1} (3.33×10^{-5} m^3 s^{-1}) and a diffusion coefficient of 1.6×10^{-5} m^2 s^{-1} for hydrogen chloride in air [9]) to be 79 cm. Except where stated, diffusion tubes were 95 cm in total length, with a coated section of 80 cm. A flow rate of 2 l min^{-1} was used throughout the work.

Absorption efficiencies for a single tube were calculated by connecting two tubes in series and testing each separately after exposure to the sample air. Absorption efficiency was then calculated as $100\ C_1/(C_1 + C_2)$, where C_1 is the first tube concentration, and C_2 the second tube concentration.

Diffusion/denuder tube coating. Diffusion/denuder tube coatings of sodium fluoride as used by Niessner and Klockow [10] for other acid gases, were used for all this work.

To confirm that no hydrogen chloride was absorbed in the uncoated 15-cm length of tube used to ensure laminar flow, measurements were made by sam-

TABLE 1

Effect of particle size on particulate deposition on diffusion/denuder tube wall by Brownian diffusion

Particle size (μm)	Diffusion coefficient ($m^2\ s^{-1}$)	Percentage absorption (n/n_0)
0.01	1.35×10^{-8}	2.6
0.1	2.21×10^{-10}	0.17
1.0	1.27×10^{-11}	2.49×10^{-2}

pling room air through two uncoated 90-cm diffusion/denuder tubes connected in series for an extended period of 18 h. No significant amount of hydrogen chloride was collected in the entire length of these uncoated tubes, confirming that no absorption of hydrogen chloride was likely to occur in the uncoated 15-cm section of tube.

Hydrogen chloride measurements in the presence of sodium chloride aerosol particles. Particulate sodium chloride and other chloride aerosols can diffuse to the diffusion/denuder tube walls by Brownian diffusion and the theoretical absorption efficiency is given by the expression quoted by Fuchs [11]: $n/n_0=2.56\ [\pi DL/F]^{2/3}$, where n is the number of particles per unit volume of air deposited on the tube wall, n_0 is the number of particles per unit volume of air entering the tube, and D is the diffusion coefficient of the particles. Table 1 shows absorption efficiencies for particles of various sizes. Diffusion coefficients were taken from Fuchs [11].

Most airborne particles tend to be in the range 0.01–4 μm and so it can be concluded that there should be insignificant deposition of these particles with the experimental conditions used here. To confirm this experimentally, tests were run with artificially generated aerosol particles from a laboratory-constructed aerosol generator based on an ultrasonic nebulizer. Details of the aerosol generator were given earlier [4]. All apparatus was thoroughly cleaned with water before the experiments were begun. Air was drawn and not pumped through the ultrasonic nebulizer and generator tube to avoid contamination from the components of the pump. A solution ($6\ \mu g\ ml^{-1}$) of sodium chloride was pumped to the ultrasonic nebulizer at 0.05 ml min^{-1} and air was drawn through the nebulizer at 15–20 l min^{-1}. Coated diffusion/denuder tubes were set up in the region of the air intake point and the aerosol generator outlet sampling point, and hydrogen chloride in air was compared with hydrogen chloride measured in the presence of sodium chloride particles. The concentration of sodium chloride particles in the air was calculated from the solution uptake rate of the nebulizer and the volume of air into which it was dispersed. The sodium chloride particulate concentration was greatly in excess of that expected to be found in ambient air. Results are given in Table 2 for tests on

TABLE 2

Determination of hydrogen chloride in the presence of sodium chloride particles

HCl found ($\mu g\ m^{-3}$)		Particulate concentration ($\mu g\ m^{-3}$ NaCl)	Absorption of particles (%)
Without particles	With particles		
0.14	0.17	16.0	0.3
0.44	0.94	15.0	5.3
0.28	0.49	15.0	2.3
0.66	0.92	17.2	2.4
0.29	0.51	16.7	2.1

five separate occasions; it can be seen that the presence of particles has only a small effect on the determination of hydrogen chloride gas in air.

Storage of diffusion/denuder tubes. Provided that the ends of the coated diffusion/denuder tubes were sealed with Parafilm immediately after preparation, the tubes could be stored for several days, with no contamination or deterioration in their adsorption capacity on first use.

To ascertain whether exposed tubes could be left before taking potentiometric measurements, room air was sampled through two separate tubes in parallel. One tube was processed immediately and the other tube was left for a period of time before the chloride measurement. Results are given in Table 3. It would appear from these results that exposed tubes can be left for at least six days without deterioration, but to comply with analytical good practice it is recommended that tube preparation be done immediately before exposure and that potentiometric measurements be made immediately afterwards.

TABLE 3

Effect of storage on exposed diffusion/denuder tubes

Hydrogen chloride found after storage period (days) ($\mu g\ m^{-3}$)					
None	One	Two	Three	Four	Six
0.53	0.55				
0.28		0.30			
0.30		0.29			
0.26			0.28		
0.12				0.11	
0.12				0.12	
0.09					0.11
0.07					0.09

TABLE 4

Absorption capacity of diffusion/denuder tubes

Exposure time (min)	Volume (l)	Hydrogen chloride ($\mu g\ m^{-3}$)		Absorption efficiency (%)
		Second tube	First tube	
20	45	2.8	330.6	99.2
60	124.7	6.4	334.3	98.1
140	274.8	86.0	222.5	72.1

Capacity of diffusion/denuder tubes. Experiments were conducted to ascertain the maximum amount of hydrogen chloride that could be absorbed in the diffusion/denuder tube. Relatively high concentrations of hydrogen chloride were produced by diluting a 0.04% hydrogen chloride mixture (BOC Special Gases) into a mixing chamber.

Coated diffusion/denuder tubes were connected in series and exposed to a high level of hydrogen chloride for varying periods of time. The results (Table 4) show that a hydrogen chloride concentration of 334.3 $\mu g\ m^{-3}$ can be sampled for 60 min without the absorption efficiency being affected. If sampling is continued for 140 min, the first tube becomes saturated as evidenced by the breakthrough of hydrogen chloride from the first to the second tube. The result for the 60-min exposure indicated that at least 42 μg of hydrogen chloride can be absorbed on the first tube (i.e., the quantity of hydrogen chloride absorbed if 124.7 l of 334.3 $\mu g\ m^{-3}$ hydrogen chloride is sampled).

Effect of large excesses of acid gases. As well as ambient air, it was envisaged that hydrogen chloride measurements would be made in power station plumes at ground level where concentrations of other acid gases, i.e., sulphur dioxide and nitrogen dioxide, could be relatively high. Experiments were therefore conducted to see whether the presence of excess of acid gases could saturate or poison the coated diffusion/denuder tubes.

To test the effect of sulphur dioxide, coated diffusion/denuder tubes were prepared in duplicate and exposed to 100 $\mu g\ m^{-3}$ sulphur dioxide from a permeation tube calibrator (Vici Metronics) for 2 h (an exposure time much greater than that expected in the field). These tubes, together with two duplicate tubes that had not been exposed to sulphur dioxide, were then used for sampling hydrogen chloride from the mixing chamber. The results (Table 5) show that large excesses of sulphur dioxide have no significant effect on hydrogen chloride measurements.

To test the effect of nitrogen dioxide, duplicate coated diffusion/denuder tubes were exposed to 270 $\mu g\ m^{-3}$ nitrogen dioxide from a cylinder (BOC Special Gases) for 30 min (again a loading much greater than that expected in the

TABLE 5

Effect of excess of sulphur dioxide or nitrogen dioxide on hydrogen chloride measurements

Tube tested	HCl found ($\mu g\ m^{-3}$)	Tube tested	HCl found ($\mu g\ m^{-3}$)
Tube 1+SO_2	30.1	Tube 1+NO_2	19.9
Tube 2+SO_2	30.9	Tube 2+NO_2	14.0
Tube 3 (SO_2 absent)	31.7	Tube 3 (NO_2 absent)	13.7
Tube 4 (SO_2 absent)	30.2	Tube 4 (NO_2 absent)	15.1

field). These tubes were tested in the same way as for exposure to sulphur dioxide. The results (Table 5) show that, although reproducibility is not as good as before, large amounts of nitrogen dioxide did not prevent the absorption of hydrogen chloride.

Performance characteristics

The performance characteristics of the analytical method were assessed. In all cases, the method as described in the recommended procedure was followed.

Calibration line. A typical calibration line for the chloride electrode is shown in Fig. 2. A fresh calibration line should be prepared for each batch of determinations. It is important that the calibration line is well defined below 100 $\mu g\ l^{-1}$ by the inclusion of as many standards as possible. Between batches, the electrode was left to stand in 0.01 mol l^{-1} nitric acid.

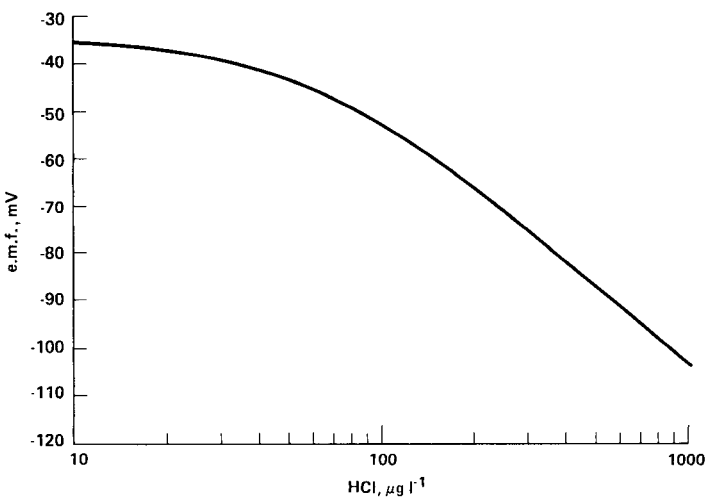

Fig. 2. Chloride electrode calibration line.

TABLE 6

Absorption efficiency of hydrogen chloride diffusion/denuder tubes

No.	Volume sampled (l)	HCl found ($\mu g\ m^{-3}$)		Absorption efficiency (%)
		Upper tube	Lower tube	
1	2,388	0.03	0.16	84.2
2	2,550	0.03	0.18	85.7
3	8,362	0.01	0.21	95.5
4	5,328	0.01	0.23	95.8
5	10 937	0.019	0.242	92.7
6	12 445	0.023	0.241	91.3
7	3,774	0.059	0.373	86.3
8	6,261	0.038	0.333	89.8
9	8,138	0.018	0.306	94.4
10	14 732	0.025	0.284	91.9

Diffusion/denuder tube absorption efficiency and blanks. The percentage of hydrogen chloride absorbed on the coated diffusion/denuder tube was measured by connecting two tubes in series and processing each tube separately. Different volumes of room air were analysed on separate occasions; the results are given in Table 6. Absorption efficiencies ranged from 84.2 to 95.8%. This scatter is probably due to the difficulty in measuring accurately the low levels of hydrogen chloride in the upper tube when the smaller volumes of air were sampled, i.e., a relatively large error was introduced because the chloride levels in the upper tube were at or near the blank level. When larger volumes of air were used (Tests 5, 6 and 10), the % absorption efficiency was far more consistent, ranging from 91.9 to 92.7%. Even for these results, it is difficult to measure accurately the hydrogen chloride absorbed in the upper tube. It is interesting to note that, when larger concentrations of hydrogen chloride are measured in the upper tube, the absorption efficiency is measured more accurately as 98–99% (Table 4).

It is important that blank tubes are included in any series of measurements, by coating, sealing and measuring in exactly the same way as for the sample tubes. The levels of hydrogen chloride found in the 5 ml of deionized/distilled water used for dissolution of the coating should be $\ll 10\ \mu g\ l^{-1}$. If high blanks ($> 10\ \mu g\ l^{-1}$ in 5 ml) are encountered, contamination is the likely source.

Precision. The precision of the method was estimated by sampling room air through two tubes in parallel on eight separate occasions. The hydrogen chloride concentration of the room-air samples ranged from 0.16 to 0.55 $\mu g\ m^{-3}$ and the standard deviation was estimated to be 0.027 $\mu g\ m^{-3}$.

TABLE 7

Hydrogen chloride concentrations in the air around Didcot

Distance from stack (km)	Site (Ordnance Survey Reference)	HCl conc. ($\mu g\ m^{-3}$)		SO_2 conc. ($\mu g\ m^{-3}$)
11.7	1. SU 405871 (3.6.85)	5.64	5.71	233
11.7	2. SU 409864 (3.6.85)	3.71	3.77	149
-	3. SU 503919 (3.6.85)	0.76	0.46	-
4.1	4. SU 502955 (1.5.85)	0.14	0.20	-

Measurements of hydrogen chloride in air. Measurements of hydrogen chloride in air at ground level were made in the field around Didcot Power Station. The sampling apparatus was mounted on a frame and powered from the CERL Mobile Air Pollution Sampling Unit. In the first series of measurements, sampling was done in duplicate for 2 h at site 1 and for 80 min at site 2, both sites being judged from concurrent measurements of sulphur dioxide to be in the plume. Duplicate clean-air samples (remote from the plume) were taken on the same day as well as on a previous occasion. Duplicate blank tubes were prepared and processed at the same time as the samples and gave negligible hydrogen chloride concentrations. Results are given in Table 7.

DISCUSSION

The analytical technique described, where gaseous hydrogen chloride is separated from particulate chloride aerosol in a diffusion/denuder tube with sodium fluoride coating, allows gaseous hydrogen chloride to be determined in the atmosphere at very low levels. Formal tests were not conducted to determine the limit of detection of the chloride electrode, but previous information [7] suggested that 20 $\mu g\ l^{-1}$ is a realistic lower level. Consequently, for the determination of very low levels of hydrogen chloride ($<1\ \mu g\ m^{-3}$) it is recommended that air is sampled for at least 4 h. If higher concentrations of hydrogen chloride are expected, the sampling time can be reduced accordingly. More sensitive methods, such as ion chromatography, could permit shorter sampling times, but contamination is an ever-present difficulty.

If 20 $\mu g\ l^{-1}$ is taken as the detection limit for chloride with the ion-selective electrode, then the detection limit, C_d, for the concentration of hydrogen chloride in air is given by $C_d\ (\mu g\ m^{-3}) = 20 \times 5/V$, where V is the total volume of air drawn through the tube, in litres. The detection limit of the method is defined as $50/t\ \mu g\ m^{-3}$ hydrogen chloride, where t is the sampling time (min). Thus 1 $\mu g\ m^{-3}$ hydrogen chloride can be detected with a sampling time of 50 min.

It is very important that the analysis is kept free of contamination, because errors can be quite large, especially for low hydrogen chloride concentrations and short sampling times. In view of this, if results of the highest precision are required, sampling should be continued for as long as possible. The diffusion-/denuder tubes have a high capacity, and levels as high as 330 $\mu g\ m^{-3}$ hydrogen chloride can be sampled for 60 min without affecting their performance.

The method was examined both theoretically and experimentally. The experimentally derived absorption efficiencies of the diffusion/denuder tubes were $>90\%$ and the standard deviation of the method was calculated at 0.023 $\mu g\ m^{-3}$ for hydrogen chloride concentrations in the range 0.16–0.55 $\mu g\ m^{-3}$. Sulphur dioxide and nitrogen dioxide at the levels normally encountered did not affect the absorption efficiency of the diffusion/denuder tubes. The theoretical expression of Fuchs [11] indicates that interference from particulate chloride salts should be negligible; this was confirmed experimentally by running tests with artificially generated aerosol particles (similar to those expected to be present in the atmosphere), from a laboratory-constructed aerosol generator.

The work was done at the Central Electricity Research Laboratories of the Technology Planning and Research Division. This paper is published with the permission of the Central Electricity Generating Board.

REFERENCES

1 L. Horvath, E. Meszaros, E. Antal and A. Simon, Tellus, 33 (1981) 382.
2 R.D. Cadle, Rev. Geophys. Space Phys., 18 (1980) 746.
3 B. Vierkorn-Rudolph, K. Bachmann, B. Schwarz and F.X. Meixner, J. Atmos. Chem., 2 (1984) 47.
4 N.A. Dimmock and G.B. Marshall, Anal. Chim. Acta, 185 (1986) 159.
5 M. Ferm, Atmos. Environ., 13 (1979) 1385.
6 P.G. Gormley and M. Kennedy, Proc. R. Ir. Acad., Sect. A, 52 (1949) 163.
7 G.B. Marshall and D. Midgley, Analyst, 103 (1978) 438.
8 G.B. Marshall and D. Midgley, Analyst, 104 (1979) 55.
9 G.M. Hidy and J.R. Brock, The Dynamics of Aerocolloidal Systems, Pergamon, Oxford, 1970.
10 R. Niessner and D. Klockow, J. Aerosol Sci., 13 (1982) 175.
11 N.A. Fuchs, The Mechanics of Aerosols, Pergamon, Oxford, 1964, p. 205.

Analytica Chimica Acta, 202 (1987) 61–73
Elsevier Science Publishers B.V., Amsterdam — Printed in The Netherlands

A PYROHYDROLYTIC METHOD FOR THE DETERMINATION OF LOW FLUORINE CONCENTRATIONS IN COAL AND MINERALS

K.J. DOOLAN

The Broken Hill Proprietary Company Limited, Central Research Laboratories, PO Box 188, Wallsend, New South Wales 2287 (Australia)

(Received 24th April 1987)

SUMMARY

Techniques are described for the pyrohydrolysis of a range of sample materials in a silica tube furnace. Samples are mixed with a catalyst and combusted at 1200°C in a stream of oxygen and steam, and the liberated fluorine is absorbed in solutions appropriate to either ion-selective electrode or ion-chromatographic measurement. Catalyst composition, furnace temperature, and gas flow rates are particular variables discussed with respect to recovery of fluorine at concentrations up to about 5% (w/w). Recovery and precision are favourable compared with those obtained by the alternative peroxide fusion and oxygen bomb combustion methods for coal analyses. Relative standard deviation is less than 0.05 for most samples. Results agree with certified values of available reference materials including ores and rocks, while new data are provided for several non-certified reference materials.

Fluorine emissions to the atmosphere provide the greatest potential individual source of environmental contamination by trace elements released from the utilization of coals [1]. Fluorine has been classified as an "element of moderate concern" to environmental quality and health [2], with the most severe impact being on plant life. The expected requirement for accurate and cost-efficient analyses for fluorine, with respect to commercial coal-marketing purposes, prompted a detailed investigation into the practical merits and quality of results obtained from different methods of sample processing.

Fluoride ion-selective electrodes or, more recently, ion-chromatographic techniques have been applied extensively to the determination of fluoride ions in solution. The problem remained, however, of determining the most effective means of sample preparation. Direct ignition of coal with sodium carbonate has been regarded as suitable [3–7], though more conveniently a high-pressure oxygen bomb combustion of the coal has been used [3,8–10]. Pyrohydrolytic techniques have also been applied with combustion tube [11,12] and induction [13] furnaces for the liberation of fluorine. Induction furnaces were

0003-2670/87/$03.50

available in the author's laboratories, but it was considered that the coal and mineral exploration areas generally would have little access to such equipment, and investigations were conducted only with conventional tube furnaces of the type used in most coal testing laboratories.

The work described below was, therefore, directed towards the development of an accurate, rapid, and straightforward procedure which could be integrated readily into any comprehensive facility for coal analysis. The pyrohydrolytic fluorine procedure has been in routine use in the author's laboratory for approximately four years [14]. Although initially devised for coal analysis, it was found also to be appropriate for fluorine determinations up to percentage concentrations in ash, minerals, and ores.

METHOD DEVELOPMENT

Four methods of coal sample pretreatment were considered to warrant investigation in order to establish comparative data with respect to analytical accuracy, precision, speed, and ease of operation. It is noteworthy that there are no commercially available coal reference materials for which a fluorine value is certified. A set of coal samples was selected, therefore, to cover a range of coal types and ash values. With sample types other than coal, there is a wide choice of reference materials, and these were used extensively to support the method development and proving phases.

Methods for pretreatment

Alkali fusion. Initial studies showed that most bituminous coal samples were incompletely oxidized during sodium carbonate fusion as described earlier [4–7] despite a preliminary 475 °C "soak" prior to fusion at approximately 1000 °C. Also, some fluorine may have been lost during this period. Sodium peroxide is more alkaline and a more powerful oxidizing flux than the sodium carbonate. Since it has been successfully applied to the determination of fluorine in inorganic materials, extension of the method to coal samples was straightforward. Samples (200 mg) mixed with 1 g of sodium peroxide in a platinum crucible were warmed overnight at 150 °C; a further 0.5 g of the peroxide was added and the mixture fused at 450 °C. Fluorine was extracted into hydrochloric acid and the solution diluted for measurement. A disadvantage of this method is that sub-bituminous coals were violently reactive, and sodium carbonate was then the more suitable flux.

Oxygen bomb combustion. A simple and convenient means of sample decomposition is available through combustion under a high pressure of oxygen in a bomb, an approach which has become accepted internationally through status as an ASTM standard test method [9]. The procedure investigated in the present work was identical in principle to this method.

Mineral matter fusion. The preparation of a mineral matter residue from the

TABLE 1

Effect of catalyst mixture on fluorine recovery

Catalyst[a]	Fluoride content found SRM 91[b] (%)	SC143[c] ($\mu g\ g^{-1}$)
None	4.63	78
SiO_2	4.85	81
WO_3	5.06	80
SiO_2/WO_3 (7+1)	5.25	88
$SiO_2/WO_3/V_2O_5$ (8+1+1)	5.65	103

[a]250 mg of catalyst was added in each case to 5 mg of NBS 91 or 250 mg of SC143, with 150 ml min^{-1} oxygen flow rate. [b]Certified value, 5.72%. [c]Cf. Table 2.

oxidation of coal in a low-temperature radiofrequency plasma asher, with subsequent fusion as described above, had potential advantages with respect to higher solution concentration, improved precision and speed of measurement, and short total analysis time once the mineral matter had been prepared. However, it was found in related work that some fluorine was lost during the low-temperature preparation of mineral matter [15] (possibly as a result of a pyrohydrolytic-type mechanism), and this approach proved unsuitable and was discontinued.

Pyrohydrolysis. Most published applications of high-temperature hydrolysis have dealt with a variety of inorganic materials, with relatively few references considering materials of organic or biological origin [11–13,16,17]. Pyrohydrolysis provides an elegant, simple procedure for the separation of fluorine from a host matrix, but attention to several experimental parameters was found to be critical to the success of the method.

The maximum temperature of the furnace used in early development studies was 1100°C, which was also the temperature specified by van Leuven et al. [11]. Variables investigated were the flow rate of oxygen, volume ratio of oxygen to steam, and catalyst mixture. The former two parameters were varied over wide ranges in order to establish the most efficient conditions for fluorine liberation; the conditions given below in the procedure were found to provide quantitative recovery most rapidly. Conditions could, however, be varied within broad limits without significant deterioration of results. Most critical was the effect of a variation in catalyst mixture, as shown in Table 1.

The catalyst mixtures used in the literature have been somewhat varied in content and effectiveness. They have consisted of acidic oxides in order to react with fluoride minerals in the sample via a heterogeneous exchange mechanism, with subsequent release of volatile fluoride species, in particular hydrofluoric acid [18,19]. Variation of the composition of the catalyst was not investigated exhaustively in this work, but the mixture of oxides initially used included the

TABLE 2

Comparison of results from methods of fluorine determination

Coal	F content ($\mu g\ g^{-1}$, dry-basis)		
	Peroxide fusion	Oxygen bomb	Pyrohydrolysis
SC143	110	75	116
SC152	158	123	147
SC154	140	98	158
SC156	255	250	277
SC158	34	35	32
T333	< 10	3	4
NBS 1632a	171	128	176

two oxides most commonly cited in the literature, silicon and tungsten, as well as that of vanadium, which with a melting point of 700°C has been found successful at lower pyrolysis temperatures [20].

Although quantitative recovery was achieved with NBS SRM 91 under the initially developed pyrohydrolysis conditions, an interlaboratory comparison of results for the coal sample set used in method development (see Table 2) with results returned by use of the NSW Department of Mineral Resources induction-furnace technique [13], indicated that incomplete recovery was being achieved with SC143. Only when the flow rate of oxygen was substantially increased was complete recovery evident. With an oxygen flow rate of 750 ml min^{-1}, the flow rate of steam was computed to be approximately 4,000 ml min^{-1}. Conversely, this higher oxygen flow yielded low recoveries for high fluorine samples, though this only became significant at fluorine concentrations greater than about 5% (w/w). A fluorine concentration of about 1% (w/w) was established to mark the preference for the higher or lower flow rate. With an oxygen flow rate of 150 ml min^{-1}, the steam flow was about 2500 ml min^{-1}.

EXPERIMENTAL

Pyrohydrolysis apparatus and reagents

The assembly used for pyrohydrolysis is illustrated in Fig. 1, and the major items of special apparatus are described below. A feature of the procedure was the use of gravimetric techniques for the addition of standard solution (ISE measurement) and the dilution of sample pyrohydrolysate. This is facilitated by the availability of an electronic top-loading balance having precision of 1 mg and a capacity exceeding 150 g. Volumetric methods can be implemented at the expense of simplicity and speed.

Combustion tube furnace. The pyrohydrolysis technique required a high-temperature combustion tube furnace and accessories similar to that required

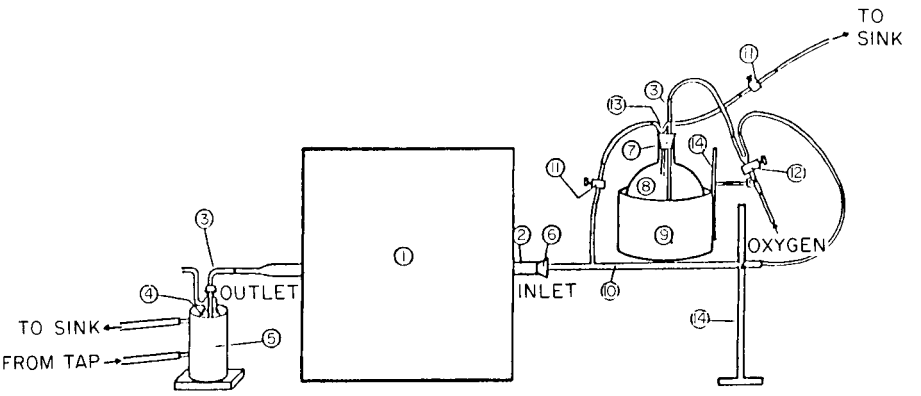

Fig. 1. Pyrohydrolysis apparatus for fluoride. (1) Furnace; (2) silica combustion tube; (3) gas distribution tubes; (4) absorption vessel; (5) water jacket; (6) silicone rubber stopper (or preferably a spring-held silica ground joint); (7) rubber stopper; (8) 2-l flask; (9) heating mantle; (10) borosilicate glass T-tube with silica push-rod; (11) stopcock; (12) three-way stopcock; (13) glass Y-piece; (14) retort stand and clamp.

in coal-testing laboratories for the conventional determination of carbon, hydrogen, sulphur and chlorine according to standard methods [21]. High-alumina porcelain or mullite combustion tubes were found to be unsuitable, owing to unfavourable thermal stress properties for the input of steam during the hydrolysis phase. It was essential, therefore, to use silica combustion tubes. These are preferably tapered at the outlet end to obviate the need for closure via rubber stoppers. Even high-temperature silicone stoppers degenerate rapidly with the passage of large volumes of superheated steam. A short length of quartz wool is inserted into the tube towards the outlet end to act as a filter (any dust particles carried over from the sample can interfere with an ion-chromatographic measurement). An iron-tipped silica rod is operated magnetically to push samples, in porcelain boats, into the hot zone of the furnace.

Gas absorption vessel. The gaseous combustion products and excess of steam were passed through a Dreschel gas-washing bottle (Quickfit MF/29/3/125) fitted with an adjustable head (MF27/3/13) and a high-porosity gas-distribution tube (3830/00, flame-bent at right angles 50–60 mm from the top, and preferably with several 1-mm holes drilled radially around the frit to reduce pressure buildup inside the furnace). The absorption vessel construction is not critical; any assemblage providing effective gas absorption would be adequate. Because the vessel becomes quite hot from the steam, a water jacket must be used to assist condensation of the bulk of the steam; with a large enough volume this jacket would not need to be a continuous flow system as illustrated in Fig. 1.

Steam generator. A 2-l round-bottomed flask, with a heating mantle, was stoppered, with a gas distribution tube for the inlet of oxygen and a glass Y-

piece for directing the outlet for excess of steam to drainage, or for carrying the steam by oxygen to the furnace.

Fluoride measurement. Two methods were developed for the determination of fluorine in the pyrohydrolysate. In the potentiometric method, a fluoride ion-selective electrode (ISE) was used with a pH/mV meter reading to 0.1 mV and a saturated calomel reference electrode. For ion chromatography, a Dionex 2010i ion chromatograph with an HPIC-AS4A anion-exchange column, conductivity detector (0–30 μS range) and anion fiber suppressor module was used with an eluent containing 0.23 g l^{-1} Na_2CO_3 and 0.063 g l^{-1} $NaHCO_3$.

Reagents. Analytical reagent-grade chemicals and distilled/deionized water should be used for all requirements. The catalyst was ground to a fine powder and ignited (800°C for 1 h); either silicon dioxide/tungsten trioxide/vanadium pentoxide (8+1+1), or silicon dioxide was used (see text). The absorption solution for the ISE method was 0.025 M sodium hydroxide; for ion chromatography, 0.56 g l^{-1} Na_2CO_3/0.15 g l^{-1} $NaHCO_3$ was used for suppressed systems (non-suppressed systems require an alternative eluent and absorption solutions based on, for example, benzoic acid). The ISE buffer contained 20 g of potassium nitrate and 250 g of ammonium acetate per litre, with the pH adjusted to 6.5 with acetic acid.

The fluoride standard solution (200 μg ml^{-1}) contained 0.221 g of sodium fluoride (ignited at 800°C for 1 h) per litre.

Procedure

Various forms of fluorine may be significant contaminants in a laboratory environment and careful attention to the cleanliness of apparatus is essential to maintain acceptable precision for results. The furnace assembly must be purged with moist oxygen before each series of analyses to ensure freedom from contamination. With appropriate care, reagent blanks should not be significant.

Maintain a setting for the heating mantle of the steam generator such that the water simmers gently. Set the furnace temperature to about 1200°C. With each day of use, position fresh quartz wool at the gas outlet end of the silica tube, loosely packed for 50–100 mm; this serves as a particulate filter as well as a WO_3 condensation medium when the triple oxide catalyst is used.

Weigh 250 mg of sample (M_s) into a pre-ignited porcelain combustion boat, add 250 mg of catalyst (use the triple oxide mixture unless the mineralogy of the sample is known from tests to require only the silica catalyst). Mix well with a small spatula or wire to achieve thorough homogenization. Secure the absorption vessel containing 50 ($\pm$1) ml of absorption solution (selected for either ISE or ion-chromatographic measurement), place the sample boat into the end of the furnace and position the three-way stopcock (Fig. 1, item 12) so that dry oxygen flows through the furnace at 750 ml min^{-1}. Push the boat into the hottest zone over a period of 3.5 min, using a schedule appropriate to the temperature profile of the furnace so that volatile matter is completely

combusted and soot deposition on the outlet tubing does not occur. Re-position the three-way stopcock so that oxygen bubbles through the steam generator, open the stopcock between the steam generator and the furnace and close that leading to the drain. For coal and oxidizable materials including sulphides, steam may be introduced at any time following ignition of the volatile matter and back-ignition of the sample; for inorganic materials, steam is introduced once the sample has been pushed into a warm zone ($>200\,^{\circ}C$). Maintain this passage of steam and oxygen for 15 min after positioning of the sample boat in the hottest furnace zone. Terminate the steam flow-through by opening the drain stopcock and closing that to the furnace. Backwash the absorption assembly bubbler by removing and re-inserting the key of the three-way stopcock several times. Rinse the solution into a tared 125-ml polystyrene phial with a minimum volume of water.

For ISE measurement, place the pyrohydrolysate on the balance and add approximately 0.5 g of standard fluoride solution by means of a dispensing bottle or adjustable micropipettor; the increased mass (M_1) allows calculation of the amount of fluorine added. (This initial fluoride addition hastens the stabilization of the electrode potential during solution measurement, but is not so high as to cause a significant reduction in sensitivity for low-fluorine sample solutions.) Dilute the pyrohydrolysate to about 120 g net (M_p) with water and cool to ambient temperature. Transfer to a second phial and weigh approximately 40 g of pyrohydrolysate (M_a), and dilute (4+1) by weight with buffer solution (M_b). Read the potential of the solution after 2–3 min (E_1). Tare the fluoride standard dispensing bottle, add sufficient fluoride to the buffered solution to cause a potential change of 20–30 mV, and read after a further 2–3 min (E_2); reweigh the dispensing bottle to determine the mass of fluoride solution added (M_2). The fluoride concentration in the sample is calculated from the following formula, adapted from the Orion Research instructions (density adjustment for calculation based on volumes rather than masses as shown yields an insignificant change in result):

$$F\ (\mu g\ g^{-1}) = \left(\frac{M_p M_2 C}{M_a \{ [(1 + (M_2/(M_a + M_b))) 10^{(E_1 - E_2)/S}] - 1 \}} - M_1 C \right) / M_s$$

where E_1 is the initial electrode potential (mV), E_2 the final electrode potential (mV), M_1 the mass of first addition of standard fluorine (g), M_2 the mass of second addition of standard fluorine (g), M_p the mass of pyrohydrolysate (g), M_a the mass of pyrohydrolysate aliquot (g), M_b the mass of buffer added to pyrohydrolysate aliquot (g), M_s the mass of sample (g), C the concentration of fluorine solution in $\mu g\ ml^{-1}$ (assumed equivalent to $\mu g\ g^{-1}$ for calculations), and S the slope of electrode response at ambient temperature (established according to the manufacturer's recommendations, except that the buffered solution matrix must be the same as used in the present work).

For ion-chromatographic measurements, simply dilute the pyrohydrolysate to 120 g net. Measure the peak areas with the ion chromatograph using 50-μl injections, with calibration solutions containing the same volume of carbonate

buffer and up to 300 μg of fluoride. The fluoride peak is the first eluted within 1.1–1.2 min. The chromatographic run should not be terminated, however, until after about 6 min, to allow for the complete elution of all chloride (1.5 min), nitrate (2 min) and sulphate (about 4 min).

The procedure is suitable generally for materials containing fluorine up to about 5% (w/w). However, it has been found that fluorine concentrations exceeding about 0.5% should be processed with proportionately reduced sample mass, so that the mass of fluoride liberated through pyrohydrolysis does not exceed about 1000 μg. Further, fluorine concentrations greater than about 1% should be processed with a reduced oxygen flow rate of 150 ml min^{-1}.

RESULTS AND DISCUSSION

A comparison of fluorine results obtained for a set of seven coals by the peroxide fusion, oxygen bomb, and pyrohydrolytic methods is presented in Table 2. These results are the means of at least quadruplicate determinations in each case. In the initial application of the procedure, ISE measurements were used but extensive tests have confirmed that ion-chromatography gives equivalent results. From Table 2, all coals except brown coal T333 returned high fluorine values from which method comparisons were possible. With four of these coals, the results from pyrohydrolysis were the highest. With the fusion method, there appeared to be a low bias in the results compared with those from pyrohydrolysis, but the ranges for the individual results overlapped and agreement between the methods was within 10% relative.

With the oxygen bomb method, however, results for five coals were significantly at variance with results from pyrohydrolysis, the latter being higher by 10–60% relative. The two samples in agreement (SC158 and T333) were those with lowest fluorine (and lowest ash) values, such differences being insignificant at these levels. There is ample additional data within the author's laboratory that this greater yield compared with the oxygen bomb method is quite common, a finding confirmed from the experience of other laboratories [13,22]. The extent of the discrepancy for a given coal is probably dependent on the mineralogical species present, as some minerals may not liberate fluorine quantitatively under bomb combustion conditions.

The international test programme conducted to support the certification of three South African reference coals confirmed the discrepancies between pyrohydrolysis and alternative methods. Six laboratories reported mean values of 81, 62 and 83 $\mu g\ g^{-1}$ by the oxygen bomb method, and two reported values averaging 114, 98 and 146 $\mu g\ g^{-1}$ by pyrohydrolysis, for SARM 18, 19 and 20, respectively [23]. Recommended values could not be assigned to these coals in the absence of firm evidence as to the validity of the methods used. In support of the results from pyrohydrolysis, Table 3 shows that proton-induced gamma emission techniques (PIGME [24]) have provided similar values. Ad-

TABLE 3

Fluorine in reference materials by pyrohydrolysis (dry basis)

Designation	Material type	This work		Other values [ref.]
		Mean	1s	
Values < 0.1%		Fluorine ($\mu g\ g^{-1}$)		
BHP-CRL SM 8	Manganese ore	82	2	80[a]
BHP-CRL SM E-8	Manganese ore	214	2	200[a]
BHP-CRL SI 11	Iron ore	96	2	90[a]
BCS 303	Iron ore sinter	910	9	920[a]
NBS 278	Obsidian rock	380	10	500[b]
NBS 688	Basalt rock	144	4	200[b]
NBS 1570	Spinach	18	3	4 [25]
NBS 1571	Orchard leaves	8	2	4[b]
NBS 1573	Tomato leaves	12	3	5 [26]
NBS 1575	Pine needles	10	1	4 [26]
NBS 1632a	Bituminous coal	176	4	92 [10]
NBS 1632b	Bituminous coal	46	2	40[c]
NBS 1633a	Fly ash	82	3	110[c]
NBS 1634a	Fuel oil	9	4	-
NBS 1635	Sub-bituminous coal	39	1	4 [25]
SARM 18	Coal	115	2	114[c]
SARM 19	Coal	103	1	93[c]
SARM 20	Coal	152	6	153[c]
T-1	Tonalite	410	2	400[a]
Values > 0.1%		Fluorine (%)		
BCS 302/1	Iron ore	0.18	< 0.01	0.17[a]
BCS 382	BOS slag	1.62	0.03	1.61[d]
BHP-CRL SF 19	Fluorspar	3.10	0.09	3.30[a]
Canmet SY-1	Syenite	0.16	< 0.01	0.12 [27]
Canmet SY-2	Syenite	0.51	0.02	0.47 [28]
CRPG BR	Basalt	0.113	0.003	0.10 [29]
CRPG GH	Granite	0.34	< 0.01	0.35 [29]
EuroStd 681/1	Iron ore	0.18	< 0.01	0.19[d]
EuroStd 876/1	Electric oven dust	0.23	0.01	0.24[d]
EuroStd 877/1	Furnace dust	0.77	0.02	0.78[d]
NBS 91	Opal glass	5.65	0.14	5.72[d]
NBS 120a	Phosphate rock	3.89	0.07	3.92[d]
NBS 120b	Phosphate rock	3.87	0.04	3.84[d]
USGS G2	Granite	0.13	< 0.01	0.13 [30]
USGS GSP-1	Granodiorite	0.39	0.01	0.37 [25]

[a]BHP-CRL peroxide fusion. [b]Certificate "information only". [c]PIGME [24]. [d]Certified.

ditional PIGME results obtained for a set of six thickener underflow materials from coal preparation plants, having ash contents of 50–60%, showed an average discrepancy compared with pyrohydrolysis of only 17 $\mu g\ g^{-1}$ at the 500

$\mu g\ g^{-1}$ level.

Although the oxygen bomb method has been implemented (albeit often inaccurately) for coals with up to 25% ash [9], application to materials with higher ash contents would demand at least the addition of benzoic acid to assist the achievement of a high combustion temperature. This method is not, however, suitable for extension to the variety of materials outlined in Table 3. The reliability of the pyrohydrolysis method is further confirmed by the good agreement of results with available certificated or "preferred" literature values for many of the inorganic materials tested in the present work. With high-fluorine minerals, such as fluorspars having concentrations greater than 10% (w/w), the recommended conditions of pyrohydrolysis are inadequate, and results are invariably low by 0.5–2% absolute. No attempt was made within the scope of this work to establish suitable conditions for the processing of such materials, as they are generally satisfactorily handled by carbonate or peroxide fusions.

In the only two previous literature references to the pyrohydrolytic determination of fluorine in coal with a tube furnace, the temperature used was 1100°C [11,12]. This temperature was used in the earlier stages of the present development work, but as there increasingly appeared to be a complex set of pyrohydrolysis variables which affect the acceptability of results, and because the equilibrium

$$MF_{2n} + nH_2O \rightleftharpoons MO_n + 2nHF$$

is forced to the right with increasing temperature [20], subsequent work was done with 1200°C. Silica tubes start to warp at significantly higher temperatures, which are therefore unsuitable. Data presented by Gao et al. [12] indicated a correspondence of results for the oxygen bomb and pyrohydrolysis methods. For coal SC143 with conditions (1100°C/SiO_2 catalyst/150 ml min^{-1} oxygen) similar to those reported [12], it was indeed found that oxygen bomb and pyrohydrolysis results [75 $\mu g\ g^{-1}$ (Table 2) and 81 $\mu g\ g^{-1}$ (Table 1), respectively] were similar. However, variation to the triple oxide catalyst and higher oxygen flow rate returned the considerably higher value of 116 $\mu g\ g^{-1}$ (Table 2). This value was not further improved by using 1200°C, though results then were marginally more precise.

The basic methodology of the procedure described in this paper was applied elsewhere to coal samples, for which it was found that a catalyst of silica alone and temperature of 1200°C yielded recoveries comparable with those for the triple oxide catalyst and 1100°C [22]. The latter conditions were used to obtain the complete set of data for the preparation of Table 3. After a higher-temperature furnace became available in the author's laboratory, a check of several reference materials using silica and the higher pyrohydrolysis temperature confirmed the general correspondence of results from either set of conditions. It can be concluded from all data obtained throughout the development work that the triple oxide catalyst is usually necessary at 1100°C, but that

TABLE 4

Comparison of fluorine results for copper ores by pyrohydrolysis[a]

	A		B	
	Mean	Range	Mean	Range
BHP-CRL SG11 ore	780	35	810	10
BHP-CRL SG12 concentrate	1520	45	1610	30
BHP-CRL SG13 ore	770	25	850	30
BHP-CRL SG14 ore	840	40	915	10
BHP-CRL SG15 ore	910	25	925	15

[a]Results (air-dry) from duplicate determinations rounded to the nearest 5 $\mu g\ g^{-1}$. Conditions: (A) $SiO_2/WO_3/V_2O_5$ catalyst, 1100°C, ion-chromatography measurement (all sample solutions required dilution); (B) SiO_2 catalyst, 1200°C, ISE measurement.

silica should suffice at 1200°C. The mineralogy of a sample is the determining factor, however, and cases of uncertainty should be resolved by obtaining results from the application of both catalysts, irrespective of temperature.

A set of copper ores and concentrates was used to examine the procedural variations described. Samples were processed at 1100°C with the triple oxide catalyst followed by ion-chromatographic measurement. They were also processed at 1200°C with silica catalyst, followed by the standard-addition ion-selective electrode measurement. Results are seen from Table 4 to be similar, though the set obtained at higher temperature tended to be the higher and more precise.

It can be seen from Table 3 that satisfactory agreement between the pyrohydrolysis and PIGME results could not be achieved for reference fly ash NBS SRM 1633a, irrespective of catalyst, temperature, oxygen flow rate, or fine grinding of the sample. Similarly, discrepancies of up to 20% relative were found with a selection of refuse materials (ash values > 75%) from coal preparation plants. Extensive investigation has failed to resolve these differences, which incongruously occur with high-ash coal-derived materials though silicate rocks, ores and other essentially inorganic reference materials have been analysed with acceptable accuracy. There is substantial practical evidence that the pyrohydrolytic method presented in this paper is rapid, cost-efficient, more reproducible, and more accurate than commonly used alternatives for the analysis of coals. The clear implication from the case of NBS SRM 1633a and similar materials is that some sample types appear to return low results by the pyrohydrolysis method. Further investigation is required to explain satisfactorily the discrepancies noted above. The general applicability of pyrohydrolysis recommends it, however, as a preferred method for the determination of trace to minor concentrations of fluorine in coals and a wide variety of minerals. Pyrohydrolysis would be beneficial in the analysis of materials included

in a recent report on methods for the determination of fluoride in environmentally relevant matrices [31], and the techniques contained in the present paper form the basis of a Standards Association of Australia method, currently in preparation, for application to coal, coke and fly ash analysis.

Development work relevant to coal analyses was supported by the National Energy Research Development and Demonstration Programme Grant No. 80/0220. Appreciation is expressed to A.C. Knott for discussions on method development, I. Oblasser and A.-L. Carter for experimental assistance, T.D. Rice and W.C. Godbeer for discussions on supporting development aspects, and to the Broken Hill Proprietary Co. Ltd. for permission to publish the work.

REFERENCES

1 K.J. Doolan, J.C. Mills and K.E. Turner, Broken Hill Proprietary Tech. Bull., 24 (1980) 17.
2 U.S. National Research Council, PECH Report, Trace Element Geochemistry of Coal Resource Development Related to Environmental Quality and Health, U.S. National Committee for Geochemistry, National Academy Press, Washington, DC, 1980.
3 H.E. Crossley, J. Soc. Chem. Ind., London, 63 (1944) 284.
4 R.R. Ruch, H.J. Gluskoter and N.F. Shimp, Environ. Geol. Notes, No. 72, Ill. State Geol. Surv., 1974.
5 J. Thomas and H.J. Gluskoter, Anal. Chem., 46 (1974) 1321.
6 R.A. Nadkarni, Anal. Chem., 52 (1980) 929.
7 R.F. Abernethy and F.H. Gibson, U.S. Bur. Mines Rep. Invest., No. 7054, 1967.
8 E.N. Pollock, in S.P. Babu (Ed.), Trace Elements in Fuel, American Chemical Society, Washington, DC, 1975, p. 23,
9 American Society for Testing and Materials, Total Fluorine in Coal by the Oxygen Bomb Combustion-Ion Selective Electrode Method, American Society for Testing and Materials, Philadelphia Method D3761, 1979.
10 R.A. Nadkarni, Int. Lab., September (1981) 26.
11 H.C. Van Leuven, G.J. Rotscheid and U.J. Buis, Fresenius' Z. Anal. Chem., 296 (1979) 36.
12 G. Gao, B. Yan and L. Yang, Fuel, 63 (1984) 1552.
13 T.D. Rice, Occurrence and Distribution of Fluorine in Sydney Basin Coal Seams, Paper presented at Coal Science Symposium, Sydney, 1982.
14 J.C. Mills, K.J. Doolan and A.C. Knott, Determination of Trace Elements in Coal and Coal Products, NERDDP EG-84-358, Department of Resources and Energy, Canberra, 1983.
15 K.J. Doolan, K.E. Turner, J.C. Mills, A.C. Knott and R.R. Ruch, Volatilities of Inorganic Elements in Coals During Ashing, Proc. Am. Chem. Soc. Div. Fuel Chem. Symposium, 29 (1984) 127.
16 G.J. Kakabadse, B. Mandhin, J.M. Bather, E.C. Weller and P. Woodridge, Nature (London), 229 (1971) 626.
17 M. Noshiro and T. Yarita, Bunseki Kagaku, 26 (1977) 721.
18 J.C. Warf, W.D. Cline and R.D. Tevebaugh, Anal. Chem., 26 (1954) 342.
19 M.J. Nardozzi and L.L. Lewis, Anal. Chem., 33 (1961) 1261.
20 A.C.D. Newman, Analyst, 93 (1968) 827.
21 Australian Standard Methods for the Analysis and Testing of Coal and Coke, AS 1038 series, Parts 6.1 and 6.3.2, Standards Association of Australia, Sydney, 1986.
22 W.C. Godbeer, CSIRO Div. Fossil Fuels, North Ryde, Australia, personal communication.
23 E.J. Ring and R.G. Hansen, Sth. Afr. Council for Min. Technology, Randberg, South Africa, Rep. M169, 1984.

24 L.S. Dale, CSIRO Div. Energy Chem., Lucas Heights, Australia, personal communication.
25 G. Troll and A. Farzeneh, Geostandards Newsl., 2 (1978) 43.
26 E.S. Gladney, Anal. Chim. Acta, 118 (1980) 385.
27 S. Abbey, A.H. Gillieson and G. Perault, Canada Cntr. Min. Energy Technol., Rep. MRP/MSL 75-132 (TR), Ottawa, 1975.
28 F.J. Flanagan, Geochim. Cosmochim. Acta, 37 (1972) 1189.
29 K. Govindaraju and H. de la Roche, Geostandards Newsl., 1 (1977) 67.
30 O. Stecher, Geostandards Newsl., 7 (1983) 283.
31 The Analytical Working Group of the Comité Technique Européen Du Fluor, Anal. Chim. Acta, 182 (1986) 1.

Analytica Chimica Acta, 202 (1987) 75–84
Elsevier Science Publishers B.V., Amsterdam — Printed in The Netherlands

RAPID COULOMETRIC TITRATIONS WITH A NEW DESIGN OF ELECTROLYTIC CELL

H.H. RÜTTINGER and U. SPOHN*

Sektion Chemie, Martin-Luther-Universität Halle, 4020 Halle, Weinbergweg 16 (German Democratic Republic)

(Received 7th May 1987)

SUMMARY

The construction of a compact coulometric titration cell with integrated injection valve and photometric and biamperometric flow-through detectors is reported. The lower part of the cell is designed as a magnetic centrifugal pump by means of which the supporting electrolyte is propelled through the other functional parts. Various rapid titration procedures were developed. The favourable flow conditions allow titration times between 10 and 100 s. The principle of continuous titration up to a preselected set-point is applied for both the photometric and biamperometric detectors. Microgram amounts of cyanide and thioglycolic acid are titrated directly with electrogenerated iodine. Full advantage of the cell design is obtained in the implementation of back-titration procedures during which the sample and the reagent in excess are injected simultaneously into the circulating electrolyte. Back-titrations are implemented to determine microgram amounts of iodine, copper(II) and iron(III).

Coulometric titrations are among the most precise analytical methods. In order fully to utilize the advantages of this technique, it is necessary to have electrolysis cells which, in terms of parameters such as sampling rate, precision of sampling and reliability, will provide rapid and complete mixing of the sample and the titration medium, and will also prevent any mixing of the anode and cathode products. Large electrode areas have to be combined with small cell volumes [1,2] to achieve short titration times, and the method of end-point detection must be capable of rapid response without interfering with the current-generating circuity. Flow-through detectors combined with coulometric cells provide improved signal-to-noise ratios, particularly in the case of electrochemical end-point detection.

Gary et al. [3] proposed a fast-circulation cell with a flow-through bypass equipped with an amperometric or a photometric flow-through detector; a centrifugal pump circulated the supporting electrolyte. De Soto Perera and Curran [4] connected an electrolysis cell completely filled with 240 ml of electrolyte to a biamperometric thin-layer detector; electrolysis cell and detector were

0003-2670/87/$03.50

connected by a closed tubing loop. A disadvantage is the enhanced noise-to-signal ratio of the biamperometric indicator signal caused by the pulsation of the peristaltic pump.

In the present paper, the construction and evaluation of a compact coulometric titration cell which meets the demands mentioned above are reported. The cell includes the generating and the auxiliary electrode chambers, a photometric and an amperometric flow-through detector, an injection valve and a magnetic centrifugal pump, all incorporated into one body. To take the full advantage of the cell design, back-titration procedures should also be included. Coulometric back-titrations are relatively seldom used [5]. However, they would greatly extend the field of application of rapid coulometric titrations. Coulometric back-titrations are advantageous for cases in which the conditions for direct titrations cannot be fulfilled, e.g., the need for rapid and quantitative reaction between titrant and analyte without side-reactions, for a sensitive method of end-point location, and for a titrant which can be electrogenerated with 100% current efficiency. In many cases, it is possible to use a suitable reagent in excess, which can be back-titrated coulometrically after its rapid and well-defined reaction with the analyte. The charge involved in the back-titration step is then subtracted from the charge consumed during the coulometric standardization of the excess of reagent to obtain the analytical result.

The performance of the proposed cell construction is evaluated here for the direct titration of microgram amounts of thioglycolic acid and cyanide, and in back-titration procedures for the determination of microgram amounts of iodine, copper(II) and iron(III).

EXPERIMENTAL

Apparatus and instrumentation

Figure 1 is a schematic diagram of the experimental arrangement. The titration cell is connected to a coulometric autotitrator. The polarization voltage used for amperometric end-point indication can be varied between 0 and ± 2 V. The photometric end-point detection operates with a phototransistor (SP-201-D) as light receiver and a luminescent diode (VQA-23-D; $\lambda_{max} = 565$ nm, $\lambda_{1/2} = 40$ nm, VEB Werk für Fernsehelektronik Berlin) as light source.

The amperometric indicator electrode or the emitter of the phototransistor, respectively, are connected to the input of the current monitor (7). The amperometric indicator current or the photocurrent can be amplified by 1 V μA^{-1} or 10 V μA^{-1}. The output of the current monitor is connected to a comparator circuit of 12 steps, in which the amplified detector signal is compared with the preselected set point. When the set point is reached, the generating current is switched on or off by means of a relay. An autozero circuit completes the photometric detection.

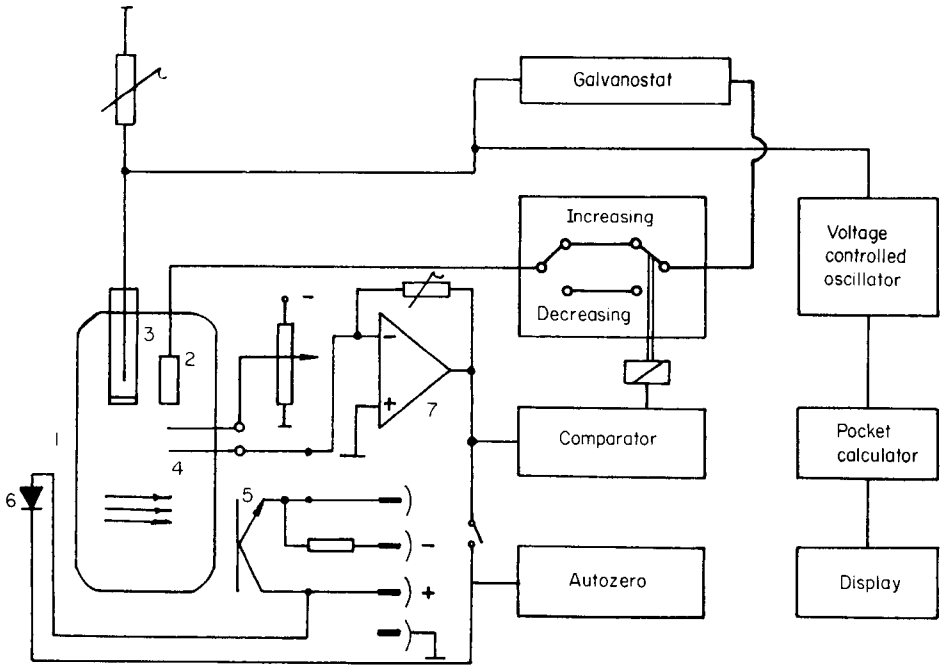

Fig. 1. Experimental arrangement: (1) titration cell; (2) generator electrode; (3) auxiliary electrode; (4) indicator electrodes; (5) phototransistor; (6) luminescent diode; (7) current monitor.

The voltage-controlled oscillator converts the voltage drop across a suitable adjusted shunt into a needle pulse sequence. A pocket calculator counts the pulses continuously. The input of a multiplying factor allows recording of the degree and the result of the titration in any desired unit. The corresponding count during the coulometric determination of the excess of reagent also provides direct reading in back-titration procedures.

Coulometric titration cell

The cell (Fig. 2) consists of four operational sections formed by cylindrical precision-planed PTFE blocks (50-mm diameter), which are pressed together between two plexiglas plates and held by four screws. The internal space of the cell (10–11 ml), completely filled with supporting electrolyte, is separated from the auxiliary electrode chamber by a cation-exchange membrane (2) (Nafion 427, DuPont, U.S.A.) or a G4 glass frit. The auxiliary electrode chamber (1) is fitted through the upper supporting plate (3) and screwed into the head section (4) so that the diaphragm is flush with the upper edge of the horizontal channel (5). The auxiliary electrode (6) is a platinum wire (0.5-mm diameter, 20 mm long). A platinum foil (7) with a surface area of 4.6 cm^2, covering the cell base and supported by a thin slice of PVC, serves as the generator electrode.

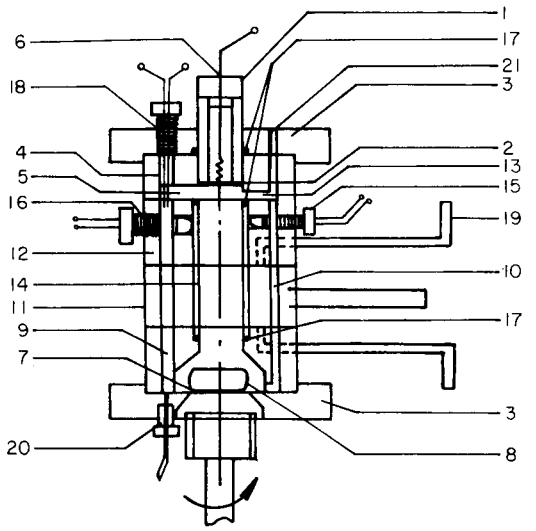

Fig. 2. Titration cell: (1) auxiliary electrode chamber; (2) Nafion-427 diaphragm; (3) supporting plates; (4) head section; (5) main horizontal channel; (6) auxiliary electrode; (7) generator electrode; (8) centrifugal pump; (9) main circulation channel; (10) sample-insertion channel; (11) injection-valve section; (12) detector section; (13) horizontal channel; (14) cuvette tube; (15) phototransistor; (16) luminescence diode; (17) neoprene O-rings; (18) amperometric detector; (19) sample solution inlet; (20) inlet for introduction of electrolyte; (21) degassing hole (for details see text).

The supporting electrolyte is propelled by a magnetic centrifugal pump (8) through the main circulation channel (9; 5-mm diameter) and the sample insertion channel (10; 3-mm diameter), then through the injection-valve section (11) and the detector section (12) to the head section. After passing through the horizontal channels (5 and 13), the electrolyte flows along the diaphragm through the cuvette tube (14), reaching the low-pressure inflow of the centrifugal pump. The centrifugal pump contains a magnetic stirring bar (7-mm diameter, 14 mm long) which is rotated by an external permanent magnet at 500 rpm.

The detector section bears the phototransistor (15) and the luminescent diode (16), which are held by fittings screwed in as far as the cuvette. The cuvette consists of borosilicate glass (14 mm i.d., 17 mm o.d., 30 mm high) and is held between the detector section and the housing of the centrifugal pump. Neoprene O-rings (17) serve as seals. The platinum wire electrodes (0.5-mm diameter, 4 mm long) of the amperometric flow detector (18) are mounted into the main circulation channel by means of a PTFE fitting.

The injection-valve section can be turned between the positions for sample input and sample injection. The injection-valve body is guided between rings protruding on both sides, which are fitted to the sections above and beneath.

In the sample-input position the sample solution flows through the inlet (19) and the corresponding channel of the injection valve. After the valve has been turned by 54°, the sample volume, established by the volume of this channel, is injected into the circulating electrolyte by connecting to the sample insertion hole.

To implement back-titration procedures, an additional loop for solution insertion is introduced into the cell body. This loop for introducing reagent in excess is designed analogously to the sample loop and displaced from it by about 90°. In this configuration, the sample solution and the reagent solution in excess are injected simultaneously into the circulating electrolyte when the valve is turned.

Chemicals and solutions

All chemicals were of analytical reagent-grade quality and were used as received. The electrolyte and stock solutions were prepared with twice-distilled water.

A ca. 0.1 M cyanide solution was prepared from recrystallized potassium cyanide in 0.05 M sodium hydroxide and standardized by titration with silver(I) solution. An approximately 0.1 M stock solution of thioglycolic acid was standardized coulometrically [6]. A 0.05 M triiodide solution was prepared by weighing and dissolving sublimed iodine in 0.2 M potassium iodide. The 0.1 M solutions of iron(III) and copper(II) were prepared by dissolving $FeCl_3 \cdot 6H_2O$ and $CuSO_4 \cdot 5H_2O$, respectively, in 0.1 M hydrochloric acid and standardized by titration with EDTA.

For the coulometric titration of cyanide, the supporting electrolyte contained 0.1 M KI, 0.1 M NaCl and 0.15 M $NaHCO_3$. For the titration of thioglycolic acid, thiosulphate and iodine, the sodium hydrogencarbonate was replaced by 0.01 M acetic acid. For the titration of iron(III), the supporting electrolyte was 0.3 M KI acidified to pH 1 with hydrochloric acid. For copper(II), the electrolyte was 0.3 M KI/0.1 M NaCl/0.2 M acetic acid. To locate the end-point photometrically, 0.5 ml of starch indicator solution (10 g l^{-1}) was added to the corresponding electrolyte; the starch solution was prepared daily.

Procedure

For the coulometric titrations, the generating current was between 0.1 and 10 mA. The platinum indicator electrodes were polarized at an applied potential of 150 mV, except for the copper(II) titration for which 180 mV was applied. The green luminescent diode was operated at a current of 28 mA during the photometric titrations. The titration curves were recorded at constant electrolytic current by means of a strip-chart recorder (Type OP-207, Radelkis, Budapest). Before a series of titrations was started, the pocket calculator was

set, as required, to sum or subtract continuously the number of pulses corresponding to a definite amount of charge or an equivalent amount of substance.

In the back-titration procedures, after every ten determinations, the injected amount of the reagent in excess was titrated coulometrically to the same set point as during the back-titration step. From the stored result of this standardization step, the charge or the equivalent amount of the excess of reagent was counted back in the analytical run.

The titration cell was filled slowly from the bottom through inlet (20) until the electrolyte flowed through the upper degassing hole (21). The magnetic centrifugal pump was only then operated. The auxiliary electrode chamber was filled with 0.2 M KCl for the direct titration procedures and for the iodine determination, but with 0.3 M KCl for the iron(III) determination and with 0.6 M KCl for the copper(II) titration.

After pretitration, the titrations were run continuously up to the preselected set point of the corresponding detector signal.

RESULTS AND DISCUSSION

In order to test the measuring device described, thiosulphate standard solutions were titrated with photometric and biamperometric end-point detection. The relative standard deviations for injections of the sample and the reagent in excess were evaluated from coulometric titrations of 0.1 M thiosulphate with iodine by using both methods of end-point indication; the value found was 0.0008 ($n=10$). A calibration graph with eight points ($n=6, r^2=1$) intersected the origin. From this plot, the injected volumes were calculated to be (57.35 ± 0.04) μl and (56.85 ± 0.04) μl. After injection of thiosulphate, both methods of end-point detection passed the switch-on value almost immediately. After 4–5 s, stable indicator signals were attained. Figure 3 shows that

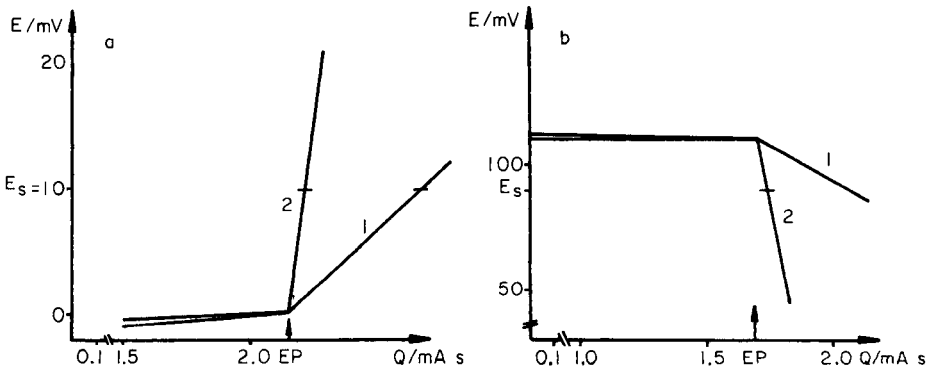

Fig. 3. (a) Biamperometric titration curves for 2.5 μg of thiosulphate; (b) Photometric titration curves for 2.0 μg of thiosulphate: (1) amplification, 1 V μA^{-1}; (2) amplification, 10 V μA^{-1}. E_s, set point; EP, equivalence point.

TABLE 1

Direct coulometric titration of thioglycolic acid and cyanide ($n=6$, $\alpha=0.05$)

Amount injected (μg)	Amount found (μg)		Generator current (mA)
	Biamperometric	Photometric	
Thioglycolic acid			
1.23	1.24 ± 0.01	1.22 ± 0.01	0.1
5.45	5.43 ± 0.03	5.46 ± 0.03	0.2
10.94	10.94 ± 0.04	10.96 ± 0.05	0.5
32.84	32.99 ± 0.18	32.95 ± 0.21	1.0
54.74	55.01 ± 0.31	54.60 ± 0.28	1.0
Cyanide			
0.528	—	0.537 ± 0.009	0.2
1.07	—	1.05 ± 0.01	0.2
4.05	—	4.06 ± 0.02	0.5
8.11	—	8.08 ± 0.03	1.0
27.7	—	27.6 ± 0.2	2.0

titration curves recorded one after the other fitted almost completely, thus allowing precise set-point titrations.

A comparison of the biamperometric titration curves with those recorded in batch-type cells showed a more favourable signal-to-noise ratio, higher sensitivity and better reproducibility for the proposed arrangement.

Direct titrations

Table 1 shows the results of the titration of thioglycolic acid and cyanide with triiodide. Even very small amounts of thioglycolic acid and cyanide can be determined with high precision and accuracy. One titration takes between 15 and 120 s. Up to 40 titrations can be done with the same supporting electrolyte filling without loss of precision. Cyanide can be titrated also biamperometrically. However, the reaction

$$CN^- + I_3^- \longrightarrow ICN + 2\,I^-$$

and the electrochemical reducibility of ICN even at polarization voltages below 100 mV cause appreciable changes in the shapes of the titration curve during a continuous series of titrations, resulting in erroneous results. This can obviously be avoided if photometric detection with starch indicator solution is applied.

Back-titrations

As the results in Table 2 demonstrate, very small amounts of iodine, iron (III) and copper (II) can be determined very precisely and accurately by means of

TABLE 2

Coulometric back-titrations for iodine, iron(III) and copper(II) ($n=6$, $\alpha=0.05$)

Amount injected (μg)	Amount found (μg)		Excess of thiosulphate[a]	Generator current (mA)
	Biamper.	Photom.		
Iodine				
1.31	1.29 ± 0.02	1.32 ± 0.02	3.71 ± 0.03	0.1
13.15	13.12 ± 0.07	13.13 ± 0.08	26.52 ± 0.12	0.5
54.3	54.2 ± 0.1	54.4 ± 0.1	109.2 ± 0.3	1.0
131.5	131.7 ± 0.4	131.0 ± 0.4	218.4 ± 0.7	1.0
208.4	207.8 ± 0.6	208.2 ± 0.6	365.3 ± 1.0	2.0
Iron(III)				
5.75	5.70 ± 0.05	5.71 ± 0.05	17.45 ± 0.11	0.5
24.65	24.48 ± 0.18	24.68 ± 0.17	77.71 ± 0.29	1.5
68.9	69.1 ± 0.3	69.2 ± 0.3	220.4 ± 0.6	3.0
120.3	121.0 ± 0.4	121.1 ± 0.4	382.3 ± 1.0	5.0
240.7	239.9 ± 0.8	240.9 ± 0.7	702.9 ± 2.1	10.0
Copper(II)				
5.05	5.01 ± 0.06	—	16.43 ± 0.08	0.2
25.18	25.42 ± 0.20	—	80.87 ± 0.29	1.0
58.5	58.7 ± 0.3	—	195.8 ± 0.6	2.5
125.9	125.5 ± 0.4	—	380.5 ± 1.0	5.0
251.8	252.7 ± 0.6	—	710.8 ± 1.9	7.5

[a]In μg-equivalents of substance determined.

coulometric back-titration of the excess of thiosulphate. Up to fifty iodine, and twenty iron(III) or copper(II) determinations can be done in the same supporting electrolyte filling. Iron(III) and iodine can be titrated with both photometric and biamperometric end-point detection. Because of Cu_2I_2 precipitate formation, only the biamperometric method of end-point detection is suitable for the set-point titration of copper(II).

The advantages of the proposed method for the determination of iodine compared to the direct titration by electrolytically generated tin(II) [7] or iron(II)-EDTA [8] are its significantly higher precision and its greater independence from contaminating oxygen. In the same way, many iodine-evolving oxidants (e.g., iodate, bromine, chlorine, hypochlorite, chloramine-T and chloramine-B) can be titrated with analogous results.

The iodometric titration of iron(III) as proposed by Rowley and Swift [9], based on the addition of excess of thiosulphate and back-titration with electrogenerated iodine, has hitherto found only a few practical applications. However, the procedure has a great advantage compared to direct coulometric titrations by electrogenerated titanium(III) [10–12] or tin(II) [13] in that interference by oxygen is appreciably smaller. Further, the end-point of the

iodometric titration can be located biamperometrically as well as photometrically with higher sensitivity and precision. The procedure is applicable for monitoring the iron(III) content in iron(III) chloride etching solutions.

To titrate copper(II) iodometrically, Cadersky [14] used the supporting electrolyte 0.1 M KI/0.5 M NH_4SCN/0.1 N H_2SO_4 and found a precision of ± 0.8 to $\pm 3.8\%$ with an accuracy of 1.5% ($n=5$) in the range of 6–100 μg Cu(II). In order to prevent the slowly occurring reduction of copper(II), the present measurements were made without thiocyanate. After the generator electrode chamber had been filled, high-purity nitrogen was passed through the supporting electrolyte for 10–15 min to remove oxygen. Up to ten-fold amounts of zinc(II) or magnesium(II) were tolerated.

The described applications demonstrate that with the proposed new concept of a coulometric titration cell, high precision can be achieved even at very short titration times. By means of the integrated valve, injection through displacement capillaries, which is usual in titration cells completely filled with electrolyte, can be avoided. Here, a more precisely defined and smaller volume of titrated electrolyte is exchanged for the same volume of sample solution. The mode of continuous titrations in series makes it possible to achieve a much higher frequency of sample and reagent additions. The implementation of large series of titrations in a relatively small volume of supporting electrolyte results in highly efficient uitilization of reagents.

The constant flow conditions provided by enhanced controlled convection at the surface of the indicator electrodes produce more reproducible biamperometric titration curves and shorter response times. The principle of hydrodynamic detection in a flow-through loop minimizes the danger of interferences between generating and indicator circuit. The small volume of the inner cell space and the large area of the generator electrode (4.6 cm^2) in combination with short mixing times contribute essentially to the high titration rates. The insertion of a third electrolyte loop into the cell body does not remarkedly influence the mixing time.

Depending on the injected amount of reagent in excess, back-titrations take between 20 and 70 s. Hitherto unattained sample rates of 40–100 h^{-1} for back-titration procedures can be achieved. The simultaneous precise injection of sample and reagent in excess means that the two-fold addition necessary in the usual back-titration procedures does not cause a significant deterioration of precision. It is obvious that many other classical direct and back-titration procedures can be achieved coulometrically in the proposed titration cell.

The authors thank Professor Hermann Matschiner for valuable discussions concerning this work and Dr. Lux for his help in translating the manuscript.

REFERENCES

1 A.J. Bard, Anal. Chem., 35 (1963) 1125.
2 A.A. Sakharov, Zavod. Lab., 50 (1984) 18.
3 A.M. Gary, E. Piement, M. Roynette and J.P. Schwing, Anal. Chem., 44 (1972) 198.
4 M.A. de Soto Perera and D.J. Curran, Anal. Chim. Acta, 119 (1980) 251, 263.
5 E. Bishop, in C.L. Wilson and D.W. Wilson (Eds.), Wilson and Wilson's Comprehensive Analytical Chemistry, Vol. IID, Elsevier, Amsterdam, 1975.
6 L.B. Oganesyan and H.F. Konkova, Zh. Anal. Khim., 35 (1980) 1995.
7 T. Takahashi and H. Sakurai, Talanta, 9 (1962) 74.
8 R.W. Schmid and C.N. Reilley, Anal. Chem., 28 (1956) 520.
9 K. Rowley and E.H. Swift, Anal. Chem., 26 (1954) 373.
10 P. Arthur and J.F. Donahue, Anal. Chem., 24 (1952) 1612.
11 H.V. Malmstadt and C.B. Roberts, Anal. Chem., 28 (1956) 1412.
12 S. Slovak and M. Pribyl, Fresenius' Z. Anal. Chem., 228 (1967) 266.
13 A.I. Kostromin, V.V. Mosolov and I.D. Juschanina, Zh. Anal. Khim., 27 (1972) 1115.
14 I. Cadersky, Fresenius' Z. Anal. Chem., 244 (1969) 122.

Analytica Chimica Acta, 202 (1987) 85-96
Elsevier Science Publishers B.V., Amsterdam — Printed in The Netherlands

TENSAMMETRY WITH ACCUMULATION ON THE HANGING MERCURY DROP ELECTRODE
Part 4. The Behaviour of Oxyethylated Alcohols (Polyoxyethylene n-alkyl monoethers)

M.K. PAWLAK and Z. ŁUKASZEWSKI*

Institute of General Chemistry, Technical University of Poznań, 60-965 Poznań (Poland)

(Received 22nd July 1986)

SUMMARY

The behaviour of polydispersed oxyethylated alcohols having a well-defined n-alkyl radical is described. Surfactants 6-14, 10-10, 10-14, 18-14, 18-10 and 18-6 (the first number denotes the number of carbon atoms in the n-alkyl radical, and the second one the average number of oxyethylene subunits) were examined. The conditions included 5 or 10 min of adsorptive preconcentration of surfactants at concentrations lower than the c.m.c. value. Only negative tensammetric peaks were examined. The relationships between the peak height and the preconcentration potential were investigated for potentials more negative than −1.0 V vs. SCE. More hydrophilic surfactants (i.e., 6-14, 10-10 and 10-14) form one wide tensammetric peak. The relationship of this peak to the preconcentration potential is simple and is similar to the negative branch of the adsorption isotherm. More hydrophobic surfactants (i.e., 18-6, 18-10 and 18-14) form a narrow peak, caused by the monomer form of the surfactant. If the threshold concentration of surfactants 18-6 and 18-10 is exceeded, a second very narrow peak appears, which is caused by the premicellar form of the surfactant formed at concentrations lower than the c.m.c. The dependences of the peak height on the preconcentration potential for surfactants 18-6, 18-10 and 18-14 are complicated; each plot shows a maximum, but the curves greatly depend on the surfactant concentration, which makes the choice of preconcentration potential difficult. Within the 10-(30-50) $\mu g\ l^{-1}$ range of surfactant concentration, the plots of peak height vs. surfactant concentration are approximately linear. Results for the lowest concentrations are very imprecise because of strong adsorption of the surfactants on the surface of the cell.

Earlier investigations [1–3] showed that there is considerable potential for tensammetry with accumulation on the hanging mercury drop electrode (HMDE) in the determination of trace concentrations of surfactants. The complexity of the behaviour of surfactant mixtures under tensammetric conditions also became evident. The possibilities for the determination of particular components in the complex mixtures were examined by using, as an example, mixtures of poly(ethylene glycols) having different molecular weights

0003-2670/87/$03.50

and Triton X-100. The differentiating action of the preconcentration potential was used for the determination of components of the mixtures. In the work described below, the same problems in relation to oxyethylated alcohols (polyoxyethylene alkyl monoethers) are considered. Oxyethylated alcohols belong to the most popularly used group of nonionic surfactants. In their structure, different oxyethylated alcohols have different lengths of the alkyl chain (i.e., the hydrophobic part of the molecule) as well as different lengths of the oxyethylene chain (i.e., the hydrophilic part of the molecule). Such differentiation is necessary in order to achieve a desirable range of practical properties.

The behaviour of oxyethylene monoethers of lauryl alcohol under conditions of classical tensammetry (i.e., with the dropping mercury electrode, DME) has been described by Jehring in his monograph [4]. The tensammetric behaviour of other oxyethylated alcohols has not previously been described. The aim of the present work was to examine the behaviour of oxyethylated alcohols having different ratios of hydrophobic and hydrophilic parts in their structures under conditions of tensammetry with accumulation on the HMDE. Thus oxyethylated alcohols having different lengths of the n-alkyl chain and the oxyethylene chain were investigated. Because of the unavailability of chemically well-defined polyoxyethylene n-alkyl monoethers, polydispersed oxyethylated alcohols were used, but these materials have an exactly defined n-alkyl radical, unlike the commercial products. As in our previous work, only the cathodic tensammetric peaks were investigated; otherwise, the required anodic tensammetric peaks would be recorded alongside dissolution peaks from metals deposited in the accumulation stage. Several such additional peaks would seriously affect the identification of the tensammetric peaks, as well as the determination of the surfactant. Main attention was concentrated on the possible differentiating action of the preconcentration potential. The dependences of the peak heights for all the investigated oxyethylated alcohols on the preconcentration potential were therefore examined; however, these investigations were restricted to the range of potentials more negative than -1.0 V vs. SCE, in order to keep experimentation within manageable proportions.

EXPERIMENTAL

A Radelkis OH-105 polarograph was used with a voltage scan rate of 400 mV min^{-1}. The applied amplitude of the alternating voltage was 2 mV. Controlled-temperature HMDE equipment (Radiometer) having an additional molybdenum-rod auxiliary electrode was used. In the glass cell, a small teflon beaker was placed so that the investigated solution was only in contact with teflon. The potential was checked with a N-517 digital voltmeter (Mera-Tronic, Poland).

Oxyethylated alcohols synthesized at the Institute of Chemical Technology and Engineering of this University were used. These surfactants were obtained by oxyethylation of the relevant n-alcohols (reagent grade). Thus these sam-

TABLE 1

The content of impurities in the examined polyoxyethylene n-alkyl monoethers

Surfactant	Abbreviation	Content of PEG[a] (%)	Content of free alcohol (%)
Tetradecyloxyethylene n-hexyl monoether	6-14	10.3	1.4
Decyloxyethylene n-decyl monoether	10-10	3.5	3.4
Tetradecyloxyethylene n-decyl monoether	10-14	6.6	1.8
Tetradecyloxyethylene n-octadecyl monoether	18-14	3.5	0.8
Decyloxyethylene n-octadecyl monoether	18-10	4.7	2.5
Hexyloxyethylene n-octadecyl monoether	18-6	0.8	11.7

[a]Poly(ethylene glycols).

ples were polydispersed products, and contained free n-alcohol and poly(ethyleneglycols) as well as the main products. The investigated substances, together with the content of impurities and the abbreviations used further in the text, are listed in Table 1. The concentrations of impurities were determined by Miesiąc [5]. Although these surfactants are not the most strictly defined chemical substances, they are better defined than commercial products.

The sodium sulphate used for preparation of the base electrolyte was purified by double recrystallization and heated at 600°C. All solutions were prepared in water thrice-distilled from quartz. Only freshly distilled water was used. Only glass and quartz vessels were used. The supporting electrolyte in all the studies was aqueous 0.5 M sodium sulphate.

The investigated solutions were first thermostated at 25°C in measuring flasks; they were then introduced into the thermostated (25°C) measuring cell and deaerated by bubbling oxygen-free nitrogen. Just before preconcentration was started, the stirrer was switched on, the required preconcentration potential was set and a new mercury drop was formed. The preconcentration time, which was 5 or 10 min, was measured from this moment. The tensammetric curve in the negative direction was recorded for this solution, after a 1-min quiescent period.

RESULTS

For the six surfactants listed in Table 1, the tensammetric curves were recorded after adsorptive preconcentration at different applied potentials. The

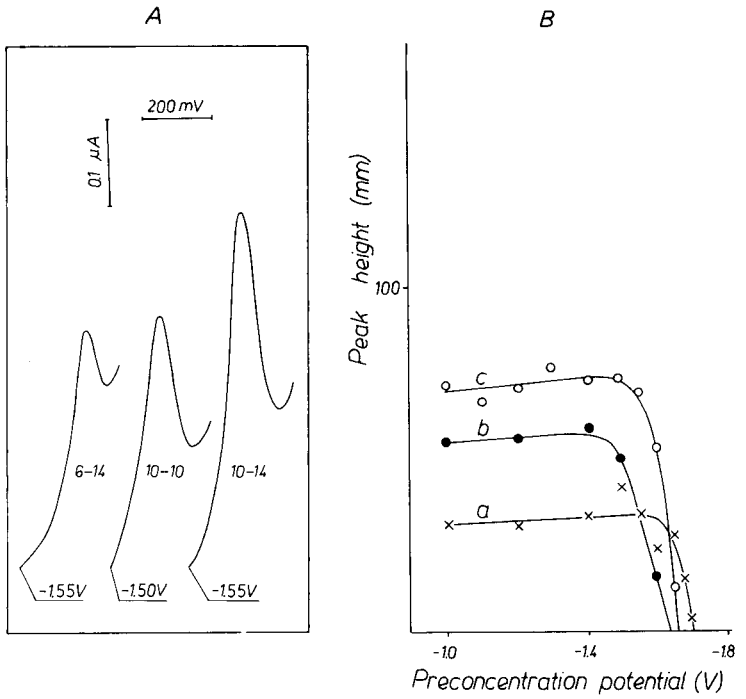

Fig. 1. The tensammetric curves of surfactants 6-14, 10-10 and 10-14 (A), and the relationships between the peak height of surfactants 6-14, 10-10 and 10-14 and the preconcentration potential (B) (curves a, b and c, respectively). Concentration of surfactants, 0.20 mg l^{-1}; preconcentration time, 5 min.

preconcentration potential was changed within the range of −1.0 to −1.8 V vs. SCE.

The behaviour of surfactants 6-14, 10-10 and 10-14, under conditions of tensammetry with accumulation on the HMDE, is simple. Each of them forms one wide peak; examples of these peaks are shown in Fig. 1A. The dependences on preconcentration potential of the peak heights of these surfactants are shown in Fig. 1B. These dependences, obtained for 0.20 mg l^{-1} solutions after 5-min preconcentration periods, are also simple in shape, and are similar to the cathodic part of the adsorption isotherm.

The behaviour of surfactants 18-14, 18-10 and 18-6 is much more complicated. The relationships of the peak height to the preconcentration potential for these surfactants depend strongly on the concentration of the surfactant, and were therefore examined for 2 or 3 different concentrations. At low concentrations of the surfactants, there was the problem of adsorption of the surfactant on the cell surface. Of course, this phenomenon occurs at all levels of surfactant concentration, but only at small concentrations do the losses caused by such adsorption play an important role in quantitative work. This effect

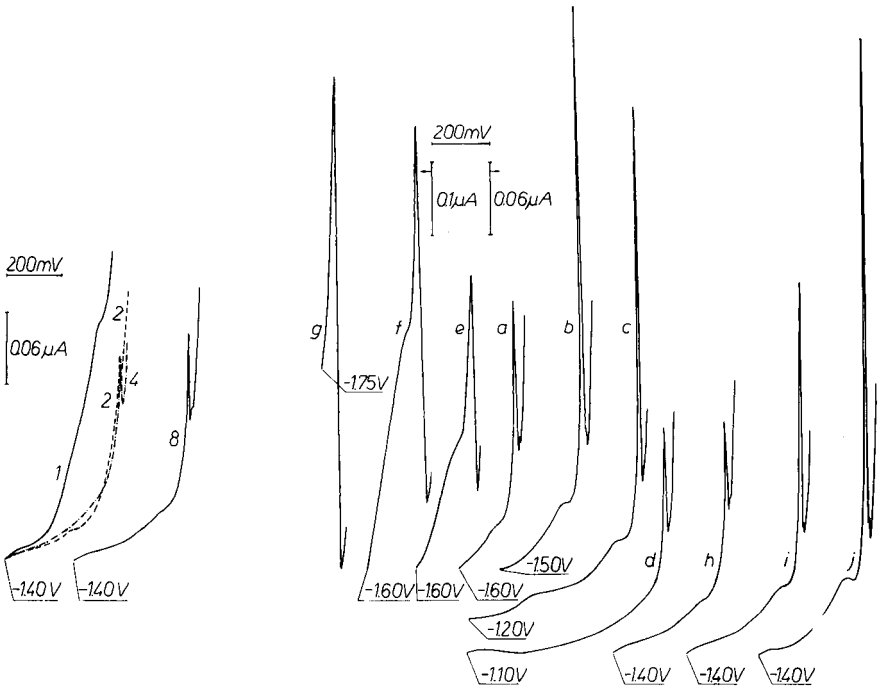

Fig. 2. The influence of adsorption of surfactant 18-14 on the surface of the teflon cell on the peak height of the surfactant. Concentration of surfactant, 0.01 mg l^{-1}; preconcentration at −1.40 V vs. SCE for 10 min. The numbers of the curves denote the sequence of measurements.

Fig. 3. The tensammetric curves of surfactant 18-14 recorded under different conditions. Concentration of surfactant: (a-d) 0.025, (e) 0.10, (f, g) 0.20, (h) 0.010, (i) 0.020, (j) 0.030 mg l^{-1}. Preconcentration time: (a-d) and (h-j) 10 min, (e-g) 5 min. Preconcentration potential given on the curves.

was examined for the case of surfactant 18-14 with a 10-min preconcentration period; a 0.025 mg l^{-1} solution of the surfactant was added to a freshly cleaned teflon cell and deaerated and the usual procedure was applied. After the measurements, the solution was removed, a fresh solution of the same concentration was added and the deaeration and measurement were repeated. This procedure was repeated several times, until a stable peak height was obtained. The results of 1, 2, 4 and 8 repetitions of the procedure are shown in Fig. 2. Almost total adsorption of the surfactant on the teflon cell is evident in the first measurements; however, the results obtained with a glass cell were much worse. To prevent errors arising from such losses, the cell surface was first saturated with surfactant in all later experiments involving low concentrations of surfactant. Such saturation greatly improved the results.

Tensammetric curves of surfactant 18-14 are characterized by the presence of a single narrow peak; typical curves obtained for different concentrations,

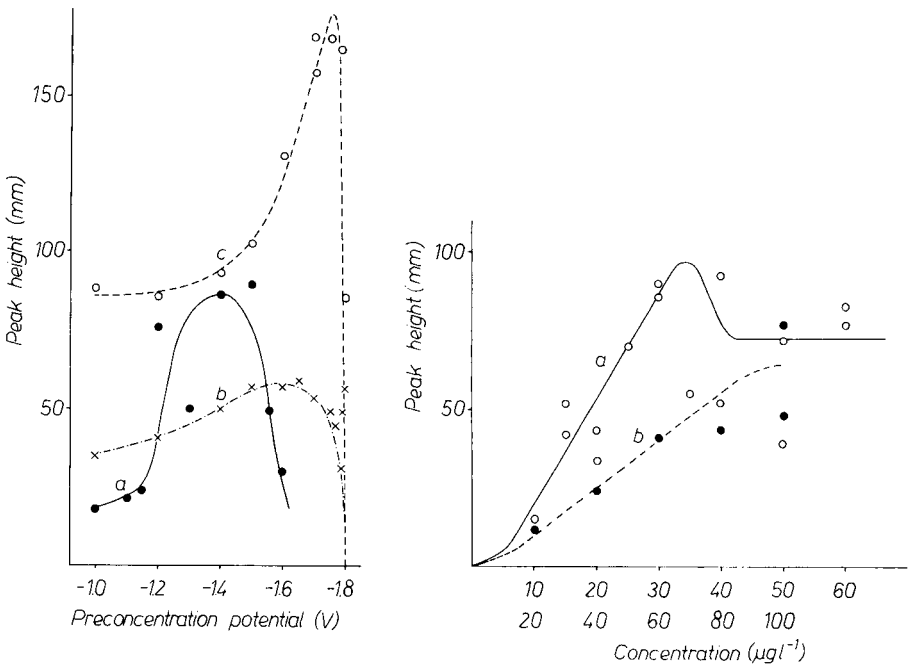

Fig. 4. The dependences of the peak height of surfactant 18-14 on preconcentration potential for different concentrations and preconcentration times. Concentration: (a) 0.025, (b) 0.10, (c) 0.20 mg l^{-1}. Preconcentration time: (a) 10 min, (b, c) 5 min. 100 mm = 400 nA.

Fig. 5. The dependences of the peak height on the concentration of surfactant 18-14 under different preconcentration conditions. Preconcentration potential: (a) −1.40 V, (b) −1.60 V vs. SCE. Preconcentration time: (a) 10 min, (b) 5 min. 100 mm = 480 nA.

preconcentration potentials and times, are shown in Fig. 3. As can be seen, an additional small peak or shoulder appears to the left of the main peak in many curves and grows with increasing surfactant concentration. At a sufficiently high concentration of surfactant, this peak combines with the main narrow peak to form a common bulging peak (curves e and f, Fig. 3). Also, a very small peak to the right of the main peak is visible on many curves.

The dependences of the peak height on the preconcentration potential were investigated for concentrations of surfactant 18-14 of 0.025, 0.10 and 0.20 mg l^{-1} with appropriate preconcentration times. The obtained dependences are shown in Fig. 4 and characteristic tensammetric curves in Fig. 3 (curves a–g). The large scatter of the points at the lowest concentration is probably caused by adsorption of the surfactant on the cell wall. All three dependences (Fig. 4) have a maximum but its position is shifted in a negative direction with increasing surfactant concentration. This effect makes the choice of preconcentration potential more difficult.

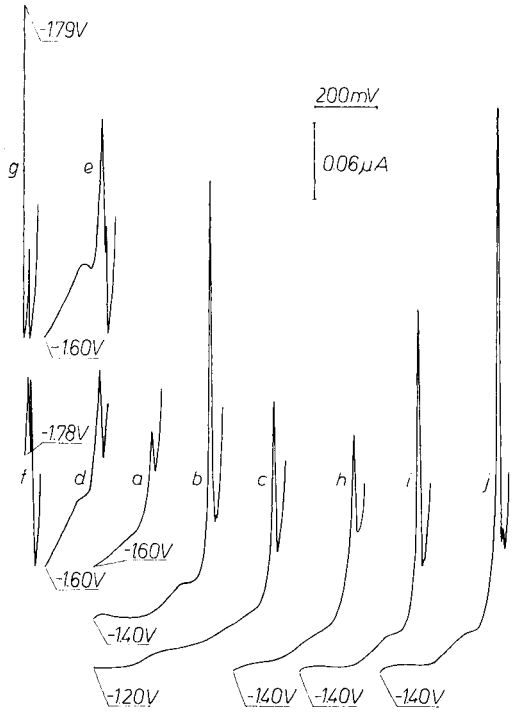

Fig. 6. The tensammetric curves of surfactant 18-10 recorded under different conditions. Concentration of surfactant: (a–c) 0.025, (d) 0.10, (e–g) 0.20, (h) 0.010, (i) 0.020, (j) 0.030 mg l^{-1}. Preconcentration time: (a–c) and (h–j) 10 min, (d–g) 5 min. Preconcentration potential given on the curves.

The relationship between the peak height of surfactant 18-14 and its concentration was also investigated. Two preconcentration potentials and times were selected: −1.40 V (i.e., at about the maximum of curve a in Fig. 4) for 10 min, and −1.60 V vs. SCE (i.e., at about the maximum of curve b) for 5 min. The curves obtained are shown in Fig. 5; three selected tensammetric curves are given as curves (h–j) in Fig. 3. Both curves in Fig. 5 are approximately linear over narrow ranges. Curve (a), which was obtained with the longer preconcentration, has a roughly horizontal section for concentrations higher than 0.03 mg l^{-1}; this indicates saturation of the electrode surface with surfactant under these conditions. Curves (a) and (b) are both essentially sigmoidal; this is more pronounced in the case of curve (a), which was obtained for a longer preconcentration time. Losses of surfactant by adsorption onto the cell may account for this shape and for the great scatter of points in curve (a).

The tensammetric curves for surfactant 18-10 are also basically characterized by the presence of a single narrow peak, as for surfactant 18-14 (Fig. 6). At concentrations $\geqslant$0.20 mg l^{-1}, a second very narrow, more negative peak

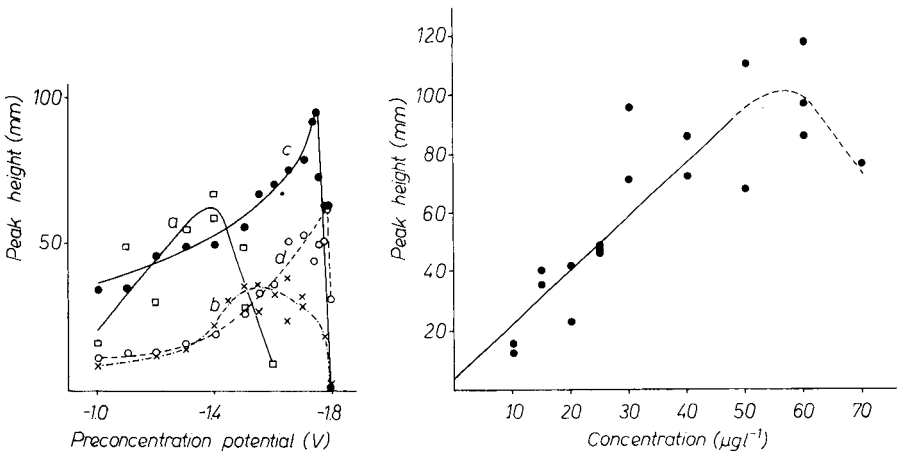

Fig. 7. The dependences of the peak height on the preconcentration potential for surfactant 18-10, as obtained at different concentrations of surfactant: (a) 0.025, (b) 0.050, (c) 0.20 (the first peak), (d) 0.20 mg l^{-1} (the second peak). Preconcentration time: (a) 10 min, (b–d) 5 min. 100 mm = 0.40 μA.

Fig. 8. The dependence of the peak height on the concentration of surfactant 18-10. Preconcentration potential, −1.40 V vs. SCE; preconcentration time, 10 min. 100 mm = 480 nA.

appears on the tensammetric curves (see curves e and f). A trace of this peak is visible on a few curves obtained at lower concentrations. A small hump appears to the left of the main peak but this peak influences the main peak only in the case of curve (e), which was obtained at a concentration of 0.20 mg l^{-1}. The dependence between peak height and preconcentration potential was investigated for 0.025–0.20 mg l^{-1} solutions of surfactant 18-10 (Fig. 7). Two curves are shown for the 0.20 mg l^{-1} because there are two peaks on the tensammetric curve for this concentration (see curves e and f, Fig. 6). Each relationship in Fig. 7 has a maximum, and the positions of the maxima are shifted towards more negative values with the increasing surfactant concentration, as in the case of surfactant 18-14 (cf. Fig. 4). On the basis of Fig. 7, a preconcentration potential of −1.40 V vs. SCE (i.e., at the maximum of curve a) was selected as most suitable for the determination of surfactant 18-10 within the range 0.010–0.050 mg l^{-1}.

A calibration curve obtained for a 10-min preconcentration period is shown in Fig. 8. This curve can be described as approximately linear within the range 0.010–0.050 mg l^{-1}. For higher concentrations of the surfactant, the deviation from the linear relationship can be ascribed to saturation of the electrode surface. The large scatter of the points is again ascribed to the variable effects of adsorption of surfactant on the cell surface at these low concentrations.

In the case of surfactant 18-6, two narrow, overlapping peaks appear on the

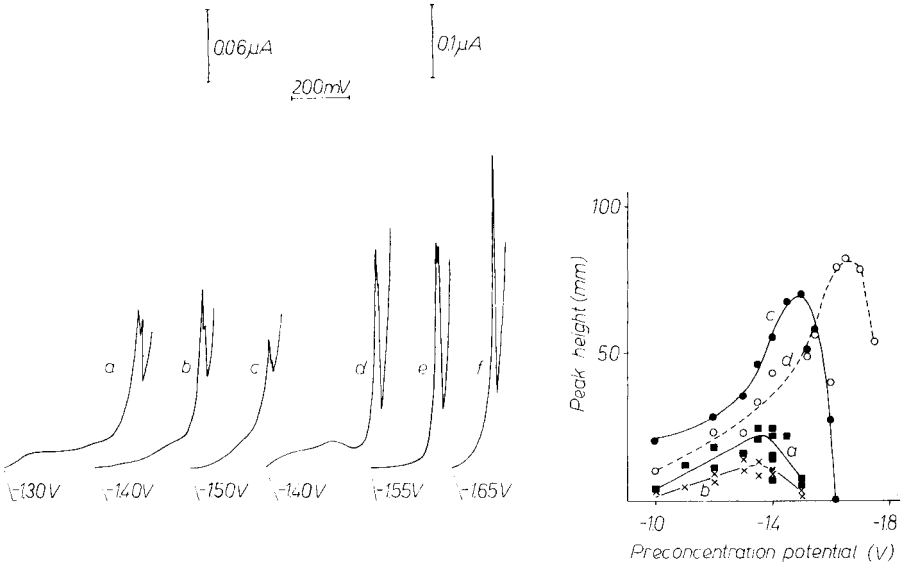

Fig. 9. The tensammetric curves of surfactant 18-6 measured under different conditions. Concentration of surfactant: (a–c) 0.025, (d–f) 0.20 mg l^{-1}. Preconcentration time: (a–c) 10 min, (d–f) 5 min. Preconcentration potential given on the curves.

Fig. 10. The dependences of the peak height on the preconcentration potential for surfactant 18-6, as obtained at different concentrations of surfactant: (a, b) 0.025, (c, d) 0.20 mg l^{-1}; (a, c) the "first" peak, (b, d) the "second" peak. Preconcentration time: (a, b) 10 min, (c, d) 5 min. 100 mm = 400 nA.

tensammetric curves over a wide range of concentration, almost regardless of the preconcentration potential or time (Fig. 9). The influence of preconcentration potential on the heights of both peaks was investigated under the same conditions (Fig. 10). For each concentration of surfactant 18-6, two curves are shown in Fig. 10, corresponding to the two peaks on the tensammetric curves in Fig. 9. Each curve in Fig. 10 has a maximum. The positions of the maxima are again shifted towards negative potentials with increasing surfactant concentration. The ratios of the peaks vary with change of preconcentration potential, especially in the case of the 0.20 mg l^{-1} solution; this is clearly visible both in Fig. 9 (curves d–f) and in Fig. 10 (curves c and d). The distance between the maxima in curves (c) and (d) in Fig. 10 makes it possible to obtain a well-separated peak for surfactant 18-6 (curve f, Fig. 9), as discussed below.

DISCUSSION

The reason for the differences in the behaviour of the investigated surfactants under tensammetric conditions with accumulation on the HMDE is to

be found in the different possibilities for association of these surfactants. This association depends on the ratio between the hydrophilic and hydrophobic parts of the surfactant molecule. In the considered group of surfactants, the ratio of the hydrophilic part of the molecule, which is represented by the oxyethylene chain, to the whole molecule decreases in the following sequence: 6-14, 10-14, 10-10, 18-14, 18-10, 18-6; these ratios are 0.88, 0.82, 0.76, 0.71, 0.64 and 0.53, respectively. In the same sequence, an increase in the tendency of the molecules to associate and so decreasing values of the critical micelle concentration (c.m.c.) are also to be expected. The available literature data on the c.m.c. values, which is rather incomplete, is in agreement with this sequence. The values available are: 1.49 mM for surfactant 10-14 [5], 1.20 mM for surfactant 10-10 [5], 0.06 mM for surfactant 18-14 [6], 0.03 mM for surfactant 18-10 [6], and 0.0002–0.004 mM for surfactant 18-6, depending on the method of measurement used [5]. Although the surfactants examined were polydispersed mixtures (and for that reason in this paper all concentrations have been expressed in mg l^{-1}), the concentrations are easily recalculated to mM for purposes of comparison. The highest investigated concentration (i.e., 0.20 mg l^{-1}) may also be expressed as 0.0002–0.0004 mM, depending on the molecular weight of the surfactant. This is lower by 2–3.5 orders of magnitude than the c.m.c. values for the investigated surfactants, with the exception of surfactant 18-6. In this last case, the concentration of 0.20 mg l^{-1} is 0.000375 mM, which is either the same order of magnitude as the c.m.c. value or about an order of magnitude lower, depending on the method of measuring the c.m.c. It is relevant to add that Miesiąc, who determined the c.m.c. values for surfactant 18-6 [5], used this same polydispersed surfactant for his measurements. Even if the 0.20 mg l^{-1} solution of surfactant 18-6 is of the same order of magnitude as the c.m.c., lower concentrations of this surfactant (e.g., 0.025 mg l^{-1}) are distinctly below the c.m.c. value. Thus, in almost all cases, the concentration of surfactant was much lower than the c.m.c.

In spite of this, only the tensammetric curves of surfactants 6-14, 10-14 and 10-10 are characterized by the presence of a single broad peak, which can be attributed to the monomer form of the surfactant [4,7]. These three surfactants have the highest ratios of the hydrophilic part in the molecule, and for these surfactants the difference between the concentration used (0.20 mg l^{-1}) and the c.m.c. is greatest. Conversely, the tensammetric curves of surfactants having the lowest ratios of the hydrophilic part in the molecule (i.e, surfactants 18-6 and 18-10) are characterized by the presence of two narrow cathodic tensammetric peaks, though in the case of surfactant 18-10 this happens only at distinctly higher concentrations. The more negative of these peaks is often attributed to the micellar form of the surfactant [4]. However, it is doubtful that this is the case for a solution having micelles of the surfactant in the considered range of concentration because the c.m.c. value is much higher than the concentration of the surfactant. Yet, the formation of the micelle occurs

gradually and involves a premicellar stage. It is precisely the premicellar forms, which are smaller than the micelle, that are responsible for the presence of the second cathodic peak in the tensammetric curves of surfactants 18-6 and 18-10. The same conclusion was previously drawn in the case of Triton X-100 [3]. Of course, in the case of surfactant 18-10, a premicellar form (as well as a second peak) appears only at a sufficiently high concentration. Reduction of the concentration of surfactant 18-10 from 0.20 mg l^{-1} to 0.10 mg l^{-1} causes the disappearance of the second peak on the tensammetric curve (see curves e and d, Fig. 6). This means that the new concentration of the surfactant is too low for the formation of a premicellar form of the surfactant. In the case of surfactant 18-6, the curves have two peaks even at the lowest investigated concentration (i.e., 0.025 mg l^{-1}). It is difficult to decide if the strong tendency to association of this surfactant is an original property of the pure surfactant or if it is partly caused by the presence of more than 10% of the free nonoxyethylated n-octadecanol, which would be the core of any premicellar form of the surfactant.

In the case of surfactant 18-6, the use of a sufficiently negative preconcentration potential causes the formation of this peak alone, which is related to the premicellar form of the surfactant (see curve f, Fig. 9). For surfactant 18-10, such a possibility is available only for a very narrow range of preconcentration potential values (see curve g, Fig. 6). The possibility of the separate formation of a second peak provides evidence for the preconcentration of the premicellar form of the surfactant coming from the solution during the preconcentration stage. Another reason for the appearance of the "second" peak could be the formation of the premicellar form from the monomer on the electrode surface during the preconcentration stage. However, the above observation eliminates this possibility because, at a sufficiently negative potential, the monomers do not adsorb on the electrode surface. Thus, only transportation of the premicellar form from the bulk of solution can be the reason for the appearance of the "second" peak on the tensammetric curve. The same conclusion was previously drawn by Retter [8] on the basis of the relation between the tensammetric peaks and the diffusion of different forms of surfactant towards the surface of DME under conditions of classical tensammetry.

The dependences of the peak height on the preconcentration potential, which are very important for a proper choice of this potential, are complicated in the cases of surfactants 18-14, 18-10 and 18-6, but quite simple in the cases of surfactants 6-14, 10-14 and 10-10. For the former set of surfactants, there is a maximum on the plot of peak height vs. preconcentration potential (Figs. 4, 7 and 10); such maxima are more typical of mixtures than of homogeneous substances [2,3]. This is easily explained because surfactants 18-14, 18-10 and 18-6 are polydispersed mixtures. The question then arises as to whether it is reasonable to conduct an investigation with inhomogeneous compounds. However, the present state of synthesis in the area of homogeneous polyoxyethy-

lene alkyl monoethers means that homogeneous standard substances are not available, particularly in the cases of compounds having a long alkyl chain (C_{16}, C_{18}) and a large number of oxyethylene subunits. The availability of such homogeneous surfactants is unlikely to improve in the near future, but the practical situation demands that attempts be made to develop new methods of surfactant analysis. Moreover, commercial surfactants are also very complicated mixtures and the exact content of these inhomogeneous surfactants in waters, sediments, etc., ought to be determined. Accordingly, investigations must be done with such inhomogeneous standard surfactants as are available, both to develop tensammetry with accumulation on the HMDE as an analytical method and to determine the concentrations of polydispersed commercial products. When homogeneous standard substances become available, the properties of the already examined surfactants will have to be retested.

A very important barrier in determining trace concentrations of these surfactants by the proposed method is their adsorption on the cell surface. This phenomenon causes very great scatter in the results, and the precision of such measurements is very poor. Obviously, the effect of adsorption of the surfactant on the cell surface increases with increasing time of contact of the solution with the cell and with decreasing surfactant concentrations. This can be seen by comparison of the results in Fig. 5 obtained for lower concentrations and longer preconcentration time (curve a) with those for higher concentrations and shorter preconcentration time (curve b). The adsorption effects are due to the use of very diluted solutions, rather than to the tensammetric method itself, so that all measurements of trace concentrations of surfactants will be affected, regardless of the measuring technique used. Tensammetry with accumulation on the HMDE seems to be a very useful means of investigating losses of surfactants on the surfaces of different materials.

This work was supported by Research Program CPBP 01.17. We thank Dr. I. Miesiąc for kindly providing the oxyethylated alcohols used in these investigations.

REFERENCES

1 H. Batycka and Z. Łukaszewski, Anal. Chim. Acta, 162 (1984) 207.
2 H. Batycka and Z. Łukaszewski, Anal. Chim. Acta, 162 (1984) 215.
3 Z. Łukaszewski, H. Batycka and W. Zembrzuski, Anal. Chim. Acta, 175 (1985) 55.
4 H. Jehring, Elektrosorptionsanalyse mit der Wechselstrompolarographie, Akademie-Verlag, Berlin, 1974.
5 I. Miesiąc, Doctoral Thesis, Technical University of Poznań, 1983.
6 P. Becher, in M.J. Schick (Ed.), Micelle Formation in Aqueous and Nonaqueous Solutions; Nonionic Surfactants, M. Dekker, New York, 1966.
7 E. Müller and H.D. Dörfler, Z. Chem., 21 (1981) 28.
8 U. Retter, Doctoral Thesis, Akademie der Wissenschaften der DDR, Berlin, 1972.

Analytica Chimica Acta, 202 (1987) 97–116
Elsevier Science Publishers B.V., Amsterdam — Printed in The Netherlands

TENSAMMETRY WITH ACCUMULATION ON THE HANGING MERCURY DROP ELECTRODE
Part 5. The Behaviour of Mixtures of Oxyethylated Alcohols

M. K. PAWLAK and Z. ŁUKASZEWSKI*
Institute of General Chemistry, Technical University of Poznań, 60-965 Poznań (Poland)
(Received 19th September 1986)

SUMMARY

The behaviour of the following mixtures of polydispersed oxyethylated alcohols having a well-defined n-alkyl radical was investigated: 18-14/6-14, 18-14/10-14, 18-14/18-10, 18-14/18-6, 18-6/18-10, 6-14/10-14 and 18-6/18-10/18-14 (the first number denotes the number of carbon atoms in the n-alkyl chain, and the second is the number of oxyethylene subunits). The influence of preconcentration potential in the range more negative than −1.0 V vs. SCE is described in detail. The results are compared with the behaviour of model mixtures of poly(ethylene glycols). The surfactant mixtures 18-14/6-14 and 18-14/10-14 behave similarly to a model mixture of components having sufficiently different properties. Separate peaks for both components appear on the tensammetric curves of the mixtures, but only at certain preconcentration potentials are the peak heights similar to the peak heights for the individual components alone. The behaviour of the 18-14, 18-10 and 18-6 mixtures, in all combinations, depends strongly on whether premicellar (associated) forms are present in the solution. These premicellar forms are indicated by a common very narrow peak on the tensammetric curves. If the monomeric forms predominate (i.e., at low-total surfactant concentrations) the peak heights for the mixtures are approximately additive after preconcentration at a suitable potential. If premicellar forms predominate (as at total concentrations >0.1 mg l^{-1}), the behaviour of the mixtures is a result of competition between the monomeric and premicellar forms in the adsorption process. This behaviour approximates the behaviour of a mixture consisting of sufficiently different components; monomeric forms behave like the first component, and premicellar forms like the second component of the model mixture. For the surfactant mixture 18-14/18-10, which behaves additively under certain conditions, it is possible to determine the total concentration within the range 10–35 $\mu g\ l^{-1}$. The 6-14/10-14 mixture forms a single nonadditive peak.

The determination of components of surfactant mixtures is a much more difficult problem than the determination of individual surfactants. Mixtures of surfactants undergo complicated mutual influences of the components both in the bulk solution [1] and on the electrode surface [2]. The latter effect is peculiarly important for the determination of trace concentrations of surfactants by means of tensammetry with accumulation on the hanging mercury drop electrode (HMDE). The mutual effects of surfactants in the layer adsorbed on the mercury surface lead to very complicated dependences of the heights of the tensammetric peaks on the concentrations of particular components of the mixture and on the preconcentration potential [3–6]. The cre-

0003-2670/87/$03.50

ation of a good working theoretical model for the calculation of these phenomena seems to belong to the future. However, it is possible to establish experimentally the dependences of the peak height on the preconcentration potential or preconcentration time. From a knowledge of such dependences for all the peaks of a mixture, it can be estimated whether or not it is possible to determine some component of the mixture without separation, by means of a proper choice of preconcentration potential. Such possibilities are important, especially because the methods available for the separation of one surfactant from a surfactant mixture are very few or non-existent. The use of a properly chosen preconcentration potential for differentiation of the adsorption conditions for components of the surfactant mixture make it possible to determine trace concentrations of polyethylene glycols (PEG's) having higher molecular weight (m.w.) in the presence of an excess of PEG's having lower m.w. [4] or Triton X-100 [5].

In model systems consisting of unassociated PEG's having different m.w., three different types of behaviour were selected [4]: (1) a mixture consisting of similarly behaving components such that the changes of peak height are additive; (2) a mixture consisting of differently behaving components; and (3) a mixture consisting of similar components which do not behave additively. In the first case, one can determine the sum of concentrations of the components of the mixture, and the peak height responds very similarly to changes in the concentration of each component. In the second case, it is possible to determine one of the components of the mixture in the presence of an excess of the second component by using a properly chosen preconcentration potential. The third case is almost useless from the analytical point of view. In the case of surfactants which undergo association, it was found that both a monomer and an associated form of the surfactant behave like two independent components of the mixture [5]. In such cases, it is possible to record the peak of the premicellar form of the associating surfactant.

The purpose of the present work was to examine the behaviour of mixtures of oxyethylated alcohols under conditions of tensammetry with accumulation on the HMDE. The behaviour of the same individual surfactants has been examined [6]. This study was undertaken both to extend present knowledge about the behaviour of surfactant mixtures, and for the more practical purpose of seeking good methods for the determination of oxyethylated alcohols. The area of investigation necessary for reasonably comprehensive knowledge of the properties of mixtures of oxyethylated alcohols is very wide. Accordingly, this investigation was restricted to selected combinations of components of the mixtures and to one or two selected concentrations of surfactants with a selected range of preconcentration potential. Most of the studies were concerned with two-component mixtures of surfactant 18-14 (see [6]) with some other surfactant. Surfactant 18-14 was selected for extensive investigation because of practical reasons. The n-octadecyl and n-dodecyl radicals are the most fre-

quently represented in alcohols obtained from natural raw materials, but for n-octadecyl the number 14 is close to the optimal number of oxyethylene subunits for many practical properties. Thus the two-component mixtures investigated contained surfactant 18-14 with surfactants 6-14, 10-14, 18-10 and 18-6, i.e., with surfactants having different ratios of the hydrophobic and hydrophilic parts in their molecular structure. These investigations were extended for two two-component mixtures, i.e., 6-14/10-14 and 18-6/18-10, which are mixtures of the two most hydrophilic and two most hydrophobic surfactants, respectively, as well as for a three-component mixture of surfactants 18-14, 18-10 and 18-6.

EXPERIMENTAL

The polarographic equipment was the same as described recently [6]. A small teflon beaker was placed in the glass cell so that the solution was in contact with teflon.

Oxyethylated alcohols were synthesized as described previously [6], by oxyethylation of n-alcohols. They were polydispersed products, and together with the main products these materials contained free n-alcohol and poly(ethylene glycols). The contents of these impurities were listed in Table 1 of Part 4 [6]. Although these surfactants are not very strictly defined, they are better defined than commercial products.

Purified sodium sulphate was used for preparation of the aqueous 0.05 M base electrolyte [6]. All solutions were prepared in water thrice-distilled from quartz. Only freshly distilled water was used. Only glass and quartz vessels were used, except for the teflon measuring cell.

Test solutions were thermostated at 25 °C, introduced into the measuring cell and deaerated with oxygen-free nitrogen, whilst still being thermostated at 25 °C. Preconcentration was done in stirred solution at the required potential with a new mercury drop [6]. The preconcentration time was measured from the moment of drop formation. The tensammetric curve was recorded in the negative direction after a 1-min quiescent period [6].

RESULTS

The dependences of the negative tensammetric peaks on the preconcentration potential were investigated for six two-component mixtures of surfactants (18-14/6-14, 18-14/10-14, 18-14/18-10, 18-14/18-6, 6-14/10-14 and 18-6/18-10) and for one three-component mixture (18-14/18-10/18-6). In all cases, the investigations were restricted to the range of preconcentration potential more negative or equal to −1.0 V vs. SCE. The 18-14/6-14, 18-14/10-14 and 6-14/10-14 mixtures and the three-component mixture were investigated only

at a concentration of 200 $\mu g\ l^{-1}$ for each component in the mixture. In all these cases, the preconcentration time was 5 min. The mixtures 18-14/18-10, 18-14/18-6, and 18-10/18-6 were investigated at two concentration levels and at two preconcentration times. The lower level of concentration was 12.5 $\mu g\ l^{-1}$ for each of the surfactants and the preconcentration time was 10 min. For the higher level of concentration, the preconcentration time was 5 min; for the 18-14/18-10 and 18-14/18-6 mixtures, the concentration of surfactant 18-14 was 100 $\mu g\ l^{-1}$ and that of the second component was 200 $\mu g\ l^{-1}$. For the mixture of surfactants 18-6/18-10, the concentration of each component was 200 $\mu g\ l^{-1}$.

The results are summarized in the form of relationships between the tensammetric peak heights and the preconcentration potential in the various figures. For comparison, the corresponding curves for the individual surfactants alone, taken from Part 4 [6], are given as dashed lines in these figures. Char-

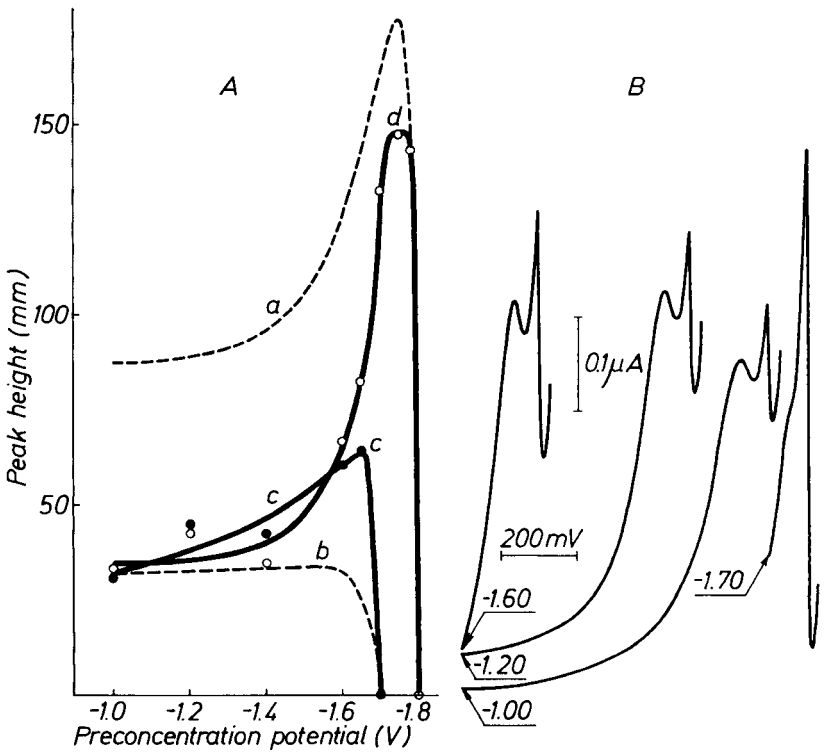

Fig. 1. The dependences of the peak height on the preconcentration potential for the mixture of surfactants 18-14 and 6-14 (A), with examples of the tensammetric curves obtained after preconcentration at the potentials shown on the curves (B). Curves: (a) 200 $\mu g\ l^{-1}$ surfactant 18-14 alone; (b) 200 $\mu g\ l^{-1}$ surfactant 6-14 alone; (c,d) the mixture, 200 $\mu g\ l^{-1}$ each, for the first (●) and second (○) peaks, respectively. Preconcentration time 5 min; 100 mm = 0.40 μA.

acteristic tensammetric curves obtained after different preconcentration potentials are also shown.

Surfactants 18-14 and 6-14

In the case of the mixture of surfactants 18-14 and 6-14, two peaks appear on the tensammetric curve (Fig. 1B), except for the most negative preconcentration potential. The relationships of peak height to preconcentration potential for this mixture and for the individual surfactants are shown in Fig. 1A. With preconcentration potentials of -1.0 to -1.4 V, the height of the less negative of these peaks is similar to the height of the peak of surfactant 6-14 alone, which enables this peak to be assigned to this surfactant in the mixture. The narrower of the two peaks probably can be identified as the peak of surfactant 18-14 in the mixture, but it is lower than the peak of surfactant 18-14 alone at the same concentration within the whole examined range of preconcentration potentials. The reduction in the peak height is comparatively small

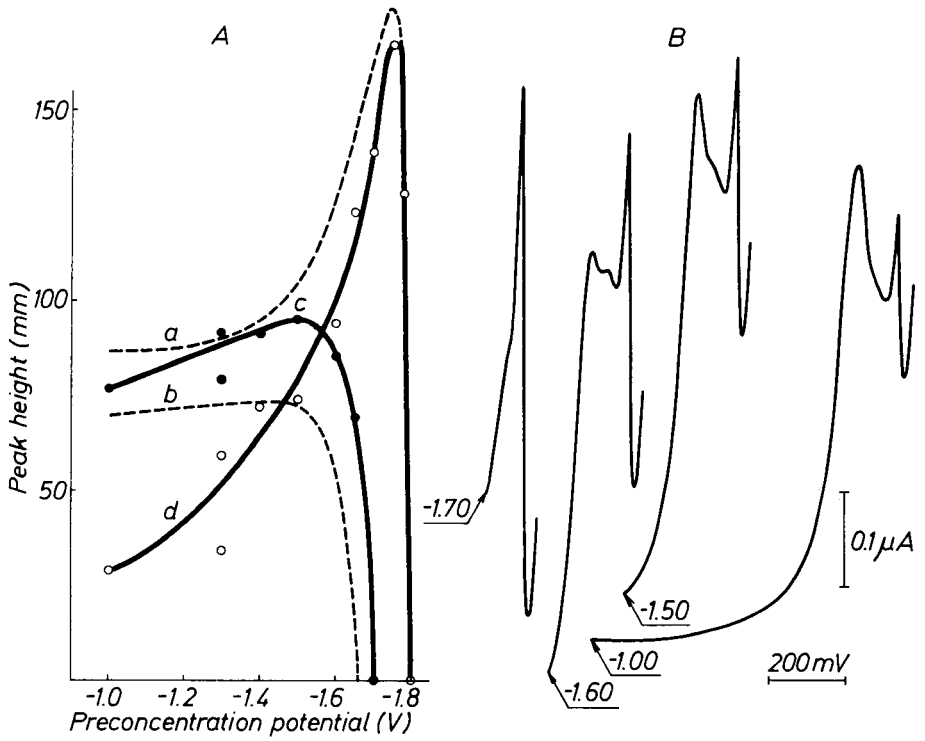

Fig. 2. The dependences of the peak height on the preconcentration potential for the mixture of surfactants 18-14 and 10-14 (A), with examples of the tensammetric curves obtained after preconcentration at the potentials shown on the curves (B). Curves: (a) 200 $\mu g\ l^{-1}$ surfactant 18-14 alone; (b) 200 $\mu g\ l^{-1}$ surfactant 10-14 alone; (c,d) the mixture, 200 $\mu g\ l^{-1}$ each, for the first (●) and second (○) peaks, respectively. Preconcentration time 5 min; 100 mm = 0.40 μA.

within the potential range −1.7 to −1.89 V vs. SCE, where the peak from the mixture is about 85% of the peak height for surfactant 18-14 alone.

Surfactants 18-14 and 10-14

The mixture of surfactants 18-14 and 10-14 yields two peaks on the tensammetric curve (Fig. 2B). The less negative and wider of these peaks can be assigned to surfactant 10-14 in the mixture, from its shape, height and potential. The second, narrower peak can be assigned to surfactant 18-14. The dependence of the peak height on the preconcentration potential for both peaks of this mixture are shown in Fig. 2A (curves c and d, for the first and second peaks, respectively). The dashed curves relate to the individual surfactants. The less negative of the peaks is slightly higher than the corresponding peak of surfactant 10-14 alone for the preconcentration potentials tested. The difference between the peak height of surfactant 10-14 alone and in the mixture

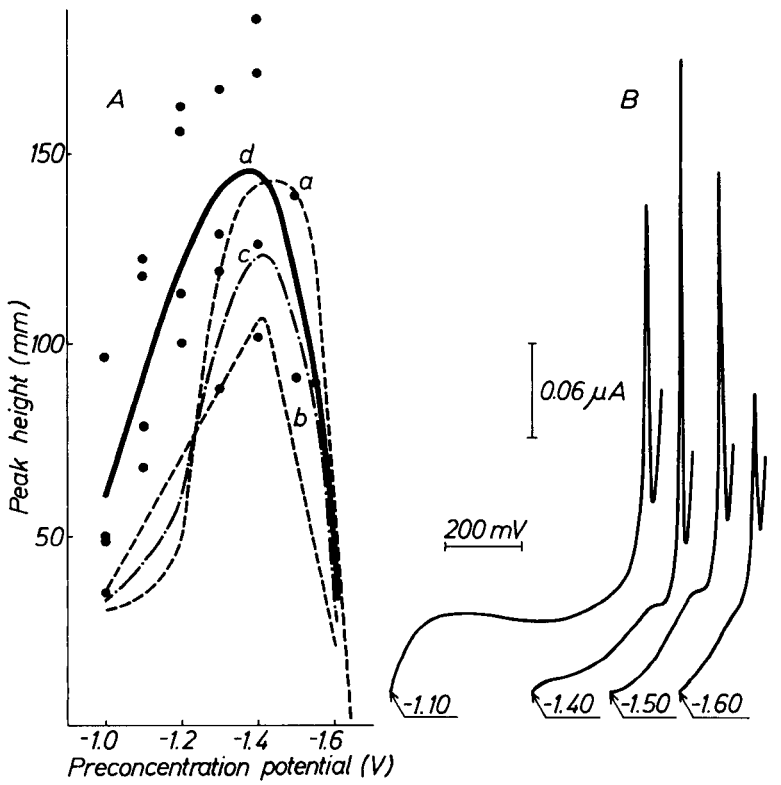

Fig. 3. The dependences of the peak height on the preconcentration potential for a 1:1 mixture of surfactants 18-14 and 18-10 at low total concentration (A), with examples of the tensammetric curves obtained after preconcentration at the potentials shown on the curves (B). Curves: (a) 25 $\mu g\ l^{-1}$ surfactant 18-14 alone; (b) 25 $\mu g\ l^{-1}$ surfactant 18-10 alone; (c) mean of curves a and b; (d) the mixture (25 $\mu g\ l^{-1}$ total). Preconcentration time, 10 min; 100 mm = 0.24 μA.

decreases as the preconcentration potential approaches −1.0 V. It seems probable that further changes of preconcentration potential in the same direction would eliminate this difference. For all the potentials tested, the second peak of the mixture (curve d) is smaller than the corresponding peak of surfactant 18-14 alone (curve a) at the same concentration; but the difference decreases at the most negative potentials tested, beginning from the potential corresponding to the disappearance of the wider peak. A third very small peak appears on the tensammetric curve between the two peaks discussed above when the preconcentration potential is −1.50 or −1.60 V (Fig. 2B).

Surfactants 18-14 and 18-10

For the mixture of surfactants 18-14 and 18-10, one well-defined narrow peak, or two almost overlapping peaks, appear on the tensammetric curves, depending on the total concentration of the mixture. At the lower total con-

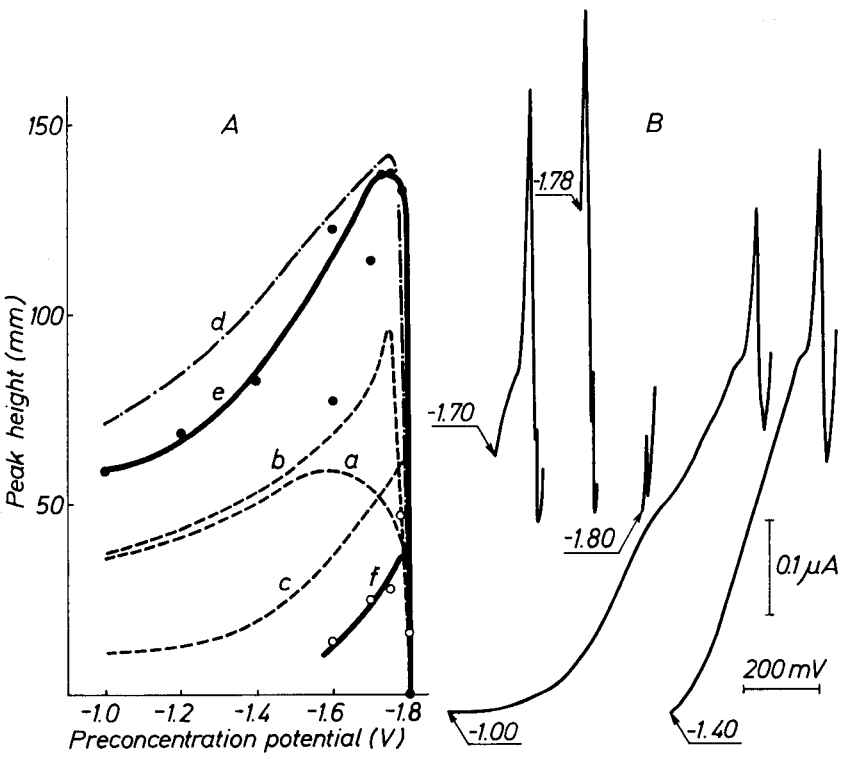

Fig. 4. The dependences of the peak height on the preconcentration potential for a 1:2 mixture of surfactants 18-14 and 18-10 at high total concentration (A), with examples of the tensammetric curves obtained after preconcentration at the potentials indicated on the curves (B). Curves: (a) surfactant 18-14 alone (100 $\mu g\ l^{-1}$); (b,c) surfactant 18-10 alone (200 $\mu g\ l^{-1}$) for the first and second peaks, respectively; (d) mean of curves a and b; (e) the mixture with a total concentration of 300 $\mu g\ l^{-1}$; (f) the small narrow peak of the mixture. Preconcentration time, 5 min; 100 mm = 0.40 μA.

centration ($25\ \mu g\ l^{-1}$) only one peak appears (Fig. 3B), regardless of the preconcentration potential. At the higher total concentration ($300\ \mu g\ l^{-1}$), a second very narrow peak is clearly visible in the tensammetric curves corresponding to preconcentration potentials of -1.70 and -1.78 V (Fig. 4B). This peak can be obtained separately at a sufficiently negative potential (-1.80 V; Fig. 4B). In the range of total concentration of surfactants 10–60 $\mu g\ l^{-1}$ the second peak does not appear. Because the mixture of surfactants 18-14 and 18-10 at sufficiently low concentrations produces only one peak, this peak can be identified as the common peak of the monomers of these surfactants. A second narrow peak, which appears only at a sufficiently high total concentration of the two surfactants, can be asigned to a premicellar form of the surfactants, as in the case of surfactant 18-10 alone [6].

The heights of the peaks for the mixture of surfactants 18-14 and 18-10 plotted against the preconcentration potentials are shown in Figs. 3A and 4A for total surfactant concentrations of 25 $\mu g\ l^{-1}$ and 300 $\mu g\ l^{-1}$, respectively. In Fig. 3A, the points are very scattered, which is caused by adsorption of surfactant on the surface of the measuring cell [6] and makes interpretation of the results difficult. In Fig. 3A, the results obtained for the 1:1 mixture of surfactants 18-14 and 18-10 (curve d) are compared with those obtained for 25 $\mu g\ l^{-1}$ of surfactants 18-14 and 18-10 alone. The strictly additive behaviour of the two surfactants is represented by curve (c), which was constructed by calculation of the mean of curves (a) and (b). The experimentally obtained results (curve d) are obviously higher, and the difference between curves (c) and (d) increases as the preconcentration potential becomes less negative; within the range -1.4 to -1.6 V, the difference is not substantial.

For a higher total concentration of the mixed surfactants 18-14 and 18-10 ($300\ \mu g\ l^{-1}$; Fig. 4A), the experimental points related to the main peak (curve e) are slightly below the curve calculated on the assumption of additivity (curve d). The difference between the calculated and experimental curves is especially small for potentials in the range -1.6 to -1.8 V, where these curves almost overlap. The experimental points for the small narrow peak of the surfactant mixture (curve f) are much lower than the curve for surfactant 18-10 alone at the same concentration.

A calibration curve was prepared in order to check the additivity for the main peak from 1:1 mixtures of surfactants 18-14 and 18-10 having a total concentrations in the range 10–60 $\mu g\ l^{-1}$. The results are shown in Fig. 5 (curve d). For comparison, the linear calibrations for the individual surfactants (reproduced from Part 4) are given (curves a and b). The results for the mixture can be described as approximately linear; the negative intercept may indicate a slightly sigmoidal character of the relationship, as in the case of surfactant 18-14 alone [6]. The slope and the intercept of the calibration curve have mean values between the corresponding values for surfactants 18-14 and 18-10 alone

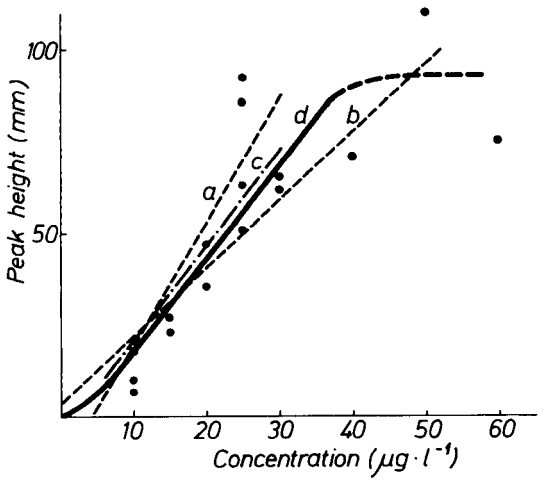

Fig. 5. The dependence of the peak height on the total concentration of 1:1 mixtures of surfactants 18-14 and 18-10. Curves: (a) surfactant 18-14 alone; (b) surfactant 18-10, alone; (c) mean of curves a and b; (d) the mixture. Preconcentration time, 10 min; preconcentration potential, −1.40 V vs. SCE; 100 mm = 0.48 μA.

(compare curves d and c). This supports the conclusion about the additivity of the behaviour of surfactants 18-14 and 18-10 under the conditions of the experiment. At the higher concentrations of the mixture, the response is not linear (Fig. 5) because of saturation of the electrode surface with surfactant, as previously discussed [6].

Surfactants 18-14 and 18-6

The mixture of surfactants 18-14 and 18-6 produces two very closely located narrow peaks on the tensammetric curves (Figs. 6B and 7B). Only when a high total concentration of the mixture is examined by using very negative preconcentration potentials is it possible to obtain a separate extremely narrow high second peak (see the curve corresponding to −1.79 V in Fig. 7B). The first of these peaks can be identified as a common peak of the monomer form of the surfactants present in the mixture; the second peak seems to belong to the premicellar form of the surfactants, produced in the mixture, as in the case of surfactant 18-6. However, it may be that free n-octadecanol, about 10% of which is present in surfactant 18-6, participates in the formation of the peak related to the premicellar form.

The reactions of the tensammetric curves to changes in preconcentration potential present very different pictures, depending on the total concentration of the surfactant mixture. When the total concentration of the 1:1 mixture was very low ($25\ \mu g\ l^{-1}$) and a 10-min preconcentration time was used, the second peak changed irregularly and was significantly lower than the first, less nega-

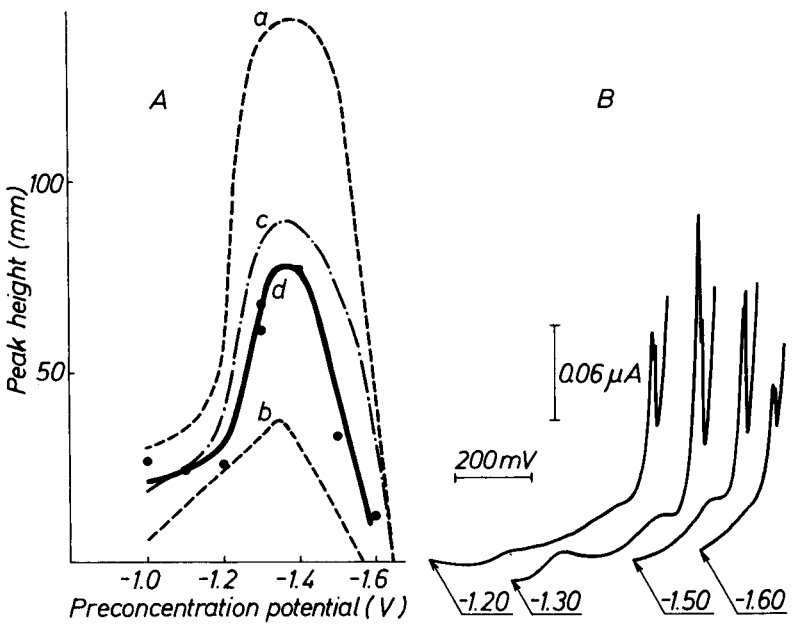

Fig. 6. The dependences of the peak height on the preconcentration potential for a 1:1 mixture of surfactants 18-14 and 18-6 at low total concentration (A), with examples of the tensammetric curves obtained at different preconcentration potentials (B). Curves: (a) 25 $\mu g\, l^{-1}$ surfactant 18-14 alone (first peak); (b) 25 $\mu g\, l^{-1}$ surfactant 18-6 alone (first peak); (c) mean of curves a and b; (d) the mixture (25 $\mu g\, l^{-1}$ total). Preconcentration time, 10 min; 100 mm = 0.24 μA.

tive peak. Because of this irregularity, the relationship between the peak height and the preconcentration potential (Fig. 6A) concerns only the first peak. In contrast, when the total concentration of the mixture was high (300 $\mu g\, l^{-1}$ at a ratio of 1:2) and the preconcentration time was 5 min, the second peak plays a more important role in the tensammetric curve than the first peak (Fig. 7). Accordingly, Fig. 7A concerns both peaks for the mixture.

The relationships for the mixtures of these surfactants (Figs. 6A and 7A) are also completely different at different total concentrations. In Fig. 6A, which concerns the lower total concentration, the experimental points (and curve d) are compared with the corresponding relationships for the individual surfactants [6] and with the strictly additive behaviour of the examined mixture (curve c). Within the preconcentration potential range -1.0 to -1.3 V vs. SCE, the experimental points are similar to the values for additive behaviour, but in the range -1.3 to -1.6 V, the values are lower than those expected for additive behaviour.

For the higher total concentration of the same surfactants (Fig. 7A), the relationship is completely different. Within the potential range tested, the first peak, which is probably a common peak of the monomers for both surfactants,

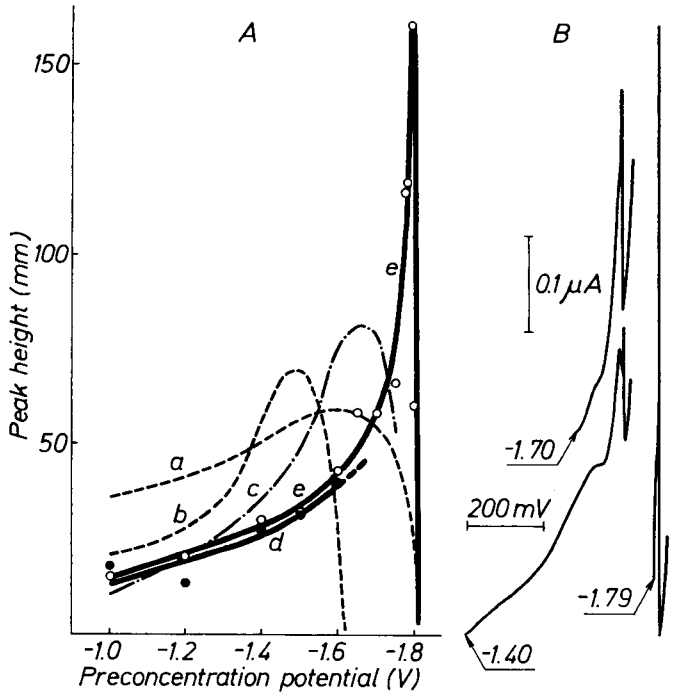

Fig. 7. The dependences of the peak height on the preconcentration potential for a 1:2 mixture of surfactants 18-14 and 18-6 at high total concentration (A), with examples of the tensammetric curves obtained at different preconcentration potentials (B). Curves: (a) 100 $\mu g\, l^{-1}$ surfactant 18-14 alone; (b) 200 $\mu g\, l^{-1}$ surfactant 18-6 alone (first peak); (c) 200 $\mu g\, l^{-1}$ surfactant 18-6 alone (second peak); (d,●) the first peak of the mixture (300 $\mu g\, l^{-1}$ total); (e,○) the second peak of the mixture. Preconcentration time, 5 min; 100 mm = 0.40 μA.

is smaller than either the sum of the peak heights for the individual surfactants or the height of each of these peaks separately (curve d). The second, very narrow peak of the mixture, can be assigned to the premicellar forms of the surfactants in the mixture. The relationship of this peak (curve e) is completely different from the corresponding curve for surfactant 18-6 alone (curve c). The spectacular increase of the second peak of the mixture within the range of preconcentration potentials closest to the desorption potentials of both surfactants 18-6 and 18-14 (i.e., −1.75 to −1.79 V) is especially surprising.

Surfactants 18-10 and 18-6

These surfactant mixtures produce two closely located narrow peaks on the tensammetric curves (Figs. 8B and 9B), as in the case of mixtues of surfactants 18-14 and 18-6. However, with a very negative preconcentration potential, a high total concentration of the mixture produces only the second, more negative of these peaks (see curve corresponding to a potential of −1.79 V, Fig. 9B). The first (less negative) peak for the mixture can be identified as a

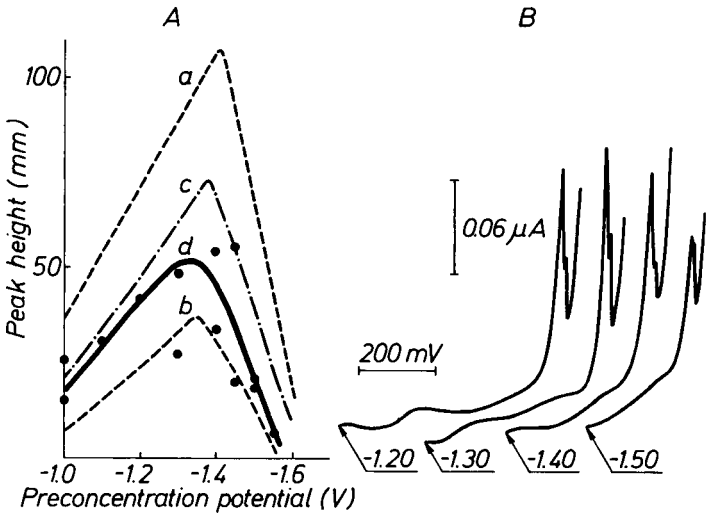

Fig. 8. The dependences of the peak height on the preconcentration potential for a 1:1 mixture of surfactants 18-10 and 18-6 at low total concentration (A), with examples of the tensammetric curves obtained at different preconcentration potentials (B). Curves: (a) 25 $\mu g\, l^{-1}$ surfactant 18-10 alone (first peak); (b) 25 $\mu g\, l^{-1}$ surfactant 18-6 alone (first peak); (c) mean of curves, a and b; (d) first peak of the mixture (25 $\mu g\, l^{-1}$ total). Preconcentration time, 10 min; 100 mm = 0.24 μA.

common peak of the monomers of the surfactants present, and the second as a common peak of the premicellar forms of these surfactants. The relationships between peak height and preconcentration potential are quite different for low (25 $\mu g\, l^{-1}$, Fig. 8A) and high (400 $\mu g\, l^{-1}$, Fig. 9A) total concentrations, as was the case for surfactants 18-14 and 18-6 (see above). In Fig. 8A, the results obtained for the first peak are compared with the corresponding relationships for the individual surfactants. The results for the mixture (curve d) are only slightly lower than those corresponding to strictly additive behaviour (curve c) in the preconcentration potential range -1.0 to -1.3 V vs. SCE. Within the range -1.3 to -1.6 V, the results resemble those for surfactant 18-6 alone (curve b) rather than the additive behaviour. The height of the second, more negative peak of the mixture changed irregularly with varying preconcentration potential and so is not shown.

For the high total concentration of the mixture of these surfactants (400 $\mu g\, l^{-1}$ at the ratio 1:1), the results were again compared in a similar way. In this case, the second peak is important and both the first and second peaks are considered in Fig. 9A. Both these peaks behave quite differently from the individual surfactants. The first, less negative of these peaks (again a common

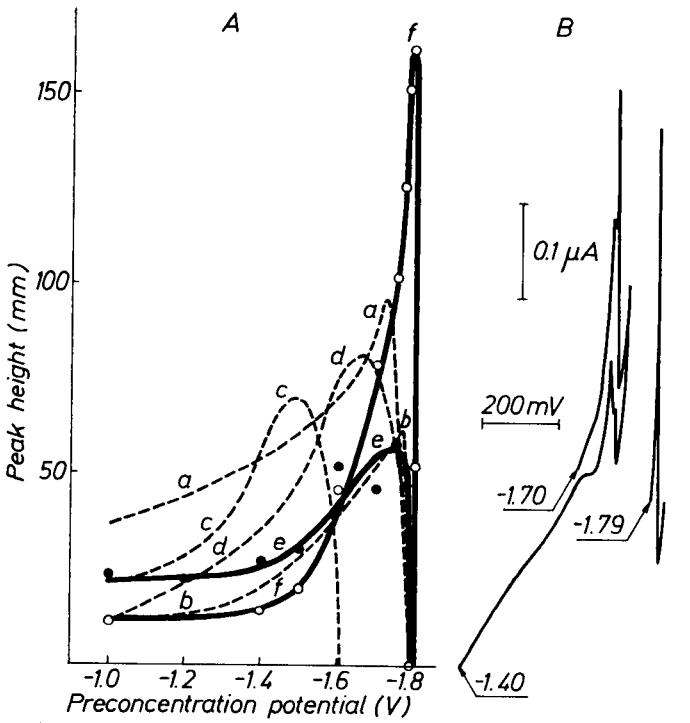

Fig. 9. The dependences of the peak height on the preconcentration potential for a 1:1 mixture of surfactants 18-10 and 18-6 at high total concentration (A), with examples of the tensammetric curves obtained at different preconcentration potentials (B). Curves: (a) surfactant 18-10 alone (200 $\mu g\ l^{-1}$) for the first peak; (b) as in (a) but for the second peak; (c) surfactant 18-6 alone (200 $\mu g\ l^{-1}$) for the first peak; (d) as in (c) but for the second peak; (e,●) first peak of the mixture (400 $\mu g\ l^{-1}$ total); (f,○) second peak of the mixture. Preconcentration time, 5 min; 100 mm = 0.40 μA.

peak of the monomers) is much lower than the sum of the corresponding peak heights for the individual surfactants; at most potentials, it is even lower than the peaks for each surfactant alone (compare curve e with curves a and c). The second peak (probably from the premicellar forms) is also much lower than the summed heights of the individual peaks of the surfactants (compare curve f with curves b and d) at most preconcentration potentials tested. However, at potentials located between the desorption potentials of the two surfactants (i.e., −1.6 to −1.8 V) this second peak increases suddenly, as in the case of the mixture of surfactants 18-14 and 18-6 (Fig. 7A).

Mixtures of surfactants 18-14, 18-10 and 18-6

The behaviour of the three-component mixture of surfactants 18-14, 18-10 and 18-6 (1:1:1) was investigated only at a comparatively high total concentration (600 $\mu g\ l^{-1}$). This behaviour is similar to the case just discussed. Two

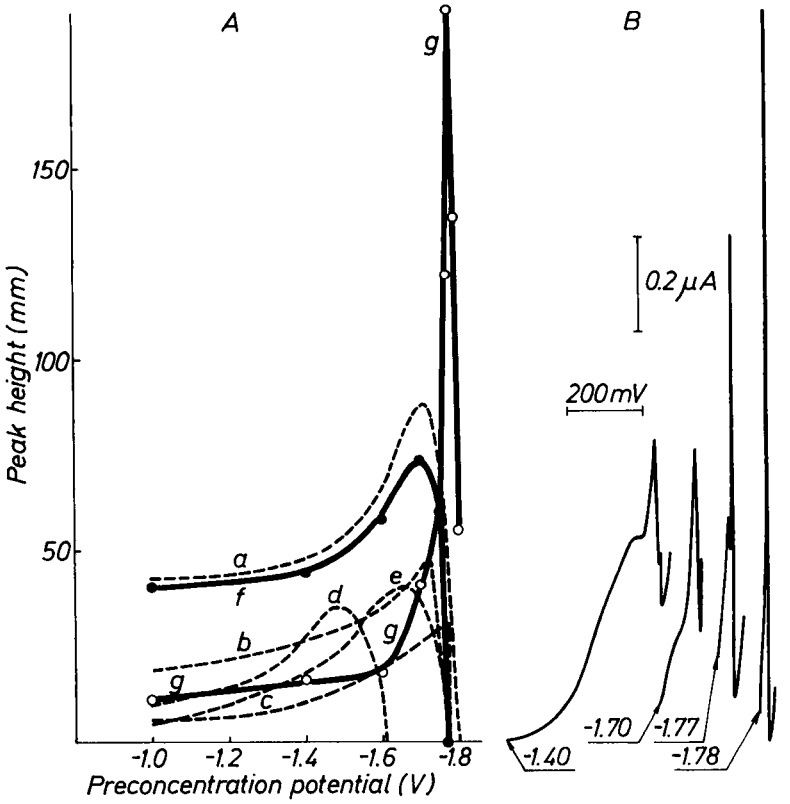

Fig. 10. The dependences of the peak height on the preconcentration potential for a 1:1:1 mixture of surfactants 18-14, 18-10 and 18-6 (A), with examples of tensammetric curves obtained at different preconcentration potentials (B). Curves: (a) surfactant 18-14 alone (200 $\mu g\, l^{-1}$); (b,c) surfactant 18-10 alone (200 $\mu g\, l^{-1}$) for the first (b) and second (c) peaks; (d,e) surfactant 18-6 alone (200 $\mu g\, l^{-1}$) for the first (d) and second (e) peaks; (f,●) first peak of the mixture; (g,○) second peak of the mixture. Total concentration of the mixture, 600 $\mu g\, l^{-1}$; preconcentration time, 5 min; 100 mm = 0.80 μA.

narrow peaks appear on the tensammetric curves for the mixture (Fig. 10B); the ratio of their heights depends on the preconcentration potential. Additionally, to the left of these peaks, a bulge is visible, which is also characteristic for surfactant 18-14 alone. The two narrow peaks are similar to the peaks of surfactants 18-10 and 18-6 alone but the behaviour of these peaks with varying preconcentration potentials is completely different from that for the separate surfactants. The dependences are shown in Fig. 10A. Curve (f), corresponding to the less negative of the peaks for the mixture, is similar to curve (a) for surfactant 18-14 alone, but it is slightly lower than that curve and is obviously much lower than the sum of the corresponding curves for the three individual surfactants. For most preconcentration potentials, the second peak for the

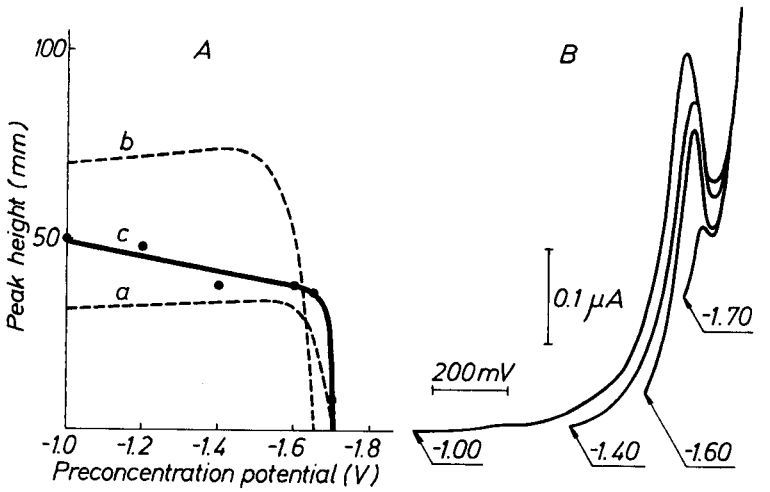

Fig. 11. The dependence of the peak height on the preconcentration potential for a 1:1 mixture of surfactants 6-14 and 10-14 (A), with examples of tensammetric curves obtained at different preconcentration potentials (B). Curves: (a) surfactant 6-14 alone (200 $\mu g\, l^{-1}$); (b) surfactant 10-14 alone (200 $\mu g\, l^{-1}$); (c) the mixture (total concentration 400 $\mu g\, l^{-1}$). Preconcentration time, 5 min; 100 mm = 0.40 μA.

mixture (curve g) is also lower than the sum of the second peak heights of the separate components. However, for preconcentration potentials close to the desorption potential (i.e., -1.75 to -1.80 V), the second peak suddenly increases spectacularly.

Surfactants 6-14 and 10-14

For the mixture of surfactants 6-14 and 10-14, i.e., both surfactants have a distinct excess of hydrophilic oxyethylene chain in the molecular structure, only one wide peak appears on the tensammetric curves (Fig. 11B) This peak is similar in shape and potential to the peaks obtained for the individual components of the mixture. Thus, this peak cannot be assigned to either surfactant but rather is a common peak. The dependence of peak height on the preconcentration potential is shown in Fig. 11A (curve c). As can be seen, the peak height for the mixture is much smaller than the sum of the heights for the separate components. This is, therefore, a case of nonadditivity of tensammetric peaks.

DISCUSSION

The investigated mixtures of polyoxyethylene n-alkyl monoethers represent different types of behaviour under conditions of variable preconcentration potential.

The components of the mixtures of surfactants 18-14/6-14 and 18-14/10-14 have different adsorptive properties. In contrast to the other cases considered above, each surfactant in these mixtures forms a separate peak on the tensammetric curve (see Figs. 1B and 2B). The less negative of these peaks belongs to surfactant 6-14 or 10-14. Within a defined range of preconcentration potential, this peak is slightly higher in the presence of surfactant 18-14 than in the case of surfactant 6-14 or 10-14 alone. However, at preconcentration potentials close to the desorption potential of surfactant 6-14 or 10-14 (curves c, Figs. 1A and 2A), a maximum appears, which is typical of the behaviour of many mixtures. The peak of surfactant 18-14 (the second peak) is decreased by the presence of surfactant 6-14 to 10-14; only at preconcentration potentials more negative than the desorption potential of surfactant 6-14 or 10-14 does the peak for surfactant 18-14 increase and become only slightly lower than it is when the other surfactant is absent. Thus, the use of a properly selected preconcentration potential provides, albeit with some error, a determination of the first or second components of the mixture. The surfactant mixtures 18-14/6-14 and 18-14/10-14 can thus be classified as mixtures of surfactants having sufficiently different properties that one component can be estimated in the presence of the other, as in the case of PEG-9000 in the presence of either PEG-1500 [4] or Triton X-100 [5]. There are, however, distinct differences in the behaviour of mixtures of the present surfactants on the one hand, and mixtures of PEG's or PEG-9000 and Triton X-100 on the other hand. With regard to the weaker surfactant in the mixture (i.e., the one having less negative desorption potential), for the model mixture of PEG-1500 and PEG-9000 [4] the peak for PEG-1500 in the mixture was lower than the peak for PEG-1500 alone, over the whole range of preconcentration potentials tested. The weaker surfactant Triton X-100 behaved similarly in the presence of the stronger surfactant PEG-9000 [5]. With the mixtures of the polyoxyethylene n-alkyl monoethers 18-14/6-14 and 18-14/10-14, the peaks for the weaker surfactant (i.e., 6-14 or 10-14) were slightly higher than the corresponding peaks for these surfactants alone. The behaviour of the stronger surfactant in the mixture (i.e., the one having more negative desorption potential) also differs to some extent for the 18-14/6-14 and 18-14/10-14 mixtures compared to the model mixture of PEG's. The presence of PEG-1500 in the mixture decreases the peak for PEG-9000 within the adsorption range of PEG-1500, but causes a very strong increase in the peak height for PEG-9000 when the preconcentration potential is located between the desorption potentials of PEG-1500 and PEG-9000. Triton X-100 similarly influences the peak for PEG-9000; but in this case only the increase in the peak for PEG-9000 is well expressed. In the cases of the 18-14/6-14 and 18-14/10-14 mixtures, the weaker surfactant decreases the peak height of the stronger surfactant (18-14) within the range of adsorption of surfactants 6-14 or 10-14. This property is the same as in the case of the model mixture of PEG-1500 and PEG-9000. At a preconcentration

potential more negative than the adsorption range of surfactants 6-14 or 10-14, the peak height for surfactant 18-14 is increased (Figs. 1A and 2A), but this increase is less than in the case of the PEG mixture, and the peak height for surfactant 18-14 does not exceed the peak height for this surfactant alone.

The differences described above between the behaviours of the PEG-1500/PEG-9000 mixture and the 18-14/6-14 and 18-14/10-14 mixtures, as well as some differences between the model PEG mixture and the Triton X-100/PEG-9000 mixture, indicate that several subtypes of behaviour can be identified.

Three general properties can be selected for mixtures of components having sufficiently different behaviour under conditions of tensammetry with accumulation on the HMDE: (i) peaks for both components of the mixture are obtained when preconcentration is done at a potential less negative than the desorption potential of the weaker surfactant in the mixture; (ii) the peak for the stronger surfactant in the mixture is decreased when the preconcentration potential is less negative than the desorption potential of the weaker surfactant (though in the case of the Triton X-100/PEG-9000 mixture, the peak for PEG 9000 is only slightly decreased); and (iii) the peak height for the stronger surfactant in the mixture is increased after preconcentration at potentials between the desorption potentials of the weaker and stronger surfactants. The differences in the behaviour of the particular subtypes are related to the following properties: (i) the peak height for the weaker surfactant can be either increased or decreased by the stronger surfactant compared to the response for the weaker surfactant alone; (ii) the peak height for the stronger surfactant, which is greatly increased by the weaker surfactant if the preconcentration potential is located between the desorption potentials of the weaker and stronger surfactants, can still be decreased under some conditions, compared to the response for the stronger surfactant.

The cases discussed above have little practical significance and were considered mainly to improve knowledge of surfactant mixtures. For that reason, these mixtures were not investigated in the detail necessary for analytical purposes.

In the cases of the mixtures of surfactants 18-14, 18-10 and 18-6, in all combinations, there were no peaks belonging to particular components of these mixtures but rather one or two closely located peaks, which are common peaks. The less negative of these peaks can be attributed to a common peak of the monomeric forms of the surfactants; the second peak is probably a common peak of the premicellar forms of the surfactants. In considering the behaviour of the binary or ternary mixtures of surfactants 18-14, 18-10 and 18-6, it must be recalled that these surfactants are not pure substances, but polydispersed products. For example, surfactant 18-10 consists of about twenty individual derivatives of n-octadecanol, having equal, lower or higher numbers of oxyethylene subunits than the average value of 10. Surfactants 18-14, 18-10 and

18-6 consist essentially of the same pure chemical compounds, but in different ratios. That is why in these mixtures one common peak of the monomeric forms is formed. The question arises if the behaviour of this common peak is additive, as in the case of the mixture of PEG-9000 with PEG-20000 [4]. The answer is more easily given for a low total concentration of surfactant, in which case only the monomer is present in the solution and there are no complications connected with the competition of the monomer and associated forms of the surfactant (e.g., with the mixture of surfactants 18-14 and 18-10), or the monomer is in excess compared to the associated forms (as for the mixtures 18-14/18-6 and 18-10/18-6).

In the case of the 18-14/18-10 mixture, the calibration plots show the additivity of the behaviour of the two surfactants at a preconcentration potential of -1.40 V vs. SCE (Fig. 5). The picture becomes slightly different when the plot of experimental peak height vs. preconcentration potential for the same surfactant mixture is compared with the corresponding plot calculated on the assumption of additivity of behaviour (curves d and c, Fig. 3A). The experimental results are higher than the calculated ones, and this difference increases as the preconcentration potential is shifted towards less negative values. Although these results suffer from severely scattered experimental points, and the precision of the measurements on which curves (c) were based was similarly poor, close study of Fig. 3A suggests that additivity of the peak heights is maintained within a certain range of the most negative preconcentration potentials; outside that range, the experimental results are higher than the calculated values, i.e., the peaks are not additive.

The situations for the 18-14/18-6 and 18-10/18-6 mixtures are slightly different. Within a certain range of preconcentration potential, the experimental curves are lower than those expected if full additivity is assumed (see Figs. 6A and 8A). This difference in the behaviours of the 18-14/18-10 mixture on the one hand, and the 18-14/18-6 and 18-10/18-6 mixtures on the other hand, is probably caused by the presence of premicellar forms in the solution in the latter case. The presence of premicellar forms in the latter cases is evidenced by the appearance of the second very narrow peaks on the tensammetric curves (see Figs. 6B and 8B). The monomeric and the premicellar forms probably compete in the adsorption/desorption process on the mercury surface, which causes the deviation from peak-height additivity. However, these deviations are not very great because at a total concentration of 25 $\mu g\, l^{-1}$, the concentration of the premicellar forms is lower than that of the monomeric forms; additionally, the larger premicellar forms must diffuse more slowly to the electrode surface than the monomeric forms. The differences between the experimental and calculated peak heights are clearly visible in all the above-mentioned cases, but they are not very significant and it is possible to find suitable preconcentration potentials at which the errors caused are minimal. Under such conditions, tensammetry with accumulation on the HMDE can be used for

determining the total concentration of polyoxyethylene n-octadecyl monoethers within the range of concentrations lower than 30–50 $\mu g\, l^{-1}$, i.e., lower than the concentrations needed to saturate the electrode surface with the surfactant. When the total concentrations of the mixtures of polyoxyethylene n-octadecyl monoethers exceeded 100 $\mu g\, l^{-1}$, the tensammetric peaks were generally not additive. This can be ascribed to competition between the monomeric and premicellar forms of these surfactants or to mutual influences in the adsorbed layer. Preconcentration for 5 min at a total concentration exceeding 100 $\mu g\, l^{-1}$ is enough to saturate the electrode surface, i.e., to give an adsorptive equilibrium state. This can be concluded from the calibration curves for surfactants 18-14 and 18-10 alone [6] or for the mixture of these surfactants (Fig. 5). However, the electrode surface is quickly covered by the smaller, faster monomer forms. Further preconcentration (i.e., the last part of the preconcentration) probably leads to partial displacement of the monomeric forms from the surface layer by the premicellar forms, which diffuse more slowly to the mercury surface but predominate in the solution and are probably stronger surfactants. The last supposition is based on the more negative desorption potential of the premicellar forms compared to the monomer. The conditions which govern competition between the monomer and premicellar forms can be changed by utilizing the differentiating action of the preconcentration potential. The relationships between the peak height and the preconcentration potential for the surfactant mixtures 18-14/18-6, 18-10/18-6 and 18-14/18-10/18-6 at sufficiently high total concentrations (see Figs. 7A, 9A and 10A) can be classified as the same type of behaviour as is shown by the model mixture consisting of sufficiently different components. However, in these cases, the monomeric and the premicellar forms of the surfactants compete, rather than the different components of the mixture. In Figs. 7A, 9A and 10A, the peaks of the monomers (i.e., the first peaks) are much lower than the expected values, presumably because of the presence of the premicellar forms (i.e., the stronger surfactant). Similarly, PEG-9000 influenced the peak of PEG-1500 in a model mixture [4]. The monomers also influence the peak for the premicellar forms. Within the range of their adsorption, the monomers decrease the peak height for the premicellar forms (i.e., the second peak). The monomeric forms, outside the range of their adsorption, cause a spectacular increase in the peak height for the premicellar forms. A very narrow high single peak appears on the tensammetric curves corresponding to these conditions (see Figs. 7B, 9B and 10B). The peak of PEG-9000 (i.e., the stronger surfactant in the model mixture of PEG-1500 and PEG-9000) behaves similarly [4].

The behaviour of the surfactant mixture 18-14/18-10 differs significantly. In the considered range of total concentration of surfactants, the concentration of premicellar forms is comparatively low and the premicellar forms have a comparatively weak effect on the peak of the monomer. Thus the first peak, which corresponds to the monomer, behaves almost additively in this case. The

predominance of the monomer forms decreases the peak height of the premicellar forms (see curve f, Fig. 4A).

The formation of the premicellar forms is a stage in the process of formation of the micelle which is still difficult to observe. The use of tensammetry with accumulation on the HMDE offers the chance for better examination of this important stage. That is why studies of the behaviour of the surfactants and their mixtures are important, not only within the range for predominance of the first peak (monomer), but also within the range of higher concentrations corresponding to the production of premicellar forms.

The case of the surfactant mixture 6-14/10-14 is completely different from all previously considered mixtures. This mixture forms one common nonadditive peak (Fig. 11). Formally, this case can be classified as a mixture consisting of similar components which behave nonadditively, but it is quite different from the model mixture of PEG-4000, PEG-6000, PEG-9000 and PEG-20000. It is probably a subtype of nonadditive behaviour of surfactant mixtures but this needs more detailed investigation.

This work was supported by Research Program CPBP 01.17. We thank Dr. I. Miesiąc for kindly providing the oxyethylated alcohols used in these investigations.

REFERENCES

1 P. Becher, in M.J. Schick (Ed.), Nonionic Surfactants, M. Dekker, New York, 1966.
2 H. Jehring, Elektrosorptionsanalyse mit der Wechselstrompolarographie, Akademie Verlag, Berlin, 1974.
3 H. Batycka and Z. Łukaszewski, Anal. Chim. Acta, 162 (1984) 207.
4 H. Batycka and Z. Łukaszewski, Anal. Chim. Acta, 162 (1984) 215.
5 Z. Łukaszewski, H. Batycka and W. Zembrzuski, Anal. Chim. Acta, 175 (1985) 55.
6 M.K. Pawlak and Z. Łukaszewski, Anal. Chim. Acta, 202 (1987) 85.

Analytica Chimica Acta, 202 (1987) 117–122
Elsevier Science Publishers B.V., Amsterdam — Printed in The Netherlands

SIMULTANEOUS DETERMINATION OF MERCURY(II), COPPER(II) AND BISMUTH(III) IN URINE BY FLOW CONSTANT-CURRENT STRIPPING ANALYSIS WITH A GOLD FIBRE ELECTRODE

HUANG HUILIANG[a], DANIEL JAGNER* and LARS RENMAN

Department of Technical Analytical Chemistry, Chemical Center, P.O. Box 124, S-221 00 Lund (Sweden)

(Received 6th April 1987)

SUMMARY

Urine samples are treated with concentrated nitric acid and potassium permanganate at 70°C for 10 min prior to injection. The flow electrode system consists of a 10-μm diameter gold fibre working electrode, a glassy carbon reference electrode and a platinum counter electrode. In the fully automated constant-current stripping procedure, the gold fibre is first covered with a fresh gold film after which the sample is electrolyzed for 1 min prior to stripping in 0.1 M hydrochloric acid with a current of 0.1 μA. The procedure is repeated on a spiked sample after which the sample analyte concentrations are evaluated and presented digitally and graphically on a printer/plotter. The results obtained for bismuth, copper and mercury in a urine reference sample were 36.9, 39.7 and 47.7 $\mu g\ l^{-1}$ with standard deviations ($n=10$) of 3.2, 4.2 and 2.1, respectively. The certified values for copper and mercury were 45 and 51 $\mu g\ l^{-1}$; no certified value was available for bismuth.

It has recently been shown that carbon and metal fibres can be used successfully as sensors in flow potentiometric and constant-current analysis, the main advantages of the fibre electrodes being their increased sensitivity, improved stability and simplified handling [1,2].

Mercury(II) in urine has been determined electrochemically by means of differential-pulse anodic stripping voltammetry with a gold disc electrode [3] and by means of stripping potentiometry with either a copper-coated glassy carbon electrode [4] or a gold disc electrode [5]. Considering the recent progress in instrumentation for potentiometric and constant-current stripping analysis [6] and in flow fibre technology [1,2], it was decided to re-investigate the determination of mercury(II) in urine and to include the possibility of simultaneous determination of copper(II). Because the work on reference urine material revealed that these samples contained rather high concentrations of bismuth(III), the possibility of simultaneously determining this element was also studied.

[a]Permanent address: Scientific Instrumentation Department, Xiamen (Amoy) University, Fujian Province, China.

0003-2670/87/$03.50

EXPERIMENTAL

Instrumentation

A computerized flow potentiometric and constant-current stripping analyzer was used [6]. In this instrument, six different solutions can be sucked through the electrodes in random choice order. Flow rate, electrode potential and magnitude of the stripping current are controlled by the computer. During stripping, the potential vs. time transient is recorded with a real-time sampling rate of 25.6 kHz. After recording the stripping curve and subtracting the background, the computer locates and integrates the stripping peaks for the various elements [6]. After processing of another sample spiked with the analytes, the computer evaluates the sample concentrations, using the normal equations for standard addition. Finally, the results are presented digitally and graphically, the stripping curve E vs. time being illustrated by the differentiated plot dt/dE vs. electrode potential E.

The flow rate in all the experiments described below was 1 ml min^{-1}.

Electrodes and reagents

A 10-μm diameter gold fibre (99.99+% purity; Goodfellow, Cambridge, England) inserted perpendicularly to the flow direction of a Viton tube (inner diameter 1.0 mm) was used as the working electrode (cf. [1,2]). A glassy carbon rod (length 10 mm, diameter 1 mm; Ringsdorff, F.R.G.) glued perpendicularly to the flow direction of a PVC tube (inner diameter 2 mm) was mounted downstream from the gold fibre electrode and used as reference electrode. The potential of the glassy carbon reference electrode (GCE) was -0.50 ± 0.12 V vs. the saturated calomel electrode. The platinum tube counter electrode (length 10 mm, inner diameter 0.7 mm; Goodfellow) was mounted downstream from the reference electrode.

All reagents were of analytical-reagent grade except the mineral acids which were of Suprapur grade (Merck). Seronorm urine reference standard (batch 108), with a creatinine concentration of 1.5 g l^{-1} was obtained from Nycomed, Oslo, Norway. All dilutions were made with Millipore-Q water.

The gold-plating solution contained 100 mg l^{-1} gold(III) in 0.10 M hydrochloric acid. The electode cleaning solution was 0.10 M hydrochloric acid in 50% (v/v) ethanol. The stripping solution was 0.10 M hydrochloric acid.

Procedure for urine

To 10 ml of urine sample, 5 ml of concentrated nitric acid and 1 ml of 10 mM potassium permanganate was added. The mixture was heated at 70°C for 10 min and, after cooling, was diluted to 100 ml. From this solution, two 40-ml portions were taken and, to one of these, standard additions of 10 μg l^{-1} mercury(II), copper(II) and bismuth(III) were made. These solutions were placed at two inlets of the analyzer.

In the fully automated constant-current stripping procedure, the stripping solution was first allowed into the flow cell and a potential of 0.10 V vs. GCE was applied for 5 s in order to remove mercury which might have accumulated on the gold fibre electrode during storage. A fresh surface of gold was then plated onto the gold fibre by means of electrolysis in the gold-plating solution at −0.40 V vs. GCE for 10 s. The gold-plating procedure was ended by applying a potential of 0.10 V vs. GCE for 1 s in order to remove possible metal impurities. After this, the sample was sucked into the cell and electrolysis was done according to a pulsed procedure whereby a potential of −0.70 V vs. GCE was applied for 5 s followed by a potential of −0.60 vs. GCE for 1 s. After ten such pulse sequences, the stripping solution was sucked into the cell and 20 s later stripping was initiated with a constant curent of 0.10 μA. Stripping was terminated at a potential of 0.20 V vs. GCE, and after 2 s at this potential, a potential of −0.60 V vs GCE was applied for 2 s and the background was recorded. Finally, the rinsing solution was sucked through the cell for 5 s at a potential of 0.10 V vs. GCE. The same procedure was repeated with the spiked urine sample.

RESULTS AND DISCUSSION

Stripping solution composition

It has been shown [2] that the stripping potentials for mercury and copper on gold electrodes are highly dependent on chloride concentration in the stripping medium. At chloride concentrations above approximately 3 M, mercury is oxidized before copper and at lower chloride concentrations after copper. The dependence of the bismuth, copper and mercury stripping potentials on the chloride concentration of the stripping medium is illustrated in Fig. 1. A 0.50 M nitric acid sample containing 10 μg l^{-1} each of bismuth(III), cop-

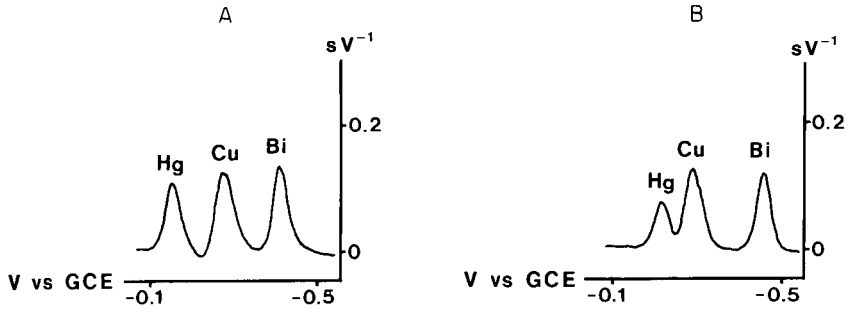

Fig. 1. Differentiated background-corrected constant-current stripping curves obtained after 1 min of electrolysis in 0.50 M nitric acid containing 10 μg l^{-1} each of bismuth(III), copper(II) and mercury(II), and subsequent stripping with a current of 0.1 μA in (A) 0.1 M hydrochloric acid and (B) 0.5 M hydrochloric acid.

per(II) and mercury(II) was electrolyzed for 1 min in the pulse potential mode described above for digested urine samples and subsequently stripped in 0.10 M (Fig. 1A) and 0.50 M (Fig. 1B) hydrochloric acid. As can be seen, 0.10 M hydrochloric acid is capable of completely resolving the stripping peaks of the three elements. At higher chloride concentrations, the copper and mercury signals tend to overlap (cf. Fig. 1B) and at lower concentrations the bismuth and copper signals overlap. This can be seen from the results of the interference study (Fig. 2) where 0.04 M hydrochloric acid was used as stripping medium.

Interferences

Elements which can be reduced to the elemental state on the gold electrode at −0.70 V vs. GCE and at the same time are soluble in gold are likely interferents. These include antimony(III), arsenic(III), silver(I) and platinum. Experiments showed that platinum is stripped anodic to the three elements under study and does not interfere when present in a 100-fold excess. In 0.10 M hydrochloric acid, the stripping peaks of silver and mercury can be resolved provided that the silver(I) concentration is lower than the mercury(II) concentration. In urine samples, this is very likely to be the case because of the limited solubility of silver(I) in body fluids. The presence of silver(I) in the sample does, however, decrease the sensitivity and long-term stability of the gold fibre electrode.

Antimony and arsenic do not interfere in the analysis of digested urine samples because these elements will exist in the pentavalent state. Even so, the interference from antimony(III) and arsenic(III) was investigated. Figure 2 shows the constant-current stripping peaks obtained after one minute of pulsed electrolysis (−0.80 V vs. GCE for 5 s and −0.60 V vs. GCE for 1 s, repeated

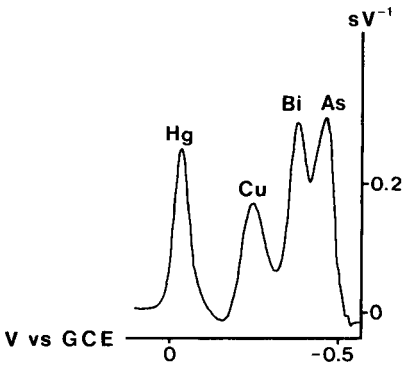

Fig. 2. Differentiated background-corrected constant-current stripping curves obtained after 1 min of electrolysis in 0.50 M nitric acid containing 20 $\mu g\ l^{-1}$ each of arsenic(III), bismuth(III), copper(II) and mercury(II), and subsequent stripping with a current of 0.1 μA in 0.04 M hydrochloric acid.

10 times) in a 0.50 M nitric acid solution containing arsenic(III), bismuth(III), copper(II) and mercury(II) and subsequent stripping in 0.04 M hydrochloric acid. As can be seen, the presence of arsenic(III) would interfere with the bismuth signal. The interference from antimony(III) was investigated under the same experimental conditions as those for Fig. 1(A) except that 50 $\mu g\ l^{-1}$ antimony(III) was added to the sample; no interference was observed.

Accuracy and precision

The linear range for bismuth(III), copper(II) and mercury(II) was investigated by examining 0.50 M nitric acid samples containing 5, 10, 20 and 50 $\mu g\ l^{-1}$ each of these elements under the experimental conditions recommended for digested urine samples. No significant deviations from linearity were obtained. The experiments were repeated with stripping currents of 0.20, 0.30 and 0.50 μA instead of 0.10 μA. As expected, the stripping peak areas varied inversely with the magnitude of the stripping current. Linear relationships between peak area and sample concentration of analytes were obtained for all three elements under study in the stripping current range investigated.

The accuracy of the procedure was investigated by analyzing a 0.50 M nitric acid sample containing 10 $\mu g\ l^{-1}$ each of bismuth(III), copper(II) and mercury(II), as in the standard addition procedure described for urine digests. Four different magnitudes of the standard addition were used (10, 20, 30 and 50 $\mu g\ l^{-1}$) for each of the three elements; for each magnitude, the sample was processed five times. The average values for 20 analyses were 11.6 $\mu g\ l^{-1}$ bismuth(III), 11.0 $\mu g\ l^{-1}$ copper(II) and 10.0 $\mu g\ l^{-1}$ mercury(II), the relative standard deviations being 9.8, 7.0 and 5.8%, respectively. The high relative standard deviations are mostly due to the single standard addition technique used for quantification [7]. Improved precision would be possible by using two or three standard additions, by increasing the time of electrolysis, or by using computer accumulation of several stripping scans. In the latter procedure, which has been used successfully in other applications [8], the unspiked sample is first processed and the stripping curve is stored in computer memory; then the spiked sample is processed and the stripping curve stored. This procedure is repeated any number of times, after which all stripping curves obtained from the unspiked sample are summed as are those for the spiked sample. Finally, the sample concentration of analyte is evaluated by means of the normal equations for standard addition.

Analysis of urine reference sample

Ten different acid digests of the urine reference sample were analyzed for bismuth, copper and mercury by the procedure described above. The results are summarized in Table 1 together with the certified values. As can be seen,

TABLE 1

Precision and accuracy in the determination of bismuth(III), copper(II) and mercury(II) in Seronorm (batch 108) urine reference sample

Element	Concentration found[a] ($\mu g\,l^{-1}$)	Certified value ($\mu g\,l^{-1}$)
Bismuth	36.9 ± 3.2	-
Copper	39.7 ± 4.2	45
Mercury	47.7 ± 2.1	51

[a]Mean and standard deviation for 10 determinations.

the values obtained for copper and mercury are in good agreement with the certified values. No certified value was available for bismuth.

Conclusions

Flow constant-current stripping analysis is useful for the simultaneous determination of bismuth, copper and mercury in urine samples, and presumably for similar materials. The computerized flow instrumentation provides highly automated performance including graphical display and digital evaluation of the results. The gold fibre is a reliable sensor provided that it is coated with a fresh gold film prior to each analytical cycle. Most results reported above were, in fact, obtained with the same gold fibre electrode.

This work was supported by the Swedish Work Environment Fund and the Carl Trygger Research Foundation.

REFERENCES

1 Huang Huiliang, Chi Hua, D. Jagner and L. Renman, Anal. Chim. Acta, 193 (1987) 61.
2 Huang Huiliang, D. Jagner and L. Renman, Anal. Chim. Acta, 201 (1987) 1.
3 J. Wang, Stripping Analysis, VCH, Deerfield Beach, FL, 1985.
4 D. Jagner, Anal. Chim. Acta, 105 (1979) 33.
5 D. Jagner, M. Josefsson and K. Årén, Anal. Chim. Acta, 141 (1982) 147.
6 L. Renman, D. Jagner and R. Berglund, Anal. Chim. Acta, 188 (1986) 137.
7 M.I. Gardner and A.M. Gunn, Fresenius' Z. Anal. Chem., 225 (1986) 263.
8 Chi Hua, D. Jagner and L. Renman, Anal. Chim. Acta, 197 (1987) 257.

Analytica Chimica Acta, 202 (1987) 123–129
Elsevier Science Publishers B.V., Amsterdam — Printed in The Netherlands

FLOW CONSTANT-CURRENT STRIPPING ANALYSIS FOR ANTIMONY(III) AND ANTIMONY(V) WITH GOLD FIBRE WORKING ELECTRODES
Application to Natural Waters

HUANG HUILIANG[a], DANIEL JAGNER* and LARS RENMAN

Department of Technical Analytical Chemistry, Chemical Center, University of Lund, P.O. Box 124, S-221 00 Lund (Sweden)

(Received 14th May 1987)

SUMMARY

Antimony(III) is determined by means of electrolysis at −0.40 V vs. Ag/AgCl on a gold-coated gold fibre electrode for 0.5–10 min in a redox buffer containing 0.01 M iron(II) in 0.10 M hydrochloric acid, and subsequent stripping with a constant current of 0.50 μA either in 2 M hydrochloric acid or in 4 M hydrochloric acid/4 M calcium chloride. Antimony(V) is determined by the same procedure in 4 M hydrochloric acid medium. Bismuth(III) is masked by the addition of iodide to the sample prior to electrolysis. Antimony(III) and antimony(V) are determined by standard addition methods; the whole procedure including digital and graphical evaluation of the results is fully automated. The antimony(V) concentrations in the river water reference sample SLRS-1 and the seawater reference sample NASS-1 were found to be 0.63 and 0.31 $\mu g\ l^{-1}$ with standard deviations of 0.046 and 0.051 $\mu g\ l^{-1}$, respectively ($n = 15$). The certified value for SLRS-1 is $0.63 \pm 0.05\ \mu g\ l^{-1}$; no certified value is available for NASS-1.

Although the polarographic behaviour of antimony is well known [1], very few attempts have been made to determine antimony electrochemically at the concentrations normally occurring in natural waters, i.e., 0.1–1 $\mu g\ l^{-1}$. The most successful attempts are those of Gilbert and Hume [2] and Gillain et al. [3], who used anodic stripping voltammetry on mercury film and mercury drop electrodes, respectively. A major problem in determining antimony with mercury electrodes is the potential overlap from the copper stripping peak. Recent work on flow potentiometric and constant-current stripping analysis with gold fibre working electrodes has shown that the potential of the copper stripping peak can be altered dramatically simply by varying the chloride con-

[a]Permanent address: Scientific Instrumentation Department, Xiamen (Amoy) University, Fujian Province (China).

0003-2670/87/$03.50

centration of the stripping medium [4]. Antimony is soluble in gold, and so it would appear that gold electrodes should be more suitable than mercury electrodes as sensors for stripping determinations of antimony.

A highly automated method for the determination of both antimony(III) and antimony(V) by means of flow constant-current stripping analysis using gold fibre sensors is described in this paper.

EXPERIMENTAL

Instrumentation

The computerized flow potentiometric and constant-current stripping analyzer has been described in detail [5]. In this analyzer, six different solutions can be sucked into the flow cell in random choice order, the electrode potential, flow rate, magnitude of stripping current and opening and closing of inlet magnetic valves being controlled by the computer. During stripping, the electrode potential (E, V) vs. time (t, s) was registered with a real-time sampling rate of 25.6 kHz. After recording of the stripping curve and subtraction of the background, the computer program located and integrated the stripping peaks of the analytes and displayed the results digitally and graphically, as the differentiated plot $dt(dE)^{-1}$ vs. E, on a printer plotter [5].

The flow rate in all investigations was 1 ml min^{-1}.

Flow electrodes and reagents

A 10-μm diameter gold fibre (99.99+% purity, Goodfellow, Cambridge, G.B.) mounted perpendicularly to the flow direction in a Viton tube, with an inner diameter of 0.80 mm, was used as the working electrode. A 10-mm silver tube with an inner diameter of 0.70 mm and lined with silver chloride was mounted downstream from the working electrode and used as reference. All potentials given below are vs. the Ag/AgCl electrode at the chloride concentration of the solution in the flow reference cell. A 10-mm platinum tube with an inner diameter of 0.70 mm was mounted downstream from the reference electrode and used as the counter electrode.

All reagents used were of analytical grade except the mineral acids which were of Suprapur grade (Merck). All dilutions were made with Millipore-Q water.

The seawater reference sample NASS-1 and the river water reference sample SLRS-1 were obtained from the National Research Council, Ottawa, Canada.

The gold film plating solution was a 100 mg l^{-1} solution of gold(III) in 0.10 M hydrochloric acid.

Constant-current stripping procedure

The constant-current stripping analysis consisted of three operations, plating of a fresh gold film onto the gold fibre, electrolysis in the sample and finally

stripping in a suitable medium. In the gold-film procedure, a potential of −0.10 V was applied for 5 s in the gold plating solution after which the potential was increased to 0.50 V in order to oxidize trace metal impurities in the plating solution. This was repeated three times, after which the sample solution was sucked into the cell for 20 s at a potential of 0.50 V. An appropriate electrolysis potential was then applied to the sample, and finally the stripping solution was sucked through the cell prior to application of the stripping current of 0.50 μA. After recording of the stripping curve in the potential region between the electrolysis potential and 0.60 V, the electrolysis potential was again applied and 2 s later the background was recorded.

In the graphical display, an averaging filter of 15 mV and a Savitsky–Golay filter of 30 mV were used, the potential resolution being 1 mV [5].

RESULTS AND DISCUSSION

Stripping medium composition

The purpose of the stripping medium is to resolve the stripping peaks of the elements which might have been co-deposited with antimony on the gold fibre electrode. Such elements are, for example, bismuth, copper, mercury and arsenic. Bismuth(III) can be masked by iodide in the sample solution and thereby prevented from depositing on the working electrode. It has been shown previously that the stripping peak potentials of mercury and copper on the gold fibre electrode are highly dependent on the chloride concentration of the stripping medium [4]. Thus in order to separate these elements, and at the same time separate antimony, stripping media with high chloride concentrations can be exploited. Furthermore, the medium must be acidic in order to prevent formation of antimony hydroxides during stripping.

Figure 1 shows the differentiated stripping peaks obtained after electrolysis at −0.30 V for 60 s in 1 M hydrochloric acid containing 5 $\mu g\ l^{-1}$ each of mercury(II), copper(II) and antimony(III) and 15 $\mu g\ l^{-1}$ arsenic(III) by stripping in a 4 M calcium chloride/4 M hydrochloric acid mixture. As is apparent from this figure, this stripping medium is capable of resolving the four elements. If, however, only separation between antimony and the other elements is required, a stripping medium of 2 M hydrochloric acid is sufficient. In this medium, the antimony stripping peak is more reproducible; this medium was therefore used in the analysis of natural waters. In 2 M hydrochloric acid, the stripping peaks of antimony and bismuth overlap and bismuth(III) must be masked with iodide prior to the electrolysis step. The efficiency of masking bismuth(III) was investigated by analyzing a 0.20 M hydrochloric acid solution containing 20 $\mu g\ l^{-1}$ antimony(III) according to the standard addition procedure with an addition of 100 $\mu g\ l^{-1}$ antimony(III). Ten consecutive analyses, one of them shown in Fig. 2(a), yielded a mean value of 19.1 $\mu g\ l^{-1}$ with a standard deviation of 1.9 $\mu g\ l^{-1}$. The procedure was repeated after the addi-

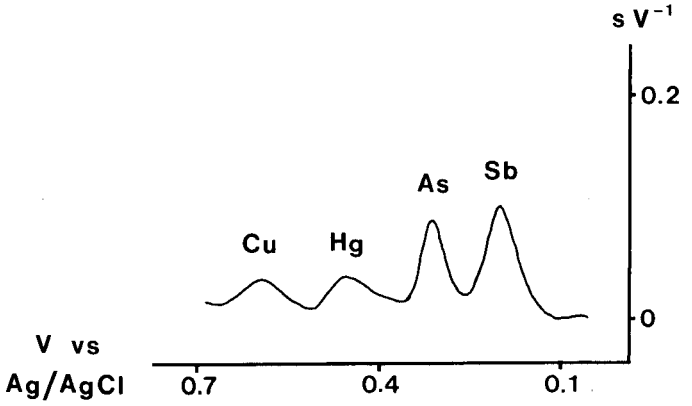

Fig. 1. Differentiated background-corrected constant-current stripping curve obtained after electrolysis at −0.30 V vs. Ag/AgCl for 60 s in 1 M hydrochloric acid containing 5 $\mu g\ l^{-1}$ each of copper(II), mercury(II), antimony(III) and 15 $\mu g\ l^{-1}$ arsenic(III). Stripping in 4 M hydrochloric acid/4 M calcium chloride with a current of 0.50 μA.

tion of 20 $\mu g\ l^{-1}$ bismuth(III) to the sample, as shown in Fig. 2(b). The result thus obtained, 39.1 $\mu g\ l^{-1}$ with a standard deviation of 2.6 $\mu g\ l^{-1}$, showed that the sensitivities for antimony(III) and bismuth(III), when expressed in μg

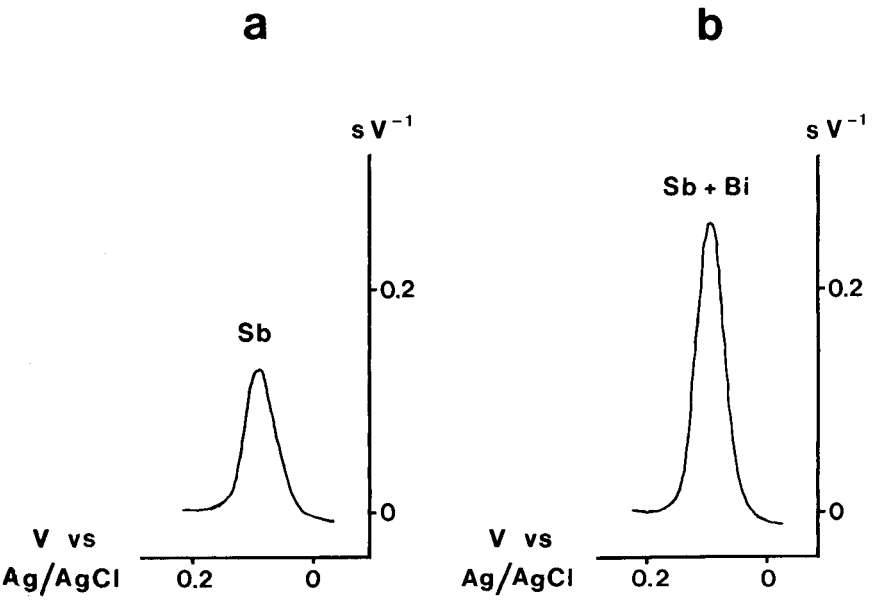

Fig. 2. Differentiated background-corrrected constant-current stripping curves obtained after electrolysis at −0.30 V vs. Ag/AgCl for 30 s in 0.20 M hydrochloric acid containing (a) 20 $\mu g\ l^{-1}$ antimony(III) and (b) 20 $\mu g\ l^{-1}$ each of antimony(III) and bismuth(III). Stripping in 2 M hydrochloric acid with a current of 0.50 μA.

l^{-1}, are very similar. After the addition of 50 μM potassium iodide, a value of 18.9 $\mu g\ l^{-1}$ with a standard deviation of 1.9 $\mu g\ l^{-1}$ was obtained, showing that bismuth(III) is completely masked by iodide.

Composition of the sample medium for the determination of antimony(III) and antimony(V)

Antimony can exist in both the trivalent and the pentavalent states, the latter being dominant in natural waters. Antimony(III) is easily reduced on a gold fibre electrode whereas antimony(V) is not. If the concentrations of the two species are to be determined, it is necessary to find a medium which, after sampling, prevents antimony(III) from being oxidized and antimony(V) from being reduced. It is also necessary to find a medium where antimony(V) is reduced to antimony(III), thus facilitating the determination of total antimony in the sample.

A redox buffer based on iron(II) in hydrochloric acid was found to be satisfactory for the preservation of the oxidation states of antimony. In 0.10 M hydrochloric acid containing 0.01 M iron(II), antimony(III) and antimony(V) were stable for at least two weeks. This was shown by analyzing a solution containing 20 $\mu g\ l^{-1}$ antimony(III) and 100 $\mu g\ l^{-1}$ antimony(V), based on a standard addition of 100 $\mu g\ l^{-1}$ antimony(III). The sample was electrolyzed for 30 s at -0.30 V vs. Ag/AgCl prior to stripping in 2 M hydrochloric acid. Eight analyses yielded a mean value of 18.9 $\mu g\ l^{-1}$ for antimony(III) with a standard deviation of 1.3 $\mu g\ l^{-1}$. The procedure was repeated two weeks later and no significant difference was obtained. When the electrolysis potential was decreased from -0.30 V to -0.60 V vs. Ag/AgCl, it was found that approximately 20% of antimony(V) was reduced. At potentials above -0.50 V, no antimony(V) was reduced.

It is well known that antimony(III) is stabilized in strong hydrochloric acid. The hydrochloric acid concentration needed to convert antimony(V) to antimony(III) was investigated by analyzing a solution containing 20 $\mu g\ l^{-1}$ antimony(V) and using a standard addition of 100 $\mu g\ l^{-1}$ antimony(III). The sample was electrolyzed for 30 s at -0.30 V vs. Ag/AgCl prior to stripping in 2 M hydrochloric acid. The sample concentration of hydrochloric acid was increased in steps of 0.50 M. At a hydrochloric acid concentration of 2 M, approximately 50% of the antimony(V) was reduced. At 4 M, all antimony(V) was reduced, as indicated by the result, 20.2 ± 0.6 $\mu g\ l^{-1}$ ($n=8$), obtained by the standard addition procedure. This was further confirmed by testing a 4 M hydrochloric acid solution containing 10 $\mu g\ l^{-1}$ antimony(V), based on standard addition of 50 $\mu g\ l^{-1}$ antimony(III) and an electrolysis time of 30 s at -0.30 V vs. Ag/AgCl. The result obtained, 10.1 ± 0.5 $\mu g\ l^{-1}$ ($n=8$), confirms the complete reduction of antimony(V). As is also apparent, the standard deviations obtained in 4 M hydrochloric acid medium are significantly better than those in 0.10 M acid.

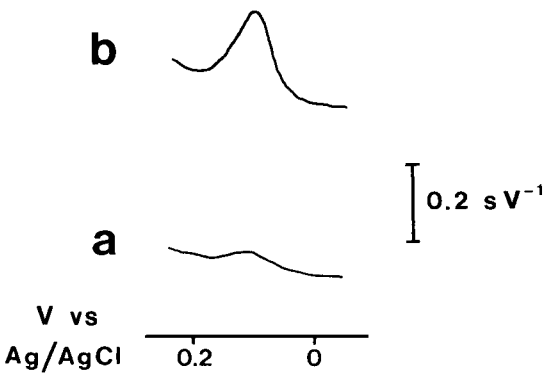

Fig. 3. Differentiated background-corrected constant-current stripping curves obtained after 10 min of electrolysis at −0.40 V vs. Ag/AgCl in seawater reference sample NASS-1 containing 4 M hydrochloric acid and 20 μM potassium iodide before (a) and after (b) the standard addition of 1 $\mu g\ l^{-1}$ antimony(V). Stripping in 2 M hydrochloric acid with a current of 0.50 μA.

Analysis of reference samples of seawater and river water

Determination of antimony(III). Potassium iodide and hydrochloric acid were added to the reference samples to give total concentrations of 20 μM and 0.10 M, respectively. The samples were electrolyzed for 10 min at −0.40 V vs. Ag/AgCl prior to constant-current stripping in 2 M hydrochloric acid. Standard aliquots of antimony(III) equal to 0.5, 1, 2, 3, 4 and 5 $\mu\ l^{-1}$ were then added to the samples, and the electrolysis/stripping cycle was repeated at each concentration. Least-square linear regression yielded antimony(III) values less than 0.04 $\mu g\ l^{-1}$ in the river and seawater reference samples, the estimated standard deviations for both determinations being 0.04 $\mu g\ l^{-1}$. Obviously, there are no significant amounts of antimony(III) in either sample. This is in agreement with previous results on the oxidation states of antimony in natural waters. For these reference samples, of course, the possibility that the nitric acid (0.01 M) added to the samples for conservation might have oxidized antimony(III) cannot be ruled out.

Determination of antimony(V). Potassium iodide and hydrochloric acid were added to the sample to yield total concentrations equal to 20 μM and 4 M, respectively. The samples were analyzed according to the procedure described above for antimony(III), with a standard addition of 1 $\mu g\ l^{-1}$ antimony(V). Figure 3 shows the constant-current stripping curves obtained in the analysis of seawater reference sample NASS-1 before (Fig. 3a) and after (Fig. 3b) this standard addition.

The mean value obtained in the analysis of fifteen different portions of the river water was 0.63 $\mu g\ l^{-1}$ with a standard deviation of 0.046 $\mu g\ l^{-1}$. This is in very good agreement with the certified value of 0.63 ± 0.05 $\mu g\ l^{-1}$. The mean

value obtained in the analysis of fifteen subsamples of the reference seawater was 0.31 $\mu g\,l^{-1}$ with a standard deviation of 0.06 $\mu g\,l^{-1}$. No value for antimony has been certified for this reference sample. The value obtained is, however, in agreement with previous results obtained by Gillain et al. [3] (0.2–0.6 $\mu g\,l^{-1}$) and Gilbert and Hume [2] (0.25–0.47 $\mu g\,l^{-1}$) for ocean waters.

Conclusions

Computerized flow constant-current stripping analysis provides a highly automated technique for the determination of antimony(III) and antimony(V) in natural waters, involving only a minimum of sample pretreatment. The gold fibre sensor is extremely reliable and, provided that it is coated with a fresh film of gold prior to each electrolysis/stripping cycle, it can be used for several hundred runs. Most of the results reported above were obtained with the same fibre electrode. Bismuth(III) interferes with the stripping peak of antimony but can be masked by the addition of iodide. In the analysis of natural waters, this addition can, however, be omitted because the bismuth(III) concentration is normally more than one order of magnitude less than the total antimony concentration.

REFERENCES

1 I.M. Kolthoff and J.J. Lingane, Polarography, Vol. II, Interscience, New York, 1965.
2 T.R. Gilbert and D.N. Hume, Anal. Chim. Acta, 65 (1973) 451.
3 G. Gillain, G. Duyckaerts and A. Disteche, Anal. Chim. Acta, 106 (1979) 23.
4 Huang Huiliang, D. Jagner and L. Renman, Anal. Chim. Acta, 202 (1987) 117.
5 L. Renman, R. Berglund and D. Jagner, Anal. Chim. Acta, 188 (1986) 137.

Analytica Chimica Acta, 202 (1987) 131–140
Elsevier Science Publishers B.V., Amsterdam — Printed in The Netherlands

A FLOW-THROUGH CELL FOR USE WITH AN ENZYME-MODIFIED FIELD EFFECT TRANSISTOR WITHOUT POLYMERIC ENCAPSULATION AND WIRE BONDING

SATORU SHIONO*, YOSIO HANAZATO, MAMIKO NAKAKO and MITSUO MAEDA

Central Research Laboratory, Mitsubishi Electric Corporation, 8-1-1 Tsukaguchi-Honmachi, Amagasaki, Hyogo 661 (Japan)

(Received 25th May 1987)

SUMMARY

A new type of flow-through cell for an enzyme-modified field effect transistor (FET) is described. The cell makes it possible to use a FET without polymeric encapsulation and wire bonding. Electrical evaluation of a FET used with the flow cell demonstrates that the flow cell has no practical problems causing sensor malfunctions. The noise and drift levels of the FET sensor with the flow cell are shown to be similar to those of an epoxy-encapsulated FET sensor. The application of the flow cell with a urease-modified FET is described. Useful responses are obtained for 0.25–50 mg l^{-1} urea with relative standard deviations of $<3\%$.

There have been significant advances in the development of enzyme-modified field effect transistors (FET), since the description of the penicillin-sensitive enzyme-modified FET by Caras and Janata [1]. Enzyme-modified FETs sensitive for several clinically important chemicals have been fabricated and their performances evaluated [2–18]. Substances which can be determined in such a way include glucose [2,3,5–15], urea [3,5,8–10,16], triglycerides [4,6], acetylcholine [16] and adenosine triphosphate [17]. An enzyme-modified FET has been experimentally proven to be usable for in vitro glucose and urea determinations with practical sensitivity and accuracy [5,9].

There are many possible advantages of using FET-based chemical sensors [1]. Among them, the small size of the sensor has been stressed most, because it permits the use of a chemical sensor for in vivo applications, thus possibly providing new physiological information [18,19], and allowing its use as an embedded sensing device for an artificial organ [11–13,20]; much effort has been made along these lines. However, another important advantage is that a FET chemical sensor can be produced much less expensively than a conventional electrode-based chemical sensor. The potential for making a chemical sensor much more cheaply would allow its use as a disposable sensor.

As was discussed in detail for an ion-sensitive FET with a neutral carrier

0003-2670/87/$03.50

membrane [21], an insulated-gate FET can be mass-produced very easily and economically. But after FET production, the ion-sensitive membrane deposition, polymeric encapsulation for electrical insulation and device packaging usually require tedious processes which are generally difficult to convert to economical mass-production processes. Some ideas have been proposed to solve these problems. Similar problems arise for production of an enzyme-modified FET.

In order to realize the full potential of mass-production of a cheap enzyme-modified FET by normal semiconductor production facilities, there have been two major problems to overcome. One is the selective deposition of enzyme-immobilized membranes on specific areas of the FET surface; the other is polymeric encapsulation. The first problem has been almost completely solved in recent years: three research groups have proposed photolithographic techniques for enzyme-membrane deposition [5–10]. These techniques are thought to be compatible with ordinary silicon wafer processes. With regard to the second problem, it should be noted that two major improvements of an ion-sensitive FET have been reported [9,22] which avoid most but not all of the tedious work of encapsulation. While an ion-sensitive FET of the conventional design requires the encapsulation of both the bare lateral sides and the bonding pad region of the FET chip, the improved design requires only the encapsulation of the bonding pad region. Abe et al. [22] fabricated a probe-type FET with a three-dimensional Si_3–N_4 passivation layer around almost all its surface, although the probe-type FET needed three-dimensional processes which were uncommon for the usual semiconductor facility. Based on similar ideas, but in order not to depend on three-dimensional processes, Kuriyama et al. [9] proposed that a silicon-on-sapphire (SOS) wafer should be used for FET fabrication so that normal semiconductor manufacturing equipment could be applied. However, it is still believed that an ordinary silicon-based FET is more favorable than an SOS-FET in terms of producing a cheap FET sensor, because silicon wafers are much more widely used in the semiconductor industry and are thus less expensive than SOS wafers. Ho et al. [21] reported a tape and dry film photoresist process as a solution to the second problem for a silicon-based ion-sensitive FET

In this paper, improvements in a flow-through cell for use with FET chemical sensors are described for in vitro measurements, rather than improvement of the FET transducer itself. The flow-through cell enables a silicon-based FET chemical sensor with no polymeric encapsulation to be used. Therefore, tedious and time-consuming encapsulation can be completely omitted. A little less importantly, it has another advantage in that the FET sensor to be used with it requires no wire bonding. Although the application of the flow cell is limited to in vitro measurements, it may offer a means for construction of cheap and thus disposable chemical sensors. After the description of the flow-

cell design and its electrical evaluation, experimental results are given for a urea-sensitive enzyme-modified FET used with the flow cell.

EXPERIMENTAL

Materials

Urease (EC 3.5.1.5, from jack beans; P-L Biochemicals (Milwaukee, WI)) had an activity of 50 U mg^{-1}. The poly-L-lysine used had an average molecular weight of 25 000 (Sigma, St. Louis, MO). Glutaraldehyde (25% in water; Ishizu Pharmaceuticals, Osaka) and polyvinylpyrrolidone (PVP) with an average molecular weight of 360 000 (Nakarai Chemicals, Osaka) were used as received. The sodium salt of 2,5-bis(4′-azido-2′-sulfobenzal)cyclopentanone (BASC) was donated by Mr. Miyazawa of Tokyo Ohka Kogyou (Kanagawa). All other chemicals were of analytical-reagent grade and all solutions were made with distilled/deionized water.

Sensor construction

The fabrication of an integrated ion-sensitive FET having two hydrogen ion-sensitive elements from an epitaxially grown silicon wafer was described in previous reports [5–7]. Figure 1 is a photograph of the integrated FET. The chip size is 6.5×5.0 mm. It has five bonding pads to be electrically connected; the center one is a substrate pad for electrical isolation of the two FET elements. The pad size is 0.7×0.5 mm. In the lower part of the chip the FET has two ion-sensitive gates, 20 μm wide and 1 mm long.

The structure of the FET sensor is schematically depicted in Fig. 2. The plastic card (S, Fig. 2), which was made by injection molding of a polycarbonate resin, has a rectangular hollow on its surface. A FET chip on whose bottom a small amount of a rapidly curing adhesive has been put is placed into the hollow. The dimensions of the hollow are such that the surface of the FET is 0.1 mm higher than the surface of the card. An immobilized urease membrane, 0.2 mm wide and 1 mm long, is made by the photolithographic technique [5]. An immobilizing solution of urease was prepared by dissolving 7.5 mg of urease and 2.5 mg of poly-L-lysine in 200 μl of aqueous solution containing 10% (w/v) PVP and 1% (w/v) BASC. The urease membrane was formed by spin-coating this urease solution on the FET, ultraviolet irradiation of a limited area around one of the two gate surfaces, and treatment with 3% glutaraldehyde solution. (The other gate of the FET would normally have a similar membrane having no urease activity to minimize the noise amplitude of the sensor output caused by the difference between a washing solution and an analyte solution [1], but in this study such a membrane was omitted because the washing and analyte solutions were prepared under controlled conditions and kept under the same conditions, so that the difference between the two solutions was expected to be negligible.)

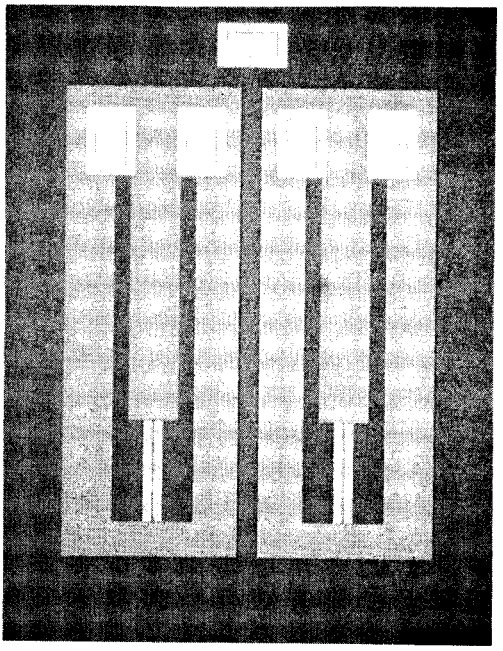

Fig. 1. Photograph of integrated FET with two hydrogen ion-sensitive FET elements (for scale, see text).

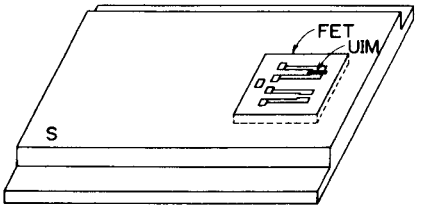

Fig. 2. Structure of enzyme-modified FET sensor: S, plastic card; FET, enzyme-modified FET chip; UIM, immobilized urease membrane.

The drain-source voltage of each FET element was set at 3.0 V and the gate voltage at −1.0 V. The substrate was biased at 5.0 V. The differential output voltage between the FET elements with and without the immobilized urease membrane was measured by the source follower mode circuit [2].

Flow-through cell

Figure 3(a) is a schematic illustration of the flow-injection apparatus used in this study. A wash solution is continuously supplied from a wash solution bottle (WS) to a flow-through cell (SC) by means of a peristaltic pump (P). A sample solution is injected into the wash solution flow via an injection port (IP) from a microsyringe (MS). The sample solution is diluted by the wash

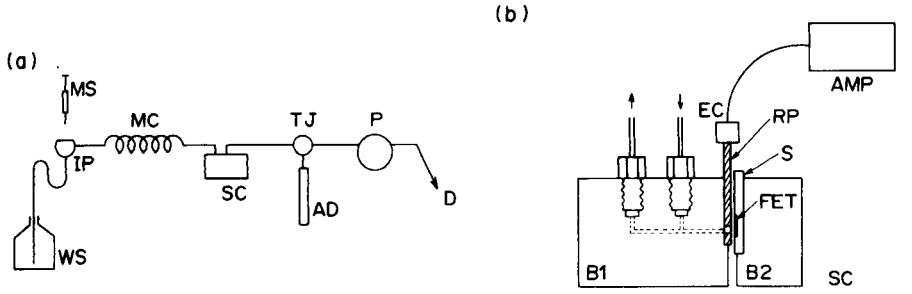

Fig. 3. Schematic diagram of flow-injection apparatus. (a) Flow system: WS, wash solution bottle; IP, injection port; MS, microsyringe; MC, mixing coil; SC, flow-through cell; TJ, three-way joint: AD, air damper; P, peristaltic pump. (b) Detailed structure of flow-through cell: B1, fixed sensor cell block; B2, movable sensor cell block; SC, flow-through cell; EC, electrical connector; RP, silicone rubber sheet; AMP, amplifier. For other abbreviations, see Fig. 2.

solution in a mixing coil (MC) between the flow cell and the injection port. To decrease fluctuations in the solution flow rate, a home-made air damper (AD) is placed between the flow cell and pump by using a three-way joint (TJ).

The cross-section of the flow cell is shown in Fig. 3(b). The flow cell is composed of two epoxy laminate blocks: the first (B1) is fixed and has an inlet and an outlet tube and a silicone rubber sheet (RP), 2 mm thick, on its right side; the second (B2) is movable and has a place to hold an FET sensor (S). A sensor is put into the block after it has been moved to the right, and the sensor is pressed against the silicone rubber sheet by moving the block to the left. To explain the structure of the flow cell in more detail, Fig. 4(a) shows the front view of the part of the flow cell containing the sensor, and Fig. 4(b) is an exploded diagram. Figure 4(c) is a cross-section, showing how the sensor is in contact with the rubber sheet. The rubber sheet, which is attached to the right side of B1 with adhesive, has a rectangular hole (c; $1.1 \times 3.0 \times 2.0$ mm) corresponding to the inlet (ip) and outlet tubes (op) on the left-hand side and at the same time to the two FET gates on the right-hand side. The area of the FET which the solution touches is a rectangular area surrounded by the dashed lines in Fig. 4(b). The rubber sheet has a polyimide flexible printed-circuit film with five gold-deposited lines (g) on its right surface. For simplicity, the lower edge of the polyimide film is not shown in Fig. 4; it lies between the hole and the lower ends of the five gold lines so that the FET surface around the two gates is in direct contact with the silicone rubber sheet. The lowest regions of the five gold lines (0.5×0.3 mm) are attached to the five corresponding contact pads (cp) when the sensor is pressed against the rubber sheet, as shown in Fig. 4(a). Thus electrical initiation of the sensor is possible simply by pressing the sensor against the rubber sheet. The rubber sheet has an electric connector (EC) at its upper end as shown in Fig. 3(b). Electrical operation is

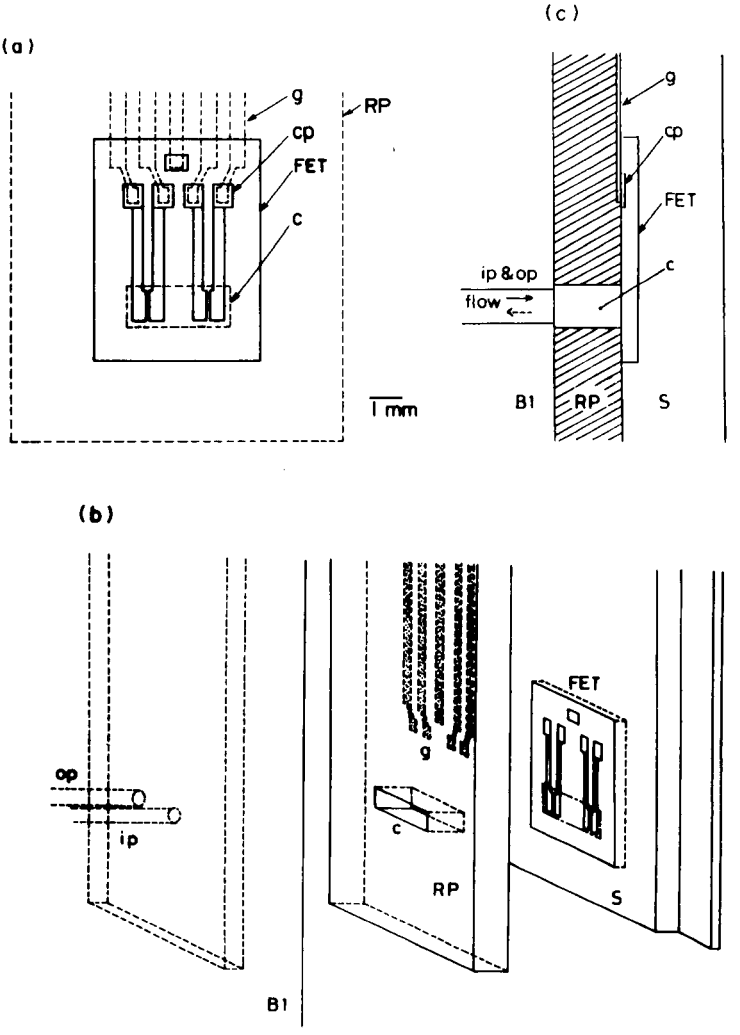

Fig. 4. Illustrations to show how the enzyme-modified FET sensor is set into the flow-through cell: (a) front view; (b) exploded view; (c) cross-section. Parts: g, gold deposited line; cp, contact pad; c, hole in silicone rubber sheet; op, outlet tube; ip, inlet tube. Other abbreviations as in Figs. 2 and 3.

achieved with an amplifier (AMP) outside the flow cell. A small gold electrode acting as a pseudo-reference electrode [2] is fixed at the center of the hole of the rubber sheet and between the edges of the inlet and outlet pipes (for simplicity, it is not shown in Figs. 3 and 4). The gold electrode is also electrically connected to the amplifier via the electrical connector.

All experiments were done at room temperature and all solutions were prepared in potassium phosphate buffer (0.02 M, pH 6.9), 1 mM in EDTA and 0.05% (w/v) in sodium azide [5]. The solution flow rate used for the flow-injection apparatus was 0.6 ml min^{-1}.

Electrical evaluation of the FET sensor used with the flow cell was done with a Yokogawa Hewlett-Packard (Tokyo) 4145A semiconductor parameter analyzer. A Kyouwa Riken (Tokyo) K-161MA150 wafer probe was also used.

RESULTS AND DISCUSSION

Electrical evaluation of the flow-through cell

The electrical operation of the FET sensor was done by physical contact of the FET contact pads (cp in Fig. 4) with the gold deposited lines (g) rather than by bonded wires, as is described above. Therefore, it was necessary to evaluate the contact resistance between them. This was achieved by taking advantage of a p-n junction of the FET which had been made for the purpose of element isolation [7]. The current-voltage characteristics of the junction could be measured by applying a potential between the FET substrate and source contact pads. The forward directed voltages required to feed a constant current were measured for ten different FET sensors, using the flow cell. Concurrently, those required voltages were also measured for the ten identical FET sensors with the wafer probe and compared with the former voltage values. The results obtained showed that in no case were the former values significantly different from the latter, and that consequently the contact resistances between the contact pads and the gold deposited lines were always negligibly small for FET operation.

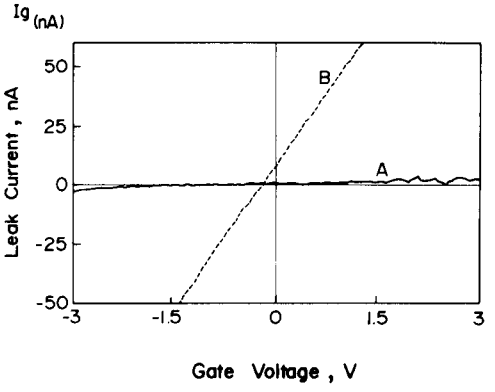

Fig. 5. Typical leakage current from the FET substrate to aqueous solution: (A) when the surfaces of the FET sensor and silicone rubber sheet are dry before the sensor is placed in the flow-through cell; (B) when one of those surfaces is wet. The FET source is connected to electrical ground and bias potential is applied to the gold reference electrode.

The electric insulation of the flow cell was checked by measuring the leakage current from the FET substrate to an aqueous solution. It is very critical for FET operation in aqueous environments to keep the leakage current lower than a certain limit [23–25]. Leakage current was measured with a FET sensor put into the flow cell through which phosphate buffer was pumped, by a procedure similar to that reported by Sibbald et al. [23]. The source of the FET was connected to electrical ground and a bias potential, sweeping from -3 to $+3$ V in 50-mV increments, was applied to the gold reference electrode with the computer-controlled electrical equipment. The leakage current flowing through the reference electrode was measured. Typical results are shown in Fig. 5. Line A is a leakage current curve over the gate voltage range of -3 to $+3$ V. As long as the surfaces of the FET sensor and silicone rubber sheet were dry before the sensor was placed in the flow cell, about twenty different sensors gave almost the same results as line A. The leakage currents observed were $\leqslant 5$ nA. These results compare favourably with the fact that FET leakage currents should not exceed 20 nA [24] or 30 nA [25]. However, if the surface of the sensor or the rubber sheet was wet, an undesirably high leakage current was observed, such as that shown by line B in Fig. 5. Therefore, it is concluded that current leakage is not a significant problem as long as care is taken to keep the surfaces of the FET sensor and rubber sheet dry before the sensor is placed in the flow cell.

Finally the noise and drift levels of the FET sensor in the flow cell were compared with those of the epoxy-encapsulated FET sensor reported earlier [5], for which a somewhat different flow cell was used. In both cases phosphate buffer was pumped through the cell at 0.6 ml min^{-1}. The noise for the encapsulated sensor was 27 ± 7 μV (mean $\pm$ standard deviation, $n=12$) whereas that for the new sensor was 31 ± 7 μV ($n=10$). The drifts were 180 ± 160 and 230 ± 180 μV min^{-1}, respectively, for measurements over the first 10 min from initiation of sensor activity. Thus the new sensor and cell show statistically the same noise and drift levels as those of the epoxy-insulated sensor. Noise and drift were also measured over longer times, up to 5 days. Neither the noise nor the drift showed a tendency to increase beyond the values given above. Therefore, it can be concluded that the design of the FET sensor used with the new flow cell gives rise to no noise and drift problems.

Application of the flow cell with a urea-sensitive enzyme-modified FET. The flow-through cell was applied with the urea-sensitive FET described above. After the urea-sensitive sensor was set into the flow cell, 100 μl of analyte solution was injected into the flowing wash solution (Fig. 3a). Figure 6 shows the response curves obtained for urea concentrations from 0.25 to 50 mg l^{-1}. Peak output voltages were obtained at almost identical times (ca. 25 s) after peak onset when urea concentrations were <10 mg l^{-1}. With greater urea concentrations the time required to reach peak maximum was prolonged. The response had a relative standard deviation ($n=5$) of $<3\%$ over this entire

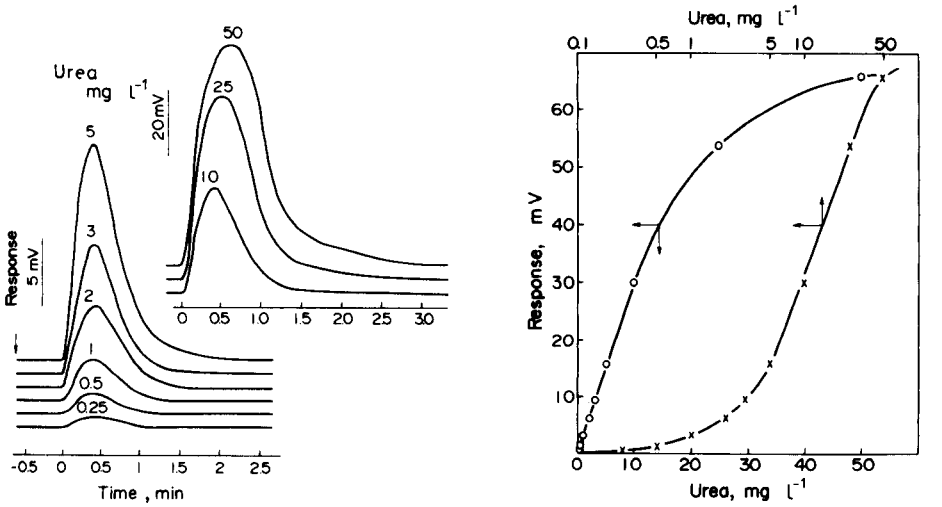

Fig. 6. Response curves of the urea-sensitive enzyme-modified FET sensor used with flow-through cell. Flow rate of wash solution was 0.6 ml min^{-1}; 100 μl of analyte solution injected at the time indicated by the arrow.

Fig. 7. Calibration graphs for urea-sensitive enzyme-modified FET sensor.

concentration range. Figure 7 shows the calibration curves on both linear and semilogarithmic scales. The urea sensor output is linear up to ca. 10 mg l^{-1}. On the semilogarithmic plot, there is a linear region from 5 to 25 mg l^{-1}.

In the work reported here, the urease-immobilized membrane was deposited on the FET gate surface after the FET sensor (Fig. 2) had been made. The order of sensor fabrication should be reversed from the viewpoint of mass production: the enzyme membrane should first be deposited on the FET gate surfaces on the wafer, then the wafer diced into enzyme-modified FET chips, and finally the FET chip attached to a plastic card to make the FET sensor. However, it is basically reasonable to think that the techniques applied here can allow this proper sequence of sensor fabrication to be adopted. A study to prove this possibility is now being undertaken, along with experiments to test the reproducibility of the response of the enzyme-modified FET fabricated by using such a sequence.

The authors are grateful to Mr. Miyazawa for donating the BASC and to Mr. Hatou and Mr. Kitazaki of the Manufacturing Development Laboratory, Mitsubishi Electric Corporation, for designing the new flow-through cell.

REFERENCES

1 S.D. Caras and J. Janata, Anal. Chem., 52 (1980) 1935.
2 Y. Hanazato and S. Shiono, Proc. 1st Int. Meet. Chem. Sensors, Fukuoka, Japan, Sept., 1982, Kodansha, Tokyo, 1983, p. 513.
3 Y. Hanazato, M. Nakako and S. Shiono, IEEE Trans. Electron Devices, 33 (1986) 47.
4 M. Nakako, Y. Hanazato, M. Maeda and S. Shiono, Anal. Chim. Acta, 185 (1986) 179.
5 S. Shiono, Y. Hanazato and M. Nakako, Anal. Sci., 2 (1986) 517.
6 Y. Hanazato, M. Nakako, M. Maeda and S. Shiono, Proc. 2nd Int. Meet. Chem. Sensors, Bordeaux, France, July, 1986, Imprimerie Biscaye, 1986, p. 576.
7 Y. Hanazato, M. Nakako, M. Maeda and S. Shiono, Anal. Chim. Acta, 193 (1987) 87.
8 Y. Miyahara, T. Moriizumi and K. Ichimura, Sensors and Actuators, 7 (1985) 1.
9 T. Kuriyama, J. Kimura and Y. Kawana, Chem. Econ. Eng. Rev., 17 (1985) 22.
10 J. Kimura, T. Kuriyama and Y. Kawana, Sensors and Actuators, 9 (1986) 373.
11 S.D. Caras, J. Janata, D. Saupe and K. Schmidt, Anal. Chem., 57 (1985) 1917.
12 S.D. Caras, D. Petelenz and J. Janata, Anal. Chem., 57 (1985) 1920.
13 S.D. Caras and J. Janata, Anal. Chem., 57 (1985) 1924.
14 M.J. Eddowes, Sensors and Actuators, 7 (1985) 97.
15 M.J. Eddowes, D.G. Pedleys and B.C. Webb, Sensors and Actuators, 7 (1985) 233.
16 Y. Miyahara, F. Matsu, T. Moriizumi, H. Matsuoka, I. Karube and S. Suzuki, Proc. 1st Int. Meet. Chem. Sensors, Fukuoka, Japan, Sept., 1982, Kodansha, Tokyo, 1983, p. 501.
17 K. Inatomi, Y. Hanazato, M. Nakako and M. Maeda, Proc. 50th Spring Meet. of Chem. Soc. Japan, April, 1985, Chemical Society of Japan, Tokyo, 1985, p. 604.
18 B.A. Mckinley, J. Saffe, W.S. Jordan, J. Janata, S.D. Moss and D.R. Westenskow, Med. Instrum. (Baltimore), 14 (1980) 93.
19 Y. Oomura, personal communication (1986).
20 H.H. van den Vlekkert, Ch. Arnoux, Ph. Lamazzi and N.F. de Rooij, Proc. 2nd Int. Meet. Chem. Sensors, Bordeaux, France, July, 1986, Imprimerie Biscaye, Bordeaux, 1986, p. 462.
21 N.J. Ho, J. Kratochvil, G.F. Blackburn and J. Janata, Sensors and Actuators, 4 (1983) 413.
22 H. Abe, M. Esashi and T. Matsuo, IEEE Trans. Electron Devices, 26 (1979) 1939.
23 A. Sibbald, P.D. Whelly and A.K. Covington, Anal. Chim. Acta, 159 (1984) 47.
24 S.D. Moss, J.B. Smith, P.A. Comte, C.C. Johnson and L. Astle, J. Bioenerg., 1 (1976) 11.
25 U. Oesch, S. Caras and J. Janata, Anal. Chem., 53 (1981) 1983.

Analytica Chimica Acta, 202 (1987) 141-149
Elsevier Science Publishers B.V., Amsterdam — Printed in The Netherlands

AN ELECTROANALYTICAL STUDY OF THE ANTICANCER DRUG DACARBAZINE

A.J. MIRANDA ORDIERES, A. COSTA GARCIA and P. TUÑÓN BLANCO*

Department of Physical and Analytical Chemistry, University of Oviedo, 33004 Oviedo, Asturias (Spain)

W. FRANKLIN SMYTH

Department of Pharmacy, The Queen's University of Belfast, 97 Lisburn Road, Belfast BT9 7BL (Great Britain)

(Received 3rd October 1986)

SUMMARY

The electrochemical behaviour of dacarbazine [5-(3,3-dimethyl-1-triazenyl)imidazole-4-carboxamide; DTIC] was investigated by Tast and differential pulse polarography (d.p.p.) at the dropping mercury electrode, by cyclic and differential pulse voltammetry at the hanging mercury drop electrode and by anodic voltammetry at the glassy carbon electrode. Calibration graphs were obtained for 2×10^{-8}–2×10^{-5} M DTIC by d.p.p., for 5×10^{-9}–1×10^{-5} M by adsorptive stripping voltammetry at a hanging mercury drop electrode, and for 1–10×10^{-5} M by high-performance liquid chromatography with oxidative amperometric detection at a glassy carbon electrode. The methods are compared and applied to determine DTIC added to blood serum after a simple clean-up procedure.

In the last ten years, the anticancer drug dacarbazine [5-(3,3-dimethyl-1-triazenyl)imidazole-4-carboxamide; DTIC] has been accepted clinically for the treatment of some malignant diseases, singly and together with other drugs [1,2]. The drug is normally administered intravenously at 250 mg daily for 5 days, repeated at 3-week intervals. The major side effects are nausea and vomiting. After intravenous injection, DTIC has a half-life in human plasma of ca. 35 min with cumulative urinary excretion in 6 h of 43% of the injected dose in man. DTIC is not appreciably bound to human plasma proteins at concentration of 5 μg ml^{-1}. The only metabolite of DTIC that has been positively identified in man is 5-aminoimidazole-4-carboxamide, AIC [3].

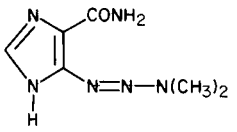

DTIC

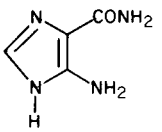

AIC

0003-2670/87/$03.50

Methylation of nucleic acids and urinary excretion of ^{14}C-labelled 7-methylguanine has been observed in man and rat species after administration of DTIC labelled on the dimethyl entity [4].

The first method for the determination of DTIC was described by Loo and Stasswender [5] and involved decomposition by ultraviolet irradiation to produce 5-diazo-imidazole-4-carboxamide (DZC) which was derivatized with the Bratton-Marshall reagent to produce an azo dye, which was measured at 540 nm; DTIC was determined in the concentration range 0.1–5.0 $\mu g\ ml^{-1}$ in pure solutions. The method was extended to real serum samples, but is lengthy and suffers from interferences through reaction of the Bratton–Marshall reagent with other species present in the sample. High-performance liquid chromatography (h.p.l.c.) has been applied in the reverse-phase mode with a C-18 column, methanol/acetate buffer as mobile phase, and ultraviolet detection at 300 nm for the determination of DTIC in serum in the low $\mu g\ ml^{-1}$ concentration range [6]. AIC was not detectable by this method but could be determined by paired-ion h.p.l.c. on a C-18 column with 0.005 M heptane sulphonic acid (pH 4) and methanol (95+5) as the mobile phase and detection at 270 nm. A detection limit of 60 ng ml^{-1} was recently achieved for the determination of DTIC and AIC by ion-pair h.p.l.c. in separate chromatographic experiments [7].

To date, only d.c. polarographic studies on the parent drug DTIC have appeared in the literature [8–10]. This paper is concerned with the behaviour of the drug in Tast and differential-pulse polarography, and cyclic and differential-pulse voltammetry and with h.p.l.c. with anodic amperometric detection and their application to the trace determination of dacarbazine.

EXPERIMENTAL

Apparatus

Polarographic and pulse voltammetric measurements were made with a Metrohm E-506 polarograph, equipped with an E-505 polarographic stand. For cyclic voltammetry, a Metrohm VA-612 scanner was coupled with a Metrohm VA-611 potentiostat and a Graphtec WX 4421 X-Y recorder. As working electrodes for the study of cathodic processes, a dropping mercury electrode (DME; $m = 2.970\ mg\ s^{-1}$, $t = 2.20$ s, measured in open circuit in 0.1 M perchloric acid) and a hanging mercury drop electrode (HMDE; Metrohm E-410, drop area 2.20 mm^2) were used, together with a saturated calomel reference electrode (SCE) and a platinum wire auxiliary electrode. For anodic voltammetry, a glassy carbon disk (Metrohm EA-286, geometric area: 7.06 mm^2) served as working electode and potentials were measured against a Ag/AgCl/sat. KCl reference electrode.

Oxidative amperometric detection in h.p.l.c. was made with the three-electrode wall-jet type cell (Metrohm 656) fitted with a glassy carbon working

electrode and an Ag/AgCl/sat. KCl reference electrode. A μ-Bondapak C-18 column (30 cm $\times$ 4 mm, particle size 10 μm), a Waters M-510 dual-piston pump and a Waters U6K injection port were used.

Reagents

DTIC standards were supplied by Dome Laboratories (purity 97.3%). Stock solutions (1.00×10^{-2} M) were stored in the dark at 4 °C. Cells and volumetric flasks were protected from light by means of aluminium foil to avoid DTIC photodecomposition. 5-Aminoimidazole-4-carboxamide hydrochloride (98%) was from Sigma.

Britton–Robinson buffers ($I = 0.1$ M, adjusted with sodium perchlorate) and 0.1 M sodium hydroxide were used as background electrolytes. The mobile phase for h.p.l.c. was a (9+1) mixture of 0.05 M ammonium acetate buffer, pH 5.5, and methanol.

Procedures

The biological sample examined was a pooled human blood serum collected from at least five different persons. Adequate amounts of DTIC were added to achieve the desired dug concentrations. Samples were treated according the following procedure.

Dilute 1.0 ml of serum sample with 10 ml of 0.1 M phosphate buffer (pH 7.0). Mix thoroughly. Pass the resulting solution through a C-18 cartridge (Sep-Pak, Waters). Wash the cartridge with 20 ml of water and elute the retained materials with 2.0 ml of methanol. Collect the eluate and evaporate the solvent in a water bath at 60 °C under an inert gas flow. Dissolve the dry serum extract in 10 ml of 0.1 M perchloric acid. Transfer to the cell and, after degassing, record the DTIC peak at -0.69 V (vs. SCE) using the following instrumental settings: pulse amplitude 100 mV; drop time 1 s; scan rate 10 mV s^{-1}. Use the standard additions method for quantitation.

An identical sample clean-up procedure was applied for the h.p.l.c. determination of DTIC in serum. The dry serum extract was redissolved in 300 ml of mobile phase and an aliquot of 50 μl was injected. The chromatograms were recorded under the following conditions: flow rate 1.3 ml min^{-1}; column temperature 27 °C; applied potential +0.98 V (Ag/AgCl/sat. KCl). Quantitation of the DTIC peak ($k' = 5.3$) was achieved by the external standard method.

RESULTS AND DISCUSSION

Tast and differential-pulse polarographic behaviour of DTIC

A 1×10^{-4} M solution of DTIC at various pH's was subjected to Tast polarography (drop time 0.4 s, scan rate of 10 mV s^{-1}). In 0.1 M perchloric acid solution (pH 3.0), two waves were evident, the first wave occurring at more positive potentials and being twice the height of the second wave (Fig. 1). Only

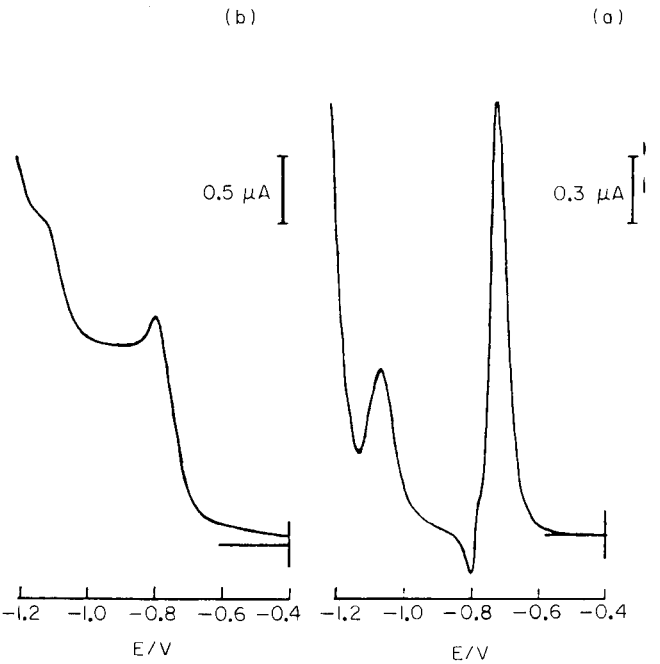

Fig. 1. Differential-pulse (a) and d.c. Tast (b) polarograms of 1.0×10^{-4} M DTIC in 0.1 M perchloric acid. Drop time 0.4 s; scan rate 10 mV s^{-1}; pulse amplitude 50 mV.

the first wave was observed in the pH region 4.0–7.0 At pH 6.0, this wave began to decrease being replaced by a third wave at more negative potentials. By pH 9.0, this third wave had assumed the height of the first wave observed at pH 6.0. The plot of $E_{1/2}$ vs. pH for the first wave had a slope of 50 mV $(pH)^{-1}$ in the pH range 4.0–8.5; that for the third wave had a slope of 37 mV $(pH)^{-1}$ in the pH range 7.0–13.0. All three waves were diffusion-controlled, indicated by their linear i_{lim} vs. $h^{1/2}$ plots.

The differential-pulse polarographic (d.p.p.) behaviour of DTIC in the same supporting electrolytes, with a pulse amplitude of 50 mV, was similar. The sharpest (peak width at half height of 60 mV) and most sensitive signal was observed for the first peak in 0.1 M perchloric acid (Fig. 1). The third peak in 0.1 M sodium hydroxide had a peak width at half height of 100 mV and a peak height of 0.75 μA compared to a peak height of 1.95 μA for the first wave in 0.1 M perchloric acid. A concentration of 35 mg l^{-1} Triton X-100 was sufficient to suppress the maximum observed on the d.c. polarograms of DTIC in acidic supporting electrolytes.

The calibration graph of the d.p.p. current in 0.1 M perchloric acid vs. concentration was linear in the range 2.0×10^{-8} M–2.0×10^{-5} M with a correlation coefficient of 0.999 (scan rate 10 mV s^{-1}; pulse amplitude 100 mV; drop time 1 s).

In order to obtain information on the reduction mechanism of DTIC at the DME, coulometry was applied at applied potentials of −0.94 V and −1.17 V in 0.1 M perchloric acid, and at −1.70 V in pH 12.0 supporting electrolytes containing 2.20 μmol of DTIC; these potentials correspond to the plateaux of the three waves. The results indicated that the first and third waves each involved the consumption of four electrons and that the second wave involved two electrons. Information on the chemical nature of the reduction product(s) at mercury electrodes was found from exhaustive electrolysis of DTIC solution in 0.1 M perchloric acid at potentials corresponding to the plateaux of the first and second waves, followed by recording of the first derivative anodic voltammetric signals at the glassy carbon electrode. After exhaustive electrolysis at −0.94 V at the mercury electrode, the resulting anodic voltammogram gave a main peak at +0.49 V (vs. SCE) and several small peaks at more positive potentials. Exhaustive electrolysis at −1.17 V gave rise to a single anodic peak at the glassy carbon electrode at +0.82 V (vs. SCE). Voltammetry of a standard AIC solution gave an identically shaped peak at this same potential. Ammonia was identified as a product of this exhaustive electrolysis at −1.17 V. The DTIC solutions electrolyzed at −1.70 V in pH 12.0 supporting electrolytes gave ultraviolet spectra with a maximum at 274 nm; AIC also gave a single maximum at 274 nm.

From this information, one may postulate the following acid-base and electrochemical behaviour of DTIC at the dropping mercury electrode:

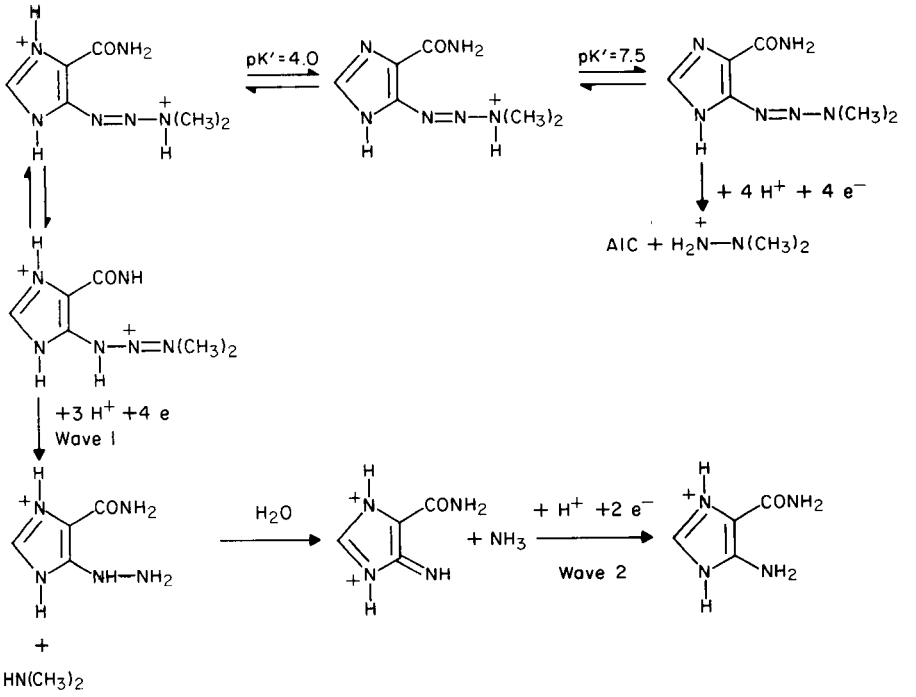

It is reasonable to suppose that the singly and doubly protonated forms of DTIC undergo similar electrochemical steps. The above mechanism for DTIC reduction in acidic medium is supported by the fact that in aromatic and heterocyclic hydrazo compounds, electroreduction occurs through quinoid intermediate species [11]. Further, the generation of quinoid forms by hydrolytic breakdown of the N–N bond has been reported as a necessary chemical step prior to the reduction of substituted azobenzenes to the corresponding amines [11]. The existence of a chemical step prior to the charge transfer in the second wave is also supported by the observed cyclic voltammetric behaviour of DTIC, as indicated below. With regard to the tautomerization equilibrium prior to electron transfer for the first wave, a similar explanation has been given for asymmetric 1,3-diphenyltriazenes [12].

Determination of DTIC in a spiked serum extract. Standard amounts of DTIC in the range 0.18–19.7 μg were added to the extract of 1 ml of serum dissolved in 10 ml of 0.1 M perchloric acid and examined by d.p.p. (pulse modulation amplitude 100 mV, drop time 1 s, scan rate 10 mV s^{-1}). The DTIC peak was observed at -0.69 V and a linear relationship was observed between the peak current of the first wave and concentration in the given range ($r=0.999$). No interfering peaks from the serum extract were observed. The procedure indicated in the Experimental section was then applied to the DTIC assay in serum samples spiked with different amounts of the drug. The precision (relative standard deviation) was 10.5% at the 0.91 μg ml^{-1} concentration ($n=5$), with 46% recovery. The detection limit found was 90 ng ml^{-1}.

Cyclic and differential pulse voltammetric behaviour of DTIC

Cyclic voltammetry of 1.0×10^{-4} M DTIC in 0.1 M perchloric acid showed two irreversible reduction processes at the HMDE (Fig. 2). Both processes would appear to be diffusion-controlled; linear plots of peak current vs. the square root of scan rate (v) were obtained over the range 5–200 mV s^{-1}. But for scan speeds higher than 800 mV s^{-1}, the current of the second reduction process decreased with increasing scan speed, and disappeared at a scan speed of 2 V s^{-1}. This suggests that the second reduction process is kinetically controlled and supports the proposed mechanism for the second polarographic wave in perchloric acid solutions.

The effect of the concentration of DTIC on the cyclic voltammetric curves was also studied. At concentrations $<5.0\times10^{-6}$ M, DTIC was adsorbed at the HMDE. At such concentrations the firt peak was nearly symmetrical and the peak current increased linearly with the first power of scan rate above 50 mV s^{-1}. The peak current also increased with the electrode/solution contact time, t_{acc} (Fig. 3). Linear plots of i_p vs. $t_{acc}^{1/2}$ were found, indicating a diffusion-controlled adsorption process [13].

An adsorptive stripping voltammetric method for the determination of trace

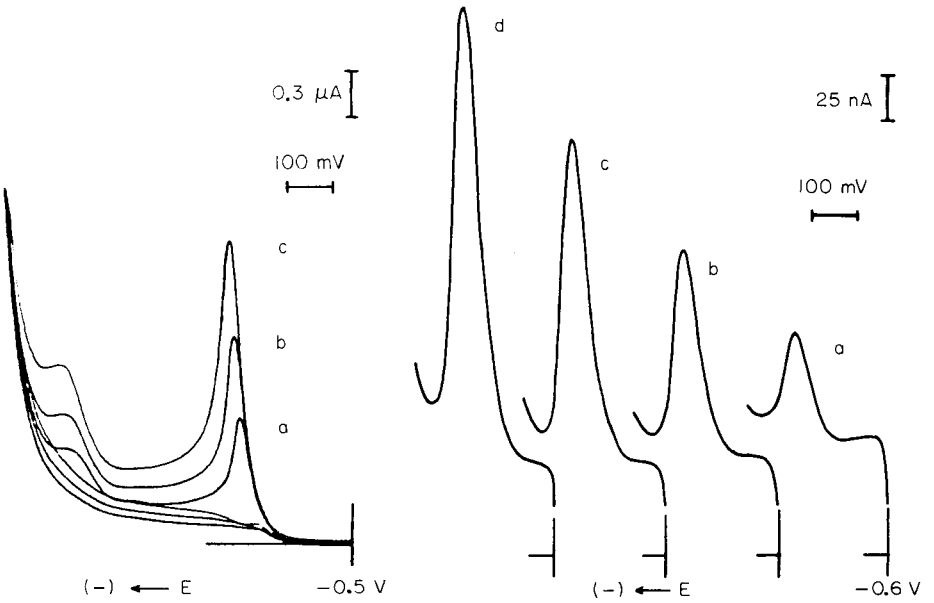

Fig. 2. Cyclic voltammograms of 1.0×10^{-4} M DTIC in 0.1 M perchloric acid. Scan rate: (a) 20, (b) 50, (c) 100 mV s^{-1}.

Fig. 3. Effect of preconcentration time on peak current for DTIC reduction in 0.1 M perchloric acid (DTIC concentration 2.5×10^{-6} M; scan rate 100 mV s^{-1}). Preconcentration time: (a) 0, (b) 10, (c) 30, (d) 80 s.

concentrations of DTIC at the HMDE was then tested. With 1.0×10^{-6} M DTIC and an accumulation time (t_{acc}) of 80 s, the other optimum operating conditions were found to be: accumulation/deposition potential −0.50 V; pulse amplitude 100 mV; scan rate 25 mV s^{-1}. Under these conditions, the ratio of the stripping signal to the direct voltammetric response (zero preconcentration time) was 4.5. Calibration under the specified operating conditions produced linear plots of peak height vs. concentration in the range 5×10^{-9}–1.0×10^{-5} M DTIC ($r=0.999$) with a detection limit ($S/N=2$) of 4.0×10^{-9} M. This is approximately 5 times more sensitive than differential pulse polarography at the DME.

Anodic voltammetric behaviour of DTIC at the glassy carbon electrode and its application to oxidative amperometric detection of DTIC

DTIC is oxidized at the glassy carbon electrode over the pH range 1–12. A plot of E_p vs. pH showed three linear portions with slopes of 55 mV $(pH)^{-1}$ for pH 1–4.8, 30 mV $(pH)^{-1}$ for pH 4.8–8.1, and 45 mV $(pH)^{-1}$ for pH 8.1–12. The breaks at pH 4.8 and 8.1 agree reasonably well with the pK' values of 4.0 and 7.5 observed in the Tast polarographic study. The peak height was con-

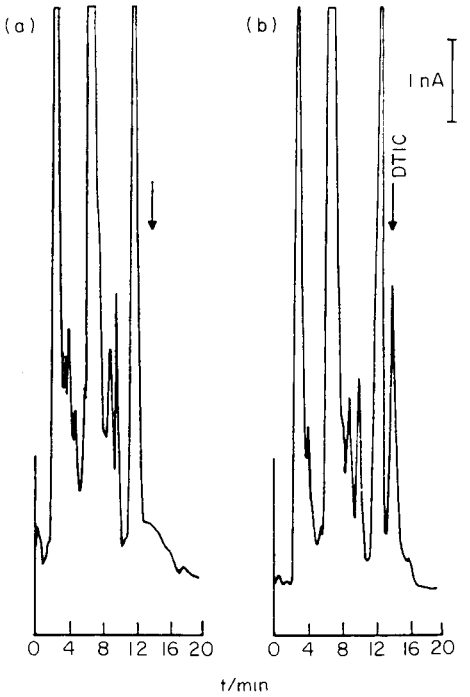

Fig. 4. Determination of DTIC added to serum by h.p.l.c. with amperometric detection: (a) blank; (b) serum spiked with 0.11 μg ml^{-1} DTIC. Applied potential, +0.98 V (vs. Ag/AgCl/sat. KCl); flow rate, 1.3 ml min^{-1}; mobile phase, 0.05 M ammonium acetate buffer pH 5.5/methanol (9+1).

stant over the pH range 1–5 and then decreased to a constant of 70% of the original peak height at pH 8. This suggests that the neutral species at pH 7.5 and pH 8 is oxidized by a different mechanism from the protonated form(s).

When a (9+1) mixture of 0.05 M ammonium acetate buffer and methanol was used as supporting electrolyte and the scan rate was 5 mV s^{-1}, peak and half-peak potentials for oxidation of DTIC at the glassy carbon electrode were +0.98 and +0.92 V (vs. Ag/AgCl/sat. KCl), respectively. Increasing the scan rate from 10 to 100 mV s^{-1} shifted the peak 25 mV towards more positive potentials. The peak height was linearly related to the square root of the scan rate over the range 5–100 mV s^{-1} and to the concentration of DTIC in the range $1\text{–}10\times10^{-5}$ M. A hydrodynamic voltammogram was constructed by repetitive injections of a fixed amount of DTIC into the h.p.l.c. system with electrochemical detection at different applied potentials. The $E_{1/2}$ value found was about +0.95 V, with maximum peak current being obtained at a potential of +1.05 V.

Under the stated conditions, the peak height for DTIC was linearly related to the amount injected in the range 3.6–360 ng (r=0.999). The method was applicable to assay of DTIC added to human serum after a simple clean-up

procedure. The elution conditions described above provided a good separation of DTIC from the naturally occurring compounds in serum. No interference of AIC was found, the metabolite being eluted in the dead volume. Figure 4 shows typical chromatograms obtained for serum samples. The lowest concentration of DTIC in serum detectable ($S/N=2$) was 18 ng ml^{-1}. The precision estimated from a set of five serum samples containing 0.36 μg ml^{-1} DTIC was 8.8%, and the mean recovery was 47%.

We thank the Spanish Government (C.A.I.C.y.T.) for financial support (Project 1182/81).

REFERENCES

1 J.K. Luce, W.G. Thurman and R.W. Talley, Cancer Chemother. Rep., 54 (1970) 119.
2 J.M. Buesa, private communication, Hospital General de Asturias, Oviedo, Spain, 1985.
3 G.E. Housholder and T.L. Loo, J. Pharmacol. Exp. Ther., 179 (1971) 386.
4 J.L. Skibba and G.T. Bryan, Toxicol. Appl. Pharmacol., 18 (1971) 707.
5 T.L. Loo and E. Stasswender, J. Pharm. Sci., 56 (1967) 1016.
6 J. Benvenuto, S. Halla, D. Farquart, K. Lu and T.L. Loo, J. Chromatogr. Sci., 10 (1979) 377.
7 H. Breithaupt, A. Damman and K. Aigner, Cancer Chemother. Pharmacol., 9 (1982) 103.
8 G. Kazemifard, F. Moattar and H. Zia, Arch. Pharm. (Weinheim, Ger.) 312 (1977) 573.
9 L. Wassilewska, Acta Pol. Pharm., 36 (1979) 451 (Chem. Abstr., 93, 13144).
10 L. Wassilewska and J. Deres, Acta Pol. Pharm., 38 (1981) 565 (Chem. Abstr., 96, 192826).
11 F. Thomas and K. Boto, in S. Patai (Ed.), The Chemistry of Hydrazo, Azo and Azoxy groups, Wiley, New York, 1975, Part 1, p. 478.
12 P. Krueger, in S. Patai (Ed.), The Chemistry of Hydrazo, Azo and Azoxy groups, Wiley, New York, 1975, Part 1, pp. 158, 159.
13 P. Delahay and Ch. T. Fike, J. Am. Chem. Soc., 80 (1958) 2628.

Analytica Chimica Acta, 202 (1987) 151–157
Elsevier Science Publishers B.V., Amsterdam — Printed in The Netherlands

INTERMETALLIC COMPOUNDS AND THE DETERMINATION OF COPPER AND ZINC BY ANODIC STRIPPING VOLTAMMETRY

GIOVANNI PICCARDI* and ROBERTO UDISTI
Institute of Analytical Chemistry, University of Florence, 50121 Firenze (Italy)
(Received 14th January 1987)

SUMMARY

The intermetallic Cu–Zn compounds produced during the simultaneous deposition of copper and zinc at a preformed mercury film electrode were studied. Over a wide range of metal concentration ratios, the real concentrations of metals in the amalgam were calculated from the peak areas obtained by anodic stripping voltammetry. The results indicate the formation of CuZn (insoluble) and $CuZn_2$ (soluble) compounds with $K_{SO}=5\times10^{-4}$ and $\beta_2=100$, respectively. The electrodeposition potential of -0.85 V vs. SCE for the reduction of copper in presence of zinc is confirmed as correct.

The apparent complexing capacity of a natural water indicates the extent to which the chelating substances present can be responsible for the formation of inert complexes of trace metals. Because the toxicity of some metals is apparently related to the concentration of the free ion, knowledge of the apparent complexing capacity is needed in studies of the speciation of metals in aquatic environments.

Various methods have been used to assess complexation in sea water [1–3] but anodic stripping voltammetry (ASV) is usually preferred [4–6]. This application of ASV is based on the assumption that the peak currents obtained, after addition of copper(II) ions to the sample, are due only to free Cu^{2+} ions and labile copper(II) complexes. Copper is preferred as a spiking agent because it can form strong complexes with numerous organic substances. Plavsic et al. [7] found that copper had the highest apparent complexing capacity when the same sea water was spiked with cadmium, lead and copper. The great sensitivity of ASV allows direct determinations of apparent complexing capacity.

As is well known, copper combines with zinc, present in natural waters, to form intermetallic compounds that modify the peak current of copper. Usually, a deposition potential more positive than the potential of the zinc peak is selected. Lazar et al. [8] observed, however, that even under these conditions

0003-2670/87/$03.50

zinc interfered because of some deposition of zinc. The break in the curve of i_p vs. added Cu^{2+} concentration was ascribed to the formation of a Cu–Zn intermetallic compound in mercury rather than to the copper-complexing capacity. The experimental results were in reasonable agreement with the numerical simulation of the proposed model.

The aims of the work described here were to reconsider the procedure for determination of apparent complexing capacity and to re-investigate the effects of intermetallic compound formation.

EXPERIMENTAL

An AMEL 473 polarographic analyzer was used with a Hewlett-Packard 7044-A X-Y recorder. The working electrode was either a Metrohm EA-276/2 glassy carbon electrode or a Metrohm E-410 hanging mercury drop electrode. The mercury film was plated from stirred oxygen-free 3% (w/v) NaCl/2.5×10^{-5} M mercury(II) acetate at -1.0 V for 20 min and then held at -0.1 V for 5 min. Before each measurement, the electrode was held at -0.1 V for 1 min, with stirring to avoid memory phenomena. The reference electrode was a saturated calomel electrode (Metrohm EA-404), to which all stated potentials are referred; the auxiliary electrode was a paraffin-impregnated graphite rod. All solutions used were deoxygenated with ultrapure nitrogen prior to measurements, all of which were obtained at 25 ± 0.2°C.

Merck Suprapur sodium chloride, sodium acetate and acetic acid were used to prepare the supporting electrolyte (3% NaCl, 1×10^{-2} M acetate buffer of pH 4.7). Standard solutions of reagent-grade copper and zinc were diluted daily to 1×10^{-5} M. Demineralized water was twice-distilled in all-silica apparatus.

Peak areas were measured with a manual planimeter (Salmoiraghi model 236) on the d.c. stripping voltammograms.

RESULTS AND DISCUSSION

The model proposed by Lazar et al. [9] was based on both voltammetric experiments and zinc-65 radiometric measurements on a sample of Gulf of Eilat sea water spiked with copper and zinc [8,9]. Successive voltammograms were run from -1.40 V to -0.90 V; the first was commenced after 2 min of electrodeposition at -1.40 V, with stirring, and the others simply by switching again to -1.40 V before starting the run. The peak currents of eight successive scans reported by Lazar et al. (Fig. 4 [8]) are reported in Fig. 1 as a function of the scan number. The stripping peak current decreases, reaching a value which depends on the amount of zinc deposited during the scan. The data in Fig. 1 seem to indicate that only 50% of the zinc accumulated is oxidized off the electrode in the first scan. The experiment of Lazar et al. was reproduced in 3% (w/v) NaCl solution with the instrumentation described above. The

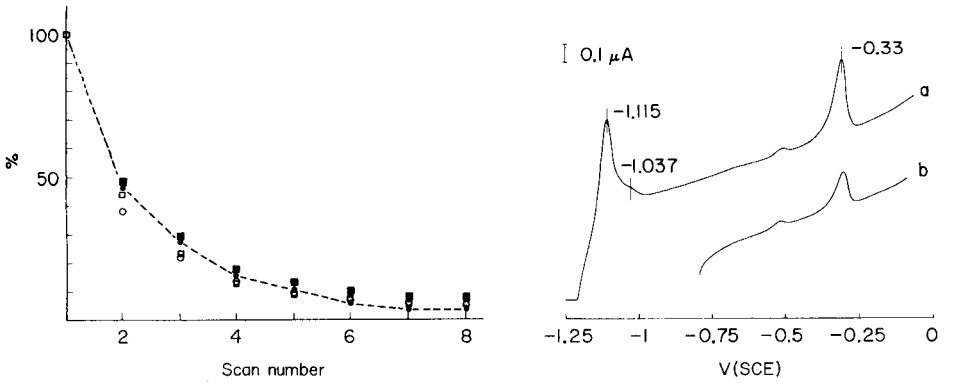

Fig. 1. Successive stripping scans of zinc. Conditions for differential-pulse ASV: pulse amplitude 50 mV, scan rate 5 mV s^{-1}, deposition time 180 s, rest time 30 s. Curves: (●) data from Lazar et al. [8]; (○) MFE with $E_d = -1.40$ V, $[Zn^{2+}] = 5 \times 10^{-7}$ M; (■) HMDE with $E_d = -1.40$ V, $[Zn^{2+}] = 5 \times 10^{-6}$ M; (□) HMDE with $E_d = -0.85$ V, $[Cd^{2+}] = 2 \times 10^{-6}$ M. The peak height obtained in the first scan is regarded as 100%.

Fig. 2. D.c. stripping voltammograms at the MFE for a 1.94×10^{-7} M Cu^{2+}/4.85×10^{-7} M Zn^{2+} solution. Deposition potential: (a) −1.40 V; (b) −0.85 V. Deposition time, 180 s.

values obtained with a mercury film electrode (MFE) are in accord (Fig. 1) with the earlier values [8].

It seems improbable that the phenomenon can be ascribed to undervoltage deposition of zinc because zinc and cadmium show the same behaviour on a hanging mercury drop electrode (HMDE) (Fig. 1). However, prolonged electrodeposition (30 min) of zinc solutions at −0.90 V, a potential at which "undervoltage" deposition of zinc should occur, resulted in a peak of the same amplitude as the peak obtained by switching the potential to −1.40 V and starting the scan. This peak was the same as that obtained from electrodes without "memory", e.g., a new MFE.

The correct interpretation of the electrode behaviour shown in Fig. 1 is that zinc does not remain as metal on the electrode but slowly diffuses as ion back into the bulk solution. When the potential is switched again to −1.40 V to start the next scan in the unstirred solution, the Zn^{2+} still around the electrode rapidly diffuse back to the electrode and are reduced. Indeed, when the solution was stirred for 2 s at the end of scan 1 (Fig. 1), the peak current for scan 2 was the same as for scans 7 or 8.

The agreement of radiochemical zinc-65 measurements with the voltammetric measurements is only apparent because the results were misinterpreted [10]. The authors [9] also did not take into account the possible difference between Zn^{2+} adsorption at a potential of −0.7 V (4080 cpm) and with an open circuit (3086 cpm). The absence of undervoltage phenomena in the described conditions indicates that it should be possible to determine copper ion

without interference from zinc at the MFE if the electrolysis potential is sufficiently more positive than the zinc oxidation peak. The intermetallic Zn–Cu compound, however, interferes in the zinc determination by ASV. With the small volume of mercury on the MFE, very high amalgam concentrations of both metals are produced, and the peak current for zinc decreases as increasing concentrations of Cu^{2+} are added to the solution [5]. Kemula et al. [11] were the first to recognize the formation of intermetallic Cu–Zn compounds. Later, different authors [4,12–14] concluded that the stoichiometry was 1:1 and, assuming that the compound in mercury was of limited solubility, they reported solubility products ranging from 1×10^{-8} to 1×10^{-5}. More recently, Shuman and Woodward Jr. [5] showed that three soluble compounds are formed, with copper-to-zinc ratios of 1:1, 1:2 and 1:3; an insoluble 1:3 compound is also formed at high amalgam concentrations. The instability constant $K_1=1.9\times10^{-3}$ was obtained from measurements at the HMDE; with the MFE the values calculated were $K_2=7.6\times10^{-2}$, $K_3=2.1$ and $K_{so}=3.1\times10^{-5}$ [5].

In differential-pulse anodic stripping voltammetry (DPASV), successive additions of Cu^{2+} to a zinc solution decrease the peak current for zinc and, at low pulse amplitudes (ΔE), the increase in the copper peak is greater than expected. This phenomenon can be ascribed to the oxidation of free copper and of zinc in the intermetallic compound at the same potential. For $\Delta E \geqslant 50$ mV, the total peak current for Cu+Zn at a deposition potential (E_d) of -1.40 V is the same as that for copper alone with $E_d=-0.85$ V. In DPASV, the total peak currents for free zinc (-1.11 V) and for the intermetallic compound ($E=-0.35$ V) are always less than the total peak currents for zinc and copper separately. The difference between the values decreases as ΔE decreases. Therefore, the differential-pulse technique does not seem useful for studying intermetallic compounds, or for distinguishing their oxidation potentials.

Direct-current stripping voltammograms obtained from a Cu^{2+}/Zn^{2+} solution in 3% (w/v) sodium chloride at pH 4.7 are shown in Fig. 2. Near the zinc peak at -1.11 V, a small peak appears at -1.04 V when some copper ion is added; the copper peak itself is at -0.33 V. The peak area at -0.33 V in curve (a) is greater than that in curve (b) where only copper is stripped from the MFE. The difference in area can be attributed to the charge needed for the oxidation of zinc in the intermetallic compound. Increasing the Cu^{2+} concentration in the Zn^{2+} solution decreases the peak area for zinc (-1.11 V), and increases the peak area at -0.33 V equivalently, as shown in Fig. 3. For both curves, the break point is situated at a 1:1 Cu/Zn ratio in the solution, and corresponds to the same 1:1 ratio in the amalgam, because the accumulation coefficients for zinc and copper are the same [5]. The charge for oxidation of copper alone after accumulation at -0.85 V is also shown in Fig. 3.

To obtain the stability constants of intermetallic compounds, the concentrations of the separate free components in the amalgam must be known. The quantities of Cu, Zn and Hg can be obtained from the number of coulombs

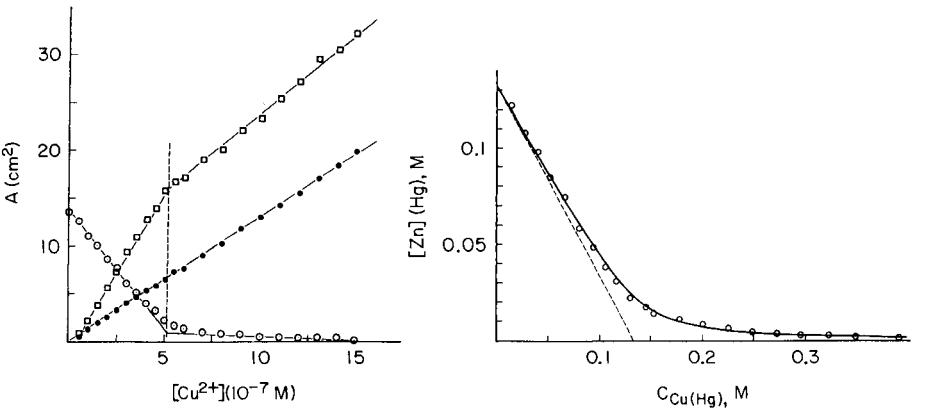

Fig. 3. Dependence of the area (A) of the stripping peaks for 5×10^{-7} M Zn^{2+} vs. the Cu^{2+} concentration: (○) $E_p=-1.115$ V, $E_d=-1.40$ V; (□) $E_p=-0.33$ V, $E_d=-1.40$ V; (●) $E_p=-0.33$ V, $E_d=-0.85$ V.

Fig. 4. Concentration of free zinc in mercury vs. total copper concentration in mercury. The continuous line is calculated for $K_{so}=5\times10^{-4}$ and $\beta_2=100$.

corresponding to the oxidation peaks if the number of electrons (n) involved is known. The number of electrons needed for the oxidation of copper in sea water was estimated by measuring the areas of the copper peaks obtained by stripping in 3% (w/v) sodium chloride at pH 4.7 and in the same solution after addition of 5×10^{-3} M EDTA. In the second experiment, EDTA was added immediately before the stripping scan so that the deposition of copper was the same in both cases. The peak area recorded with EDTA added was twice the size of the one in sodium chloride alone, indicating the formation of copper(I) in the latter medium. Further evidence of $n=1$ for the oxidation of copper in 3% (w/v) NaCl is given by the ratio (2) of the peak areas for zinc and copper. As the accumulation coefficients are the same (see above), the difference in area can be attributed to the different numbers of electrons involved in oxidation. Abdullah et al. [15], who eventually used gallium to prevent intermetallic compound formation in the determination of Cu, Pb, Cd and Zn in sea water, observed an electrode "memory" effect and attributed the copper problem to the metal remaining as an amalgam in the mercury film. The phenomenon should rather be ascribed to the formation of an insoluble film on the MFE. The effect of pH on the copper "memory" [15] substantiates this; at natural pH, an apparent release of only 60% of the copper present in the mercury film was observed, whereas at pH 3.2 there was no measurable copper. It seems plausible, therefore, that the electrode memory corresponds to the solubility of the corrosion products of copper in sea water [16], e.g., $K_{so}=1\times10^{-6}$ for CuCl and $K_{so}=1\times10^{-14}$ for Cu_2O [17].

At the end of each series of measurements, solid potassium iodide was added

to the solution to give a 0.2 M concentration, and the potential was scanned to −0.1 V, which enabled the oxidation peak of mercury to be recorded. In this medium, mercury forms tetraiodomercurate(II) ion [18], thus the quantity and volume of the mercury film can be calculated from the peak area. However, the charge thus calculated was only 93% of the charge measured during the deposition stage from mercury(II) chloride solution. The latter estimate is more reliable than the calculation based on the assumption of 100% current efficiency.

From the volume of mercury thus calculated ($4–5\times10^{-10}$ l), the total zinc and free zinc concentrations in mercury were estimated from the areas of the peaks at −1.11 V in absence of copper and with increasing concentrations of copper, respectively. The total concentration of copper was obtained from the area of the peak at −0.33 V, obtained after deposition at −0.85 V. The concentrations of free zinc in mercury, $[Zn]_{Hg}$, obtained in the presence of different concentrations of total copper in mercury, $C_{Cu(Hg)}$, are shown in Fig. 4. The dotted line, corresponding to the mole ratio 1:1, indicates that CuZn is the predominant compound that is oxidized to give a peak at the same potential as free copper.

Crosmun et al. [19], who used zinc-65, observed that at −0.75 V all the zinc bound to copper is stripped after a total elapsed time of 2 h. This seems to confirm the very low solubility of CuZn indicated by anodic stripping [13,20,21] and potentiometric [21,22] measurements. If a mercury-soluble compound were formed, very slow dissociation would explain the complete stripping of zinc at the copper stripping potential. The peak at −1.04 V (Fig. 2) appeared with the first addition of copper and decreased when the copper concentration in the amalgam was very high. This peak may be caused by dissolution of a mercury-soluble $CuZn_2$ compound which is stripped between copper and zinc; if CuZn is insoluble, $CuZn_2$ must be soluble. If both compounds were insoluble, the free zinc concentration would correlate with the ratio of solubility products, not with the amalgam composition as shown in Fig. 4.

From the experimental data, it is possible to obtain the equilibrium constants:

$$Cu(Hg) + Zn(Hg) \rightleftharpoons CuZn(Hg); K_{so} = [Cu]_{Hg}\,[Zn]_{Hg}$$

$$Cu(Hg) + 2Zn(Hg) \rightleftharpoons CuZn_2(Hg); \beta_2 = [CuZn_2]_{Hg}/[Cu]_{Hg}\,[Zn]^2_{Hg}$$

The constants calculated by the least-squares fitting were $K_{so}=5\times10^{-4}$ and $\beta_2=100$. The formation constants obtained by considering CuZn soluble and $CuZn_2$ insoluble, or both compounds soluble, provided less satisfactory fits. Stability constants were calculated on the assumption that copper is present totally as the amalgam, although a solubility of $6–10\times10^{-3}$ atom-% has been reported [22]. However, under the conditions of these experiments, no deviation from linearity of the $[Cu]_{Hg}$ vs. $[Cu^{2+}]$ relation was observed. The solubility products reported here are different from the literature data, probably

because of the larger number of experimental points and the wider range of metal concentrations considered.

The formation of intermetallic compounds is, of course, less of a problem with hanging drop mercury electrodes because of the high dilution of metals in the amalgam. Therefore, zinc can be determined accurately in presence of copper in natural waters even with the differential-pulse technique. With the MFE, interference effects can be eliminated by adding gallium, which preferentially forms intermetallic copper-gallium rather than copper–zinc compounds [15,23]. Further work on the effect of gallium and the optimal conditions for its use is in progress.

REFERENCES

1 S.F. Sugai and M.L. Healy, Mar. Chem., 6 (1978) 291.
2 P. Figura and B. McDuffie, Anal. Chem., 51 (1979) 120.
3 R.J. Stolzberg and D. Rosin, Anal. Chem., 49 (1977) 226.
4 W.L. Bradford, Chesapeake Bay Institute, Johns Hopkins University, Baltimore, MD, 1972, Report no. 76.
5 M.S. Shuman and G.P. Woodward Jr., Anal. Chem., 48 (1976) 1979.
6 D.A. Roston, E.E. Brooks and W.R. Heineman, Anal. Chem., 51 (1979) 1728.
7 M. Plavsic, D. Krznaric and M. Branica, Mar. Chem., 11 (1982) 17.
8 B. Lazar, A. Nishri and S. Ben Yaakov, J. Electroanal. Chem., 125 (1981) 295.
9 B. Lazar, A. Katz and S. Ben Yaakov, Mar. Chem. 10 (1981) 221.
10 M. Plavsic, D. Krznaric and M. Branica, Mar. Chem., 11 (1982) 17.
11 W. Kemula, Z. Galus and Z. Kublik, Nature (London), 182 (1958) 1228.
12 A.G. Stromberg, M.S. Zakharov and N.A. Mesyats, Elektrokhimiya, 3 (1967) 1440.
13 N.A. Mesyats, A.G. Stromberg and M.S. Zakharov, Elektrokhimiya, 4 (1968) 987.
14 R.G. Rudolph, Ph.D. Thesis, University of Nebraska, Lincoln, NE, 1969.
15 M.I. Abdullah, B. Reusch Berg and R. Klimek, Anal. Chim. Acta, 84 (1976) 307.
16 G. Bianchi and P. Longhi, Corros. Sci., 13 (1973) 853.
17 Stability Constants of Metal-Ion Complexes, The Chemical Society, London, 1964.
18 R. Neeb, Inverse Polarographie und Voltammetrie, Verlag Chemie, Weinheim, 1969, p. 195.
19 S.T. Crosmun, J.A. Dean and J.R. Stokely, Anal. Chim. Acta, 75 (1975) 421.
20 A.G. Stromberg and V.E. Gorodovykh, Zh. Neorg. Khim., 8 (1963) 2355.
21 P. Ostapczuk and Z. Kublik, J. Electroanal. Chem., 83 (1977) 1.
22 M. Kozlovsky and A. Zebreva, in P. Zuman and I.M. Kolthoff (Eds.), Progress in Polarography, Vol. 3, Interscience, New York, 1972, p. 157.
23 T.R. Copeland, R.A. Osteryoung and R.K. Skogerboe, Anal. Chem., 46 (1974) 2093.

Analytica Chimica Acta, 202 (1987) 159–166
Elsevier Science Publishers B.V., Amsterdam — Printed in The Netherlands

DETERMINATION OF TOTAL BASICITY AND AVAILABLE LYSINE IN PROTEINS BY NONAQUEOUS TITRIMETRY

I. MOLNÁR-PERL* and M. PINTÉR-SZAKÁCS

Institute of Inorganic and Analytical Chemistry, L. Eötvös University, Múzeum Krt. 4/B, H-1088 Budapest (Hungary)

(Received 7th May 1986)

SUMMARY

A simple method is presented for the determination of the available lysine residues of proteins. The sample is titrated directly with 0.05 or 0.1 M perchloric acid in anhydrous acetic or propionic acid to a potentiometric end-point. The titration is repeated after acylation of the sample. The difference between the two basicity values gives the available lysine content of the proteins. Results are provided for the available lysine contents of bovine serum albumin, human γ-globulin, β-casein, soya bean meals meat meal and milk protein; in most cases, they agree closely with literature data obtained by other methods. The standard error for the procedure is $<3.9\%$.

Knowledge of the available lysine content, i.e., the lysine residue possessing a free ϵ-amino group, is important in protein chemistry from both the biological and nutritional points of view. The well-known classical chemical methods for the determination of available lysine with a few exceptions [1–8] necessitate the hydrolysis of proteins [9–17]. Protein hydrolysis is a time-consuming and drastic procedure, and correction factors are required when it is applied [6].

In this paper, a new, simple method is described for the potentiometric determination of proteins in nonaqueous media. Samples are titrated with perchloric acid in anhydrous acetic or propionic acid; the difference between the results of direct titration, which corresponds to the total basicity, and of the same titration after acylation, enables the available lysine content to be obtained. No similar data seem to be available in the literature. Direct potentiometric monitoring of proteins in aqueous solutions, based on the interaction of silver or copper electrodes with the sulphur-containing residue of proteins, has been summarized recently [18–22].

0003-2670/87/$03.50

EXPERIMENTAL

Materials and apparatus

All reagents were of analytical purity (Reanal, Budapest). Bovine serum albumin (BSA), human γ-globulin (HG) and β-casein were from the Institutes for Serobacteriological Production and Research, Budapest. Soya bean meal (SBM) 1 and 3 were imported separately from the U.S.A.; soya bean meal 2 was from Brazil. Meat meal and milk protein were both of Hungarian origin. Milk protein was first treated enzymatically then with acid. Meat meal was prepared by pressing and extracting in order to remove all fat.

The soya bean meal and meat meal were powdered to a particle size of <60 mesh. The particle size of BSA was very small; to avoid agglomeration, the protein was mixed with glass beads (particle size, 80/100 mesh; Analab, North Haven, CT, U.S.A.) in a ratio of 1:10.

A Precision Digital pH-Meter (OP-208/1, Radelkis) was used. Electrodes for nonaqueous solvents were a glass electrode (type Ac-OH-B-10) and a silver/silver chloride reference electrode (type AgCl-10), both from Tacussel (Lyon, France).

Procedures

Determination of the total basicity of proteins (Procedure A). The protein or protein-containing matrix (usually 50–200 mg weighed to 0.1 mg) was placed in a 100-ml glass beaker, and 30 ml of anhydrous acetic acid or anhydrous propionic acid was added. The covered beaker was placed on a boiling water-bath for different times. After various soaking times, the solution was cooled to ambient temperature and titrated with standard 0.05 M or 0.1 M perchloric acid dissolved in anhydrous acetic acid or propionic acid, as appropriate. This procedure yields the A values mentioned in the Tables.

Determination of the total basicity of proteins after acylation (Procedure B). The above procedure was followed except that 15 ml of anhydrous acetic acid and 15 ml of propionic anhydride were used. In this case, the soaking and acylation of the protein proceeded simultaneously. This procedure yields the B values in the Tables. The available lysine content of the protein is calculated from A – B.

RESULTS AND DISCUSSION

Characteristic titration curves of representative standard proteins and protein matrices (Figs. 1–5) illustrate that the potential jumps at the equivalence points are large and steep in most cases, whether the medium is anhydrous

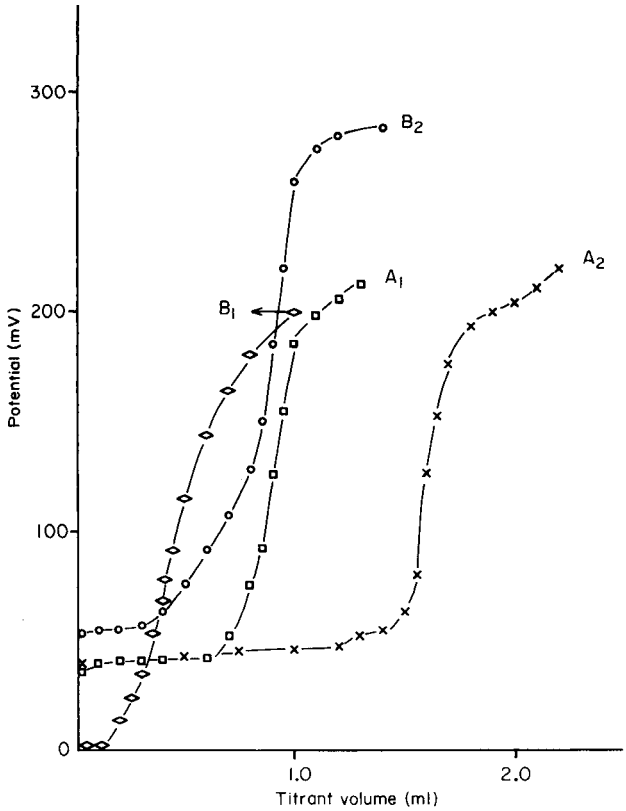

Fig. 1. Titration curves for different amounts of BSA in anhydrous acetic acid. Curves: (A) measurements without acylation for samples weighing 0.0526 g (A_1) and 0.0919 g (A_2); (B) measurements after acylation for samples weighing 0.0527 g (B_1) and 0.1028 g (B_2). (Evaluation is presented in Table 3.)

acetic or propionic acid. Unambiguous evaluation of the end-points is readily achieved by using the classical second-derivative method. The magnitude of the jumps obtained is independent (± 20 mV) of the amount of the protein titrated (Figs. 1, 4 and 5), but depends on the nature of the protein and on the procedure applied, varying from 180 mV to about 440 mV. The potential jumps tend to be larger for the titrations in anhydrous propionic acid compared to those in acetic acid, with the exception of the protein in soya bean meal which gave nearly the same jumps in both media (200–250 mV).

The above features can be explained by the fact that both propionic acid and propionic anhydride are stronger Lewis bases than acetic acid. In the case of the soya bean protein, the effect of the increased basicity is counteracted by its relatively high (50% w/w) saccharide content.

Preliminary investigations for each protein began with establishing the optimum times of soaking and acylation. The results obtained are summarized

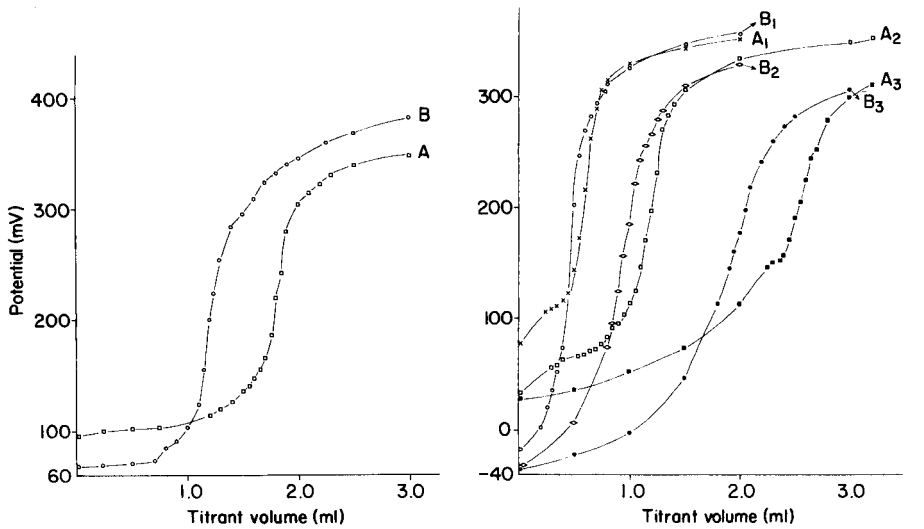

Fig. 2. Titration curves for human γ-globulin in anhydrous acetic acid: (A) without acylation for 0.1050 g of sample; (B) after acylation for 0.1021 g of sample. (Evaluation is presented in Table 3.)

Fig. 3. Titration curves for different amounts of soya bean meal 1 in anhydrous acetic acid. Curves: (A) measurements without acylation for 0.0507 g (A_1), 0.0963 g (A_2) and 0.2024 g (A_3) of sample; (B) measurements after acylation for 0.0509 g (B_1), 0.1021 g (B_2) and 0.2016 g (B_3) of sample. (Results are summarized in Table 3.)

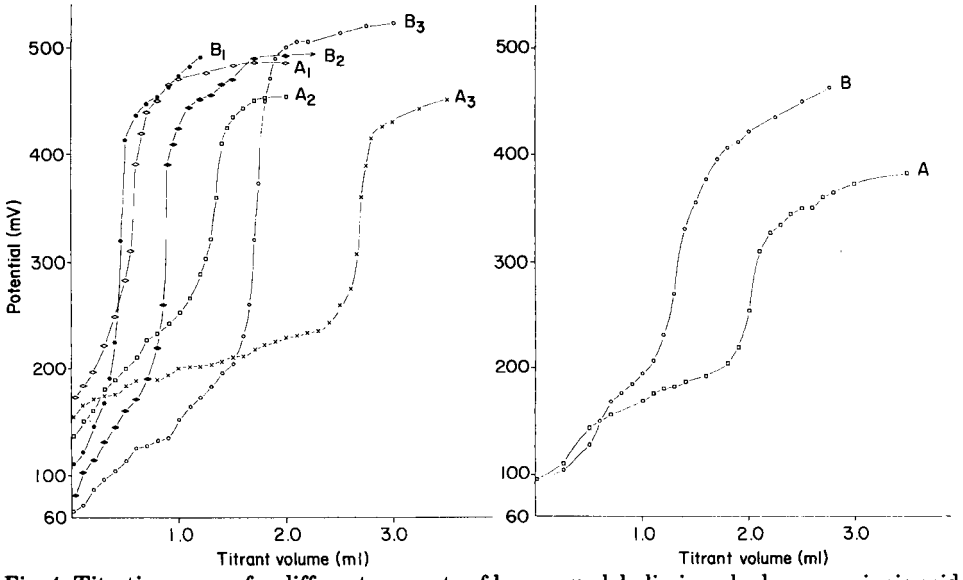

Fig. 4. Titration curves for different amounts of human γ-globulin in anhydrous propionic acid. Curves: (A) measurements without acylation for 0.0446 g (A_1), 0.1052 g (A_2) and 0.2128 g (A_3) of sample; (B) measurements after acylation for 0.0532 g (B_1), 0.1064 g (B_2) and 0.2120 g (B_3) of sample.

Fig. 5. Titration curves for meat meal in anhydrous propionic acid: (A) without acylation for 0.2524 g of sample; (B) after acylation for 0.2588 g of sample.

TABLE 1

Total basicity and available lysine content of various proteins as a function of the time of soaking (A values) and that of acylation (B values), measured with perchloric acid in anhydrous acetic acid

Sample/ protein content[a] (% w/w)	Proc.	Basicity equivalent (mM/g^{-1} protein)									Available lysine	
		Time of soaking (A) or acylation (B) (min)						Mean	SD	SE (%)	Found[b]	Lit. data
		5	10	15	20	30	60					
HG/ 85.0	A	1.79	1.65	ND[c]	1.79	1.78	1.73	1.75	0.060	3.4	0.56	0.54 [8]
	B	1.20	1.21	ND	1.20	1.22	1.21	1.21	0.012	1.0		
BSA/ 88.7	A	ND	1.66	ND	1.69	1.72	1.70	1.69	0.025	1.5	0.91	0.87 [8] 0.88 [5] 0.89 [3]
	B	ND	0.78	ND	0.78	0.76	0.81	0.78	0.024	3.1		
β-Casein/ 76.0	A	ND	0.980	ND	1.00	0.980	ND	0.987	0.007	0.71	0.55	0.47 [3,8] 0.57 [6] 0.56 [12]
	B	ND	0.434	0.439	0.436	0.440	ND	0.437	0.005	1.0		
SBM-1/ 44.0	A	2.51	2.60	ND	2.62	2.58	2.62	2.59	0.046	1.8	0.49	0.44 [7,8] 0.41 [6] 0.49 [5]
	B	ND	2.09	ND	2.10	2.10	2.10	2.10	0.006	0.3		
SBM-2/ 45.4	A	2.53	2.60	2.60	2.61	2.57	ND	2.58	0.035	1.3	0.50	-
	B	ND	2.03	2.04	2.11	2.13	ND	2.08	0.050	2.4		
SBM-3/ 46.4	A	2.57	2.59	2.59	2.45	2.50	2.52	2.54	0.057	2.2	0.52	-
	B	2.02	2.00	2.02	2.04	2.04	2.02	2.02	0.015	0.7		
Meat meal/ 61.0	A	2.13	2.17	2.09	2.13	2.12	ND	2.13	0.005	0.2	0.65	0.38 [12]
	B	1.47	ND	1.50	1.47	1.49	ND	1.48	0.015	1.3		
Milk protein/ 83.7	A	2.03	2.04	2.04	ND	2.02	2.04	2.03	0.010	0.5	0.74	-
	B	1.26	1.28	1.30	ND	1.30	1.29	1.29	0.022	1.7		

[a] $N \times 6.25$. [b] From A − B. [c] No data obtained.

in Tables 1 and 2. In all the cases studied, it was proved that the maximum time consumption required for soaking the sample and for acylation was 20 min, and that the basicity values measured did not vary even after 60 min (Tables 1 and 2). Thus the values of quantitative measurements obtained after

TABLE 2

Total basicity and available lysine content of various proteins as a function of the time of soaking (A values) and that of acylation (B values), measured with perchloric acid in anhydrous propionic acid

Sample	Proc.	Basicity equivalent: mM g^{-1} protein									Available lysine
		Time of soaking (A) or acylation (B) (min)						Mean[a]	SD	SE (%)	
		5	10	15	20	30	60				
HG	A	1.54	1.54	1.56	1.55	1.55	ND[b]	1.55	0.009	0.6	0.55
	B	ND	1.00	1.00	0.99	0.99	ND[b]	1.00	0.008	0.8	
β-Casein	A	ND	ND	ND	ND	0.556	0.571	0.563	-	-	0.272
	B	ND	ND	ND	ND	0.290	0.291	0.291	-	-	
SBM-1	A	(1.36)	(1.61)	1.77	1.86	1.76	1.82	1.80	0.046	2.6	0.44
	B	(0.46)	(1.15)	1.40	1.36	1.34	1.35	1.36	0.026	1.9	
SBM-2	A	(1.64)	1.75	1.81	1.82	ND	1.79	1.79	0.031	1.7	0.50
	B	ND	1.29	1.29	1.27	ND	1.29	1.29	0.012	0.9	
Meat meal	A	(1.25)	ND	1.42	ND	1.44	1.46	1.44	0.020	1.4	0.33
	B	(0.99)	ND	1.13	ND	1.11	1.10	1.11	0.016	1.4	

[a]Without data in parentheses. [b]No data obtained.

15–60 min of soaking and/or acylation served as the basis for reproducibility calculations. The relative standard error (SE) for the reactions of different matrices was less than 3.4% (Tables 1 and 2).

The reproducibility of the method for titrating different amounts of proteins in acetic acid is shown in Table 3 and Fig. 4. The greatest standard error found was 3.9%, thus the reproducibility of the method suggested can be regarded as appropriate.

The goal of this research was to determine the amount of available lysine from the difference of the basicities measured before and after acylation of the protein. The following points should be noted. The available lysine data vary over a large range [1–17]; some values selected as representative of different methods are summarized in Table 1. The available lysine values measured here by the titrations in acetic or propionic acid media are generally in good agreement with each other and with the mean values of the literature data cited (Tables 1–3). The two exceptions are the available lysine contents of meat meal and of β-casein measured in acetic and propionic acid solutions. The agreement of the results obtained for the soya bean meals is remarkable if one takes into account the different origins and times of acquisition of the samples.

TABLE 3

Reproducibility of the total basicity and available lysine determinations for different amounts of standard proteins and soya bean meal, measured with perchloric acid in anhydrous acetic acid

Sample/ protein content[a] (% w/w)	Basicity equivalent (mM g^{-1} protein)								Available lysine
	Without acylation (A)				After acylation (B)				
	Sample (mg)	Single result	Mean	SD/ SE(%)	Sample (mg)	Single result	Mean	SD/SE (%)	
BSA/ 88.7	23.8	1.69	1.68	0.02/ 1.4	54.4	0.72	0.77	0.03/ 3.9	0.91
	25.2	1.66			51.0	0.78			
	36.8	1.70			52.7	0.77[b]			
	50.6	1.70			103.6	0.78			
	52.6	1.68[a]			110.0	0.81			
	91.9	1.67[a]			102.8	0.76[b]			
HG/ 85.0	27.5	1.79	1.73	0.09/ 3.2	27.5	1.18	1.18	0.04/ 3.7	0.55
	50.9	1.62			52.1	1.10			
	105.0	1.76[b]			102.1	1.18[b]			
	209.2	1.79			204.3	1.20			
	308.2	1.61			304.1	1.23			
	406.8	1.81			406.8	1.20			
SBM-1/ 44.0	50.7	2.57[c]	2.60	0.05/ 1.7	50.9	2.12[c]	2.11	0.04/ 1.9	0.49
	96.3	2.69[c]			102.1	2.15[c]			
	202.4	2.62[c]			201.6	2.16[c]			
	255.1	2.58			253.7	2.07			
	426.3	2.59			450.0	2.06			
	601.7	2.59			604.0	2.12			

[a]$N \times 6.25$. [b-d]Calculated from curves presented in Figs. 1, 2 and 3, respectively.

The total basicity values of the proteins are reproducible properties and so can be utilized in protein chemistry.

We thank J. Kunovics, Á, Kövágó, J. Máthyás and I. Petróczy for valuable discussions. This work was supported in part by the State Office of Technical Development of Hungary, and the Hajduság Agrarian Industrial Association.

REFERENCES

1 M. Hennecke and B.V. Plapp, Anal. Biochem., 136 (1984) 110.
2 J.E. Ramirez, J.R. Cavanaugh, K.S. Schweizer and P.D. Hoagland, Anal. Biochem., 63 (1975) 130.
3 G.C. Goodno, H.E. Swaisgood and G.L. Catignani, Anal. Biochem., 115 (1981) 203.
4 M. Friedman and L.D. Williams, Anal. Biochem., 54 (1973) 333.

5 S.L. Snyder and P.Z. Sobocinski, Anal. Biochem., 64 (1975) 284.
6 R.F. Hurrel, P. Lerman and K.J. Carpenter, Food Sci., 44 (1979) 1221.
7 I. Molnár-Perl, M. Pintér-Szakács, Á. Kövágó and J. Petróczy, Food Chem., 16 (1985) 163.
8 I. Molnár-Perl, M. Pintér-Szakács, Á. Kövágó, J. Petróczy, U.P. Kralovánszky and J. Mátyás, Food Chem., 20 (1986) 21.
9 A.F.S.A. Habeeb, Anal. Biochem., 14 (1966) 328.
10 L.C. Mokrash, Anal. Biochem., 18 (1967) 64.
11 M.L. Kakade and I.E. Leiner, Anal. Biochem., 27 (1969) 273.
12 R.J. Hall, N. Trindner and D.I. Givens, Analyst, 98 (1973) 673.
13 J. Ernest and K. Kim, J. Biol. Chem., 21 (1974) 6770.
14 H. Falter, Anal. Biochem., 67 (1975) 359.
15 M. Friedman, Diabetes, 31 (1982) 5.
16 M. Friedman, L.D. Williams and M.S. Masri, Int. J. Pept. Protein Res., 6 (1974) 183.
17 M. Friedman and J.W. Finley, Int. J. Pept. Protein Res., 7 (1975) 481.
18 P. D'Orazio and G.A. Rechnitz, Anal. Chem., 49 (1977) 41.
19 P.W. Alexander and C. Maitra, Anal. Chem., 53 (1981) 1590.
20 P.W. Alexander and G.A. Rechnitz, Anal. Chem., 46 (1974) 250, 860.
21 M.L. Hitchman, F.W.M. Nyasulu, A. Aziz and D.D.K. Chigakule, Anal. Chim. Acta, 155 (1983) 219.
22 J.J. Tombeux, C.T. Schaubroeck, C.T. Huys, H.F. De Brabender and A.M. Goemine, Z. Anorg. Chem., 517 (1984) 235.

Analytica Chimica Acta, 202 (1987) 167–174
Elsevier Science Publishers B.V., Amsterdam — Printed in The Netherlands

A HIGH-PERFORMANCE LIQUID CHROMATOGRAPHIC ASSAY OF THE ELECTRO-OXIDATION OF PURINES
Uric Acid and the Nucleotide Drug Tubercidin-5′-Monophosphate

T. CHILDERS-PETERSON and A. BRAJTER-TOTH*
Department of Chemistry, University of Florida, Gainesville, FL 32611 (U.S.A.)

(Received 8th July 1987)

SUMMARY

A high-performance liquid chromatographic assay is described for establishing the completeness of electro-oxidation of a purine nucleotide drug tubercidin-5′-monophosphate (TMP) and the sequence of product formation. The assay shows that TMP was completely oxidized after ca. 2 h of electrolysis and that the product distribution continued to change after this time. The same assay was also used to show the sequence of product formation in the electro-oxidation of uric acid. Both separations were isocratic, with a 0.02 M potassium dihydrogenphosphate (pH 4.6–5.1) mobile phase.

Electrochemical methods can provide valuable insights into biologically important redox reactions of xenobiotics and naturally occurring compounds [1,2]. In the determination of pathways of redox reactions, electrochemical methods frequently require the support of other techniques. For example, spectroelectrochemistry with ultraviolet (UV)/visible and/or infrared (IR) spectroscopy, gas chromatography/mass spectrometry (GC/MS) and separations including gel-permeation and high-performance liquid chromatography (HPLC) have been successfully combined with electrochemical measurements to provide a complete picture of reaction products and, where possible, intermediates.

This paper describes a high-performance liquid chromatographic assay which was developed to determine unequivocally the completeness of the exhaustive redox reaction under conditions for which methods frequently used for this purpose (cyclic voltammetry and UV spectroscopy) cannot be applied. The HPLC assay offers a clear advantage, not previously emphasized, in the studies of complicated electrochemical reactions.

The assay was tested on a model purine system (uric acid) and was then applied to the study of the electro-oxidation of a purine nucleotide drug, tubercidin-5′-monophosphate. Biological degradation pathways of this drug are

0003-2670/87/$03.50

largely unknown, and the electrochemical study was undertaken to provide information about potential biological reactivity. Electro-oxidation of this purine is complicated and involves coupling of a series of electron transfers and chemical reactions [3]. In addition, the reactant and products have strong surface affinity to graphite electrodes. This complicates interpretation of electrochemical data, and makes the elucidation of the reaction pathway based on existing theories impractical under biologically relevant conditions. Instead, as is practical for such complicated organic reactions, the method of elucidation of reaction pathway was based on analysis of products and intermediates formed in the exhaustive oxidation. In this study, HPLC was an important tool.

EXPERIMENTAL

Uric acid, tubercidin-5′-monophosphate (TMP), alloxan, allantoin and hydantoin (Sigma) were used without further purification. All solutions were prepared in phosphate buffer, ionic strength 0.5 M.

An EG & G Princeton Applied Research (PAR) model 173 potentiostat with a model 179 coulometer was used in electrochemical experiments. Typically, 600 μM solutions of TMP in pH 7.0 phosphate buffer and 200 μM uric acid in pH 5.0 buffer were electrolyzed. The constant-potential electrolysis was done in a three-compartment cell in which the compartments were separated by type P-1010 cation-exchange membranes (RAI Research Corp., Hauppauge, NY). Working electrodes were two rectangular plates of pyrolytic graphite (6.3 $\times$ 1.8 cm). These were resurfaced on 600-grit silicon carbide paper (Carbimet, Buehler, IN) followed by thorough rinsing with deionized water. The reference and counter electrodes were saturated calomel electrode (SCE) and platinum, respectively. During electrolysis, the solution was continuously stirred and deaerated with nitrogen. Typically, 10 ml of solution was electrolyzed. Tubercidin-5′-monophosphate and uric acid were electrolyzed at ca. 1.0 and 0.7 V vs. SCE, respectively.

In cyclic voltammetric experiments, the working electrode was rough pyrolytic graphite which was prepared by sealing a piece of graphite (Pfizer, Minerals Division) into glass tubing with inert epoxy (Dexter Co., Hysol Division).

For HPLC, an Altex model 110 pump and solvent programmer were coupled to a Kratos Spectroflow variable-wavelength UV detector. A Resolvex (Fisher) C-18 reversed-phase column (4.6 mm $\times$ 25 cm) was used. The separation was isocratic with 0.02 M KH_2PO_4 solution (pH 4.6–5.1) as the mobile phase. This separation procedure has been shown to be useful for purines, their nucleosides and nucleotides [4]. The mobile phase was prepared with triply-distilled deionized water which was treated with UV radiation for 24 h. The potassium dihydrogenphosphate solutions were prepared by diluting the salt solution to the desired concentration and adjusting the pH with phosphoric acid; these

solutions were filtered through a 0.45-μm filter before use. Sample volumes for HPLC were 20 μl. The column was equilibrated with the mobile phase for 1 h at a flow rate of 2.0 ml min^{-1}. The flow rate during separations was 1.0 ml min^{-1}.

The known products of uric acid oxidation that were used as standards all absorb in the region 200–220 nm; the HPLC separations were monitored at 215 nm. Tubercidin-5′-monophosphate also absorbs in this region [3]. The spectra of TMP oxidation products were obtained from 200 to 400 nm [3]. All UV-absorbing products absorbed at 225 nm [3] where the separation was monitored.

RESULTS AND DISCUSSION

HPLC in the study of uric acid electro-oxidation

From studies of the electro-oxidation of uric acid by a combination of spectroelectrochemistry, gel-permeation liquid chromatography and gas chromatography/mass spectrometry it has been shown that allantoin, 5-hydroxyhydantoin-5-carboxamide and, at pH ca. 3, alloxan are the oxidation products [2]. Bicyclic imine alcohol (BCA) has been confirmed as an intermediate in the degradation of uric acid to the final products [5]. It has been shown that the same or structurally closely related products form in the electrochemical oxidation of all other naturally occurring purines and purine nucleosides [1] as well as their derivatives, purine drugs [6,7].

To establish if a fast and reliable HPLC assay could be developed to monitor the electrochemical oxidation of purines, the constant-potential oxidation of a purine, uric acid, was first studied with HPLC. This method has not been applied previously to the study of this electro-oxidation, but the analysis of the biological degradation products of uric acid by HPLC has been described recently [8]. It has been shown that the reversed-phase separations of biological purines and their degradation products can be effective under isocratic conditions with aqueous dihydrogenphosphate as the mobile phase [4,8]. The pH of the mobile phase determines the retention time and must be controlled [4]. In this separation, the pH of the mobile phase was 5.1, below the $pK_{a1}=5.75$ of uric acid [9], where it exists predominantly in the neutral form. As expected, liquid chromatograms of standard solutions show (Fig. 1) that at this pH, uric acid has a relatively high capacity factor ($k'=2.1$) and is well separated from its major oxidation product, allantoin ($k'=0.14$), and alloxan which is unretained ($k'=0$). A 5-hydroxyhydantoin-5-carboxamide standard is not commercially available but the capacity factor of a structurally similar hydantoin ($k'=0.76$) indicates that this product should be separated from uric acid and all other products (Fig. 1).

Figure 2 includes the HPLC results which were obtained during constant-potential oxidation of uric acid. As the electrolysis proceeds, formation of four

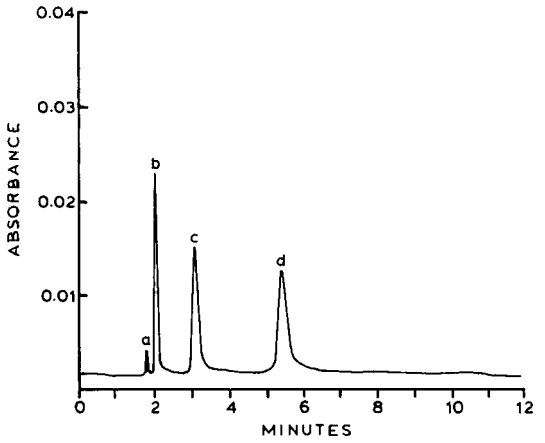

Fig. 1. Reversed-phase HPLC of standard solutions. Peaks: (a) mobile phase blank; (b) 108 μM allantoin; (c) 155 μM hydantoin; (d) 60 μM uric acid. Alloxan (not shown) co-elutes with peaks a and b. Mobile phase 0.02 M KH_2PO_4, pH 5.1; flow rate 1.0 ml min^{-1}. Absorbance monitored at 215 nm.

peaks is observed. Peaks a, b and d increase throughout the electrolysis. Peak c reaches a maximum before uric acid is completely oxidized and decreases as the electrolysis is continued. It was estimated from the HPLC data that after ca. 10 min of oxidation (Fig. 2C), ca. 85% of the uric acid had been oxidized. In the oxidation of uric acid, allantoin is the major product and at pH 7.0 forms in ca. 90% yield.

Peaks a and b were identified as due to alloxan and allantoin, respectively, based on the agreement between their capacity factors and those of standards. Peak d was assigned to 5-hydroxyhydantoin. The assignment was based on the close agreement between the k' value of standard hydantoin and the product eluting at peak d. Recent results from combined electrochemistry and thermospray tandem mass spectrometry indicate that 5-hydroxyhydantoin forms in the oxidation of uric acid and may be a decomposition product of 5-hydroxyhydantoin-5-carboxamide [10]. Peak c was assigned to 5-hydroxydantoin-5-carboxamide. A standard of this product is not available commercially. Structurally, this product is related to hydantoin; therefore, it is likely to have a similar k' value. The decrease in height of peak c and the increase in peak d during electrolysis may be due to the postulated decomposition of 5-hydroxyhydantoin-5-carboxamide to 5-hydroxyhydantoin [10].

The HPLC results show that this method can provide useful information about the number and the sequence of formation of UV-absorbing products in the electrochemical reaction. The end of electrolysis can also be unambiguously determined by the complete disappearance of the HPLC peak of the reactant.

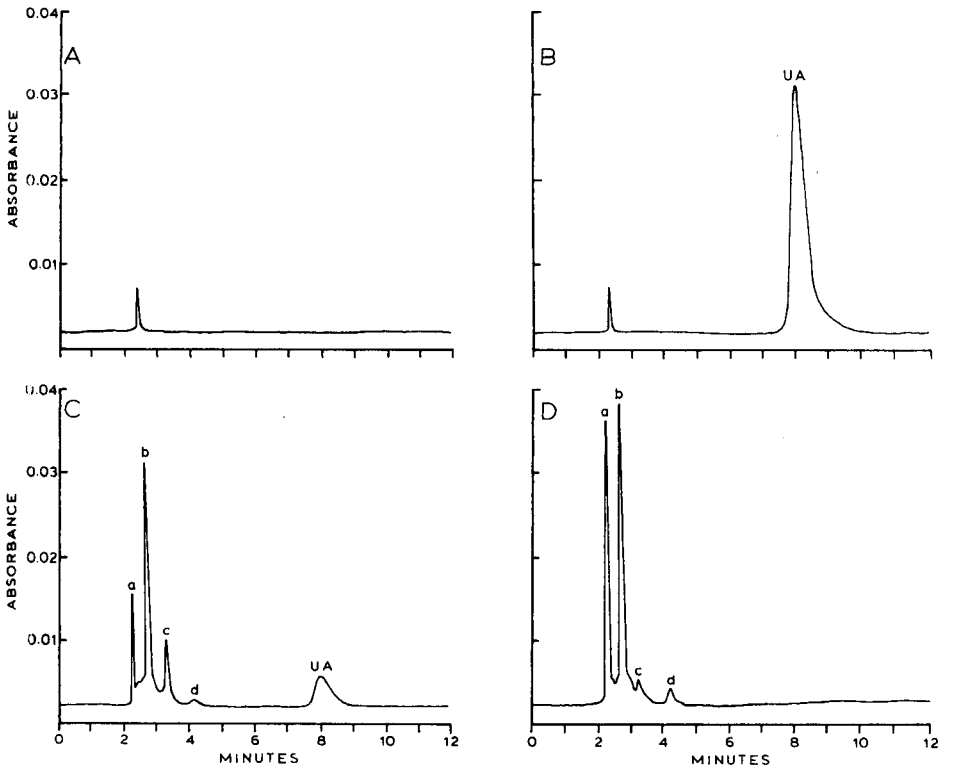

Fig. 2. Chromatograms obtained during constant-potential oxidation (0.70 V vs. SCE) of 127 μM uric acid (pH 5.1, 0.5 M phosphate buffer). Chromatographic conditions as in Fig. 1. (A) Mobile phase blank; (B) liquid chromatogram before start of oxidation; (c) 10 min of oxidation; (D) 24 min of oxidation. UA is uric acid.

HPLC in the study of electro-oxidation of a purine nucleotide drug, tubercidin-5'-monophosphate (TMP)

In the study of electro-oxidation of TMP [3], cyclic voltammetry and UV spectroscopy did not show conclusively when the drug was completely oxidized. Cyclic voltammetry at a rough pyrolytic graphite electrode shows that TMP is oxidized at very positive potentials (ca. 0.90 V vs. SCE). As TMP is oxidized, products form which can be oxidized at the same potentials; the end of TMP oxidation is impossible to determine. In the UV spectra, the absorption peaks of intermediates and products of the oxidation overlap with the absorption bands of TMP at 220 and 270 nm.

An HPLC assay was, therefore, developed to monitor the electro-oxidation of TMP. The pH of the mobile phase was 4.6. At this pH ($<pK_a=5.3$) the purine base of TMP is present in the predominantly protonated form and the phosphate group of the nucleotide is negatively charged [3]. At a mobile-phase

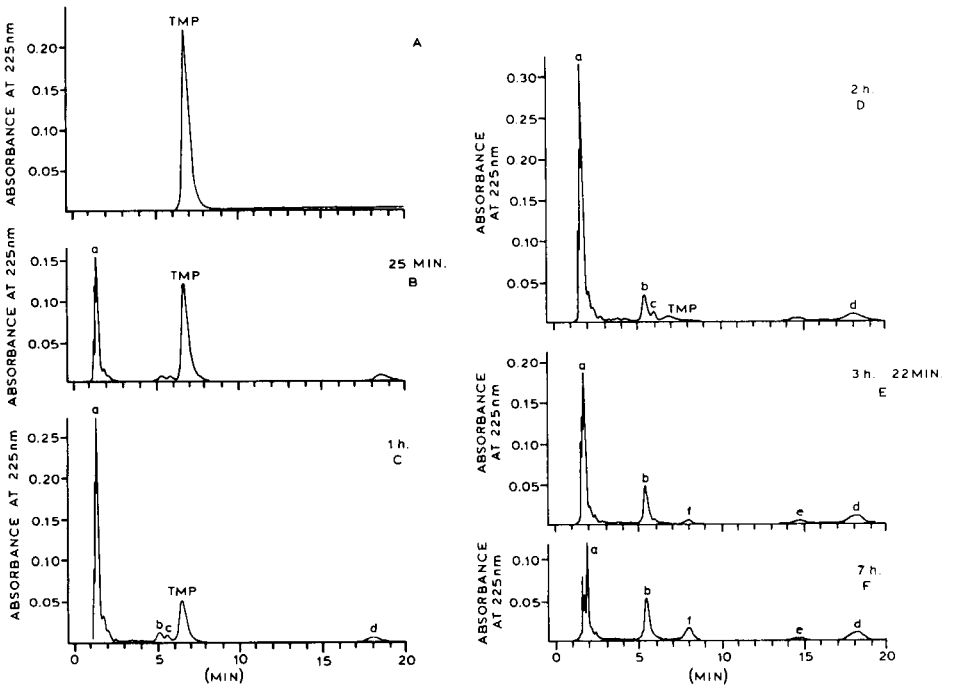

Fig. 3. Chromatograms obtained during constant-potential oxidation (0.97 V vs. SCE) of 600 μM tubercidin-5′-monophosphate (pH 7.0, 0.5 M phosphate buffer, rough pyrolytic graphite electrode). Oxidation time: (A) 0 min; (B) 25 min; (C) 60 min; (D) 120 min; (E) 202 min; (F) 7 h. For peak identification, see text. Mobile phase: 0.02 M KH_2PO_4, pH 4.6; flow rate: 1.0 ml min^{-1}. Absorbance monitored at 225 nm.

pH of ca. 5.0, where this behavior is observed, it has been shown [4] that 5′-monophosphate nucleotides of purines containing an amino group have relatively high capacity factors under the reversed-phase HPLC conditions used in this separation (see Experimental). This is in agreement with the behavior expected for neutral molecules. A relatively high capacity factor of TMP ($k' = 2.4$) was found at pH 4.6. The mobile phase pH of 4.6 also allows better retention and separation of otherwise difficult-to-retain pyrimidine nucleotides [4] which are the oxidation products of TMP (see below).

Figure 3 shows the HPLC data which were obtained during the constant-potential oxidation of TMP. Immediately after the initiation of electrolysis, a product forms which has a short retention time (peak a). As the electrolysis proceeds, peaks a–d increase and a new peak (e) forms. The HPLC results clearly show that TMP is oxidized after ca. 2 h when the products eluting under peaks a–e have formed. If the oxidation is continued, peaks a and c decrease, peaks b and d continue to increase and a new peak (f) forms.

Product separation and identification by mass spectrometry, nuclear magnetic resonance (NMR) and Fourier-transform infrared spectroscopy (FTIR), after exhaustive oxidation at ca. 0.9 V vs. SCE in pH 7.0 phosphate buffer, led to the identification of compounds eluting under peaks a and b [3].

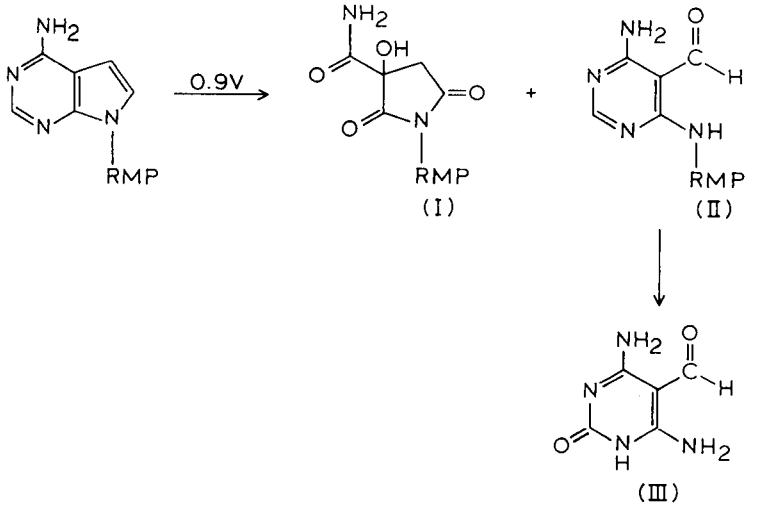

Scheme 1.

Product **I** elutes at peak a. Product **II** is present in a mixture which elutes at peak b. The products are structurally similar and both form early in the oxidation. Their structure and their nearly simultaneous detection by HPLC indicates that they may form by parallel pathways. The exceedingly small amounts of products eluting under peaks c, d and e prevented their positive identification. The structure of product **III**, which has a retention time similar to that of peak f, is consistent with its late appearance in the oxidation. Glycosidic bond cleavage, which had to occur to form this product, is difficult as has been shown from the biological oxidation studies of TMP [11]. Although this has not been confirmed, the HPLC results indicate that the product eluting under peak c may be further oxidized to product **III**.

Conclusions

The HPLC assay of the electro-oxidation of uric acid and TMP was demonstrated to be a useful method for the determination of the sequence of product formation as a function of the extent of oxidation of the parent compound. At present, the method is limited to the UV-absorbing products, but work is in progress on extending the range of applications of this approach by using different detection methods such as mass spectrometry [10].

This research was partly supported by the Research Corporation and by the

Division of Sponsored Research at the University of Florida. We thank Dr. J.G. Dorsey and his group and Dr. K. Williams for their helpful assistance. Partial support by the U.S. Army Research, Development and Engineering Center (No. DAAA15-85-C0034) and the NIH (BMT 1 R01 GM35451-1A2) is gratefully acknowledged.

REFERENCES

1 G. Dryhurst, Electrochemistry of Biological Molecules, Academic, New York, 1977.
2 G. Dryhurst, K.M. Kadish, F. Scheller and R. Renneberg (Eds.), Biological Electrochemistry, Academic, New York, 1982.
3 T. Childers-Peterson and A. Brajter-Toth, J. Electroanal. Chem., 239 (1988) 161.
4 M. Zakarla, P.R. Brown and E. Grushka, Anal. Chem., 55 (1983) 457.
5 A. Brajter-Toth and G. Dryhurst, J. Electroanal. Chem., 122 (1981) 205.
6 P.J. Kraske and A. Brajter-Toth, J. Electroanal. Chem., 207 (1986) 101.
7 D. Astwood, T. Lippincott, M. Deysher, C. D'Amico, E. Szurley and A. Brajter-Toth, J. Electroanal. Chem., 159 (1983) 295.
8 P. Durre and J.R. Andreesen, Anal. Biochem., 123 (1982) 32.
9 D.J. Brown and S.F. Mason, J. Chem. Soc., (1957) 682.
10 K. Volk, M. Lee, R.A. Yost and A. Brajter-Toth, Anal. Chem., in press.
11 J.J. Fox, K. Watanabe and A. Bloch, Prog. Nucleic Acid Res. Mol. Biol., 5 (1966) 257.

Analytica Chimica Acta, 202 (1987) 175–186
Elsevier Science Publishers B.V., Amsterdam — Printed in The Netherlands

PATTERN RECOGNITION STUDY OF BIOCHEMICAL ASSAYS FOR LIVER FUNCTION

C. ARMANINO* and R. LEARDI

Istituto di Analisi e Tecnologie Farmaceutiche ed Alimentari, Via Brigata Salerno, I-16147 Genoa (Italy)

A. RODA

Istituto di Chimica Analitica, Via dei Verdi 7, I-98100 Messina (Italy)

P. SIMONI

Istituto di Clinica Medica e Gastroenterologia, Via Massarenti 9, I-40138 Bologna (Italy)

(Received 15th April 1987)

SUMMARY

To extract discriminant information from analytical data, results from eight conventional biochemical tests of liver function and from determinations of two serum bile acids are studied by supervised pattern recognition methods. The population comprised healthy subjects and seven groups of people affected by different liver diseases. The principal components, linear discriminant, k nearest neighbours and Bayesian methods were applied. Because the prediction ability computed on the whole data set was poor, the problem was simplified by dividing the data set into three subsets, each comprising two liver diseases which were contiguous and overlapped in the hyperspace of variables. The prediction ability of the Bayesian method reached 96% at best, 75% at minimum, in the three subsets. Best performance was achieved in distinguishing between healthy subjects and those with mild liver diseases on the basis of four biochemical assays.

The diagnosis of liver diseases requires the use of combined tests for biochemical and histological function, because of overlap of the characteristics of the different liver diseases. Many conventional biochemical tests for liver function are available, but, as a consequence of their "organ" and/or "function" selectivity, accurate diagnosis is possible only by taking into account the information produced by several such tests. In recent years, several studies have been reported on the diagnostic usefulness of the serum bile-acid determination in liver diseases, but the results are often conflicting. Differences both in the assay and in the statistical approach, as well as differences in the populations studied, can be considered as the underlying causes of the discrepancies reported [1]. Several studies have shown that increases of serum bile acids parallel liver damage, and some authors [2,3] have proposed determi-

0003-2670/87/$03.50

nation of serum bile acid as a method capable of defining the histological severity of the diseases. Increases in serum bile acid, however, do not seem to be capable always of discriminating between different liver diseases.

In this study, involving seven different liver disorders, multivariate methods of feature selection and data evaluation were used in order to select the diagnostic tests that discriminate best between the different diseases, as well as to verify the diagnostic efficiency of two serum bile acids determined by a new method, and to find the classification method that could best discriminate between the liver diseases considered. In previous work, pattern recognition techniques were applied to the classification and prediction of two liver diseases by means of some enzyme concentrations in blood [4], and the Bayesian model was used for computer diagnosis of jaundice [5].

EXPERIMENTAL

Data

A data matrix of 414 objects and 10 variables (Table 1) was evaluated. The objects were subdivided into eight categories, i.e., controls (93 healthy subjects) and seven groups of patients suffering from different liver diseases. The diagnosis of liver diseases was based on clinical evaluation and on agreement of the biopsy results obtained by two experienced pathologists. Each pathologist, who was unaware of the clinical and biochemical data, examined the samples without knowledge of the other pathologist's diagnosis; cases in which diagnoses were discrepant were rejected. Diabetic, dyslipidemic and gallstone patients, and patients whose gall bladder had been removed, were excluded from the study. The control subjects showed no clinical or laboratory evidence of liver or gastrointestinal diseases and were not receiving any drug. The use of different criteria for selecting samples (only biochemical and clinical findings in controls, and liver biopsy in patients) was chosen for obvious ethical reasons.

On each subject, ten variables were measured (Table 1). The levels of serum cholic acid (CA) and serum chenodeoxycholic acid (CDCA) were evaluated by a new solid-phase enzyme immunoassay [6–8]; the other eight variables (Table 1) were determined by conventional biochemical tests of liver function.

Packages and methods

Multivariate data evaluation and graphics were done with the PARVUS-Ese package [9]. The three classification methods used were linear discriminant analysis (LDA), the k nearest neighbours (kNN) method and the Bayesian technique. The linear discriminant technique is a parametric classification method [10]. Categories supposed to have equal covariance matrices can differ if their centres of gravity (centroids) have different positions in the hyperspace of the variables. The pooled covariance matrix is calculated as the

TABLE 1

Data matrix

Categories Index	Name	No. of subjects
1	Controls	93
2	Acute hepatitis	26
3	Fibrosis	14
4	Steatosis	19
5	Chronic persistent hepatitis	51
6	Chronic active hepatitis	113
7	Cirrhosis	87
8	Cholestasis	11

Variables Index	Abbreviation and name
1	CA : Serum conjugated cholic acid
2	CDCA : Serum conjugated chenodeoxycholic acid
3	GOT : Glutamic oxalacetic transaminase
4	GPT : Glutamic pyruvic transaminase
5	AP : Alkaline phosphatase
6	γGT : γ-Glutamyl transpeptidase
7	BIL : Bilirubin
8	QK : Prothrombin (quick) time
9	ALB : Serum albumins
10	GLO : γ-Globulins

weighted mean of the covariances of the categories. For each object, the Mahalanobis distance from all the category centroids is computed, and the object is classified into the category having the nearest centroid. In spite of the wide differences between the covariance matrices of the categories in this study, a very simplified model of LDA produced some good results.

The kNN method [11] is a non-parametric classification method, based on computation of the inter-object distance matrix. For every object, the k nearest objects are taken into account; k points are given to the category of the nearest one, $k-1$ to the category of the second nearest and so on (1 point to the category of the kth nearest one). The object is classified into the category with the highest score. In this study, Euclidean distance and $k=5$ were used. The kNN rule has been often applied in classification problems in connection and in comparison with other techniques; it is very useful when some categories are not normally distributed (as some pathological categories are in this study) to validate the results of parametric techniques.

The Bayesian technique [12] is a parametric classification and modelling method. With L categories, the a priori probability $P(G_j)$ and the density

functions must be known for each category G_j. Each category has a separate model, given by the centroid of the category and the covariance matrix of the category, the conditional probability density $P(\mathbf{x}_i|G_j)$ being computed from the multivariate normal distribution. The a posteriori probability that an object i (i.e., data vector $\mathbf{x}_i$ belongs to class G_j is given by

$$P(G_j|\mathbf{x}_i) = P(G_j)\ P(\mathbf{x}_i|G_j) \Big/ \sum_{j=1}^{L} P(G_j)\ P(\mathbf{x}_i|G_j)$$

Object i is assigned to the class with the largest such probability. In this study, the a priori probability was assumed to be unity for each category, because it is a parameter of limited significance and also should be used jointly with loss factors that were unknown. The projections of the confidence hyperellipsoids of the class models were used to display the classification boundaries at different confidence intervals.

RESULTS AND DISCUSSION

Evaluation with all objects included

The raw data were normalized by autoscaling [13] to make the range between the variables comparable. The interdependences among some of the ten variables were identified by the correlation coefficient matrix: CA was positively ($r>0.5$) correlated to variables CDCA, GOT, and GPT; GOT and GPT were very significantly correlated ($r=0.93$).

Multivariate stepwise methods of feature selection, based on both LDA [14] and the Bayesian technique [15], were applied. All the variables were retained, because none of them could be discarded without a significant reduction in the ability to classify some categories.

Principal components analysis. The eigenvectors of the covariance generalized matrix were computed. The significance of eigenvectors was estimated by the cross-validation method [16] and the average variance criterion [17]. Two eigenvectors were found to be significant by the former method and three by the latter; they contained, respectively, 36, 18 and 14% of the total variance.

Figure 1 shows the plot of scores for the first two eigenvectors; all the objects are spread along two directions of largest variation, the objects of category 2 (acute hepatitis) being well separated from the others and distributed along one direction. In contrast, all the remaining categories are grouped and greatly overlapped (but in a gradient of increasing hepatocellular damage) along a quite orthogonal direction of variation.

On the plot for eigenvectors 1 and 3, the objects of category 8 were better displayed and spread along a third direction of variation. These three directions are probably factors with pathological significance; suitable interpreta-

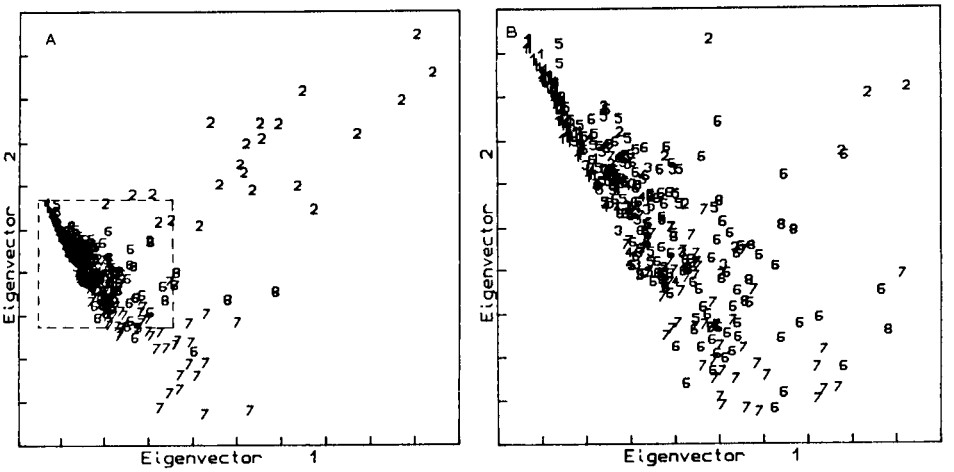

Fig. 1. (A) Eigenvector plot of the 8-category data set (55% retained variance): (1) controls; (2) acute hepatitis; (3) fibrosis; (4) steatosis; (5) chronic persistent hepatitis; (6) chronic active hepatitis; (7) cirrhosis; (8) cholestasis. (B) Enlargement of the boxed part of A.

tions may be provided by clinicians, but here the directions are simply called factors *A*, *B*, *C*. After Varimax orthogonal rotation [18] in the space of the three principal components, the three factors become nearly parallel to the new axes and their chemical significance becomes easy to evaluate. Figure 2 shows the bar graphics of the variable loadings on varivectors 1, 2 and 3. Factor *A* is characterized by cholic acids and transaminases, while the largest contribution to factor *B* comes from variables QK, ALB and GLO. Variables AP and γGT provide information on the variation of factor *C*.

Classification and modelling methods. Classification (LDA and *k*NN) and modelling (classical Bayesian) methods were applied to find the best means of discriminating among the eight categories.

The mean classification ability (i.e., the percentage of training set objects correctly classified) was 59.7% by *k*NN, 57.3% by LDA and 63.3% by the Bayesian method. The classification matrix by the Bayesian method, for which all the objects in the training set were retained, is shown in Table 2. The two columns on the right show the percent classification and prediction abilities; prediction ability was computed as the mean of a sequence of several Bayesian analyses with different random subdivisions between training and evaluation sets, the latter being composed by 30% of the total objects.

The objects of categories 1 and 2 were very well classified and predicted. Among categories 3–7, several misclassifications occurred and the prediction abilities were sometimes very poor. In particular, the centroids of classes 3, 4 and 5 are very close together so that their objects overlap severely; moreover, categories 3, 4 and 8 had very few objects. For these reasons, the preceding

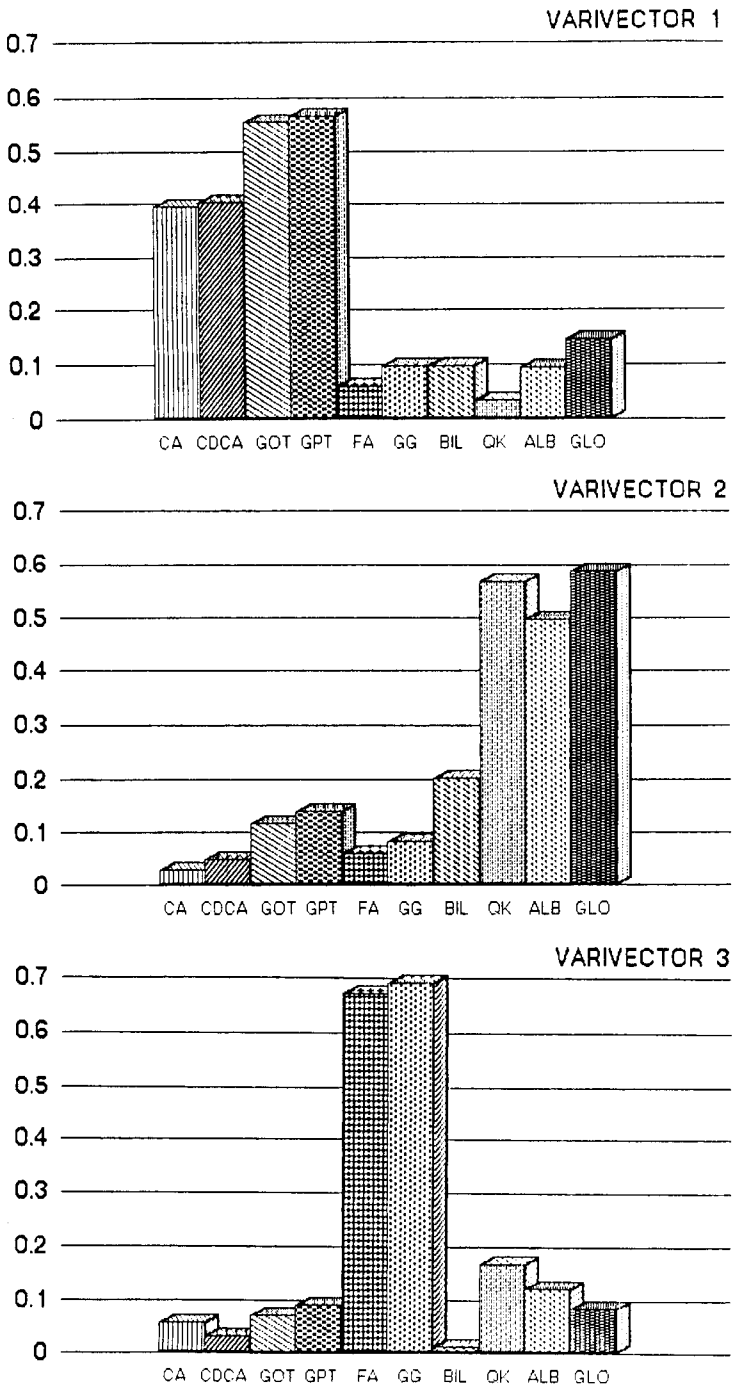

Fig. 2. Bar graphics of the variable loadings on varivectors 1, 2 and 3 (absolute values).

TABLE 2

Classification matrix of the eight categories by the Bayesian method. The number of objects correctly classified and the computed categories are reported. For each category, the percent classification and prediction abilities are listed

True category	Computed category								Ability (%)	
	1	2	3	4	5	6	7	8	Class.	Pred.
1	92	—	—	1	—	—	—	—	99	95
2	—	23	—	—	1	2	—	—	88	88
3	1	—	11	3	4	—	—	—	58	15
4	—	—	—	14	—	—	—	—	100	2
5	3	—	3	14	30	2	—	—	58	60
6	1	2	7	10	37	47	9	—	42	35
7	1	—	7	7	10	23	39	—	45	38
8	—	—	—	—	—	—	—	11	100	11

analysis was considered as preliminary. In order to extract more useful information from this data system, a new mode of creating categories was tested, in which efforts were focussed on discriminating between the categories spread along factor *B*, as suggested by diagnostic interest.

The data matrix was rearranged in the following way. The former categories 3 (fibrosis), 4 (steatosis) and 5 (chronic persistent hepatitis), which overlapped severely (Fig. 1) were grouped into a new category termed "mild liver diseases". The former categories 2 (acute hepatitis) and 8 (cholestasis) were eliminated because they were already quite well separated from the other categories. Moreover, in practice, discrimination between acute hepatitis and the remaining liver diseases is not a problem, and category 8 had too few data vectors. Thus, the new categories were: (1) controls (93 objects); (2) mild liver diseases (84 objects); (3) chronic acute hepatitis (113 objects); and (4) cirrhosis (87 objects).

To simulate the real problem that physicians must solve, the data were evaluated by pairs of contiguous categories, in order of increasing hepatocellular damage, in an attempt to discriminate best between controls and mild liver diseases, mild liver diseases and chronic active hepatitis, and chronic active hepatitis and cirrhosis.

Controls/mild liver disease subset

Only four of the ten original variables were selected by stepwise LDA (minimizing the squared Mahalanobis distance between groups): CDCA, GPT, BIL and ALB. Their loadings on eigenvectors 1 and 2 are shown in Fig. 3A; the first eigenvector is significant. In Fig. 3B, the projection on the first two eigenvectors of the 177 objects of this subset is plotted. The control category overlaps

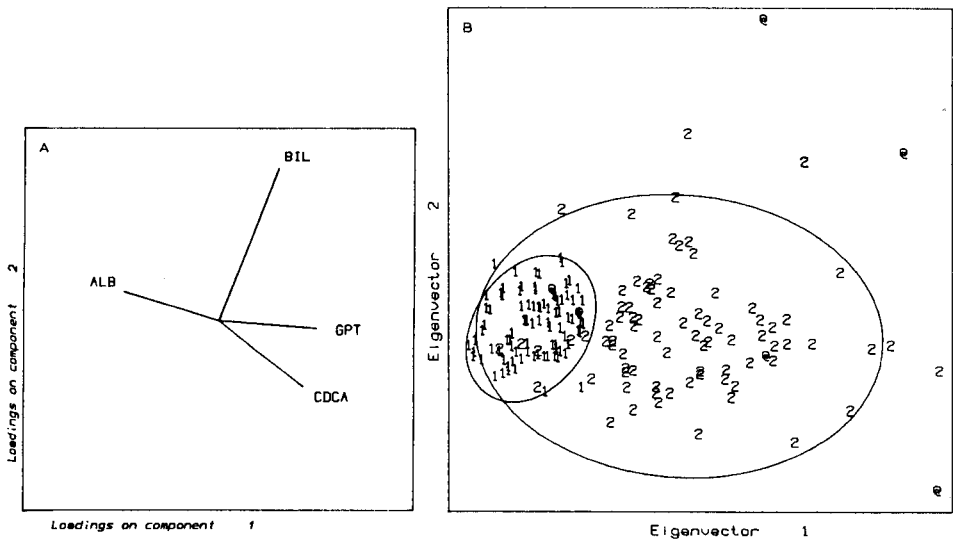

Fig. 3. Subset of controls (1) and mild liver diseases (2). (A) Loading plot of the selected variables on eigenvectors 1 and 2. (B) Eigenvector plot of the data vectors (70% retained variance); the projections of the 80% confidence hyperellipsoids of the class models of the second cycle of the Bayesian analysis are drawn; outliers are shown by symbol @.

slightly with the wider area of category of mild liver diseases. Figure 3B also shows the projections of the confidence hyperellipsoids of the category centroids of the second cycle of Bayesian treatment; six objects with confidence level >99.0 were classified as outliers in the first cycle. In this plot, the confidence hyperellipsoid for the controls is included in the mild liver disease model, but, according to the higher probability density of the control category, a classification ability of 95.9% and a prediction ability of 95.8% were obtained in the second cycle.

Table 3 summarizes the results of the classification methods. The prediction abilities were computed as the means of several different random training/-evaluation set subdivisions. The high percentages of the classification and prediction abilities achieved by the three methods indicate that it is possible to discriminate between healthy states and the mild liver diseases with the use of only four biochemical tests. Other clinical and/or biochemical tests are necessary to distinguish, within the category of mild diseases, between fibrosis, steatosis and chronic persistent hepatitis.

Mild liver disease/chronic active hepatitis subset

For these two categories, six variables were selected: CA, GPT, AP, QK, ALB, GLO. Their loadings on eigenvectors 1 and 2 are reported in Fig. 4A. The first three eigenvectors were found to be significant. The eigenvector plot in Fig. 4B shows an area in which the objects of the two categories are superim-

TABLE 3

Percentage classification and prediction abilities of the three methods

Subset		Bayesian[a]	LDA	*k*NN
		Class.-Pred.	Class.-Pred.	Pred.
Controls/ mild liver diseases	(1)	93.8-93.3	93.8-92.2	94.8
	(2)	95.9-95.8		
Mild liver diseases/ chronic active hepatitis	(1)	66.5-69.2	70.0-67.3	77.7
	(2)	81.5-76.4		
Chronic active hepatitis/ cirrhosis	(1)	74.0-70.7	75.0-68.7	72.5
	(2)	76.7-75.5		

[a]The results of the first (1) and second (2) cycles of Bayesian analysis are reported.

posed; this situation is underlined by the projections of the confidence hyperellipsoids of the Bayesian models. Despite that, the results of the classification methods show about 70% success in both classification and prediction (Table 3).

In this case, after 13 outliers (objects at confidence level >99.0) had been

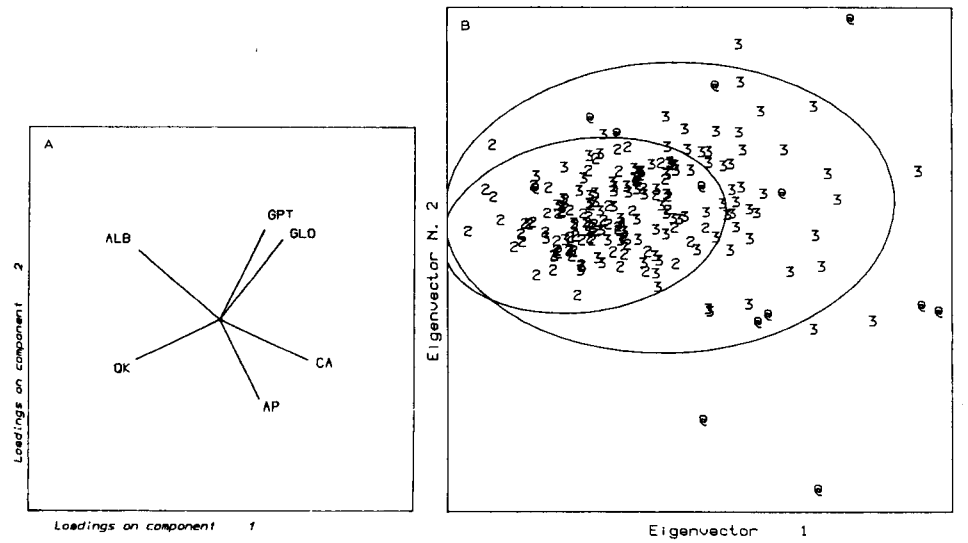

Fig. 4. Subset of mild liver diseases (2) and chronic active hepatitis (3). (A) Loading plot of the selected variables on eigenvectors 1 and 2. (B) Eigenvector plot of the data vectors (48% retained variance); the projections of the 80% confidence hyperellipsoids of Bayesian class models are drawn; outliers are shown by symbol @.

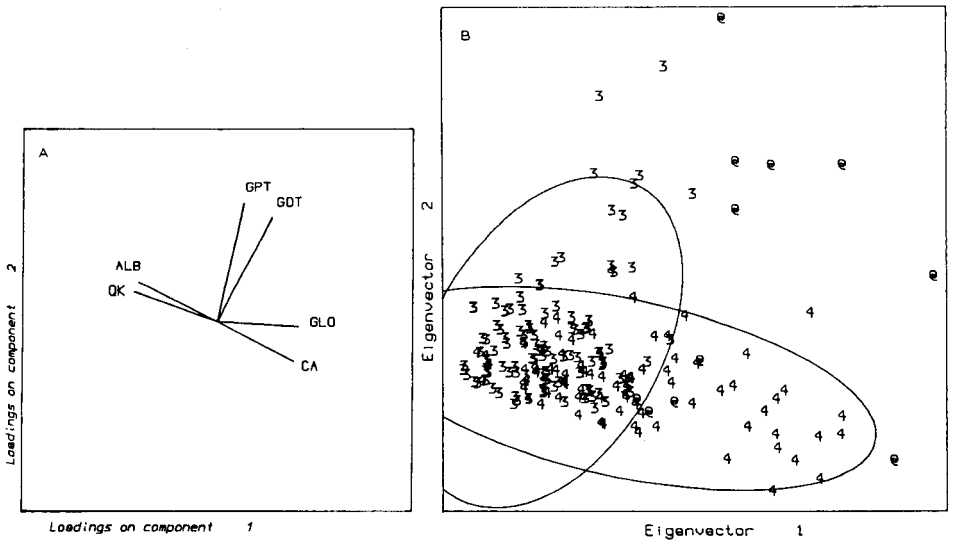

Fig. 5. Subset of chronic active hepatitis (3) and cirrhosis (4). (A) Loading plot of the selected variables on eigenvectors 1 and 2. (B) Eigenvector plot of the data vectors (65% retained variance); the projections of the 80% confidence hyperellipsoids of Bayesian (second cycle) class models are drawn; outliers are shown by symbol @.

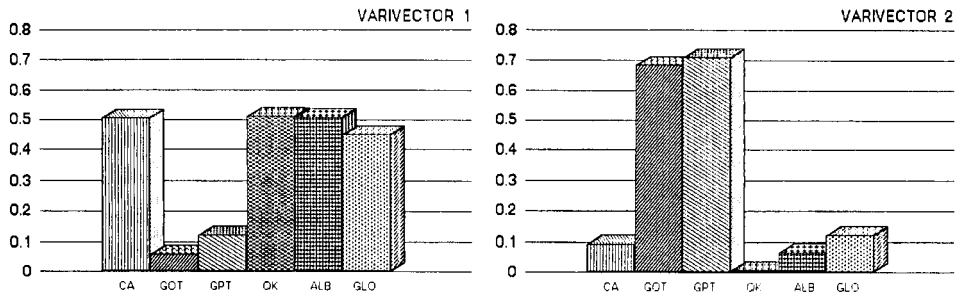

Fig. 6. Bar graphics of the variable loadings (absolute values) on varivectors 1 and 2 in subset chronic active hepatitis/cirrhosis.

discarded, the results of the Bayesian method improved to 81.5% success in classification and 76.4% in prediction. However, the 81.5% is the weighted mean of two very different values of percent classification abilities (94.9% in the mild disease category and 71.7% in the chronic active hepatitis category); these results might be improved by testing other biochemical variables.

Chronic active hepatitis/cirrhosis subset

In feature selection, six variables were chosen: CA, GOT, GPT, QK, ALB, GLO. Their loadings on eigenvectors 1 and 2 are shown in Fig. 5A. In this

subset, interesting patterns were detected. As the eigenvector plot indicates (Fig. 5B), these two categories have an abnormal distribution along two almost orthogonal directions of largest variation, with an overlapping area at the lowest scores for both categories. This plot retains 65% of the variance and the first two eigenvectors were found to be significant. New axes obtained by Varimax rotation in the plane of eigenvectors 1 and 2 almost coincided with the two directions of largest variation. In Fig. 6, the bar graphics of the variable loadings on varivectors 1 and 2 show that, in distinguishing between chronic active hepatitis or cirrhosis, the biochemical variables with increased absolute values are GOT and GPT in chronic active hepatitis and CA, QK, ALB and GLO in cirrhosis.

The projections of the confidence hyperellipsoids of the models of the second cycle of the Bayesian method (11 objects with confidence level >99.9 were considered outliers and discarded in the first cycle) show the existence of three different areas corresponding to pure chronic active hepatitis, pure cirrhosis and mixed chronic active hepatitis/cirrhosis. The mixed area probably comprises patients with both cirrhosis and chronic active hepatitis. This aspect will be discussed in a further study for which hepatocellular damage will be quantified and correlated with biochemical information.

The results in Table 3 show about 75% success in both classification and prediction. Again, the information available from the biochemical tests must be increased to achieve better discrimination between the two groups of patients.

Conclusions

The diagnostic efficiency of serum bile-acid concentrations was verified by feature selection; conjugated cholic acid or chenodeoxycholic acid is present in every selected group of variables. No significant differences were found between the classification methods used. The Bayesian technique tended to give the best results despite the sometimes non-linear distribution of objects. The Bayesian technique is a modelling, as well as classification, method; thus it was possible to discard objects which were very far from the original model, and to compute a new model with the remaining objects.

Remarkable differences were found between the classification and prediction abilities for the different diseases. In some cases (controls, acute hepatitis), very good results were obtained, but less success was achieved for the remaining categories. This means that the chemical information from all the assays applied was sufficient to discriminate among some but not all of the diseases considered. However, some practical success was attained. When the Bayesian method was applied to the whole data set, the four variables selected in the classification of the control and mild disease categories (CDCA, GPT, BIL, ALB) provided a classification and prediction success rate of 95.8% for the control group. This might serve as a preliminary test to distinguish between the absence or presence of liver disorders. In cases of suspected liver

malfunction, it would be possible to estimate whether or not a patient comes within the control model simply by testing four biochemical variables and applying the Bayesian method with the new patient in the test set. If the patient is classified in the control category, the hypothesis of liver disease can be rejected with sufficient security, otherwise the remaining tests must be applied.

We are grateful to Dr. Ing. A.M. Morselli Labate and Dr. A.G. Rusticali, Istituto di Clinica Medica e Gastroenterologia, Universita' di Bologna, for helpful discussions. This work received financial support from the Education Department (MPI 40%) and from the National Council of Research. The paper was presented in part at the Third Meeting of the Chemometrics Society, Lerici, Italy in May, 1986.

REFERENCES

1 A.C. Hofmann, Hepatology, 2 (1982) 512.
2 M.G. Korman, A.C. Hofmann and W.H.J. Summerskill, N. Engl. J. Med., 290 (1974) 1399.
3 P.S. Monroe, A.L. Baker, J.F. Schneider, P.S. Krager, P.D. Klein and I. Scholler, Hepatology, 2 (1982) 317.
4 B.R. Kowalski, Anal. Chem., 47 (1975) 1152A.
5 R.P. Knill-Jones, R.B. Stern, D.H. Girmes, J.D. Maxwell, R.P.H. Thompson and R. Williams, Br. Med. J., 1 (1973) 530.
6 A. Roda, S. Girotti, S. Lodi and S. Preti, Talanta, 31 (1984) 895.
7 A. Roda, S. Girotti, P. Filippetti, A. Piacentini and P. Simoni, in G. Galli and E. Bosisio (Eds.), Liver, Nutrition and Bile Acids, NATO A.S.I. Course, Plenum, London, 1985, p. 65.
8 A. Roda, S. Girotti, A. Piacentini, S. Preti and S. Lodi, Anal. Biochem., 156 (1986) 267.
9 M. Forina, Trends Anal. Chem., 3 (1984) 38.
10 W.R. Dillon and M. Goldstein, Multivariate Analysis: Methods and Applications, Wiley, New York, 1984, p. 360.
11 D.L. Massart, A. Dijkstra and L. Kaufman, Evaluation and Optimization of Laboratory Methods and Analytical Procedures, Elsevier, Amsterdam, 1978, p. 418.
12 R.O. Duda and P.E. Hart, Pattern Classification and Scene Analysis, Wiley-Interscience, New York, 1973, p. 10.
13 B.R. Kowalski and C.F. Bender, J. Am. Chem. Soc., 94 (1972) 5632.
14 W.R. Dillon and M. Goldstein, Multivariate Analysis: Methods and Applications, Wiley, New York, 1984, p. 375.
15 M. Forina, S. Lanteri and R. Leardi, Feature Selection by Stepwise Bayesian Analysis, COBAC IV, Graz, Austria, September, 1986, Book of Abstracts.
16 B.R. Kowalski, Chemometrics; Theory and Application, Wiley, New York, 1977.
17 E.R. Malinowski and D.G. Howery, Factor Analysis in Chemistry, Wiley-Interscience, New York, 1980, p. 82.
18 M.A. Sharaf, D.L. Illman and B.R. Kowalski, Chemometrics, Wiley, New York, 1986, p. 206.

Analytica Chimica Acta, 202 (1987) 187–197
Elsevier Science Publishers B.V., Amsterdam — Printed in The Netherlands

RESOLUTION OF OVERLAPPED CHROMATOGRAMS BY MEANS OF THE KALMAM FILTER
Data Processing of Liquid Chromatographic Signals without Solvent Peaks

YUZURU HAYASHI*, TOSHIO SHIBAZAKI, RIEKO MATSUDA and MITSURU UCHIYAMA

Division of Drugs, National Institute of Hygienic Sciences, 1-18-1 Kamiyoga, Setagaya-ku, Tokyo (Japan)

(Received 23rd April 1987)

SUMMARY

If several samples are injected successively at short intervals into a liquid chromatograph, overlapped chromatograms of the samples will result. This paper describes an application of this successive-injection method to determination of samples without solvent peaks. Twenty peaks in the overlapped chromatograms resulting from five successive injections of samples with four components (phenetole, biphenyl, pyrene and perylene) were resolved and quantified by a reduced four-dimensional Kalman filter. The period of the single chromatogram of the four components is ca. 14 min, and the period of the five overlapped chromatograms ca. 26 min, for injection intervals of 3 min. The calibration lines for the four components are all straight and satisfactory; the slope, A, of every line was $1.005 > A > 0.9996$ with correlation coefficients better than 0.999992. This successive-injection method with the reduced Kalman filter is time-saving for trivial routine work.

Overlapped chromatograms will result from successive injections at short intervals of many samples into a high-performance liquid chromatograph (HPLC) [1]. A rapid, precise method for peak resolution of the overlapped chromatograms would save much time for assays of a series of samples in various areas of analytical chemistry. For example, industrial process control often requires the determination of numerous samples which have the same known components at unknown concentrations. Successive injections of the samples at regular intervals will give overlapped chromatograms of simple or periodic pattern, which will provide information concerning the peak shapes of the components in a contracted form.

The Kalman filter is a powerful candidate for handling such a situation; this filter is characterized by a linear recursive least-squares algorithm and real-time processing of signals. Recently, the various analytical uses of the Kalman

0003-2670/87/$03.50

filter have been reviewed [2]. Peak resolution with the filter has been reported for ultraviolet-visible spectra [3–6], voltammograms [7–10] and HPLC peaks [11]. The most critical problem of the filter, when applied to the successive-injection method, is the large dimensionality of the matrices involved in the algorithm. The dimensionality is usually defined as equal to or more than the number of peaks to be resolved and must be augmented as additional samples are successively injected. It is difficult to calculate the large matrices rapidly on small laboratory computers.

This dimensional problem was successfully solved by the re-initialization method described recently for resolution of many Gaussian peaks [1]. The dimensionality of the proposed algorithm, called a reduced Kalman filter, is very small and is independent of the number of peaks to be resolved, thereby allowing practical implementation on desk top computers [1]. Twenty partly overlapping Gaussian peaks were resolved successfully by a reduced filter of four dimensions.

The aim of this paper is to demonstrate an application of the successive-injection method with the reduced Kalman filter in the analysis of samples without solvent peaks. First, the term "least square", often encountered in Kalman filter theory, is briefly reviewed from a mathematical point of view, because its definition is a little confused in some literature [2].

THEORY

A brief mathematical interpretation of Kalman filter theory may be helpful for intuitive understanding. The term "least square", is discussed with special emphasis on similarities between the filter and the commonly used linear least-squares fitting. Detailed formulation of the filter is available in the chemical [2], engineering [12,13] and mathematical [14] literature.

For simplicity, a one-dimensional problem of noise reduction from raw data is considered. X is the variable to be estimated, e.g., the concentration of a required component. A noise-contaminated piece of raw data Y_k at point k is assumed to be described by

$$Y_k = F_k X + W_k \quad (k=1, 2,..., N) \tag{1}$$

where W_k denotes white noise (Gaussian distribution) in the observation process of X. If the noise is negligible or reduced completely, the observed value Y_k can be reduced to a simple form $Y_k = F_k X$. Thus, F_k is a function of k which denotes the idealized chromatogram or spectrum for the variable of unit quantity ($X=1$). The values of F_k must be known at every point k ($k=1,..., N$) for the Kalman filter analysis before evaluation is started.

Let X' be an estimate for X. Linear regression analysis yields the optimal

value $\tilde{X}$ of X' when the square "distance" or square sum S of the difference between an estimate F_kX' and the raw data Y_k

$$S=\sum_{k=1}^{N}(Y_k-F_kX')^2 \tag{2}$$

has a minimum ($\tilde{X}=X'$). Let $\mathbf{y}$ be a column vector described by $(Y_1,...,Y_N)^T$ and $\mathbf{f}$ be $(F_1,...,F_N)^T$, where the superscript T denotes the transpose. The optimal value $\tilde{X}$ is well-known to be given by a linear algebra description [15]

$$\tilde{X}\mathbf{f}=[(\mathbf{f},\mathbf{y})/(\mathbf{f},\mathbf{f})]\mathbf{f} \tag{3}$$

where the parentheses denote a scalar product of vectors and the right-hand side represents the projection of vector $\mathbf{y}$ onto the straight line of direction $\mathbf{f}$. Of importance is that the linear regression algorithm is described by the orthogonal projection.

The Kalman filter covers the same situation. It is assumed that the variable X has a probability distribution (Gaussian). Thus, the Kalman filter estimate $\tilde{X}_k$ at a datum point k is also subject to the laws of probability and X, $\tilde{X}_k$, Y_k and W_k are called random variables. The white noise W_k is assumed to be $E[W_k]=0$ and $E[W_kW_l]=c\delta_{kl}$ $(k,l=1,...,N)$, where $E[\cdot]$ denotes the expected random variables, c the variance and δ_{kl} is Kronecker's delta. The Kalman filter finds an optimally estimated distribution $\tilde{X}_k$ so that a square "distance" P_k from an estimate X_k' to the true distribution X

$$P_k=E[(X_k'-X)^2] \tag{4}$$

takes a minimum value ($\tilde{X}_k=X_k'$). The square distance P_k shows the error of the estimate X_k'.

The difference in the definitions of the above-mentioned distances should be noted. The distance used in the usual regression analysis is founded on Euclidian space. The N-dimensional vectors $\mathbf{y}$ and $\mathbf{f}$ denote points in Euclidian space of N-dimensions, where the square distance between the points $\mathbf{y}$ and $X'\mathbf{f}$ is defined by Eqn. 2. In contrast, the definition of the square distance P_k in the theory of the Kalman filter is based on an ensemble consisting of the random variables X, $W_1,...,W_N$ and all of their linear combinations. This ensemble is called Gauss space $\mathfrak{G}(X, W_1,..., W_N)$ spanned by $X, W_1,..., W_N$ [14]. It should be noted that Y_k is contained in the Gauss space $\mathfrak{G}$, because Y_k can be described by a linear combination of X and W_k (see Eqn. 1).

Let $\mathfrak{g}_k(Y_1,..., Y_k)$ be a sub-Gauss space spanned by $Y_1,..., Y_k$:$\mathfrak{g}_k=\mathfrak{G}(Y_1,..., Y_k)$. Every estimate X_k' at a datum point k should be contained in $\mathfrak{g}_k$, while X is outside $\mathfrak{g}_k$. This means that knowledge about X is confined to the collected information $Y_1,..., Y_k$. The minimization of the square distance P_k is attained by an orthogonal projection $\tilde{X}_k$ (the optimal estimate) of the distribution X onto the sub-Gauss space $\mathfrak{g}_k$:

$$\tilde{X}_k = E[X/\sigma(\mathfrak{g}_k(Y_1,\ldots, Y_k))] \tag{5}$$

where the right-hand side is called the conditional expectation of X and $\sigma(\mathfrak{g}_k)$ is called σ-algebra [14]. It should be noted that the Kalman filter and linear regression analysis have the same formal concept of the projection in their own spaces. The term "least square" can be defined as minimization of square distance. Consequently, it can be concluded that: (i) linear regression analysis is a least-squares algorithm in Euclidian space; (ii) the Kalman filter is a least-squares algorithm in Gauss space. In addition, it can be stated that: (iii) some digitial filters based on Fourier transform are least-squares algorithms in Hilbert space.

The sub-Gauss space $\mathfrak{g}_k(Y_1,\ldots, Y_{k+1})$ enlarges as new information Y_{k+1} concerning X is collected. Thus, the distance from the point X to the subspace $\mathfrak{g}_k$ decreases with increasing k (see Fig. 1). This situation provides the recursive property of the Kalman filter algorithm.

The optimal estimate $\tilde{X}_k$ at datum point k is described by a function of Y_k, W_k, P_k, F_k, and $\tilde{X}_{k-1}$. If more estimates are required, the above scalar description should be replaced by a vector and matrix description. The matrix form of P_k is called the error covariance matrix, that of F_k is called the measurement matrix and the vector form of $\tilde{X}_k$ is termed the state estimate vector.

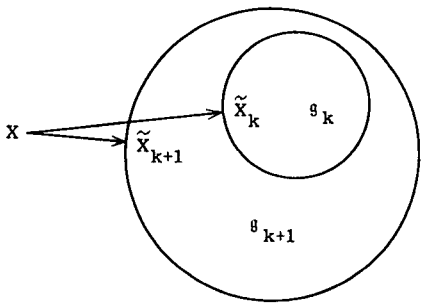

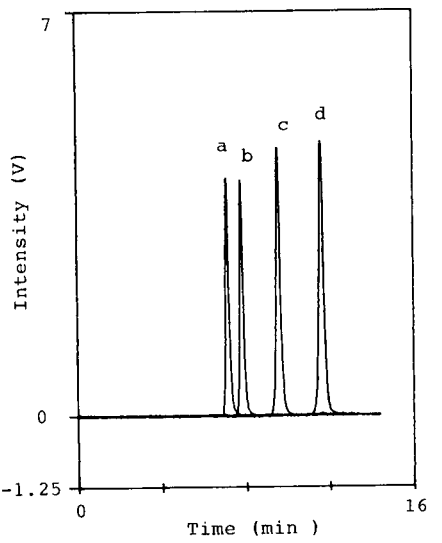

Fig. 1. Schematic diagram of expanding sub-Gauss space $\mathfrak{g}_k$ and the distribution X. The arrows denote the optimally estimated distributions $\tilde{X}_k$ and $\tilde{X}_{k+1}$. The length of the arrows denotes the error of the estimated distributions or the distance from the true distribution X to the estimated ones. Note that $\tilde{X}_k$ is contained in $\mathfrak{g}_k$, but X is not.

Fig. 2. Superimposed component peaks. Peaks: (*a*) 34 mg l^{-1} phenetole (100%); (*b*) 1.5 mg l^{-1} biphenyl (100%); (*c*) 3.0 mg l^{-1} pyrene (100%); (*d*) 3 mg l^{-1} perylene (100%).

EXPERIMENTAL

Reagents

Reagents used were phenetole and pyrene (Tokyo Kasei), biphenyl (Wako) and perylene (Aldrich). The solvent was HPLC-grade methanol (Wako). Standard solutions of phenetole (34 mg l^{-1}), biphenyl (1.5 mg l^{-1}), pyrene (3.0 mg l^{-1}) and perylene (3 mg l^{-1}) were prepared by dilution of the several-fold concentrated stock solutions with the methanol. Hereinafter, the concentrations of these standard solutions are referred to as 100% and a sample containing the four 100% components is called the 100% sample.

Methods

For the chromatographic experiments, a Hitachi 655A-11 liquid chromatograph system was used with a type 7125 loop injector (manual, 20-μl injection, Rheodyne) and a variable-wavelength ultraviolet detector (Hitachi). The eluent was monitored at 254 nm. The column used was Inertsil ODS (4.6×250 mm, Gasukuro Kogyo) and its temperature was maintained at 30°C by a Hitachi 655A-52 column oven. The mobile phase was methanol at a flow rate of 0.5 ml min^{-1}.

The outputs of the HPLC system were amplified with a Yokogawa type 3131 amplifier, collected with an Elmec EC-2325 A/D converter with 12-bit resolution and 30-μs conversion time, and transferred to the RAM of a NEC PC-9801 VX desk-top computer. The low-pass filter was adjusted to 10 Hz and the sampling intervals were 0.2 s. This computer was equipped with an Intel-80286 compatible CPU (8 MHz), 640 kbyte RAM and two 5-in. floppy disk drives (2 Mbyte). All the chromatograms displayed here were drawn by a Graphtec MP-3100 XY plotter interfaced with the computer. The ordinates of all the chromatograms are the output (V) of the d.c. amplifier (gain=100).

Data processings

The reduced Kalman filter of small dimensions has been described in detail [1]. All the programs were written in BASIC and run after compiling. The reduced filter used here is of four dimensions: the matrices and vectors involved in the algorithm are all of four dimensions. The overlapping mode adopted was to use five samples with the four components a, b, c and d injected successively at regular intervals to give twenty peaks. The peaks i_a ($i=1,...,5$) derived from the successive injections are collected in an element $\{\mathbf{F}_k\}_{11}$ of the measurement matrix $\mathbf{F}_k$ and then $\{\mathbf{F}_k\}_{11}$ becomes a periodic function of k that denotes the five peak shapes; the other peaks are manipulated in the same way. The initial condition of the state estimate vector $\tilde{\mathbf{X}}_0$ is $\tilde{\mathbf{X}}_0=0$; that of the error covariance matrix $\mathbf{P}_0$ (diagonal) is $\mathbf{P}_0=c\hat{1}$, where c denotes a constant ($=10\,000$) and $\hat{1}$ a unit matrix.

The re-initialization of the error covariance matrix $\mathbf{P}_k$ is done in inactive

regions of the filtering process [1]: $\{\mathbf{P}\}_{jj}$ is abruptly increased to the initial large value of $\mathbf{P}_0$ at the middle point m between the ith and $(i+1)$th peaks $(i=1,..., 4)$ of the same component j and the preceding estimate $\{\tilde{\mathbf{X}}_{m-1}\}_j$ before the middle point is adopted as a final estimate of the ith peak. The final estimate of the fifth peak is the estimate at the last data point 9600 (32 min). The Kalman gain $\mathbf{L}(k)$ is calculated from the periodic $\mathbf{F}_k$ and re-initialized $\mathbf{P}_k$ and then has the periodic activity of the estimation process [1].

RESULTS

The Kalman filter is an algorithm by which noise-contaminated raw data are smoothed or approximated by a linear combination of component model peaks. Thus, the examination of the effect of the overlapping procedures on the original peak shapes of the isolated components is indispensable for the successive-injection method. Figure 2 shows the component peaks in the sample (100%) to be analyzed. Retention times are: 428 s for phenetole (peak *a*), 468 s for biphenyl (*b*), 574 s for pyrene (*c*) and 697 s for perylene (*d*). In the single chromatogram, peaks *a* and *b* weakly overlap and the others are separated. An overlapping mode is adopted here: the last peak *d* in a chromatogram is outstripped by peaks *a* and *b* in the following chromatogram.

The peak shapes of the components shown in Fig. 2 were used as the measurement matrix $\mathbf{F}_k$ without any smoothing procedures except for baseline subtraction, because the noise level was very low (the variance was $<$ca. 3.5×10^{-5} V^2) under the circumstances. The simple moving-average method used for the smoothing levelled off the peak slightly and increased the Kalman filter estimates.

For examination of the precision of the short successive-injection method, the same samples were injected at regular intervals. Figure 3 shows the overlapped chromatograms derived from the five injections of the 100% samples. For 200-s injection intervals (A), peak *d* weakly overlaps with peak *b* in the following chromatogram and the ratio of the apparent height of the valley to that of the mean peak maxima is ca. 12%. For 160-s injection intervals (B), peaks *c* and *a* strongly overlap by a degree of ca. 60%. For 150-s injection intervals (C), peaks *c* and *a* fuse into one peak.

Table 1 shows the reproducibility and errors of the four component peaks in the overlapped chromatograms with the several injection intervals. The errors of the mean estimates for the component peaks which do not overlap strongly are less than 0.5%. More strongly overlapped peaks (*a* and *c* in the chromatograms from 160-s injection intervals give errors less than 2%. However, the fused peaks *a* and *c* in the 150-s interval chromatogram give large errors of ca. 10%. The relative standard deviations of all the components are good ($<0.5\%$) except for the chromatograms from the short injection intervals (160 and 150 s). Even with the shortest intervals, the weakly overlapped components (peaks

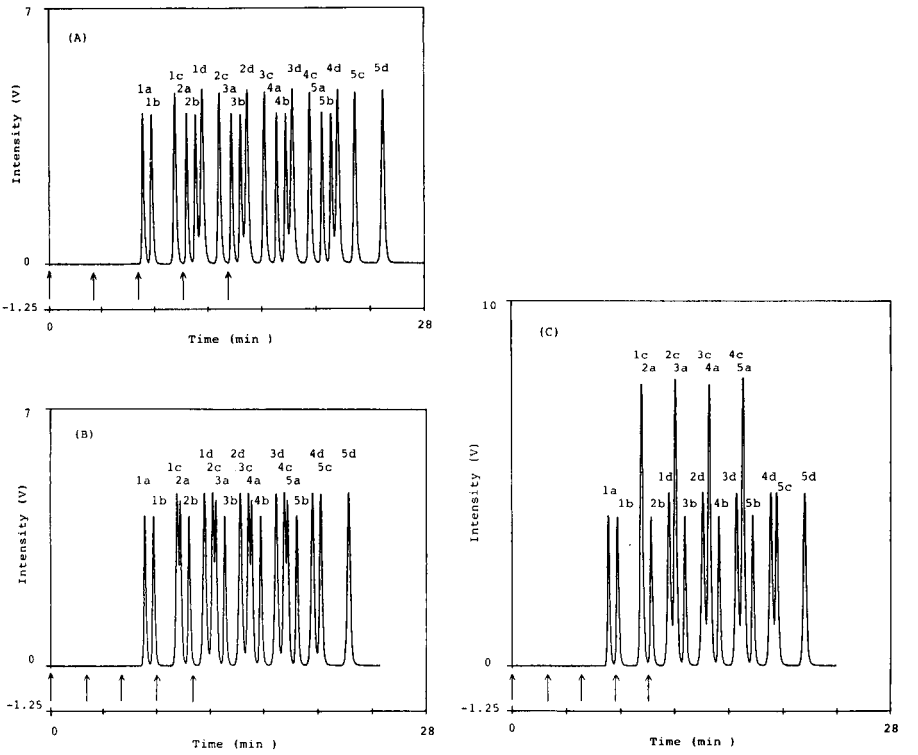

Fig. 3. Overlapped chromatograms derived from the successive-injection method. Injection interval: (A) 200 s, 1000 points; (B) 160 s, 800 points; (C) 150 s, 750 points. The arrows show the injection points of the samples.

b and *d*) give satisfactory estimates and reproducibility ($<0.5\%$). The reproducibility in the HPLC system used, measured by an isolated biphenyl, was 0.24% ($n=10$).

TABLE 1

Reproducibility (relative standard deviation, RSD) of overlapped chromatograms

Peak	Injection intervals (s)							
	200		180		160		150	
	Mean	RSD	Mean	RSD	Mean	RSD	Mean	RSD
a	100.17	0.42	100.04	0.28	101.60	1.09	112.01	6.23
b	100.05	0.14	99.89	0.21	99.89	0.24	100.05	0.17
c	100.40	0.25	100.42	0.14	99.69	0.83	91.54	6.32
d	100.15	0.22	100.49	0.10	100.17	0.45	1001.5	0.12

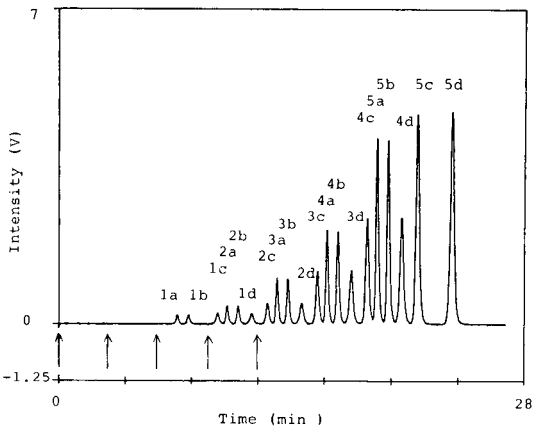

Fig. 4. An overlapped chromatogram of five samples for injection intervals of 180 s. The first injection was a 5% sample; the second, 10%; the third, 25%; the fourth, 50%; the fifth, 100%. The arrows show the injection points of the samples.

The four components were quantified simultaneously from the overlapped chromatograms obtained with the injection interval (180 s) which gave the least overlapping of the component peaks. The results allow the conclusion that if an appropriate overlapping mode is chosen, the successive-injection method is useful for the rapid, precise determination of a series of samples without solvent peaks. Figure 4 shows the total chromatogram derived from injections, at 180-s intervals, of five samples in the injection order, 5, 10, 25, 50, 100% samples. These samples had a constant ratio of the component concentrations, but of course samples with random component concentrations can be also analyzed by the reduced filter. The period of this chromatogram was ca. 26 min, which is far shorter than the total period required for five separate experiments (ca. 5×14 min).

The calibration line of peaks *a* obtained from the overlapping mode shown in Fig. 4 was straight (not shown); the slope was 1.0025, the intercept -0.0648 and the correlation coefficient 0.9999929 (see Table 2). The RSD values of the estimates of peaks *a* did not exceed 1.1% even for the 5% concentration. The errors of the mean estimates were $<1\%$ for the 100–10% samples, but 2.2% for the 5% samples. The calibration lines of the other components were also straight; their reproducibility and errors were all satisfactory (see Table 2).

Smoothed lines obtained by the reduced Kalman filter coincided with all the raw data shown in Figs. 3 and 4. This coincidence was also found for 400% samples. These results indicate that the shapes of the component peaks are not altered by the overlapping or outstripping processes of the peaks. In other words, the HPLC elution process conserves the linearity of its signals even in these overlapped chromatograms.

TABLE 2

Statistical parameters of calibration lines obtained from the 180-s interval injections

Conc.	Peaks							
	a		b		c		d	
	Mean	RSD	Mean	RSD	Mean	RSD	Mean	RSD
5	4.89	1.05	4.84	1.35	5.15	0.65	5.00	1.72
10	9.93	0.97	9.82	1.22	10.16	0.59	10.01	0.70
25	25.06	0.23	24.87	0.54	25.19	0.29	25.25	0.48
50	50.14	0.47	49.91	0.17	50.31	0.19	50.03	0.28
100	100.13	0.18	99.79	0.25	100.56	0.10	100.15	0.18
A[a]	1.0025		0.9997		1.0047		1.0011	
B	−0.0648		−0.1412		0.1012		0.0478	
r	0.9999929		0.9999934		0.9999982		0.9999922	

[a]A denotes the slope of the calibration line, B the intercept and r the correlation coefficient.

DISCUSSION

An application of the reduced Kalman filter of small dimensions described earlier [1] was presented above. The results indicate that the overlapped chromatograms can be decomposed into their constituent chromatograms or peaks precisely and that the successive-injection method can provide information concerning the HPLC signals in a contracted form. It can be concluded that the successive-injection method with the reduced Kalman filter is useful for rapid, precise determination of a series of samples without solvent peaks.

There are two main restrictions of the method: (i) the overlapping mode of the chromatograms should be chosen so that the peaks originating from the different injections do not overlap excessively; (ii) the method can be applied to at most several series of samples consisting of the same known components with unknown random concentrations. A series of samples with the same components at a constant concentration ratio was examined above. Point (i) arises from the linearity of the HPLC signals; point (ii) arises from the finite memory space of computers and the linear property of the Kalman filter. A disadvantage of the Kalman filter is that it cannot estimate unexpected or ghost peaks. However, the ghost peaks can be deconvoluted by combination of the reduced filter and the non-linear regression procedure used in the batch mode. In all cases, the experiments must be planned carefully: the injection intervals, the injection order of the series and the components of the samples must be programmed beforehand.

The reduced Kalman filter plays an important role in this sucessive-injection method [1]. Its dimensionality does not depend on the number of peaks to be estimated, but on the overlapping mode of the peaks in the total chromatogram. A practical advantage of this reduced filter is that there is no need to divide the total chromatogram into different parts containing a few peaks for economy of memory and/or execution time. If many peaks overlap without baseline-separation, most of the methods applied for the batch mode will cause some error because of the dividing procedures. The Kalman filter can circumvent this problem by the re-initialization of the error covariance matrix $\mathbf{P}_k$ and in principle the reduced filter can resolve an infinite number of peaks resulting from successive injections.

A great variety of methods has been proposed for the resolution of unresolved peaks into their components. The earliest and most commonly used technique is perpendicular-dropping and tangential-skimming [16–18]. Another approach is based on linear or nonlinear least-square fitting involving Gaussian [19–21], exponentially modified Gaussian [20–22], Weibull [20] functions, etc. Recently, a resolution method has been reported which does not involve any assumptions about peak shapes or prior knowledge of the spectra of the individual components [23]. However, a large amount of memory and/or execution time is required for these batch-mode techniques and the use of double precision further aggravates this problem [19].

The Kalman filter requires prior knowledge about the whole peak shape of each of the components as model peaks, but this requirement does not interfere with the analytical applications of the filter at all. In order to determine target components in a sample, their peak shapes or some parameters inherent in the used HPLC apparatus must be measured beforehand. Without this process, the peak resolution cannot be utilized for quantitation. During this process, the Kalman filter satisfies the requirement.

The successive-injection method presented saves much time for trivial routine work and the resulting overlapped chromatograms provide information concerning peak parameters such as height, position and width in a contracted form. This method may lead to novel designs for experimental procedures in various areas of analytical chemistry. The overlapping and outstripping effects of solvent peaks on the analysis will be considered in the next paper in this series [24].

REFERENCES

1 Y. Hayashi, T. Shibazaki and M. Uchiyama, Anal. Chim. Acta, 201 (1987) 185.
2 S.D. Brown, Anal. Chim. Acta, 181 (1986) 1 (and references therein).
3 H.N.J. Poulisse, Anal. Chim. Acta, 112 (1979) 361.
4 C.B.M. Didden and H.N.J. Poulisse, Anal. Lett., 13 (A1) (1980) 921.
5 A. Van Loosbroek, H.J.G. Debets and D.A. Doornbos, Anal. Lett., 17 (A8) (1984) 677.

6 A. Van Loosbroek, H.J.G. Debets and P.M.J. Coenegracht, Anal. Lett., 17 (B9) (1984) 779.
7 T.F. Brown and S.D. Brown, Anal. Chem., 53 (1981) 1410.
8 C.A. Scolari and S.D. Brown, Anal. Chim. Acta, 166 (1984) 253.
9 C.A. Scolari and S.D. Brown, Anal. Chim. Acta, 178 (1985) 239.
10 S.C. Rutan and S.D. Brown, Anal. Chem., 55 (1983) 1707.
11 Y. Hayashi, T. Shibazaki, R. Matsuda and M. Uchiyama, J. Chromatogr., 407 (1987) 59.
12 S. Arimoto, Kalman Filter, Sangyo Tosho, Tokyo, 1977.
13 A.H. Jazwinski, Stochastic Processes and Filtering Theory, Academic, New York, 1970.
14 H. Kunita, Estimations of Random Processes, Sangyo Tosho, Tokyo, 1976.
15 G. Strang, Linear Algebra and its Applications, Academic, New York, 1976.
16 H.A. Hancock, L.A. Dahm and J.F. Muldoon, J. Chromatogr. Sci., 8 (1970) 57.
17 A.W. Westerberg, Anal. Chem., 41 (1969) 1770.
18 J.P. Foley, J. Chromatogr., 384 (1987) 301.
19 R.A. Caruana, R.B. Searle, T. Heller and S.I. Shupack, Anal. Chem., 58 (1986) 1162.
20 R.A. Vaidya and R.D. Hester, J. Chromatogr., 287 (1984) 231.
21 R.A. Vaidya and R.D. Hester, J. Chromatogr., 333 (1985) 152.
22 S.D. Frans, M.L. McConnell and J.M. Harris, Anal. Chem., 57 (1985) 1552.
23 R.F. Lacey, Anal. Chem., 58 (1986) 1404.
24 Y. Hayashi, T. Shibazaki and M. Uchiyama, J. Chromatogr., 411 (1987) 95.

Analytica Chimica Acta, 202 (1987) 199–205
Elsevier Science Publishers B.V., Amsterdam — Printed in The Netherlands

SEQUENTIAL DETERMINATION OF GLUCOSE AND FRUCTOSE IN FOODS BY FLOW-INJECTION ANALYSIS WITH IMMOBILIZED ENZYMES

P. LINARES, M.D. LUQUE DE CASTRO and M. VALCÁRCEL*

Department of Analytical Chemistry, Faculty of Sciences, University of Córdoba, Córdoba (Spain)

(Received 14th October 1986)

SUMMARY

A sequential method for determination of glucose and fructose involving the use of enzymes (hexokinase and glucose-6-phosphate dehydrogenase) immobilized on controlled-pore glass is proposed. The flow is selected so as to determine glucose or both sugars by fluorimetric determination of the NADH formed. The method is applied to the determination of these compounds in fruit juices, yoghourt and dessert powder with good results.

Despite considerable costs and reagent instability, enzymatic methods of analysis have gained significance, thanks to their high selectivity. The problems have been minimized by immobilizing enzymes on suitable supports. Thus, the enzymes have been placed on electrodes [1–4] and packed in reactors [5–9] or different types of open tubes [10,11]. The use of flow injection analysis (f.i.a.) with immobilized enzymes adds the advantages of enzymatic analysis to the rapidity and versatility of the flow technique. The possibility of conducting many repetitive analyses in the same reactor largely avoids the problems of cost involved in the use of enzymes. Thus, numerous methods have been based on this association, particularly in clinical chemistry [12], but they have scarcely been applied in food analysis.

In this paper, a sequential determination is described for glucose and fructose by use of two reactors holding enzymes immobilized on controlled-pore glass, and fluorimetric detection. The method is based on the following coupled enzymatic reactions. First, glucose and fructose are phosphorylated to glucose-6-phosphate (G6P) and fructose-6-phosphate (F6P), respectively, by action of hexokinase (HK) and adenosine-5-triphosphate (ATP) in the presence of a doubly-charged cation [13]:

$$\text{Glucose} + \text{ATP} \overset{\text{HK}}{\rightleftharpoons} \text{G6P} + \text{ADP};\ \text{Fructose} + \text{ATP} \overset{\text{HK}}{\rightleftharpoons} \text{F6P} + \text{ADP}$$

0003-2670/87/$03.50

In the presence of glucose-6-phosphate dehydrogenase (G6PDH), G6P is oxidized by nicotinamide adenine dinucleotide phosphate ($NADP^+$) to gluconate-6-phosphate, with formation of the reduced form of the coenzyme, NADPH:

$$G6P + NADP^+ \overset{G6PDH}{\rightleftharpoons} \text{Gluconate-6-phosphate} + NADPH + H^+$$

Fructose-6-phosphate is converted to glucose-6-phosphate with the aid of phosphoglucose isomerase (PGI):

$$F6P \overset{PGI}{\rightleftharpoons} G6P$$

The G6P formed is then oxidized as above. In both cases the NADPH formed is monitored fluorimetrically at $\lambda(ex) = 340$ nm, $\lambda(em) = 460$ nm.

EXPERIMENTAL

Apparatus

A Tecator 5020 flow-injection analyzer was used. Its two peristaltic pumps start and stop individually and are synchronized with the injection system (a variable volume Tecator L100-1 injection valve). A Perkin-Elmer LS-1 LC fluorescence detector with a 4-μl flow cell was used with a Perkin-Elmer 56 recorder.

Reagents

Glucose-6-phosphate dehydrogenase (EC.1.1.1.49 type XI, with a specific activity of 325 U mg^{-1}), hexokinase (EC.2.7.1.1. type C-301, with a specific activity of 430 U mg^{-1}), and phosphoglucose isomerase (EC.5.3.1.9. type X, with a specific activity of 590 U mg^{-1}) were from Boehringer, Mannheim. Adenosine-5-triphosphate (sodium salt) and β-nicotinamide adenine dinucleotide phosphate were used as supplied by Sigma Chemical Co. Aqueous solutions of glucose and fructose were prepared from 1×10^{-2} M stock solution buffered at pH 8 with 0.1 M potassium phosphate.

The reagents used for the enzyme immobilization were 3-aminopropyltriethoxysilane (Sigma Chemical Co.) and aqueous 25% glutaraldehyde solution (Merck). The controlled-pore glass (CPG) was from Electronucleonics (Fairfield, NY); it was 80/120 mesh, with an average pore size of 202.5 nm.

Preparation of the packed reactors

The determination of glucose and fructose requires the immobilization of three different enzymes, hexokinase, glucose-6-phosphate dehydrogenase and phosphoglucose isomerase. The immobilization procedure followed was similar to that described by Masoom and Townshend [9] for glucose oxidase and was applied to each enzyme. To 0.1 g of activated controlled-pore glass was added 2 ml of 0.1 M potassium phosphate buffer, pH 6.0, containing 100 μl of hexo-

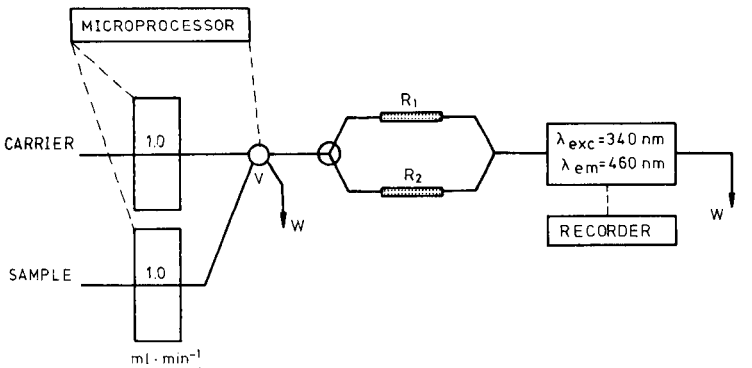

Fig. 1. Flow system used for sequential determination of glucose and fructose. The first column, R_1, contains immobilized hexokinase and G6PDH; the second, R_2, contains hexokinase, PGI and G6PDH.

kinase (64.5 U), or 100 μl of G6PDH (396 U), or 1 mg of PGI (590 U). The three solutions were kept free from oxygen at 4 °C for 2.5 h; the glass was then washed with distilled water and 0.1 M phosphate buffer, pH 6.0, to eliminate non-immobilized enzyme. Two enzymatic reactors were prepared: R_1, which was a 200×1.14 mm^2 column packed in sequence with the same weights of glass with immobilized hexokinase and G6PDH; and R_2, which was a 250×1.14 mm^2 column packed in sequence with the same weights of glass with immobilized hexokinase, PGI and G6PDH. Both reactors were stored in the 0.1 M phosphate buffer solution, pH 6.0, at 4 °C.

Sample pretreatment

Liquid samples (exactly 1 ml) were diluted to 100 ml with distilled water, from which 0.25 ml was added to a 25-ml volumetric flask, together with 12.5 ml of 0.1 M potassium phosphate buffer, pH 8.0. This solution was diluted to volume with distilled water, and placed in the aspirating tube of the peristaltic pump to fill the sample loop.

For viscous and solid samples, about 1 g of sample was weighed accurately and mixed with 100 ml of distilled water. After heating for 15 min at 60 °C, cooling and filtering through an Albet 240 filter, exactly 1 or 2 ml of this solution was mixed with 12.5 ml of the 0.1 M phosphate buffer, pH 8.0, in a 25-ml volumetric flask, and diluted to volume with distilled water. This solution was used to load the loop of the injection valve.

Flow-injection manifold

Figure 1 shows the configuration used. It consists of a single injection valve and a selecting valve which passes the injected volume sequentially through R_1 and R_2. A confluence point prior to the flow cell allows the use of a single detector. The passage of the injected sample mixture through R_1 provides a

TABLE 1

Features of the optimization and determination of glucose and fructose

Optimization	[$NADP^+$] ($\mu g\ ml^{-1}$)	[ATP] ($\mu g\ ml^{-1}$)	[Mg^{2+}] (mM)	T (°C)	V_i[a] (μl)	q[b] (ml min^{-1})	R_1 (cm)	R_2 (cm)
Range studied	0.1–1.2	0.5–4.0	0.1–2.0	20–40	30–200	0.5–2.0	5–30	5–30
Optimum value	1.0	1.0	0.5	25	100	1.0	20	25

Determination Equation[c]	Determination limit[d] (mol l^{-1})	R.s.d.[e]
$h_1 = -1.2 + 6.1 \times 10^6$[Gluc]	7×10^{-7}	1.49
$h_2 = -0.5 + 7.1 \times 10^6$[Gluc]	5×10^{-5}	1.47
$h_2 = -1.5 + 6.7 \times 10^6$[Fruc]	7×10^{-7}	0.82

[a]Volume injected. [b]Flow rate. [c]h in mV; $r = 0.9999$ and linear range $1.0 \times 10^{-6} - 1.0 \times 10^{-5}$ M in all cases. [d]10σ. [e]For 4.0×10^{-6} M ($n = 11$).

signal corresponding to glucose only, whereas the signal obtained on passage of the sample plug through R_2 results from the contribution of both analytes. The slow reaction of fructose as compared with glucose made it necessary to use the non-kinetic stopped-flow mode, the flow being halted when the sample had reached the reactor. This avoids the use of long reactors which result in increased costs and dispersion. The optimum conditions are given in Table 1.

RESULTS AND DISCUSSION

Variables were optimized by the univariate method, by using a 0.1 M potassium phosphate buffer solution containing $NADP^+$, ATP and magnesium ions as carrier, into which the samples containing $0.1–1 \times 10^{-5}$ M glucose or fructose were injected. The ranges over which the variables studied were changed and the optimum values found are shown in Table 1. An increase in the concentration of ATP or $NADP^+$ up to 1.0 mg ml^{-1} increased the analytical signal. Higher concentrations did not change the signal. A 0.5 mM magnesium solution gave the maximum signal, which decreased for lower and higher values. A pH of 9.1 gave the greatest sensitivity. Nevertheless a value of 8.0 was adopted because the immobilized enzymes were less stable at higher pH values. This pH was higher than that recommended for use with the dissolved enzymes (pH 7) [12], which is in agreement with the development of an acidic microenvironment around the immobilized enzymes caused by the generation of organic acids [6] that must be neutralized by the buffered carrier solution. Higher temperatures increased the signal but decreased reactor stability and signal reproducibility, thus a temperature of 25 °C was used.

TABLE 2

Resolution of glucose and fructose
(Equations used[a]: $H_1^M = -1.2 + 6.0 \times 10^6$[Glucose]
$H_2^M = -2.0 + 6.70 \times 10^6$[Glucose] $+ 7.10 \times 10^6$[Fructose] $- 0.3 \times 10^6$[Glucose][Fructose].)

Added ($\times 10^{-6}$ M)		Found ($\times 10^{-6}$ M)		Error (%)	
Glucose	Fructose	Glucose	Fructose	Glucose	Fructose
1.00	1.00	1.05	0.95	+5.3	−4.9
1.00	2.00	1.05	1.92	+5.0	−4.2
1.00	4.00	1.05	4.09	+5.2	+2.3
1.00	6.00	1.06	6.10	+6.1	+1.6
2.00	1.00	1.97	1.02	−1.3	+2.3
2.00	2.00	1.97	2.08	−1.4	+4.3
2.00	4.00	1.99	4.19	−0.5	+4.8
2.00	6.00	1.99	6.06	−0.2	+1.1
4.00	1.00	3.97	0.96	−0.7	−3.8
4.00	2.00	4.00	1.93	0.0	−3.4
4.00	4.00	4.03	3.91	+0.7	−2.2
4.00	6.00	4.07	5.86	+1.9	−2.3
6.00	1.00	6.00	1.07	0.0	+6.7
6.00	2.00	5.97	1.85	−0.1	−7.5
6.00	4.00	6.06	4.02	+1.0	+0.5
6.00	6.00	6.13	5.87	+2.1	−2.2

[a] H^M is the signal provided by the mixture (in mV); concentrations in M.

Increasing values of the residence time and injected volume resulted in increased signals so that a compromise between sampling rate and sensitivity had to be made (Table 1). The optimization of the stopped-flow variables yielded values of 15 for the time between injection and stopping the flow, and 30 s for the stopped-flow time. The ranges tested were 2–20 s and 10–50 s, respectively.

Determination of glucose and fructose. The calibration graphs for each analyte were linear between 1.0×10^{-6} and 1.0×10^{-5} M; the equations are given in Table 2. The r.s.d. values were $\leqslant 1.5\%$ and the sampling frequency was 30 h^{-1}.

The resolution of mixtures of glucose and fructose is feasible in ratios from 1:6 to 6:1. However, the calibration graph for fructose must be run with samples containing both analytes owing to the competition between glucose and fructose for hexokinase and then G6PDH when the sample passes through the reactor R_2 and the displacement of the equilibrium of the reactions caused by the presence of the common final reaction product. Thus the total signal obtained from the mixture is less than the sum of the signals of both substances when monitored alone. The equations used for analysis of mixtures, and the errors found are listed in Table 2.

TABLE 3

Recovery of glucose and fructose in foods

Sample (dilution)	Added ($\times 10^{-6}$ M)		Found ($\times 10^{-6}$ M)		Recovery (%)	
	Glucose	Fructose	Glucose	Fructose	Glucose	Fructose
Peach juice	-	-	2.79	2.74	-	-
(1:100 000)	2.00	2.00	4.81	4.73	100.8	99.0
	4.00	4.00	6.77	6.76	99.6	100.5
Pineapple juice	-	-	2.96	3.03	-	-
(1:100 000)	2.00	2.00	4.93	5.02	98.4	99.3
	4.00	4.00	6.91	7.02	98.9	99.9
Orange juice	-	-	3.19	2.89	-	-
(1:100 000)	2.00	2.00	5.19	4.92	100.0	101.6
	4.00	4.00	7.14	7.00	98.8	102.7
Banana	-	-	4.50	0.75	-	-
yoghourt	2.00	2.00	6.44	2.80	96.7	102.2
(1:1245)	4.00	4.00	8.40	4.77	97.6	100.4
Lemon	-	-	6.81	2.12	-	-
yoghourt	2.00	2.00	8.83	4.21	100.8	104.7
(1:1250)	4.00	4.00	10.91	6.19	102.4	101.9
Vanilla	-	-	7.04	0.71	-	-
ice cream	2.00	2.00	9.04	2.79	100.0	104.2
(1:4807)	4.00	4.00	10.99	4.74	98.8	100.9
Vanilla cream	-	-	5.54	0.81	-	-
caramel	2.00	2.00	7.67	2.83	106.5	101.2
(1:2509)	4.00	4.00	9.63	4.85	102.0	101.0

The determination of binary mixtures of these monosaccharides was examined on three different types of food: liquid (fruit juice), viscous (yoghourt) and solid (dessert powder). The recoveries found (between 96.7 and 106.5%) show the suitability of the proposed method (Table 3).

Conclusions

The efficiency of the association of columns of enzymes immobilized on controlled-pore glass and flow-injection systems is proved for the determination of mixtures of organic compounds. Nevertheless, it is necessary to mention the problems arising from the competition of both analytes for the same enzyme and the displacement of the reaction caused by the formation of the same product; these are overcome by calibrating with mixtures of both substances.

The low determination limit achieved makes it possible to dilute the samples considerably (1:2500) and hence viscous samples can be analyzed. The system has been used for at least 1500 determinations without appreciable loss of enzyme activity.

This work was supported by the C.I.C.Y.T.

REFERENCES

1 G. Marko-Varga, R. Appelquist and L. Gorton, Anal. Chim. Acta, 179 (1986) 371.
2 T. Yao, M. Sato and T. Wasa, Nippon Kagaku Kaishi, 2 (1985) 189.
3 T. Yao and T. Wasa, Anal. Chim. Acta, 175 (1985) 301.
4 F. Winquist and I. Lundström, Anal. Chem., 58 (1986) 145.
5 M. Masoom and A. Townshend, Anal. Chim. Acta, 174 (1985) 293.
6 I. Karube, J. Hara, H. Matsuoka and S. Suzuki, Anal. Chim. Acta, 139 (1982) 127.
7 R. Gnanasekaran and H.A. Mottola, Anal. Chem., 57 (1985) 1005.
8 P.J. Worsfold and A. Nabi, Anal. Chim. Acta, 179 (1986) 307.
9 M. Masoom and A. Townshend, Anal. Chim. Acta, 179 (1986) 399; 166 (1984) 111.
10 F. Morishita, Y. Hara and T. Kojima, Bunseki Kagaku, 33 (1984) 642.
11 Y. Toshio, K. Yoshiaki and M. Sochiro, Anal. Chim. Acta, 138 (1982) 81.
12 Methods of Enzymatic Analysis of Foods, Boehringer, Mannheim, 1985.
13 A.L. Lehninger, Bioquímica. Bases moleculares de la estructura y la función celular, 2nd edn., Omega, Barcelona, 1978.

Analytica Chimica Acta, 202 (1987) 207–213
Elsevier Science Publishers B.V., Amsterdam — Printed in The Netherlands

SPECTROFLUOROMETRIC DETERMINATION OF ZINC WITH 1,5-BIS(2,3-DIHYDROXYPHENYLMETHYLENE) THIOCARBOHYDRAZONE

A.M. AFONSO, M. GONZÁLEZ-DÁVILA, J.J. SANTANA and F. GARCÍA-MONTELONGO*

Department of Analytical Chemistry, University of La Laguna, La Laguna, Tenerife (Spain)

(Received 20th October 1986)

SUMMARY

1,5-Bis(2,3-dihydroxyphenylmethylene)thiocarbohydrazone was synthesized; its ionization constants are reported. A procedure is described for the spectrofluorimetric determination of 5–540 ng ml^{-1} zinc in 60/40 (v/v) ethanol/water medium, acetate-buffered to apparent pH 6.5 ($\lambda_{ex}=400$ nm, $\lambda_{em}=508$ nm). Interferences were evaluated and the procedure was applied with good results to the determination of zinc in potable waters (0.3–3 μg ml^{-1}) and lubricating oils.

Although thiocarbohydrazones have been tested as antimicrobial and antitumour agents and used in the photographic industry and as polymer stabilizers [1,2], they are not widely used in analytical chemistry. 2,2′-Bis(di-2-pyridylmethylene)thiocarbohydrazone ($\lambda_{max}=415$ nm, pH 6.2–9.8) [3], 1,5-bis(*p*-sulfophenyl)thiocarbohydrazone (500 nm, pH 3.0), 1,5-bis(salicylaldehyde)thiocarbohydrazone (390 nm, pH 5.5) [5] and some related compounds [6–8] have been used in the spectrophotometric determination of zinc(II). The thiocarbohydrazones have not so far been used for the fluorimetric determination of metal ions.

As part of an investigation on the uses of symmetric thiocarbohydrazones derived from *o*-hydroxybenzaldehyde as fluorimetric reagents for metal ions, the characteristics and analytical properties of 1,5-bis(2,3-dihydroxyphenylmethylene)thiocarbohydrazone (DPMTH) are described below, and a rapid and simple method for the spectrofluorimetric determination of zinc based on its fluorescent complex with DPMTH is reported. The procedure is applied to the determination of zinc in potable water and lubricating oils.

0003-2670/87/$03.50

EXPERIMENTAL

Apparatus

The Perkin-Elmer MPF-44A recording spectrofluorimeter used was equipped with a 150-W Osram XBO xenon arc, a DSCU-1 corrected spectra unit (0.5% Rhodamine-B in ethylene glycol as reference), a UDR-3 digital read-out, a Selecta Frigitherm ultrathermostat, and 1-cm quartz cells. The emission measuring system was calibrated daily by using the Perkin-Elmer set of fluorescent polymer blocks. A Radiometer PHM84 digital pH meter with glass and calomel electrodes was also used; pH values in aqueous 60% (v/v) ethanol media have not been corrected and are therefore given as pH*.

Reagents

The reagent was prepared as a 1.0×10^{-2} M solution in absolute ethanol. A 0.1 M zinc(II) perchlorate stock solution was prepared from zinc(II) oxide and perchloric acid and standardized complexiметrically. Working solutions were prepared daily by suitable dilution.

The ionic strength was adjusted by adding suitable amounts of 2.5 M sodium perchlorate. A 2 M acetic acid/sodium acetate buffer solution with pH 5.6 was used as indicated. All reagents and solvents were of analytical-reagent grade.

Synthesis of DPMTH

The reagent was synthesized analogously to an earlier reagent [7] by refluxing a 2:1 molar mixture of 2,3-hydroxybenzaldehyde and thiocarbohydrazide in a 1:1 (v/v) ethanol/water medium, at 70–80 °C for 3 h. After cooling, the crude yellow crystals were filtered, washed with water and diethyl ether and recrystallized from ethanol/water mixtures. The crystals obtained (yield 76%) melted at 189–192 °C. Low-resolution mass spectrometry showed a parent molecular ion (M^+) at 346 *m/z*; high-resolution mass spectrometry showed two main peaks at 151.02 *m/z* and 196.04 *m/z* with $C_7H_7O_2N_2$ and $C_8H_7O_2N_2S$, respectively, as the most probable compositions.

Determination of zinc

To up to 10 ml of sample solution, containing 0.13–13.5 μg of zinc, in a 25-ml volumetric flask, add 2.5 ml of the acetic/acetate pH 5.6 buffer solution, 1 ml of 2.5 M sodium perchlorate solution, 5 ml of ethanolic 5.0×10^{-5} M or 2.3×10^{-4} M DPMTH solution (according to the expected zinc concentration, see later), and 7.5 ml of absolute ethanol, and dilute to volume with deionized water. Measure the fluorescence at 508 nm using excitation at 400 nm, against a reagent blank. The amount of zinc present in the sample is evaluated from a calibration graph prepared under the same experimental conditions. This method is directly applicable to potable water.

Determination of zinc in lubricating oils

Weigh accurately 0.5–1.5 g of the lubricating oil, add 1 ml of concentrated sulphuric acid and evaporate to dryness. Then ignite for 2 h at 800 °C in an electric furnace. Redissolve with water to which several drops of concentrated nitric acid have been added, heating if necessary, and dilute to volume in a 100-ml volumetric flask with deionized water. Analyse suitable aliquots as described above.

RESULTS AND DISCUSSION

Characteristic of the reagent

The infrared spectrum of the reagent (KBr disk) was obtained; the bands were assigned to the stretching vibrations of phenolic hydroxyl (3400 cm^{-1}), =NH (3200–3300 cm^{-1}), -C=C- benzylic (1620 cm^{-1}), -NH-C=S (1480–1542 cm^{-1}) and -C=N- (1250 cm^{-1}). The ^{1}H-NMR spectrum (DMSO-d_6, TMS) at 90 MHz was as follows: δ = 6.68, 6.76, 6.80 (6H, d, s, d, H_4, H_5, H_6), 7.30, 9.00 (4H, s, s, OH), 8.48 (2H, wide d, $W_{1/2}$ = 50 Hz, =CH-), and 11.5 (2H, m, S=C-NH-).

The reagent is very soluble in ethanol, methanol, concentrated alkalis and mineral acids, slightly soluble in isoamyl alcohol, and insoluble in chloroform, water and diethyl ether. Aqueous alcoholic solutions of the reagent hydrolyse slowly when pH* is <1.5 or >8.5.

The reagent should behave as a pentabasic substance with deprotonation of the thiol group [R′-C(=S)-NH-NH-R⇌R′-C(-SH)=N-NH-R] and the *m*- and *o*-hydroxy groups. However, because the molecule is symmetric and the distance between the four hydroxy groups is relatively long, the values of their ionization constants would be expected to be close together and would not be distinguishable by spectrophotometric methods. The ionizations constants were calculated from the variation of the absorbance at different wavelengths with pH by application of the method of Hnilčková and Sommer [9] when the molar absorptivity of at least one species in the equilibrium could be evaluated from the absorbance/[H^+] plots; for overlapping equilibria, the SPECPK program [10] was used. The average values found were 6.97 ± 0.59 (3-OH), 8.22 ± 0.29 (-SH) and 10.76 ± 0.18 (2-OH).

The reactions of DPMTH with 50 metal ions at pH* 3.3, 5.0 and 7.5 were investigated. Only Zn(II), Ga(III), In(III), Cd(II) and La(III) gave fluorescence under ultraviolet radiation. The spectrofluorimetric characteristics of these complexes are shown in Table 1. The reagent showed no fluorescence under the experimental conditions used.

Spectrofluorimetric study of the zinc/DPMTH system

The reagent and zinc(II) form a yellow-green complex with strong yellow fluorescence under ultraviolet irradiation. The corrected excitation and emis-

TABLE 1

Spectrofluorimetric characteristics of DPMTH complexes in solution

Metal ion	λ_{ex} (nm)[a]	λ_{em} (nm)[a]	pH*
Zn(II)	411	487	7.5
Cd(II)	413	485	5.5
Ga(III)	412	488	5.5
In(III)	415	500	5.5
La(III)	382	441	3.3

[a]Corrected values.

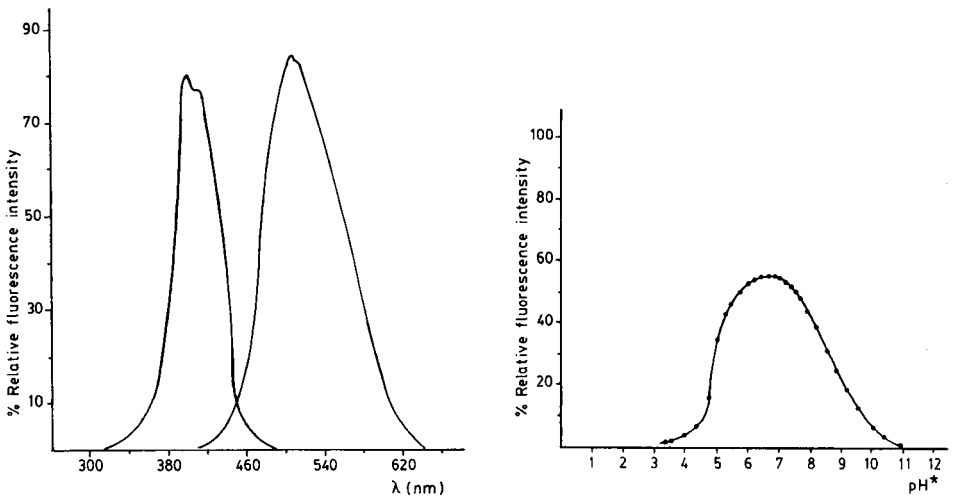

Fig. 1. Corrected excitation and emission spectra of the Zn(II) complex. pH*=6.5 (acetate), 5.0×10^{-6} M zinc, 1.0×10^{-4} M DPMTH; sensitivity 0.1, slits 6 nm.

Fig. 2. Influence of pH* on the fluorescence intensity of the Zn(II) complex. $\lambda_{ex}=411$ nm, $\lambda_{em}=508$ nm; other conditions as in Fig. 1.

sion spectra of the complex is shown in Fig. 1; the highest fluorescence emission intensity is at pH* 6.1–7.3 (Fig. 2). An aqueous 2 M acetate buffer solution of pH 5.6 gave pH* 6.5 in the aqueous 60% (v/v) ethanol medium and was used in all subsequent work.

All fluorescence measurements were made at $25\pm0.1\,^{\circ}C$, at which the fluorescence emission remained stable for at least 1 h. The fluorescence intensity decreased linearly (ca. 1.17%/°C) as the temperature increased between 15 and 45 °C.

The percentage of ethanol in the medium had a critical effect on the fluorescence intensity. A change from a mainly aqueous solution to 80% ethanol solution produced a bathochromic shift in the excitation maximum but not in

the emission maximum. This suggests that substantial changes in polarity of the complex must take place on excitation and that the solvation energy will differ on changing the solvent [11]. These effects, together with the increasing solubility of the complex in ethanolic media, are probably responsible for the enhanced fluorescence emission in ethanolic solutions. A 60/40 (v/v) ethanol/water medium is recommended because higher concentrations of ethanol limit the amounts of aqueous solutions of other reagents that can be added.

Several sodium and potassium salts were tested at different concentrations in order to study the influence of ionic strength on the fluorescence emission. Results showed that neither the ionic strength nor the salt used had any significant effect on the fluorescence emission. In all subsequent work, solutions were adjusted to ionic strength 0.3 M with sodium perchlorate. Variation in the order of addition of sample and reagents had little influence.

The stoichiometry of the complex was studied under the established experimental conditions by the continuous-variations and mole-ratio methods. A metal-to-ligand ratio of 1:1 was found, which suggests that DPMTH acts as a tetradentate ligand, without participation of the sulphur atom in chelation. The effect of reagent concentration on the fluorescence intensity of solutions containing 0.3 μg ml^{-1} zinc(II) was studied under conditions similar to those recommended under Experimental. The intensity increased as the reagent concentration was increased up to 1.1×10^{-5} M, and remained stable between 1.1×10^{-5} and 1.1×10^{-4} M. At higher reagent concentrations, the fluorescence decreased markedly, mainly because of fluorescence inversion phenomena.

Spectrofluorimetric determination of zinc

Under the conditions outlined in the recommended procedure, there was a linear relationship between emitted fluorescence intensity and Zn(II) concentration in the ranges 5–120 and 120–540 ng ml^{-1}, for 5 ml of 5.0×10^{-5} or 2.3×10^{-4} M solutions of the reagent, respectively. The detection limit as defined by IUPAC [12] was 5.2 ng ml^{-1}. When the procedure was applied to two series of eleven samples containing 52 and 240 ng ml^{-1}, relative standard deviations of 0.73 and 0.79 (95% confidence level), respectively, were obtained.

The effects of several ions on the determination of 50 ng ml^{-1} Zn(II) were studied by first applying the recommended method to solutions containing a 20 000-fold (w/w) ratio of interferent to zinc and, if interference occurred, reducing this ratio until interference ceased. Higher ratios were not tested. The criterion for interference was a variation in the concentration found for zinc of more than $\pm4\%$ from the value taken. Results are shown in Table 2. The interferences in the proposed method come mainly from ions such as Ga(III), In(III), La(III) and Cd(II), which also form fluorescent complexes with the reagent (Table 1), from ions forming coloured complexes with the reagent,

TABLE 2

Interference levels of diverse ions on the spectrofluorimetric determination of 50 ng ml^{-1} zinc(II) with DPMTH

Tolerance ratio (w/w)	Ion added
20 000	Chloride, Mg(II)
10 000	Ca(II)
4000	SO_4^{2-}
1000	NO_3^-, CO_3^{2-}
100	Se(IV), Tl(I), iodide, SCN^-, SO_3^{2-}, $B_4O_7^{2-}$, Trien
50	Sr(II)
25	HPO_4^{2-}, fluoride
20	K(I), ascorbate
10	La(III), Cd(II), bromide, tartrate, citrate
2	Ba(II), Sn(II), As(III), Zr(IV), W(VI), $S_2O_3^{2-}$
1	Ni(II), Pb(II), Cu(II), Cr(III), Au(III), Te(IV), oxalate
0.5	Fe(II), Mn(II), Ag(I), Ti(IV), UO_2^{2+}, EGTA
Strong interference	Pd(II), Co(II), Be(II), Hg(II), Fe(III), Ga(III), In(III), Al(III), V(IV), DCTA, EDTA

TABLE 3

Spectrofluorimetric determination of zinc in potable waters

Sample	1	2	3	4	5
Zn found[a] (ng ml^{-1})					
DPMTH	324	341	3537	145	220
A.a.s.	325	340	3535	143	222

[a]Mean of three determinations.

TABLE 4

Spectrofluorimetric determination of zinc in lubricating oils

Sample	Zinc content (%)	
	Present (%)	Found[a]
1 (Ca 0.18%, Mg 1.2×10^{-3}%)	0.0014	0.015
2 (Ca 0.14%, Mg 9.2×10^{-4}%)	0.011	0.011
3 (Ca 0.032%, Mg 9.5×10^{-4}%)	6.5×10^{-3}	6.7×10^{-3}
4 (Ca 0.064%, Mg 7.8×10^{-4}%)	0.010	0.011

[a]Mean of three determinations.

such as Ni(II), Co(II), Fe(II) and Mn(II), and from species forming complexes with Zn(II), such as EDTA, EGTA and DCTA.

Although DPMTH is less sensitive than benzimidazole-2-aldehyde 2-quinolylhydrazone [13], it is impossible to compare the reagents from a practical standpoint because neither an interference study nor applications were reported for the earlier reagent.

Applications

The developed method was applied to the determination of zinc in samples of potable water from the distribution systems in several cities of the Canary Islands, collected and preserved as recommended [14] and to zinc-containing lubricating oils. The results (Tables 3 and 4) show satisfactory agreement with the results obtained by atomic absorption spectrometry (a.a.s.).

The authors acknowledge financial support of this work by the C.A.I.C.y.T., grant No. 4122/79.

REFERENCES

1 F. Kurzer and M. Wilkinson, Chem. Rev., 70 (1970) 111.
2 S. Rhee, J. Pharm. Soc. Korea, 16 (1972) 162.
3 J.R. Bonilla Abascal, A. García de Torres and J.M. Cano Pavón, Microchem. J., 28 (1983) 132.
4 A.T. Pilipenko and E.N. Arendaryuk, Ukr. Khim. Zh. (Russ. Ed.), 45 (1979) 562 (Chem. Abstr., 91 (1979) 116709w.).
5 M.T. Montaña and J.L. Gómez Ariza, An. Quim., 80 (1984) 129.
6 D. Rosales and J.L. Gómez Ariza, Anal. Chim. Acta, 169 (1985) 367.
7 F.J. Barragán de la Rosa, J.L. Gómez Ariza and F. Pino, Talanta, 30 (1983) 555.
8 D. Rosales, G. González and J.L. Gómez Ariza, Talanta, 30 (1985) 467.
9 M. Hnilčková and L. Sommer, Talanta, 13 (1966) 667.
10 A. Albert and E.P. Serjeant, The Determination of Ionization Constants, 2nd edn., Chapman & Hall, London, 1971.
11 S.G. Schulman, Fluorescence and Phosphorescence Spectroscopy: Physicochemical Principles and Practice, Pergamon, Oxford, 1977.
12 H.M.H.N. Irving, M. Freiser and T.S. West (Eds.), IUPAC Compendium of Analytical Nomenclature: Definitive Rules, 1977, Pergamon, Oxford, 1978.
13 D.E. Ryan, F. Snape and M. Winpe, Anal. Chim. Acta, 58 (1972) 101.
14 American Public Health Association, American Water Works Association and Water Pollution Control Federation, Standard Methods for the Examination of Water and Wastewater, 14th edn., American Public Health Association, Washington, DC, 1976, p. 38.

Analytica Chimica Acta, 202 (1987) 215–221
Elsevier Science Publishers B.V., Amsterdam — Printed in The Netherlands

SURFACTANT CHARACTERIZATION AT AN AIR/WATER INTERFACE BY DIRECT REFLECTION ELLIPSOMETRY

ULRICH J. KRULL*, ANNIE HUM and ELAINE T. VANDENBERG

Chemical Sensors Group, Department of Chemistry, Erindale College, University of Toronto, Mississauga Road, Mississauga, Ontario L5L 1C6 (Canada)

(Received 28th January 1987)

SUMMARY

Lipid monolayers of phosphatidyl choline/cholesterol at an air/water interface are evaluated for thickness, refractive index and average molecular area by direct reflection ellipsometry. Results indicate that changes in chemical composition of monolayers can be readily detected, and that average molecular area can be reliably established. The latter results are contrasted with values obtained by monolayer-compression methods and indicate that the techniques provide data of similar accuracy and precision.

Ellipsometry is a non-destructive technique for the study of films which are usually located at the surface of a solid substrate [1]. The technique has been applied extensively in the semiconductor field and continues to be accepted in the study of organic and biological films of monolayer dimensions. Reflectance ellipsometry has been widely applied to biological and organic matrices [2–4]. It is based on the fact that monochromatic or quasi-monochromatic optical radiation which is elliptically polarized by passage through a polarizer-compensator optical train may become linearly polarized when reflected from a sample. The degree of ellipticity can be determined by means of another polarizing crystal known as an analyzer. Correlation of the angular relationships between the optical devices results in the extinction of light leaving the analyzer, and provides sufficient information to evaluate the ratio of the complex Fresnel coefficients of reflection (p_s) given [1] as:

$$p_s = \tan \psi \exp (j\Delta)$$

where $\tan \psi = |r_p|/|r_s|$, $\Delta = \delta r_p - \delta r_s$, and $j = (-1)^{1/2}$. The terms r_p and r_s represent the Fresnel coefficients of reflection for p- and s-polarized light, and δr_p and δr_s are the absolute phases of reflection of p- and s-polarized light. The Drude equations [1] are then used to convert Δ and ψ into data for the characteristic refractive index (η) and thickness (d) of the reflective film.

The Drude equations are solved by a convergent iterative calculation pro-

0003-2670/87/$03.50

cess, often using the McCrackin program [5]. What may be gleaned from these equations is that d and η for the sample may not be obtained very accurately if both are unknown. Usually the approximate value of η is used, and the thickness measurements are considered exact if relative thicknesses are compared. The Drude equations assume that: (a) the lateral surface area of the film is many times its cross-sectional thickness, (b) multiple reflecting waves combine coherently, (c) the film does not amplify light, (d) the film has a homogeneous d and η, and (e) there are plane-parallel, discrete boundaries between ambience, film and substrate. The fact that some of these assumptions are invalid limits the reliability of the absolute values of thickness and refractive index which are obtained. Ellipsometry works best when there is a large difference in η between the layers, assessed by the Fresnel coefficients. Because biological material has a refractive index of about 1.5, metal is generally used as a substrate ($\eta > 2$), and measurements taken in air ($\eta = 1.0003$) rather than water ($\eta = 1.3$) give the best results. Optimally, ellipsometry can detect changes less than 1Å in thickness, and 0.002 in η [6,7].

Limited work with direct reflection ellipsometry has been reported in the literature for surface analysis at a classical lipid monolayer located at an air/water interface [8,9]. Perhaps one of the best examples of the potential of the technique for such studies was demonstrated by comparison of ellipsometric data with radiotracer studies for a number of proteins [10]. Surface concentrations and film thicknesses of the proteins as they adsorbed from bulk solution to the air/water interface of a miniature Langmuir–Blodgett trough agreed extremely well with correlating techniques. Furthermore, continuous observations indicated the capability of ellipsometry directly to observe dynamic average alterations of protein conformation in real time.

This work demonstrates the application of direct-reflection ellipsometry to monolayers of surfactant at an air/water interface. The results indicate that structural and chemical changes within the monolayers can be readily observed as relative alterations of film thickness and refractive index. This provides a direct method of interfacial study suitable for a wide variety of industrially and biologically important surfactants, and can indicate how they chemically change with time and temperature in vitro.

EXPERIMENTAL

Reagents and apparatus

Lyophilized egg phosphatidyl choline (PC) (Avanti Biochemicals, Birmingham, AL) and cholesterol (C) (Sigma Chemical Company) were used for the preparation of monolayers. All solvents were of reagent grade. Water was obtained from a Millipore Milli-Q cartridge filtration system and was degassed under vacuum before use.

A Lauda Model 1974 thin-film balance (Brinkmann, Toronto) was used to

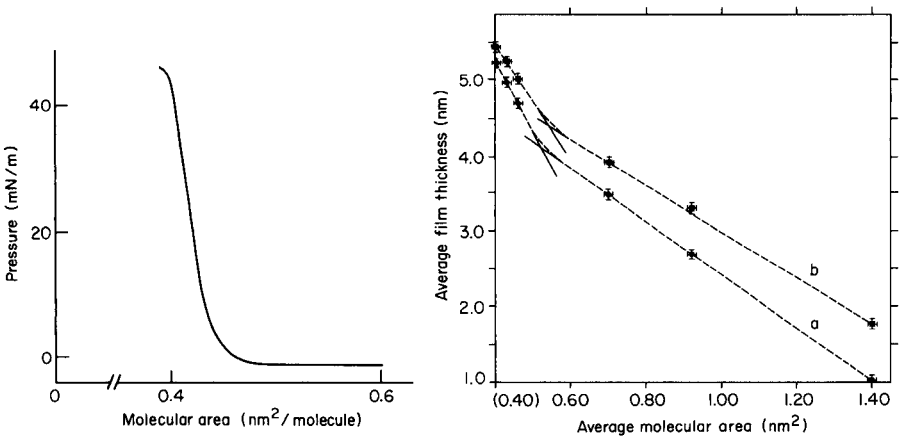

Fig. 1. Pressure/area isotherm for 1:1 weight ratio PC:C monolayer over a 0.1 M KCl solution at 22°C.

Fig. 2. Graphical determination of the average molecular area of lipids within a monolayer as surface pressure is increased: (a) unoxidized PC/C film of weight ratio 2/1; (b) slightly oxidized (ca. 5%) PC/C film of initial weight ratio 2/1.

construct pressure/area curves of lipid monolayers for correlation with ellipsometric data. Direct-reflection ellipsometry was accomplished with a Thin Film Ellipsometer Model 43702-200E (Rudolph Research, Flanders, NJ) which had a high-pressure mercury lamp as an optical source, a horizontal sample platform, a 5-mm^2 diameter exit aperture, and a photoelectric detector to establish an optical minimum when the compensator was held at +45.00° and the polarizer/analyzer crystal angles were appropriately matched. A version of the McCrackin computational program (Rudolph) suitable for a Hewlett-Packard HP-85 microcomputer was used for calculation of d and η values.

Procedures

The lipid solutions were prepared in 5 ml of hexane as weight-ratio mixtures of phosphatidyl choline and cholesterol, covering a range from 1 mg/1 mg to 3 mg/1 mg, respectively. Solutions were stored under a nitrogen atmosphere at −20°C in darkness to ensure that minimum alterations in lipid chemistry were caused by oxidation. Uncontrolled oxidation was purposefully achieved by exposure of hexane solutions at room temperature to the ambient atmosphere. Immediately before use, lipid solutions were sonicated in a bath-type sonicator for ca. 1 min to ensure homogeneous dispersion.

Lipid solutions were physically characterized by monolayer-compression experiments. Pressure/area isotherms were developed for monolayers supported on a subphase of 0.1 M potassium chloride at 25 ± 1°C (see Fig. 1). Approximately 70 μl of lipid solution was slowly transferred to the fully expanded (ca.

750 cm^2) aqueous surface over a period of 2 min. A period of at least 15 min was allowed for hexane evaporation and surface equilibration before the monolayer was compressed at a speed of 7.5 $cm^2\ min^{-1}$ until the collapse pressure was attained.

Various polyethylene trays with areas of 25.2 to 73.9 cm^2 were used as miniature troughs for preparation of monolayers for ellipsometric investigation. The trays were filled with 0.1 M potassium chloride, and the aqueous surface area was established. Various quantities of lipid solution were then added slowly to the subphase surface to prepare monolayers at different surface pressures. The known quantity of lipid solution added to the fixed aqueous surface area provided sufficient information for correlation of the physical characteristics of the tray-supported membranes with the monolayers prepared in the Lauda trough. At least four sets of polarizer and analyzer values were recorded for each experiment. The ellipsometer was partly enclosed to guard against extraneous air currents and dust.

RESULTS AND DISCUSSION

Ellipsometric characterization of the phospholipid monolayers, both in expanded and compressed forms (described later), was readily accomplished because an optical null was obvious. The precision of the experimental results was assisted by the reduction of surface vibration induced by lipid at higher surface pressures. The film thickness and refractive index values could be obtained with a maximum reproducibility of $\pm 1\%$ for repetitive measurements on a single monolayer, while comparison of different monolayers of identical chemistry provided a maximum reproducibility of $\pm 2\%$. Measurements of film thickness demonstrated that the monolayer remained constant for periods greater than 1 h. Refractive index is generally considered as a "bulk" property, and therefore may be undefined for organic films which are significantly thinner than the wavelength of the light with which they are sampled. The term refractive index is retained in this work for consistency with the parameters chosen for mathematical computations, but the limitations of physical interpretation of this term should be recognized.

The actual magnitudes of the values of film thickness and refractive index were suitable for relative comparisons at angles of incident probe radiation between 70° and 50°. For most organic and biological films, the best absolute values are obtained when the angle of incidence is just below the polarizing angle ϕ, where $\tan \phi = \eta_1/\eta_0$, with η_1 representing the refractive index of the film, and η_0 the refractive index of an underlying substrate. Results for determinations of monolayer thickness obtained by using different angles of incidence are summarized in Table 1. The results demonstrate that the optimal angle for obtaining realistic absolute thickness values is near 55.5°, and that the results are very sensitive to minor angular variations from this ideal ori-

TABLE 1

Angular dependence of ellipsometric results for molecular areas of 0.62 and 0.40[a] nm^2

Angle (degrees)	Film thickness (nm)	
	0.62	0.40
55.0[b]	8.3 ±0.2	9.5 ±0.2
55.5[b]	5.1 ±0.1	6.1 ±0.1
55.5[c]	3.4 ±0.1	4.2 ±0.1
60.0[c]	0.47±0.02	0.60±0.02

[a]Calculated area based on actual number of lipid molecules; of limited absolute value because film collapse previously initiated. [b,c]Phosphatidyl choline/cholesterol weight ratio: [b]2.6/1, [c]3.8/1.

entation. For most metal substrates, the optimal angle of incidence is between 70° and 80°, and is less sensitive to minor angular variations.

The results in Table 1 further illustrate the ability of ellipsometry to indicate monolayer structure and chemical composition. At a low surface concentration of lipids [i.e., molecular area >0.5 nm^2 per molecule (Fig. 1)], the molecules are in a mobile, randomly-interwoven configuration. As more lipid is added, the average area occupied by each lipid is decreased, and the molecules become aligned on a two-dimensional surface. With further addition of lipid, the average area available for each lipid decreases so that the acyl chains of each molecule lift from the aqueous surface and become mutually parallel in an orientation perpendicular to the plane of the subphase. This process entails alteration from a two-dimensional to a three-dimensional structure. Finally, at high surface concentrations of lipid [molecular area of about 0.4 nm^2 per molecule (Fig. 1)], the pressure causes monolayer collapse and localized multilayer structures are formed. Thus, the thickness of the lipid film increases gradually as the surface concentration of lipid is increased to form a fully compressed monolayer, and more dramatically after the point of monolayer collapse. Ellipsometry permits direct observation of such thickness variations and therefore can provide information about molecular conformation. An example of such an observation is provided in Table 1 by contrasting film thicknesses between monolayers compressed to provide two different average molecular areas.

The ellipsometric experiment samples a surface area of the order of 5 mm^2, and therefore provides results which are effectively representative of average molecular properties in the sampled region (numerous regions were sampled to ascertain monolayer homogeneity and to assess the precision of results). The relatively large sampling area precludes observation of microscopic domain structures, and therefore improves the reproducibility of results. Table 1 provides two sets of data obtained at an angle of incidence of 55.5° for two

chemically different membranes. The differences in film thickness for the two samples are obvious, and reflect the average properties of the lipid monolayers. It may be noted that a large variation in thickness between the two lipid compositions was not expected from membrane structural criteria [11]. The large differences in thickness probably originate from alterations of the refractive indices of the films caused by their different chemical contents or molecular structure arising from compression characteristics.

The ability to determine average monolayer properties provides a realistic basis for contrast between results from ellipsometric investigations and monolayer-compression experiments. The average molecular area at the monolayer-collapse pressure can be indicative of the extent of molecular interactions of lipids within a film [11]. Such interactions are dominated by polar species which are responsible for electrostatic and hydrogen-bonding processes within membranes. Figure 2 represents the ellipsometrically determined average molecular area at the point of monolayer collapse (inflection point) for membranes produced from lipids with differing contents of polar species. The linear portions of the graphs in Fig. 2 are representative of smooth and linear compression curves, as established by pressure/area experiments. The relative changes in film thickness for each independent compression experiment may be predominantly an indication of molecular alignment during monolayer compaction. The difference in film thickness between the two experiments was probably caused by changes in refractive index arising from chemical oxidation.

The surface pressure of films which were deposited in total on the polyethylene trays (fixed area) were determined by a Wilhelmy plate transducer. Quantities of lipid solution equivalent to those added to the surface of the polyethylene trays were placed onto the surface of the Lauda trough. These lipid films in the gaseous state were then compressed to surface areas equivalent to those on the polyethylene trays. The surface pressures observed for films on the trays indicated that significant deviations from the gaseous-deposited and subsequently compressed monolayers occurred at pressures greater than 30 mN m^{-1}, indicating that residual solvent and structural irregularities may have been present. Loss of lipid to the subphase was insignificant as determined by capillary gas chromatography [12] after sample preconcentration. Surface pressures of films deposited from the gaseous and liquid states were identical at surface pressures within 2 mN m^{-1} of the collapse point. Figure 2 represents data collected at surface pressures below 30 mN m^{-1} and substantially past the collapse point. Experimental results for ellipsometric work are contrasted to results from the classical monolayer compression method in Table 2 to demonstrate the applicability of ellipsometry to the determination of monolayer phenomena such as membrane collapse.

The average monolayer properties sampled in the ellipsometric experiment provide useful relative data for surfactant comparison, even though the assumptions made for use of the Drude equations may not be explicitly achieved.

TABLE 2

Phospholipid molecular areas from ellipsometric experiments

Sample	Collapse area[a] (nm^2)	Ellipsometric results[b]	
		Collapse area (nm^2)	Film thickness (nm)
Unoxidized PC/C	0.52 ± 0.01	0.52 ± 0.01	4.1 ± 0.1
Slightly oxidized PC/C	0.55 ± 0.01	0.54 ± 0.01	4.4 ± 0.1
Oxidized PC/C	0.60 ± 0.01	0.61 ± 0.01	5.1 ± 0.1

[a]PC/C weight ratio of 2.5/1, oxidation by exposure of solution to air at room temperature.
[b]Calculated from data obtained at $\theta = 55.5°$ for a PC/C weight ratio of 2.6/1.

Calibration of the ellipsometric experiments was achieved by use of the monolayer-compression technique, providing for the measurement of reliable absolute average molecular areas. The inherent sensitivity of the ellipsometric experiment to both instrumental and chemical variations implies that it is an ideal non-perturbing technique for studying relative intra- and inter-molecular interactions of surfactants at an air/water interface.

We are indebted to the Natural Sciences and Engineering Research Council of Canada for support of this work, and for provision of a summer research fellowship to A.H.

REFERENCES

1 R.M.A. Azzam and N.M. Bashara, Ellipsometry and Polarized Light, North Holland, New York, 1977.
2 A. Rothen and C. Mathot, Immunochemistry, 6 (1969) 241.
3 H. Elwing, C. Dahlgren, R. Harrison and I. Lundström, J. Immunol. Methods, 71 (1984) 185.
4 M. Horisberger, Biochim. Biophys. Acta, 632 (1980) 298.
5 F.L. McCrackin, N.B.S. Technical Note 479, N.B.S., Washington, DC, (1969) 20234.
6 M. Horisberger, Physiol. Chem. Phys., 11 (1979) 527.
7 M. Stenberg, H. Arwin and A. Nilsson, J. Colloid Interface Sci., 72 (1979) 255.
8 D. Den Engelsen and B. DeKoning, J. Chem. Soc. Faraday Trans. 1, 70 (1974) 1603.
9 D. Ducharme, C. Salesse and R.M. Leblanc, Thin Solid Films, 132 (1985) 83.
10 J.A. De Feijter, J. Bejamins and F.A. Veer, Biopolymers, 17 (1978) 1759.
11 U.J. Krull, M. Thompson, E.T. Vandenberg and H.E. Wong, Anal. Chim. Acta, 174 (1985) 83.
12 U.J. Krull, M. Thompson and A. Arya, Talanta, 31 (1984) 489.

Analytica Chimica Acta, 202 (1987) 223–230
Elsevier Science Publishers B.V., Amsterdam — Printed in The Netherlands

PRECONCENTRATION BY COPRECIPITATION OF SUBMICROGRAM AMOUNTS OF COPPER AND MANGANESE WITH 8-QUINOLINOL AND DIRECT ELECTROTHERMAL ATOMIC ABSORPTION SPECTROMETRY OF THE PRECIPITATES

KUNIHIKO AKATSUKA and IKUO ATSUYA*
Kitami Institute of Technology, 165 Koen-cho, 090 Kitami (Japan)
(Received 24th April 1987)

SUMMARY

Copper and manganese in water samples at levels at or below the $\mu g\ kg^{-1}$ level are determined by graphite-furnace atomic absorption spectrometry, after coprecipitation with 8-quinolinol followed by direct measurements on precipitate in a specially-designed furnace. The two metal ions are coprecipitated quantitatively in the pH range 7.0–8.5 with magnesium ions as carrier. The detection limits for copper and manganese are 12 and 14 $ng\ kg^{-1}$, respectively, for 300-ml portions of water samples analyzed.

Graphite-furnace atomic absorption spectrometry (AAS) has been used extensively for trace element determinations. However, when metal concentrations are below $\mu g\ kg^{-1}$ levels, the direct analysis of water samples by this technique is limited to a few elements. The detection limits are seriously degraded by the presence of matrix constituents. Thus, preconcentration is usually required. One of the currently used preconcentration techniques [1] is the extraction of metal ions with chelating reagents, and another is the use of chelating resins. In these techniques, the final analyte specimen is normally presented in the form of liquids.

Precipitation or coprecipitation of trace elements with an inselective organic reagent and subsequent collection on a filter disk results in highly enriched, uniform precipitates. The use of 8-quinolinol (8-Q) [2–8] in combination with thionalide and tannic acid is accepted to be very effective for the simultaneous recovery of a number of elements as precipitates. This method, developed by Mitchell and Scott [2–4], provides concentration factors of more than 3 orders of magnitude when the precipitates are submitted directly to atomic emission spectrometry without dissolving them.

The direct analysis of a variety of powdered solid samples by graphite-furnace (AAS) has already been proved successful [9–13]. This is based on the

0003-2670/87/$03.50

use of a specially designed graphite furnace equipped with a miniature cup (mini-cup) into which solid samples are introduced. In the present study, the direct examination of precipitates has been explored further in order to apply the technique to aqueous samples. For this purpose, a combination of 8-Q with precipitated magnesium(II) ions as carrier has proved to be excellent for the complete coprecipitation of copper and manganese in aqueous samples at sub-$\mu g\ kg^{-1}$ levels. The coprecipitates thus obtained can be used directly for graphite-furnace AAS.

EXPERIMENTAL

Apparatus and reagents

An atomic absorption spectrometer (Hitachi model Z-8000) was used in combination with an electrothermal graphite furnace of the cupped type, and a mini-cup [10,13]. A Hitachi AA data processor was used for the measurements of absorption signal as peak area and peak height. A Hitachi inductively-coupled plasma atomic emission spectrometer (ICP/AES, Super Scan Model 306) was used for recovery tests.

Acids and ammonia solution were of the purest available grade (ELSS and ELS, respectively, Kanto Chemical Co.). Ultra-clean water was obtained from a Millipore Milli-Q purification system. In all analytical procedures, such water was used. 8-Quinolinol (8-hydroxyquinoline, reagent grade, Wako Pure Chemical Co.) was dissolved in hydrochloric acid and a 2% (w/v) solution was prepared. A magnesium ion solution ($10\ mg\ ml^{-1}$) was prepared by dissolving the pure metal (99.995%) in hydrochloric acid and diluting with water. Stock standard solutions ($1.00\ g\ l^{-1}$) for each element were prepared by dissolution of the pure metals; working standards were obtained by serial dilution with water.

Procedures

Preconcentration procedure. In the standard procedure, 100 ml of a sample solution containing 20 mg of magnesium and 0.5 ml of concentrated nitric acid was placed into 250-ml pyrex flasks. A portion (5 ml) of the 2% 8-Q solution was added and then pH was adjusted to 7–8 by adding ammonia solution. The solution thus prepared was kept for 1 h at 80°C on a heater to ensure completion of precipitation. The solution was allowed to stand at room temperature for 0.5–1 h and then filtered through a weighed sintered glass filter (G4). The precipitate on the filter was washed with water. After drying at 110°C for 1 h in an oven, the filter and precipitate were weighed. The precipitate thus obtained was subjected directly to AAS using the mini-cup.

Direct AAS of precipitates. The mini-cup was first weighed on a microbalance

TABLE 1

Experimental conditions for the determination of copper and manganese after coprecipitation[a]

Conditions	
Wavelength (nm)	324.7 (Cu); 279.5, 403.1 (Mn)
Slit-width (nm)	1.3 (Cu); 0.4 (Mn)
Lamp current (mA)	10
Drying	200 °C, 30 s
Ashing	600 °C, 30 s
Atomizing	2500 °C, 10 s
Argon sheath gas	3.0 l min^{-1}
Argon carrier gas	
for drying and ashing	200 ml min^{-1}
for atomization	30 ml min^{-1}

[a]The temperatures shown were measured by a pyrophotometer (Chino Co.) standardized on the basis of the melting points of some metals.

(Mettler, model M-3). An appropriate amount (0.1–1 mg) of the precipitate was placed in the mini-cup from a small tantalum spoon, and the mini-cup was again weighed. The mini-cup was inserted into the graphite furnace, and the precipitate was dried, ashed and atomized successively according to the instrumental conditions in Table 1.

RESULTS AND DISCUSSION

Instrumental conditions for direct examination of precipitates

Typical signals for copper and manganese are shown in Fig. 1. The samples were prepared according to the standard procedure. The absorption profiles are symmetric and are quite similar to those obtained by the direct introduction of aqueous reference solutions. This suggests that 8-quinolinol and magnesium do not interfere with the determination of the other two metal ions.

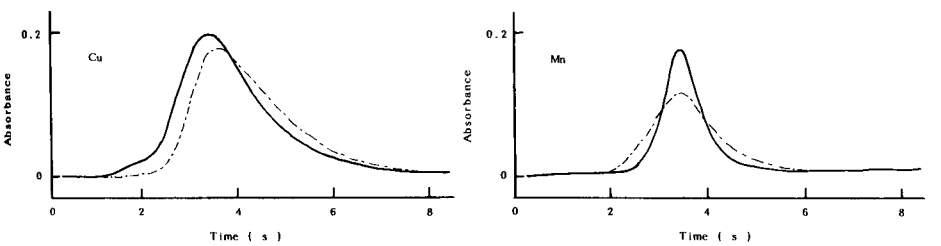

Fig. 1. Absorption/time profiles for copper and manganese: (-·-) aqueous reference solution; (-) solid sample prepared by the specified method.

In the direct examination of powdered samples by graphite-furnace AAS, the drying step was not always necessary, but it was effective for ashing organic materials smoothly. As a result, a drying temperature of 200°C for 30 s was selected.

When the temperature in the ashing step was kept in the range 400–1000°C for copper and 400–1400°C for manganese, the absorbance for these metals became constant. The relative standard deviation (RSD) of absorbances based on peak-height data were in the range 8–12%, whereas integrated (peak area) absorbances were more precise (RSD < 5%). An ashing temperature of 600°C is recommended because higher temperatures shorten the life of the graphite furnace.

An atomization temperature of 2500°C was selected, to provide maximal sensitivity. The temperature was the highest attainable when the cup-type furnace was used. Any memory effects were eliminated when the furnace was initially heated at 2500°C for 3 s. The instrumental conditions thus established are summarized in Table 1.

Recovery of copper and manganese

Although Mitchell and Scott [3,4] recommended the combined use of thionalide and tannic acid for such coprecipitation, they were precluded in this study because of high blank values. Pickett and Hankins [7], however, noted that copper was incompletely recovered by the use of 8-quinolinol alone, and that aluminum or indium ions were ineffective as carriers for improving the recovery of copper. To overcome these limitations, the effectiveness of bismuth, calcium and magnesium ions on the recovery of copper and manganese was investigated.

In order to assess the recoveries, 100-ml portions of aqueous solution containing 40 μg of copper and 80 μg of manganese were prepared. The pH of the solution was adjusted with ammonia after addition of definite amounts of 8-quinolinol and the specified carrier ion. The recoveries were examined by determining the two metal ions in the filtrates with ICP/AES. As shown in Fig. 2, the recoveries increased above pH 5 and were quantitative over the pH range 7.0–8.5 when magnesium was added. Bismuth and calcium ions were less effective than magnesium. Consequently, in subsequent experiments, precipitations were done at pH 8.0 in the presence of magnesium ions.

The concentration factor is defined as the weight ratio of the aqueous sample to the precipitate on the filter. It is ca. 1000 in the standard procedure. Both the use of small amounts of 8-quinolinol and a large amount of aqueous sample led to small amounts of final precipitates and hence an increase in the concentration factor.

The effect of the amount of 8-quinolinol on the concentration factor was examined for different weights of aqueous sample under various conditions.

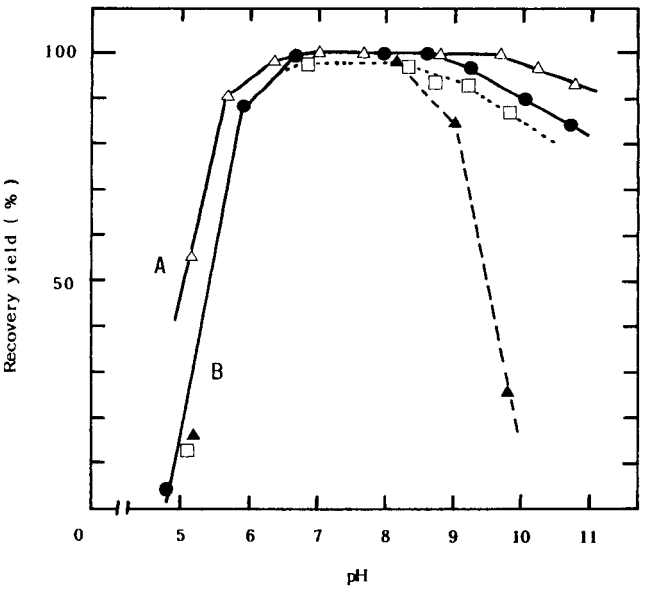

Fig. 2. Effect of pH on the coprecipitation of copper(II) and manganese(II) with 8-quinolinol and carrier ion. Curve A: (△) manganese with magnesium carrier. Curve B: copper with magnesium (●), bismuth (□) and calcium (▲) carrier ion. Conditions: 100 mg 8-Q, 20 mg of carrier ion, total volume of aqueous solution 100 ml.

TABLE 2

Conditions for quantitative recovery of copper and manganese from different weights of aqueous sample under various conditions

Sample weight (g)	Precipitant added		Concentration factor
	8-Q (mg)	Mg^{2+} (mg)	
100	60	10	1900
100	40	20	2000
160	60	20	2700
300	100	20	3800

The concentration factors attained under the conditions for quantitative recovery of the metals are listed in Table 2.

Analytical parameters

Analytical blanks were estimated according to the standard procedure except that 300 ml of the Milli-Q water was used. When 100 mg of 8-quinolinol was used, the final concentration factor was 3800. So the results for the blank

TABLE 3

Blanks and detection limits for natural water analysis at 3800-fold preconcentration

Element	Detection limit[a] ($ng\,l^{-1}$)	Blank[b] ($ng\,l^{-1}$)	Practical detection limit[c] ($ng\,l^{-1}$)
Cu	0.3	51 ± 6	12
Mn	0.2	84 ± 7	14

[a]Detection limit for AAS divided by the concentration factor (3800). [b]Average of five replicate blank values ± SD. [c]Practical detection limit; twice the blank SD, based on a 300-ml sample.

sample must be divided by 3800; the results are shown in Table 3 in which the detection limits for the AAS measurement are also divided by the final concentration factor. The detection limit depends on the blank reproducibility; twice the standard deviation of the blank obtained from five replicate determinations is shown in Table 3 as the practical detection limit. The blank values can be decreased by the use of purified precipitants.

Calibration graphs were obtained according to the standard procedure in which copper or manganese spikes (50 ng, 100 ng or 1 μg) were added to 100 ml of water. On the assumption of 100% recovery of the metals, 1 mg of the standard powder sample contained 0.427, 0.863 and 8.69 ng of the metals, respectively. Calibration graphs obtained by plotting the absorbance signals (peak area) against the amount of metals in the precipitates were essentially linear over the range 0.1–10 ng for copper, and 0.04–1.4 (279.6-nm line) and 0.5–7.5 ng (403.1-nm line) for manganese. Their slopes agreed within experimental errors with those derived from the aqueous standards, as shown in Fig. 3. This is strong evidence for the quantitative recovery of these elements down to less than $\mu g\,kg^{-1}$ level.

Application to tap and river water samples

The method was applied to the determination of copper and manganese in tap and river water samples. The results are listed in Table 4. The two elements in the sample at the $\mu g\,kg^{-1}$ level can be determined by the standard addition method, for which 40–100 ml of the samples were used. As the blank values were relatively high, the concentration of the elements in the samples was also determined from the relationship between aqueous sample weight and total amounts of the elements obtained in the final precipitate. As shown in Fig. 4, the concentration was obtained from the slope of the least-square lines. The values obtained agree well with those obtained by the standard addition method. The blank value listed in Table 4 was also obtained from the y-intercept of the line, in good agreement with the initial estimate based on calibration with samples prepared with Milli-Q water and the precipitants.

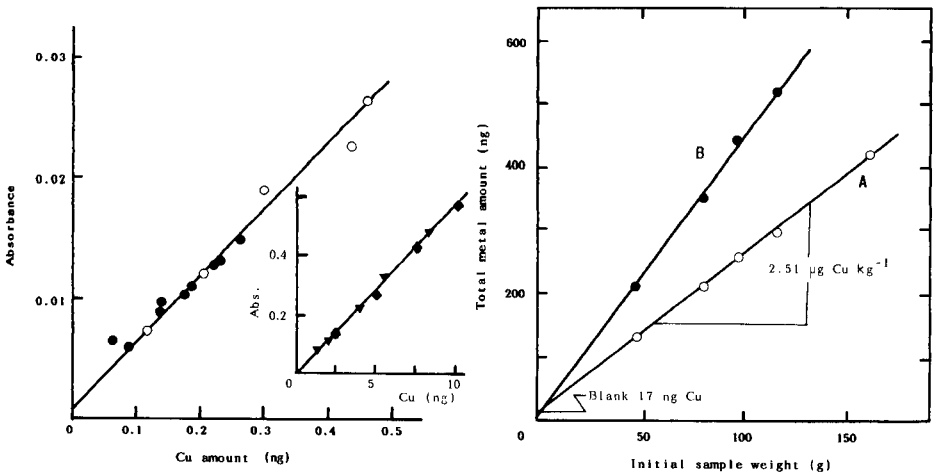

Fig. 3. Calibration graphs for copper. (♦) Aqueous standard solutions (inset). Other symbols: solid samples prepared by the coprecipitation method from 100 ml of aqueous samples containing (●) 0.5, (○) 1.0 and (▼) 10.0 ng Cu ml^{-1}.

Fig. 4. Relationship between initial weight of tap water sample and the total amount of metals in the final precipitate: (A) copper; (B) manganese. (Final samples were prepared by coprecipitation with 100 mg of 8-Q and 20 mg of Mg^{2+} at pH 8.)

In Table 4, the results obtained by the proposed method are also compared with a value for copper obtained by Murozumi and Nakamura [14] by isotope-dilution mass spectrometry (IDMS) for the same sample of river water as that used in the present study. The data indicate satisfactory agreement between

TABLE 4

Determination of copper and manganese in natural water samples

Sample	Element	Present method		IDSM[a] ($\mu g\ kg^{-1}$)
		Blank (ng)	Found[b] ($\mu g\ kg^{-1}$)	
Tap water	Cu	17±2	2.51±0.07[c], 2.65±0.21[d]	-
	Mn	28±2	3.53±0.07[c], 3.52±0.35[d]	-
River water	Cu	17±2	0.31±0.04[c], 0.34±0.07[d]	0.297
	Mn	28±2	4.04±0.03[c], 4.19±0.32[d]	-

[a]Isotope-dilution mass spectrometry [14]. [b]Blank value is subtracted; mean ±SD ($n=4$). [c]Obtained from the relationship between initial sample weights and total amounts of the elements. [d]Obtained by the standard addition method.

the results for copper. Values for manganese by IDMS are not shown because there is no suitable isotope of manganese to allow IDMS.

From these results, many elements forming complexes with 8-quinolinol can be expected to be quantitatively recovered under the same conditions. Further work is needed to decrease blank values, but the combined use of coprecipitation and the direct examination of the precipitate by graphite-furnace AAS is a promising procedure for the determination of ultra-trace elements in natural waters.

The authors thank Professor Masayo Murozumi and Mr. Siji Nakamura of the Muroran Institute of Technology for their kindness in allowing the use of their IDMS results. This study was supported by a Grant-in-Aid for Scientific Research (No. B-61470033) from the Ministry of Education of Japan, for which the authors are very grateful.

REFERENCES

1 G. Tölg, Talanta, 19 (1972) 1489.
2 R.L. Mitchell, Analyst, 71 (1946) 361.
3 R.L. Mitchell and R.O. Scott, J. Soc. Chem. Ind., London, 66 (1947) 330.
4 R.L. Mitchell and R.O. Scott, Spectrochim. Acta, 3 (1948) 367.
5 A.J. Mitteldorf, Appl. Spectrosc., 6 (1951) 21.
6 J. Smit and J.A. Smit, Anal. Chim. Acta, 8 (1953) 274.
7 E.E. Pickett and E.E. Hankins, Anal. Chem., 30 (1958) 47.
8 R.L. Dehm, W.G. Dunn and E.R. Loder, Anal. Chem., 33 (1961) 607.
9 I. Atsuya and K. Itoh, Bunseki Kagaku, 31 (1982) 708, 713.
10 I. Atsuya and K. Itoh, Spectrochim. Acta, Part B, 38 (1983) 1259.
11 K. Itoh, K. Akatsuka and I. Atsuya, Bunseki Kagaku, 33 (1984) 301.
12 K. Itoh, T. Itoh, K. Akatsuka and I. Atsuya, Bunseki Kagaku, 35 (1986) 122.
13 I. Atsuya, K. Itoh, K. Akatsuka and K. Jin, Fresenius' Z. Anal. Chem., 326 (1987) 53.
14 M. Murozumi and S. Nakamura, Muroran Institute of Technology, private communication, 1986.

Analytica Chimica Acta, 202 (1987) 231-236
Elsevier Science Publishers B.V., Amsterdam — Printed in The Netherlands

Short Communication

COULOMETRIC TITRATION OF SALTS OF STRONG MINERAL ACIDS IN ACETIC ANHYDRIDE BY APPLICATION OF A HYDROGEN/PALLADIUM ELECTRODE

VILIM J. VAJGAND*
Faculty of Science, University of Belgrade, Belgrade (Yugoslavia)
RANDJEL P. MIHAJLOVIĆ and RADMILA M. DŽUDOVIĆ
Faculty of Science, University of Kragujevac, Kragujevac (Yugoslavia)
LJILJANA N. JAKŠIĆ
Faculty of Science, University of Priština, Priština (Yugoslavia)
(Received 15th October 1986)

SUMMARY

The application of H_2/Pd electrodes as generator and indicator electrodes is described for coulometric titrations of alkali metal halides and trivalent metal sulphates in acetic anhydride with potentiometric end-point detection. In acetic anhydride, sodium fluoride is a strong enough base to be titrated directly with H^+ ions obtained by anodic oxidation of hydrogen dissolved in palladium. Other halides (NaCl, KCl, LiCl, KBr and NaBr) can be determined, after reaction of halides with mercury(II) acetate, by coulometric titration of the liberated base. Potentiometric end-point detection with a H_2/Pd–mercury(I) acetate electrode pair is satisfactory. Sulphates of Fe(III), Cr(III) and Al(III) are determined by back-titrating the excess of barium acetate after precipitation of barium sulphate. The errors in these determinations are $< 1\%$ for concentrations ranging from 0.001 to 0.003 M.

Acetic anhydride is widely used as a medium for titrations of various organic and inorganic compounds [1,2]. For quantifying bases in this solvent, perchloric acid dissolved in an organic solvent is most often used as the titrant. Because the concentration of perchloric acid in pure acetic anhydride changes with time, titrations of substances which display basic character in this solvent are usually done with solutions of perchloric acid in acetic acid or dioxane containing a small amount of water [3–6].

Pifer and Wollish [7] reported that inorganic chlorides, bromides and iodides can be converted to the corresponding basic acetates by the addition of an excess of mercury(II) acetate in anhydrous acetic acid; the liberated acetate was then titrated with perchloric acid. Goldstein et al. [8] determined sul-

0003-2670/87/$03.50

phates of tervalent cations by adding excess of barium acetate and back-titrating with perchloric acid in acetic acid; glass and saturated calomel electrodes were used.

The difficulties encountered in determining bases in acetic anhydride (change of perchloric acid concentration with time and water introduced with perchloric acid) can be avoided by using coulometrically generated hydrogen ions, obtained by direct oxidation of hydrogen dissolved in palladium, and by using a H_2/Pd–mercury/mercury(I) acetate electrode pair instead of the conventional electrode pair for potentiometric detection of end-points.

Experimental

Reagents. All chemicals used were of analytical-reagent grade (Merck). Sodium chloride, sodium fluoride, sodium bromide, potassium chloride, potassium bromide and lithium chloride were examined as 0.01 M solutions in acetic anhydride. The exact concentrations of these solutions were determined by coulometric titration in acetic anhydride, with hydroquinone as anode depolarizer and malachite green as indicator.

The barium acetate and mercury(II) acetate solutions in acetic acid were 0.02 M. Before use, acetic anhydride was redistilled by use of a fractionating column and the fraction boiling at 136–137°C was collected [1].

Apparatus. The current source was a voltage/current stabilizer (Vinča, Beograd). The current of the generator circuit was measured by means of a precise milliammeter (Iskra, Kranj). The apparatus used for the coulometric titration with visual end-point detection is shown in Fig. 1A. The tubing used in construction of the cell was of 30-mm diameter; the height was 100 mm. The anode compartment of the electrolytic cell was separated from the cathode compartment by means of a sintered glass G4 disc. A platinum cathode was used with the H_2/Pd anode. The equipment used for potentiometric end-point detection is outlined in Fig. 1B. The capacity of the electrolytic cell was 100 ml. A mercury(I) acetate electrode served as the reference with a H_2/Pd indicator electrode.

Electrodes. The mercury(I) acetate electrode was constructed as indicated in Fig. 1B. Pure mercury was placed to a height of several millimetres in the outer tube (20-mm diameter) and connected via sealed platinum wire to the pH meter. The mercury was covered with a paste made of pure mercury, mercury(I) acetate and a saturated solution of sodium perchlorate in anhydrous acetic acid or an acetic acid/acetic anhydride (1:6 or 5:95) mixture; this paste was covered with a saturated solution of sodium perchlorate in the same solvent, which was connected with the test solution through a teflon tap and capillary tube, as shown in Fig. 1B.

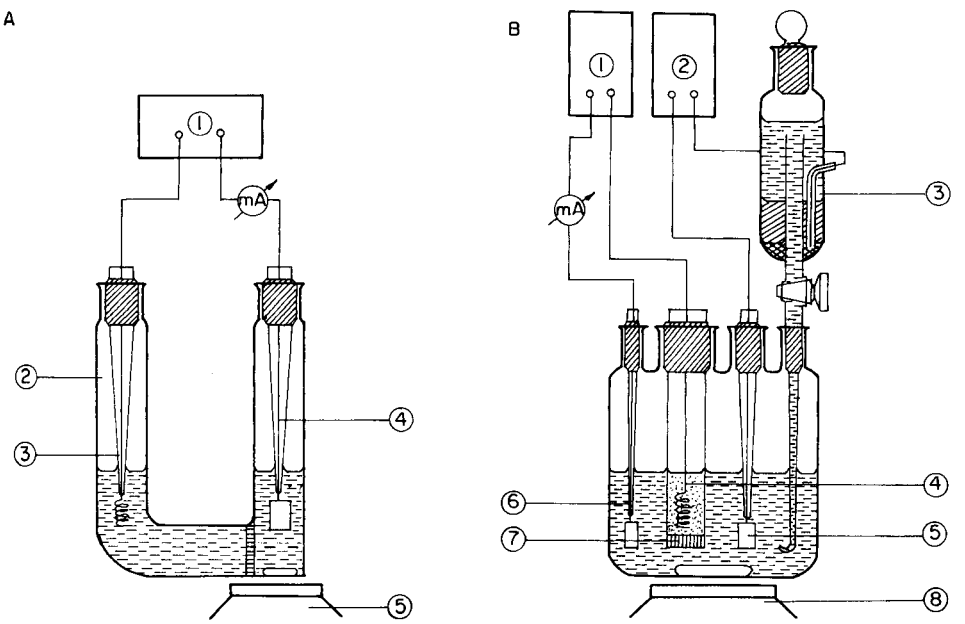

Fig. 1. Schematic diagrams of the apparatus for the coulometric titrations. (A) Visual detection of the end-point: (1) current stabilizer; (2) electrolytic cell; (3) Pt cathode; (4) H_2/Pd anode; (5) magnetic stirrer. (B) Potentiometric detection of the end-point: (1) current stabilizer; (2) pH meter; (3) mercury(I) acetate electrode; (4) Pt cathode; (5) H_2/Pd indicator electrode; (6) H_2/Pd anode; (7) sintered glass (G4); (8) magnetic stirrer.

The generator electrode was a palladium sheet (10×20×5 mm) which was sealed by means of platinum into a glass tube. The electrode was saturated with hydrogen obtained by electrolysis of water containing some drops of sulphuric acid; the hydrogen liberated at the cathode dissolves directly in palladium. Saturation was obvious from evolution of excess of hydrogen on the palladium. The indicator electrode was a spiral of 0.5-mm diameter palladium wire (99.9% pure; Johnson Matthey Metals, London). The spiral platinum cathode was sealed into a glass tube in the usual way.

Determination of halides of alkali metals. For visual detection of the end-point, the supporting electrolyte (0.2 M sodium perchlorate in acetic anhydride) was poured into the two compartments of the electrolytic cell (Fig. 1A) up to the same level. The platinum spiral electrode was dipped into the catholyte, and after the addition of 1–2 drops of indicator solution (malachite green in acetic anhydride) to the anode compartment, the H_2/Pd electrode was placed in the anolyte. Hydrogen ion was generated to titrate the supporting electrolyte, and then a measured amount (0.5–1.0 ml) of the sample solution and an excess of mercury(II) acetate were added. The current source and a chrono-

meter were switched on simultaneously, and hydrogen ions were generated until the color of the indicator changed.

For potentiometric detection of the end-point (Fig. 1B), the supporting electrolyte was added as indicated above, the electrodes were immersed, and the supporting electrolyte was titrated. Then a measured volume of the sample solution and an excess of mercury(II) acetate were added. The liberated acetate was titrated with discontinuous generation of hydrogen ions, the potential being read after each step. The end-point was evaluated from the second-derivative curve.

In each case, the amount of the liberated acetate (i.e., the concentration of halide) was calculated in the usual way from the quantity of electricity consumed.

Determination of sulphates of Fe(III), Cr(III) and Al(III). The sulphates of Fe(III), Cr(III) and Al(III), the acetates of which are weaker bases than barium acetate, were determined with the apparatus shown in Fig. 1B. These sulphates were previously dissolved in water, because their solubilities in acetic anhydride and acetic acid are very small. Water must be present because the reaction of barium acetate with solid sulphates is not quantitative, even on heating. The precipitation was done with 0.02 M barium acetate which had previously been standardized by the coulometric/potentiometric method. The water present was then removed by heating the solution with acetic anhydride in a flask with a reflux condenser for 5–10 min. The solution thus obtained was quantitatively transferred to the anode compartment of the electrolytic cell and the excess of barium acetate was titrated as described above.

Results and discussion

Sodium fluoride in acetic anhydride is a sufficiently strong base to be titrated directly with a standard solution of perchloric acid [9]. In order to eliminate the interference of water from the perchloric acid solution, fluoride has been titrated with hydrogen ions generated at a palladium anode [10]. When the H_2/Pd electrodes were used for both the generator and indicator electrodes, the potential jump at the equivalence point was about 150 mV. The results obtained by visual and potentiometric detection of the end-point were satisfactory (Table 1).

Other halides (NaCl, KCl, LiCl, NaBr and KBr) which are weak bases even in acetic anhydride, were determined by the exchange reaction: $2NaCl + Hg(OAc)_2 = 2NaOAc + HgCl_2$. The liberated acetate was titrated with hydrogen ions generated from the H_2/Pd anode. With the potentiometric end-point, equilibrium potentials during the titration were rapidly established, and the jump at the equivalence point was about 100 mV for concentrations of halides ranging from 0.001 to 0.003 M. Typical results are presented in Table

TABLE 1

Coulometric determination of halides of alkali metals in acetic anhydride with visual and potentiometric detection of the end-point (I=6 mA)

Titrated salt	Visual end-points		Potentiometric end-points	
	Taken (mg)	Recovery[a] (%)	Taken (mg)	Recovery[a] (%)
Sodium fluoride	0.623	100 ±0.5 (6)	2.659	100.1±0.4 (4)
Lithium chloride[b]	0.68	99.8±0.5 (9)	2.72	100.0±0.2 (6)
Sodium chloride[b]	0.99	100.0±0.4 (10)	4.24	100.0±0.3 (7)
Potassium chloride[b]	1.01	100.0±0.7 (10)	5.07	100.0±0.1 (7)
Potassium bromide[b]	1.84	99.8±0.6 (11)	7.67	100.0±0.5 (8)
Sodium bromide[b]	0.62	99.8±0.8 (6)	6.81	100.2±0.4 (6)

[a]The number of titrations is given in parentheses. [b]Titrated by the exchange procedure.

1. The error was <0.5%. With visual detection of the end-point, the accuracy was as good, but the precision was slightly poorer (Table 1).

The determination of the sulphate salts of Fe(III), Cr(III) and Al(III) was based on back-titration of the excess of barium acetate after precipitation of the sulphate as barium sulphate. Iron, chromium and aluminium acetates do not interfere with the titration of barium acetate, because they are much weaker bases than barium acetate. The recoveries obtained in the titrations of aluminium sulphate (2.41 mg), chromium(III) sulphate (3.2 mg) and iron(III) sulphate (3.27 mg) were 99.7±0.6%, 100.6±0.9% and 100.2±2.1% (n=5), respectively. These errors are less than 1%, which is similar to those of classical gravimetric determinations at this level.

Conclusions

The application of the H_2/Pd generator electrode in the determination of salts of strong mineral acids in acetic anhydride simplifies the procedure compared to more conventional titrations. This coulometric method also provides higher accuracy. The H_2/Pd electrode is also suitable as the indicator electrode in titrations in acetic anhydride. A stable potential is rapidly established during the titration and at the equivalence point. The H_2/Pd electrode has a low resistance in nonaqueous solutions and is simply made so that it has significant advantages over the glass electrode.

REFERENCES

1 A.P. Kreshkov, L.N. Bykova and N.A. Kazaryan, Kislotno-osnovnoe Titrovanie v Nevodnikh Rastvorakh, Khimya, Moscow, 1967.
2 Elektrokhimiya Metallov v Nevodnikh Rastvorakh, Mir, Moscow, 1974.

3 N.P. Dzyba and V.P. Georgievskii, Farm. Zh. (Kiev), 6 (1959) 26.
4 N.A. Goncharova and K.I. Evstratova, Zh. Anal. Khim., 25 (1970) 634.
5 N.P. Bezinger, G.D. Galpern and M.A. Abdurakhmanov, Zh. Anal. Khim., 16 (1961) 91.
6 D.C. Wimer, Anal. Chem., 30 (1958) 77.
7 Ch.W. Pifer and E.G. Wollish, Anal. Chem., 24 (1952) 519.
8 G. Goldstein, O. Menis and O.L. Manning, Anal. Chem., 33 (1961) 266.
9 B.W. Mather and F.C. Anson, Anal. Chem., 33 (1961) 132.
10 V.J. Vajgand, R. Mihajlović and Lj. Jakšić, Sixth Yugoslav Congress for Pure and Applied Chemistry, Sarajevo, 1979, Abstract 191; Glas. Hem. Druš., Beograd, 46 (1981) C121.

Analytica Chimica Acta, 202 (1987) 237–240
Elsevier Science Publishers B.V., Amsterdam — Printed in The Netherlands

Short Communication

PREDICTION OF CARCINOGENICITY OF POLYNUCLEAR AROMATIC HYDROCARBONS ON THE BASIS OF THEIR CHEMICAL STRUCTURES

YOSHIKATSU MIYASHITA, TOHRU OKUYAMA, KAZUTOMO YAMAURA, KIYOKATSU JINNO and SHIN-ICHI SASAKI*

School of Materials Science, Toyohashi University of Technology, Tempaku-cho, Toyohashi 440 (Japan)

(Received 17th March 1987)

Summary. The carcinogenicities of polynuclear aromatic hydrocarbons in particulates extracted from diesel engine exhaust are predicted on the basis of the combined bay–L region theory proposed earlier, in conjunction with pattern recognition techniques. The predicted carcinogenicities agree well with experimental data, thus showing the validity of the proposed model equations.

Miyashita, Sasaki and co-workers [1,2] considered the hypothetical metabolic pathways of polynuclear aromatic hydrocarbons (PAHs) and deduced model equations based on the "combined bay–L region" theory, with help from pattern recognition techniques, to explain the carcinogenicities of PAHs.

Equation 1 was obtained on the basis of fifteen PAHs which are known to be carcinogenic:

$$J = 9.47\Delta E_{\pi}^{(1)} + 10.78\Delta E_{\mathrm{deloc}} - 0.32 I_{\mathrm{L}} + 25.73 \qquad (1)$$

with $n = 15$, $s = 0.53$, $r = 0.92$ and $F = 18.80$. Equation 2 was obtained on the basis of the above 15 carcinogenic PAHs and six other PAHs known to be noncarcinogenic:

$$J = 8.64\Delta E_{\pi}^{(1)} + 12.43\Delta E_{\mathrm{deloc}} - 0.34 I_{\mathrm{L}} + 21.61 \qquad (2)$$

with $n = 21$, $s = 0.62$, $r = 0.91$ and $F = 26.45$. In the data for these equations, n, s, r, and F are, respectively, the number of compounds, the standard deviation, the multiple correlation coefficient, and the F value of the correlation. The carcinogenicities are expressed on an arbitrary scale J with values of 0, 1, 2, 3 and 4 for inactive (−), slightly active (+), moderately active (2+), more active (3+) and very active (4+), respectively [3]. In Eqns. 1 and 2, $\Delta E_{\pi}^{(1)}$

0003-2670/87/$03.50

TABLE 1

PAHs in the exhaust from a diesel engine

Peak	Name	Peak	Name
1	Benzo[ghi]perylene	7	Naphtho[8,1,2-bcd]perylene
2	Dibenzo[def, mno]chrysene	8	Naphtho[1,2,3,4-ghi]perylene
3	Coronene	9	Dibenzo[cd, lm]perylene
3a	Methyl coronene	10	Benzo[a]coronene
4	Naphtho[1,2,3,4-def]chrysene	11	Benzo[pgr]naphtho[8,1,2-bcd]perylene
5	Benzo[rst]pentaphene	12	Naphtho[8,1,2-abc]coronene
6	Dibenzo[b, def]chrysene	13	Ovalene

represents the energy change (β unit) in forming the A-region dihydrodiol from the parent PAH; I_L is the sum of two atomic superdelocalizabilities involved in the L region for the parent compounds, and ΔE_{deloc} is the change in delocalization energy (β unit); these values were calculated from the process of metabolic transformation of PAH.

Application of Eqns. 1 and 2 to PAHs with a terminal benzene ring enables the active or inactive carcinogenic character of PAHs to be predicted, apart from those used previously in developing the equations. Recently, in work on high-performance liquid chromatography (HPLC) of the particulates collected from diesel exhaust gas, Fetzer et al. [4] detected and identified 13 PAHs with 6 to 10 aromatic nuclei (Table 1). Figure 1 shows their structural formulae on the chromatogram; the carcinogenicities observed by earlier workers [5–8] for nine of these compounds are listed in Table 2. Noncarcinogenicity of the other four compounds (7, 8, 11 and 12) has been reported. The

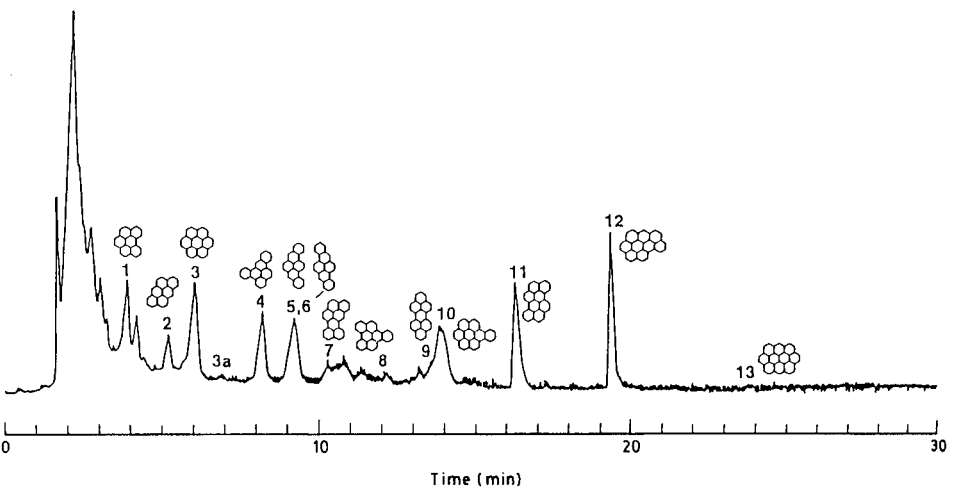

Fig. 1. Liquid chromatogram of particulates in the exhaust from a diesel engine.

TABLE 2

Carcinogenicity observed by physiological tests[a]

PAH	Terminal benzene ring	Lacassagne et al. [6]	Jones and Matthews [7]	Dipple [8]	Morgan et al. [5]
1	–			Moderate	Noncarcinogen
2	–			Inactive	Noncarcinogen
3	–				Noncarcinogen
4	+		++++	High activity	
5	+		+++	High activity	Carcinogen
6	+		+++	High activity	
7	–				
8	+				
9	–	Weak			
10	+	Inactive			
11	–				
12	–				
13	–				Noncarcinogen

[a]Carcinogenicities of PAHs 7, 8, 11 and 12 have not been measured.

presence or absence of the terminal benzene ring in each structure is noted in Table 2.

First, carcinogenicities were predicted by Eqns. 1 and 2 for compounds 4, 5, 6, 8 and 10 which have terminal benzene rings because these molecules have the bay region. The values of $\Delta E_\pi^{(1)}$ and ΔE_{deloc} for these compounds are listed in Table 3. None of these compounds has an L region, i.e., $I_L = 0$. The J values calculated from Eqns. 1 and 2 based on the $\Delta E_\pi^{(1)}$ and ΔE_{deloc} data listed are also shown in Table 3.

The carcinogenicity of compound 4 is predicted to be about +2. This predicted value is less than the results observed by Jones and Matthews [7] and

TABLE 3

Carcinogenicity calculated by Eqns. 1 and 2 on the basis of the descriptor values ($\Delta E_\pi^{(1)}$ and ΔE_{deloc})

PAH	$\Delta E_\pi^{(1)}/\beta$	$\Delta E_{\text{deloc}}/\beta$	J values	
			Eqn. 1	Eqn. 2
4	−3.3936	0.775	1.95	1.92
5	−3.2743	0.866	4.06	4.08
6	−3.2492	0.845	4.07	4.04
8	−3.3488	0.653	1.06	0.79
10	−3.3510	0.664	1.16	0.91

Dipple [8] (Table 2). The carcinogenicities of compounds 5 and 6 were predicted to be about +4; these high predicted values correspond well to those observed [5,7,8]. The present method for prediction of carcinogenicity, therefore, is useful. Both compounds 8 or 10 are predicted to have J values of about +1; the latter was found to be noncarcinogenic in actual measurements [5]. Although no observed value of compound 8 is available, it should be only slightly active according to the present prediction method.

Compounds 1, 2, 3, 9 and 13 are considered to be noncarcinogenic because of the lack of the terminal benzene ring. This prediction corresponds well to the results observed for compounds 1, 2, 3 and 13; an exception is compound 9, reported as weakly carcinogenic by Lacassagne et al. [6]. Thus, it is almost possible to say that compounds 7, 11 and 12 should be noncarcinogenic even though their carcinogenicity has not been measured. It must be noted that only one of the PAHs (4 in Table 1) used in this study was also a member of the training set used in developing the model [2].

Discussion

Model equations were proposed earlier [1,2] to predict the carcinogenicities of PAHs on the basis of the combined bay–L region theory and pattern recognition techniques were applied. The carcinogenicities of large PAHs extracted from diesel engine exhaust were studied by using these equations. The calculated predictions of carcinogenicity correspond well with the observed values, which enhances the validity of the prediction method described.

The authors thank the Computer Center, Institute for Molecular Science, for affording computation facilities. Y.M. expresses his thanks to Dr. Takahiro Kobayashi of the National Institute for Environmental Research.

REFERENCES

1 Y. Miyashita, T. Seki, Y. Takahashi, S. Daiba, Y. Tanaka, Y. Yotsui, H. Abe and S. Sasaki, Anal. Chim. Acta, 133 (1981) 603.
2 Y. Miyashita, Y. Takahashi, S. Daiba, H. Abe and S. Sasaki, Anal. Chim. Acta, 143 (1982) 35.
3 D.M. Jerina and R.E. Lehr, in V. Ullrich, I. Roots, A.G. Hildebrant, R.W. Estabrook and A.H. Conney (Eds.), Microsomes and Drug Oxidations, Pergamon, Oxford, 1977, p. 709.
4 J.C. Fetzer, W.R. Biggs and K. Jinno, Chromatographia, 21 (1986) 439.
5 D.D. Morgan, D. Warshawsky and T. Atkinson, Photochem. Photobiol., 25 (1977) 31.
6 A. Lacassagne, N.P. Buu-Hoi, F. Zadjela and G. Saint-Ruf, C.R. Acad. Sci., Ser. D, 266 (1968) 301.
7 D.W. Jones and R.S. Matthews, Prog. Med. Chem., 10 (1974) 159.
8 A. Dipple, in C.E. Searle (Ed.), Chemical Carcinogens (ACS Monograph 173), American Chemical Society, Washington, DC, 1976, p. 245.

Analytica Chimica Acta, 202 (1987) 241–246
Elsevier Science Publishers B.V., Amsterdam — Printed in The Netherlands

Short Communication

MOLECULAR EMISSION CAVITY ANALYSIS FOR ORGANIC SULPHUR COMPOUNDS AFTER ELECTROLYTIC GENERATION OF HYDROGEN SULPHIDE

N. GREKAS and A.C. CALOKERINOS*

Laboratory of Analytical Chemistry, University of Athens, 106 80 Athens (Greece)

(Received 19th March 1987)

Summary. Organic sulphur compounds (thiosemicarbazide and dithioxamide) are determined in the range 5.00–30.0 $\mu g\ ml^{-1}$. Electrolysis is done between two platinum electrodes in a closed vapour-generation system. Various parameters which affect the procedure are investigated in detail. Other sulphur-containing compounds can be determined with different sensitivities.

Molecular emission cavity analysis (m.e.c.a.) has been applied to the determination of many organic and inorganic sulphur-containing compounds [1]. The conventional technique allows the simultaneous determination of sulphur anions in binary and ternary mixtures but it also leads to various difficulties such as matrix effects and poor reproducibility [2]. Vapour-generation systems have been developed for determining a limited variety of sulphur compounds. Thus, sulphate can be determined with very good sensitivity by m.e.c.a. with a vaporizing system, after reduction of sulphate to hydrogen sulphide. The reaction is conducted in a heated system which contains a mixed tin/orthophosphoric acid reductant. However, the procedure is troublesome and requires a complex vaporizing system [3].

Sulphur compounds that produce sulphur dioxide or hydrogen sulphide on acidification can also be determined in the vaporizing system either manually [4,5] or automatically [6,7]. Application of these methods is restricted to compounds that produce such sulphur gases on acidification. Nevertheless, application of m.e.c.a. to the determination of organic sulphur compounds after evolution of sulphur vapours by reactions other than acidification seemed possible and was further investigated. Initially, electrolysis was chosen for evolution of hydrogen sulphide from various organic compounds. Previous work on electrolytic hydrogenation of organic sulphur compounds and evolution of hydrogen sulphide has shown that the method can be used analytically [8]. In this communication, development and applications of a molecular emission cavity analyzer with an electrolytic generation system are described.

0003-2670/87/$03.50

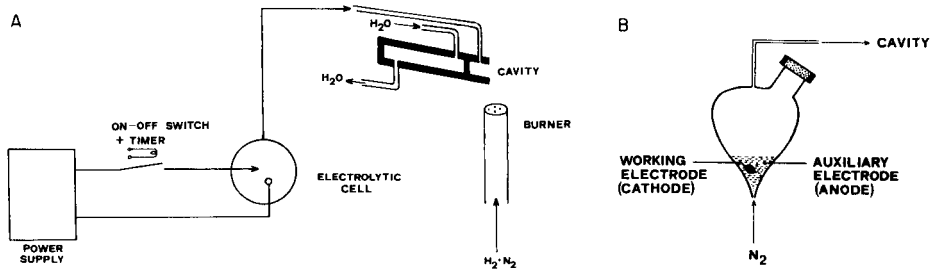

Fig. 1. (A) Schematic diagram of electrolytic unit (not to scale). (B) Electrolytic cell used for generation of hydrogen sulphide from organic sulphur compounds.

Experimental

Apparatus. The apparatus used consisted of the m.e.c.a. detector previously described [9] and an electrolysis unit (Fig. 1A). The latter consisted of a thermostatted cell, a d.c. power supply and an on-off switch controlled by a precision timer. The cell (Fig. 1B) was made of glass (internal volume ca. 15 ml) and was continuously purged by nitrogen, which ensured adequate stirring of the solution and purging of hydrogen sulphide to the cavity. Two platinum electrodes were embodied in the cell. The overall areas of the electrodes were 128 and 8 mm^2, respectively, and the distance between them was 5 mm. The timer ensured a precise and reproducible electrolysis time.

Reagents. All solutions were prepared from analytical-reagent grade materials in deionized distilled water. All solutions of organic compounds were prepared daily in 4.0 M sulphuric acid.

Procedure. Set up the instrument under the optimized conditions shown in Table 1. Ignite the flame and establish the baseline on the recorder. Introduce 2.00 ml of the analyte solution to the electrolytic cell, and start the timer and the electrolysis. The timer switches off the current automatically after the appropriate time (30 s). Record the change in emission intensity with time and record the maximum peak height in mV. After termination of electrolysis, empty the cell by suction.

Results and discussion

A potentiostat was used initially for controlling the cathode potential but the generated S_2 emission was weak owing to the small current supplied to the cell. Furthermore, electrolysis at the controlled cathode potential was not selective. It was decided, therefore, to use an ordinary d.c. power supply capable of generating high currents. All optimization studies were carried out with 20 and 40 $\mu g\ ml^{-1}$ dithioxamide (rubeanic acid) solutions.

TABLE 1

Experimental parameters for molecular emission cavity analysis for organic sulphur compounds by electrolytic hydrogenation

Parameter	Description
Cooling water flow rate	130 ml min^{-1}
Hydrogen flow rate	1.0 l min^{-1}
Nitrogen flow rate	2.1 l min^{-1}
Photomultiplier voltage	900 V
Wavelength	384 nm
Slit width	2 mm (4 nm spectral bandwidth)
Sulphuric acid concentration	4 M
Temperature of cell	28 °C
Nitrogen carrier gas flow rate	160 ml min^{-1}
Volume of analyte solution	2.00 ml
Electrolysis interval	30 s
Current	180 mA

Purging of hydrogen sulphide into the cavity is mainly controlled by the nitrogen flow rate (for a given flame composition). The electrolysis time controls the quantities of hydrogenated organic compounds and hydrogen sulphide formed. Both parameters were investigated; the results are shown in Fig. 2. At flow rates <74 ml min^{-1}, the contents of the cell ran into the nitrogen

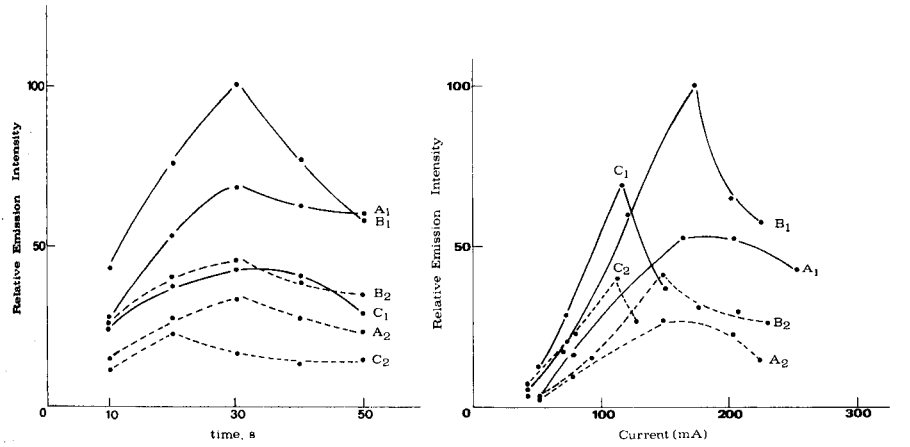

Fig. 2. Effect of electrolysis time on signal from (1) 40 and (2) 20 μg ml^{-1} dithioxamide at different flow rates of nitrogen carrier gas: (A) 136; (B) 160; (C) 188 ml min^{-1}. (Current 20 mA; volume 2.00 ml).

Fig. 3. Effect of current on signal from (1) 40 and (2) 20 μg ml^{-1} dithioxamide in different concentrations of sulphuric acid: (A) 3.0; (B) 4.0; (C) 5.0 M. (Electrolysis time 30 s; nitrogen flow rate 160 ml min^{-1}).

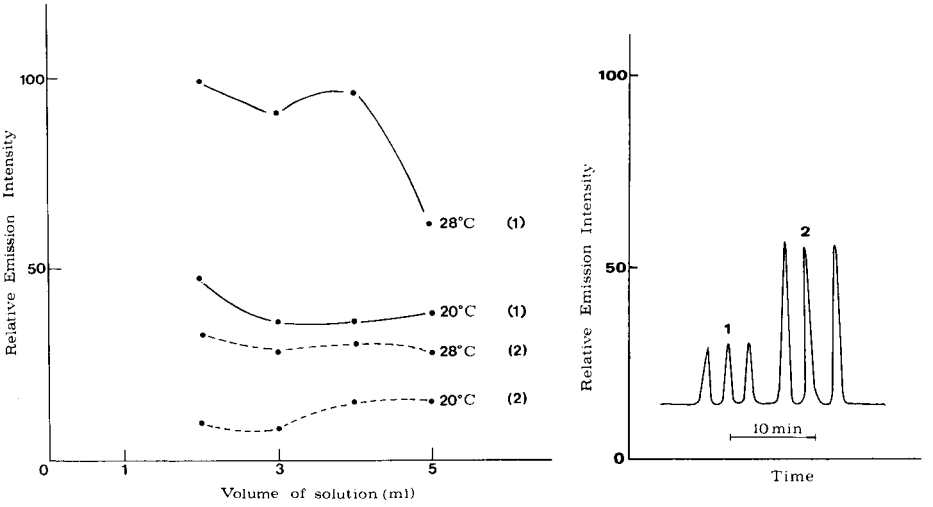

Fig. 4. Effect of solution volume containing (1) 80 and (2) 40 μg of dithioxamide at two temperatures in the electrolytic cell. (Nitrogen flow rate 160 ml min^{-1}; current 180 mA; electrolysis time 30 s.)

Fig. 5. Emission profiles from 20 μg ml^{-1} dithioxamide on platinum cathodes of different surface areas: (1) 8 mm^2 (wire); (2) 128 mm^2. (Experimental parameters as in Table 1.)

inlet at the bottom of the vessel while at flow rates >190 ml min^{-1}, the pressure in the system was too great and solution droplets were carried into the cavity.

Sulphuric acid was used as the electrolysis medium, mainly because its performance was already proven [8]. The quantity of hydrogen sulphide evolved greatly depended on the current and acid concentration, because hydrogenation occurs according to the following general scheme [10]:

$$\rangle C{=}S + 2H^+ + 2e^- \rightarrow \rangle CH\text{-}SH$$

$$\rangle CH\text{-}SH + 2H^+ + 2e^- \rightarrow \rangle CH_2 + H_2S$$

The effect of both parameters on the emission intensity is shown in Fig. 3. When acetic acid was used, no S_2 emission was obtained, owing to the insufficient acidity of the medium. Nitric acid was not tested because it can decompose many organic sulphur compounds and thus decrease the amount of hydrogen sulphide evolved. When orthophosphoric acid was used, broad and irregular peaks were obtained. The effect was attributed to the viscosity of the medium which delays evolution of hydrogen sulphide.

Because hydrogen sulphide is soluble in aqueous sulphuric acid solutions, the effect of solution volume was investigated by injecting various volumes containing the same quantity of the analyte (Fig. 4) into the cell. At least 2.0 ml was necessary to submerge the electrodes completely in the solution. The

TABLE 2

Relative emission intensities from some organic sulphur-containing compounds (as 20 μg S ml^{-1} solutions)

Compound	Relative emission intensity
Thiobarbituric acid	100
Thiosemicarbazide	75.0
Dithioxamide (rubeanic acid)	60.0
Thiodiacetic acid	17.0
Thiourea	15.0

results show that the volume of analyte solution generally had little effect on the intensity. The solubility was decreased at higher temperatures, thus giving greater intensity (Fig. 4) but it was not possible to increase the temperature to $>30\,^{\circ}$C, owing to severe carryover of water to the cavity.

During electrolysis, hydrogenation of the organic sulphur compound occurs at the cathode and oxygen is evolved at the anode. Both gases are transferred to the cavity but oxygen severely decreases the S_2 emission intensity [11]. Oxygen evolution ceases as soon as electrolysis stops, whereas hydrogen sulphide continues to evolve owing to its solubility in water. Therefore, when a solution is being electrolyzed, little or no emission is recorded, and maximum S_2 emission intensity is recorded as soon as electrolysis is interrupted.

The amount of oxygen evolved depends on the electrolysis time (Fig. 2). If short electrolysis intervals are used (<20 s), small amounts of oxygen are generated but the emission intensity is also low, because of decreased H_2S evolution. If long electrolysis intervals are used (>40 s), the amount of oxygen evolved is increased and the emission intensity is decreased. Therefore, the electrolysis time must be controlled accurately, in order to achieve maximal sensitivity and reproducibility. A 30-s electrolysis interval was used for all further work.

The amount of hydrogen sulphide formed is also affected by the electrode surface area, for a given time interval. Electrolysis of a given solution at a large cathode generates a more intense emission than at a small electrode (Fig. 5).

The main conclusion from the optimization studies is that, because oxygen is an undesirable by-product, all the experimental parameters must be adjusted so that the ratio of oxygen to hydrogen sulphide is minimized.

Analytical results. Table 2 shows the relative emission intensities from some organic sulphur-containing compounds. The calibration graph of emission intensity (I, mV) vs. concentration of compound (C, μg ml^{-1}) was sigmoidal, but the log I vs. log C calibration graph was linear over the range 5.00–30.0 μg ml^{-1} thiosemicarbazide ($\log I = -1.8 + 1.5 \log C$; $r = 0.991$, $n = 5$) or dithiox-

amide ($\log I = -1.6 + 1.4 \log C; r = 0.992, n = 5$). The limits of detection (signal/noise = 3) were 2.50 and 2.00 $\mu g\ ml^{-1}$, respectively. The relative standard deviation for 20 $\mu g\ ml^{-1}$ concentrations of both compounds was 5.0% ($n = 8$).

The manual method described is cumbersome and time-consuming, and cannot be used for routine analysis. Furthermore, the apparatus used does not allow electrolysis at temperatures above ambient because of severe carryover of water droplets into the duct and hence to the cavity. It was therefore decided to investigate whether the procedure could be automated by using a continuous flow system similar to the design developed for the determination of sulphite [6] and sulphide [7]. A continuous-flow electrolytic cell was made by embodying two platinum wires into the continuous flow debubbler described previously [6,7]. Unfortunately, continuous electrolysis of the flowing acidic solution of the organic compound generated oxygen which either was carried into the cavity and eliminated the emission or interfered severely with the flow of waste from the cell. The use of antioxidants such as hydrazine did not improve the measurement.

Conclusions

Electrolysis can be used for the determination of organic sulphur compounds after conversion to hydrogen sulphide but oxygen interferes severely and does not allow measurement of sulphur in a continuously flowing stream. The method seems more feasible for the determination of compounds (such as As, Sb, Si compounds) which generate molecular emissions under flame conditions that require oxygen. Further applications of the method will be investigated.

The authors thank C. Efstathiou for stimulating discussions. This communication was presented at the 7th SAC International Conference on Analytical Chemistry, Bristol, 1986.

REFERENCES

1 M. Burguera, S.L. Bogdanski and A. Townshend, Crit. Rev. Anal. Chem., 10 (1980) 185.
2 A.C. Calokerinos and A. Townshend, Prog. Anal. At. Spectrosc., 5 (1982) 63.
3 S.L. Bogdanski, I.M.A. Shakir, W.I. Stephen and A. Townshend, Analyst, 104 (1979) 886.
4 S.L. Bogdanski, A. Townshend and B. Yenigul, Anal. Chim. Acta, 115 (1980) 361.
5 A.C. Calokerinos and A. Townshend, Fresenius' Z. Anal. Chem., 311 (1982) 214.
6 N. Grekas and A.C. Calokerinos, Analyst, 110 (1985) 335.
7 N. Grekas and A.C. Calokerinos, Anal. Chim. Acta, 173 (1985) 311.
8 M. Wronski, Talanta, 26 (1979) 976.
9 A.C. Calokerinos and T.P. Hadjiioannou, Anal. Chim. Acta, 148 (1983) 277.
10 M.L. Girard and C. Dreux, Bull. Soc. Chim. Fr., 8 (1968) 3469.
11 S.L. Bogdanski, A.C. Calokerinos and A. Townshend, Can. J. Spectrosc., 27 (1982) 10.

Analytica Chimica Acta, 202 (1987) 247–250
Elsevier Science Publishers B.V., Amsterdam — Printed in The Netherlands

Short Communication

DETERMINATION OF NAPHTHOLS BY FLOW-INJECTION CHEMILUMINESCENCE

S.A. AL-TAMRAH

Chemistry Department, College of Science, King Saud University, Riyadh (Saudi Arabia)

ALAN TOWNSHEND*

Chemistry Department, University of Hull, Hull HU6 7RX (Great Britain)

(Received 14th April 1987)

Summary. 1-Naphthol, 2-naphthol, 2-naphthol-6-sulphonic acid, 1-amino-2-naphthol-4-sulphonic acid and 1-amino-2-naphthol hydrochloride are determined by the chemiluminescence produced by acidic permanganate oxidation in a flow system. Rhodamine B is used as sensitizer. The limits of detection are ca. 5×10^{-7} M in a 20-μl sample.

Very few chemiluminescence methods have been described for the determination of naphthols. They are indirect procedures based on the enhancement [1] or inhibition [2] of luminol/hydrogen peroxide chemiluminescence. During an investigation of the effect of other compounds on the chemiluminescence determination of sulphite by permanganate oxidation [3], it was observed that 1-amino-2-naphthol-4-sulphonic acid also gave rise to chemiluminescence with acidic permanganate. Initially, this was thought to be due to sulphite impurity in the sample, but a purified sample, and 1- and 2-naphthols, were also found to produce emissions. This reaction was therefore investigated as a means of determining naphthols. The flow-injection technique is now well known to be very effective for analyses based on chemiluminescence [4].

Experimental

Apparatus. The flow system used is shown in Fig. 1. A peristaltic pump (Ismatec Mini-S-820) was used to deliver the acidic permanganate and sensitizer solutions each at a flow rate of 1.8 ml min^{-1}. Teflon tubing (0.8 mm internal diameter) was used for the flow lines; the pump tubing was from Anachem (0.85 mm i.d.). The two solutions were mixed at a perspex T-piece placed 5 mm before the detector flow coil. Sample solution (20 μl) was injected by a Rheodyne R5020 injection valve. The flow cell and detector were as described

0003-2670/87/$03.50

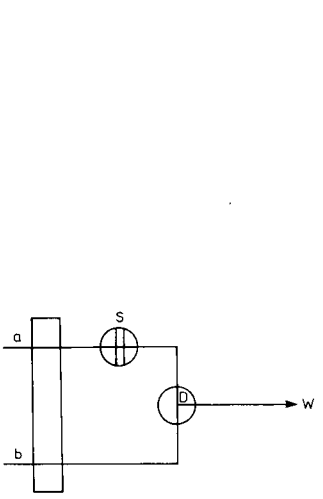

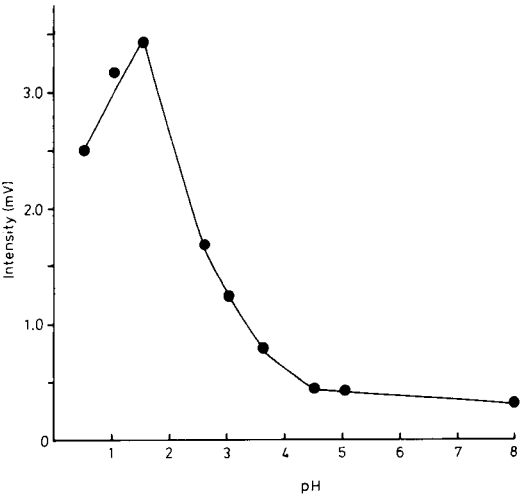

Fig. 1. Flow system used: (a) $KMnO_4/H^+$; (b) sensitizer; (S) sample injection; (W) waste; (D) detector. The distance between S and D is 25 cm.

Fig. 2. Effect of pH on emission intensity (peak height) from 2.5×10^{-5} M 1-amino-2-naphthol-4-sulphonic acid with 5×10^{-6} M permanganate in the absence of rhodamine B.

previously [5]. The signal (peak height) was recorded by an Oxford 3000 chart recorder (Oxford Electronic Instruments).

Reagents. A stock solution of 1×10^{-3} M potassium permanganate was prepared by dissolving the appropriate amount of analytical-grade potassium permanganate in deionized water. Diluted solutions were prepared as needed and the pH was adjusted by 0.2 M sulphuric acid. 2-Naphthol-6-sulphonic acid (sodium salt), 1-amino-2-naphthol-4-sulphonic acid, 1-amino-2-naphthol hydrochloride, and naphthalene-1-sulphonic acid (sodium salt), were all supplied by BDH Chemicals. 2-Naphthol (May & Baker), 1-naphthol (Hopkin & Williams) and 1-aminonaphthalene-2-sulphonic acid (R.N. Emanuel) were also used. Stock solutions (1×10^{-3} M) of each of these compounds were prepared daily in deionized water. Solutions were kept in the dark to minimize oxidation or decomposition. A 1×10^{-3} M rhodamine B solution was prepared in deionized water.

Optimization. The effect of the pH of a 5×10^{-6} M potassium permanganate solution on the emission from 2.5×10^{-5} M 1-amino-2-naphthol-4-sulphonic acid was studied in the absence of sensitizer (i.e., with water in the sensitizer channel). The results are shown in Fig. 2. The greatest sensitivity was obtained when the pH was ca. 1.5. At higher pH values, the peak height decreased and the peaks became a little broader.

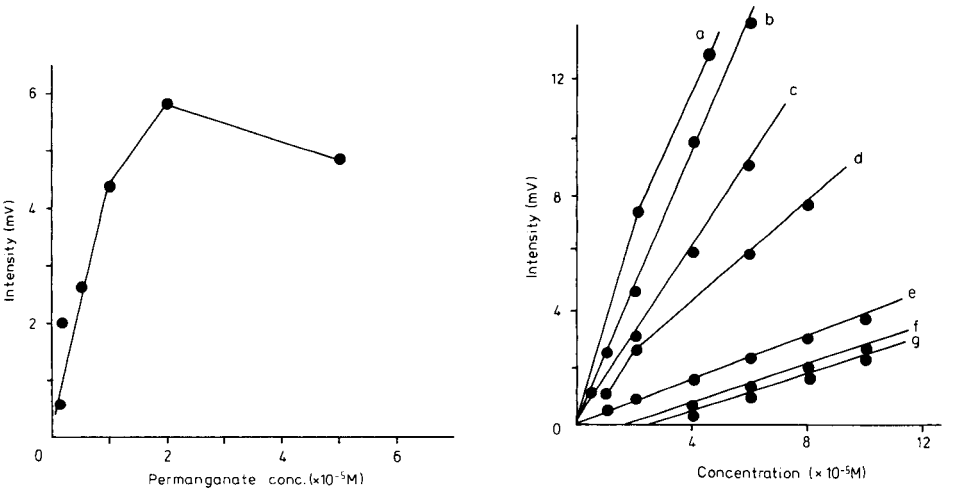

Fig. 3. Effect of permanganate concentration on the emission intensity from 2.5×10^{-5} M 1-amino-2-naphthol-4-sulphonic acid at pH 1.5, in the absence of rhodamine B.

Fig. 4. Calibration graphs for: (a, g) 1-naphthol; (b, c) 1-amino-2-naphthol-4-sulphonic aicd; (d) 2-naphthol; (e) 1-amino-2-naphthol hydrochloride; (f) 2-naphthol-6-sulphonic acid. (a, b) In presence of 3×10^{-5} M rhodamine B; (c–g) in absence of rhodamine B.

The effect of the permanganate concentration on the emission from 2.5×10^{-5} M 1-amino-2-naphthol-4-sulphonic acid in the absence of sensitizer was investigated at pH 1.5. Greatest intensity occurred at 2×10^{-5} M potassium permanganate, which was similar to the naphthol concentration (Fig. 3). At higher permanganate concentrations, the intensity decreased as a result of absorption of the emitted light by permanganate [6].

Calibration. Calibration graphs for the naphthols and derivatives tested in the absence of sensitizer are shown in Fig. 4. Unusually for chemiluminescent reactions, these are linear over the range studied. The sensitivity (slope) was dependent on the nature and position of the groups on the naphthalene ring. The greatest sensitivity was obtained for 1-amino-2-naphthol-4-sulphonic acid and 2-naphthol. The intensities produced by 1-naphthol, 1-amino-2-naphthol hydrochloride and 2-naphthol-6-sulphonic acid were weaker.

Sensitizers have been used to enhance weak emissions, and have been successfully used in the sulphite/permanganate system [3]. In the present reaction, rhodamine B considerably enhanced the signal intensity from the weaker emitters. For example, with 8×10^{-5} M 1-naphthol, the signal increased from 2 mV without the sensitizer to 23 mV when the rhodamine B concentration was increased to 2×10^{-5} M; above this concentration, the intensity gradually decreased, probably because of an inner filter effect. The more sensitive cali-

bration plots for 1-naphthol and 1-amino-2-naphthol-4-sulphonic acid under these conditions are shown in Fig. 4.

Naphthalene-1-sulphonic acid and 1-aminonaphthalene-2-sulphonic acid gave no measurable emissions, in the presence or absence of the sensitizer. This suggests that the chemiluminescent reaction involves oxidation of the hydroxyl group, probably to the corresponding quinone.

The detection limit (signal/noise=2) was 1×10^{-6} M (2×10^{-11} mol) for 2-naphthol in the absence of sensitizer and 5×10^{-7} M (1×10^{-11} mol) for 1-naphthol in the presence of sensitizer. The relative standard deviation for 13 measurements of 5×10^{-5} M 1-naphthol in the presence of rhodamine B was 0.5%.

The method described is simple, rapid and reasonably sensitive, and could readily be applied for detection of naphthols after liquid chromatographic separation, as has been done for opiates, which also give sensitive chemiluminescence with acidic permanganate [7].

REFERENCES

1 A.T. Pilipenko, I.E. Kalinichenko and E.Ya. Matreeva, Zh. Anal. Khim., 33 (1978) 1612.
2 N.M. Lukovskaya and M.I. Gerasimenko, Zh. Anal. Khim., 26 (1971) 1639.
3 S.A. Al-Tamrah, A. Townshend and A.R. Wheatley, Analyst, 112 (1987) 883.
4 See, e.g., R.W. Abbott, A. Townshend and R. Gill, Analyst, 111 (1986) 635.
5 A.A. Al-Warthan and A. Townshend, Anal. Chim. Acta, 185 (1986) 329.
6 M. Yamada, T. Nakada and S. Suzuki, Anal. Chim. Acta, 147 (1983) 401.
7 R.W. Abbott, A. Townshend and R. Gill, Analyst, 112 (1987) 397.

Analytica Chimica Acta, 202 (1987) 251–256
Elsevier Science Publishers B.V., Amsterdam — Printed in The Netherlands

Short Communication

A PYROLYSIS/GAS CHROMATOGRAPHIC METHOD FOR THE DETERMINATION OF HYDROGEN IN SOLID SAMPLES

ROBERT H. CARR[a], ROBERTA BUSTIN[b] and EVERETT K. GIBSON*

SN4 Experimental Planetology Division, NASA Johnson Space Center, Houston, TX 77058 (U.S.A.)

(Received 23rd June 1987)

Summary. A method is described for the determination of hydrogen in solid samples. The sample is heated under vacuum after which the evolved gases are separated by gas chromatography with a helium ionization detector. The system is calibrated by injecting known amounts of hydrogen, as determined manometrically. The method, which is rapid and reliable, was checked for a variety of lunar soils; the limit of detection is about 10 ng of hydrogen.

Hydrogen is present in a variety of substances, either as a contaminant or as an integral part of the material. The hydrogen can be released by chemical reaction, crushing, or heating, after which it can be determined. Methods for determining hydrogen abundance in solid samples are numerous and cover a wide range of techniques. These include manometry [1], emission spectroscopy [2], mass spectrometry [3,4], gas chromatography [5,6], thermal gravimetry [3], nuclear microprobe [7], neutron gamma techniques [8], and determination of water produced by oxidation of hydrogen [9].

Some of these methods require gram-size samples [1,9] while others can determine hydrogen in samples ranging from 10 to 250 mg [3–5]. Methods requiring large sample sizes are unsuitable in any instance in which the sample supply is limited or the sample must be retained for additional studies. For determinations such as these, it is essential to have a very sensitive method for determining hydrogen.

The technique reported here is a highly sensitive one which combines pyrolysis with gas chromatography and the ultra-sensitive helium ionization detector.

Experimental

Equipment. The experimental arrangement is outlined in Fig. 1. A small resistance wire furnace was constructed using Kanthal A wire. The furnace was operated at a temperature of 900 °C, as determined by an optical pyrometer

[a]Present address: ICI Europa Ltd., Everslaan 45, B-3078 Kortenberg, Belgium.
[b]Present address: Arkansas College, Batesville, AR 72501, U.S.A.

0003-2670/87/$03.50

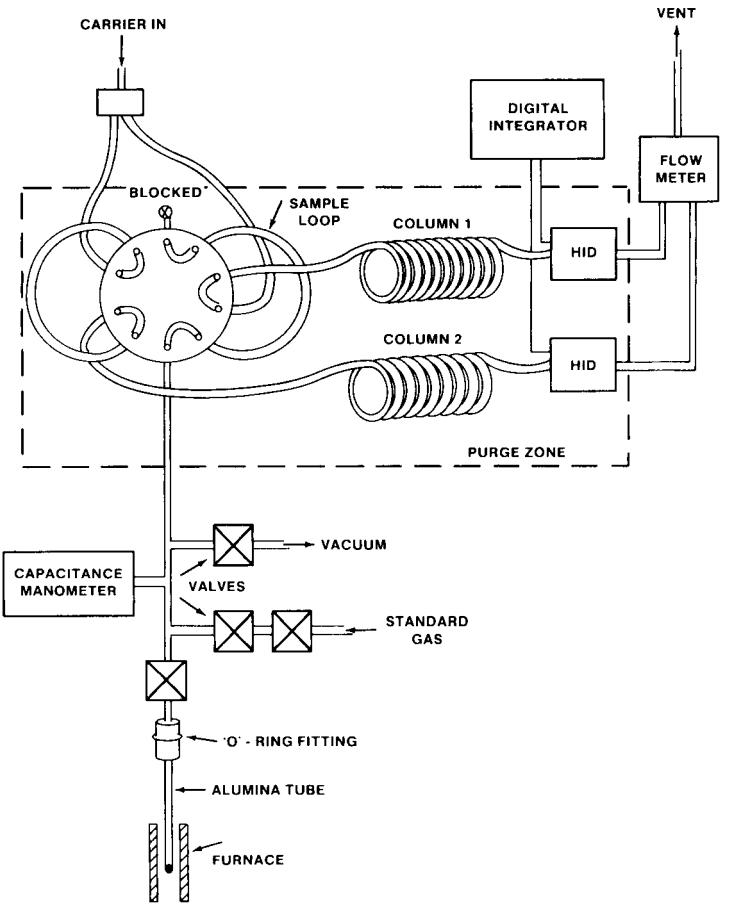

Fig. 1. The experimental set-up.

and also an emplaced thermocouple. The solid samples were placed directly in a 1/4-in. o.d. alumina sampling tube which was fitted into the sampling assembly using a vacuum-tight Cajon connector. A heating time of 3 min was adequate for the complete evolution of hydrogen in the samples studied.

Hydrogen was separated and determined by using a Valco Model 1000 Trace Gas Analyzer fitted with a helium ionization detector (HID). The detector was operated at 60°C with an applied potential of 240 V. The column was a 12-ft., 1/4-in. stainless steel tube packed with molecular sieve 5A, 80/100 mesh, operated at 50°C. The carrier gas was helium containing 92 μl l^{-1} nitrogen as an impurity. A flow rate of 17 ml min^{-1} was used.

The sampling system was evacuated prior to hydrogen extraction and injection. The instrument injection valve was reconfigured so that the sample loop became part of the extraction volume which was evacuated prior to each run.

The entire system was designed to be as leak-free as possible. High-vacuum stainless steel Nupro valves were welded into the sampling line. In the gas chromatograph itself, the injection valves, columns, and detectors were enclosed in a purge zone which was filled with helium in order to minimize atmospheric leakage effects.

Calibration. The system was calibrated by injecting known amounts of hydrogen. The volume of the entire sampling line was determined manometrically. This volume was then filled with varying amounts of standard gas containing 99.2 μl l^{-1} hydrogen in helium. The pressure in the line was measured with an MKS Baratron capacitance manometer. From the pressure and volume, the number of moles of hydrogen in the sampling line was calculated.

Chromatographic signals were monitored by a digital Spectra-Physics 4200 computing integrator.

Samples. Hydrogen abundances were determined for a variety of lunar soils. Samples of approximately 10 mg were necessary for good reproducibility.

Results and discussion

The gas chromatograph was supplied with factory-installed columns which could not be readily changed by the user. One was a Porapak-Q column, and the other was a molecular sieve 5A column. Initial experiments were undertaken to establish which of these was more suitable for the hydrogen determination. With the Porapak-Q column, variation of the chromatographic conditions failed to produce complete, baseline resolution of hydrogen and neon (Fig. 2a), even when cooling to $-45\,^{\circ}$C was used. However, hydrogen could be completely resolved from other species on the molecular sieve 5A column (Fig. 2b). A flow of 17 ml min^{-1} and a column temperature of $50\,^{\circ}$C provided a short retention time for hydrogen (about 3 min) but still allowed complete resolution of hydrogen.

Ultrapure helium was initially used as the carrier gas. This proved to be unsuitable because a linear response could not be obtained for the desired concentration range and because hydrogen peaks were sometimes negative and sometimes deformed, W-shaped peaks. Several authors have described the effects of using less pure helium as the carrier gas in order to change the response characteristics of the helium ionization detector [10–14]. Decreasing the purity of the helium carrier decreases the sensitivity of the detector but increases the upper limit of linear response. It also reverses the polarity of the hydrogen signal, giving a well-defined, positive signal. The detector gave a positive, linear response with helium containing 92 μl l^{-1} nitrogen as the carrier gas.

A linear calibration curve was obtained over the range 10–600 ng of hydrogen. In a plot of integrator counts ($\times 10^{-5}$) vs. mass (ng) of hydrogen, the equation $y = 0.0581\ x - 0.486$ was obtained, with a correlation coefficient of 0.99997 (for four points obtained by repetitive injections).

Reproducibility of the detection system was excellent. By using repetitive

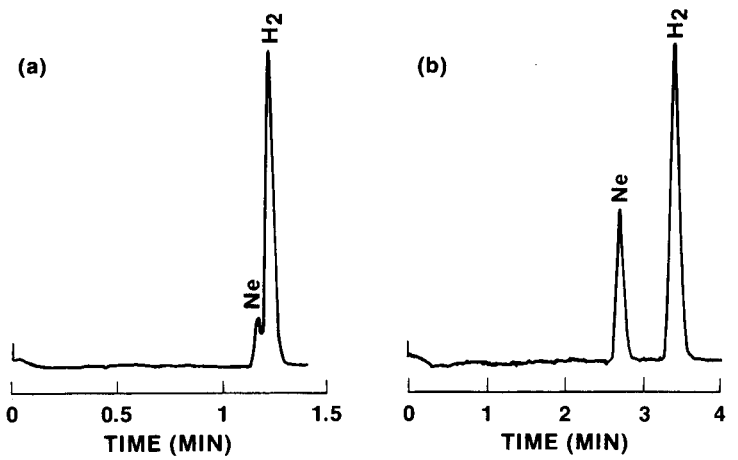

Fig. 2. Chromatograms showing the resolution of hydrogen from neon: (a) Porapak-Q column at 30°C; (b) molecular sieve column at 30°C. Ultrapure helium carrier gas, 15 ml min^{-1}. Helium ionization detector at 60°C.

injections of standard gas, the uncertainty (one standard deviation) was found to be about 0.5% (Table 1) on amounts of hydrogen in the desired range. When hydrogen was determined in bulk lunar samples, the uncertainty level was about 5%. This demonstrated that the overall reproducibility of the technique was good, considering the inherent inhomogeneity of lunar samples.

The method appears to be quite reliable. Despite inherent sample differences, values obtained from this method compare favorably with literature values (Table 2). Particle-size separates were run on two lunar soils. Mass-balance calculations showed excellent agreement between the calculated and the experimentally found values for hydrogen, providing more evidence for the validity of this method (Table 3).

The technique is rapid, sensitive, reproducible, and reliable. Very small sample sizes can be used, making this an attractive method in cases for which there is a limited supply of sample such as lunar soil or in which sample preparation is tedious or time-consuming such as hand-picking of mineral separates.

This work was supported in part by the National Aeronautics and Space

TABLE 1

Reproducibility evaluated from repetitive injections of standard gas

Hydrogen injected (ng)	35	135	405	607
Counts ±1 SD (10^4 counts)	16.2±0.06	73.5±0.27	228.6±1.32	349.0±1.34

TABLE 2

Comparison of results with literature values

Lunar sample number	Hydrogen abundance ($\mu g\ g^{-1}$)		Lunar sample number	Hydrogen abundance ($\mu g\ g^{-1}$)	
	This method	Literature values		This method	Literature values
10 084 149	54.2	44.7 [15], 45.9 [9]	69 941 36	41.7	34.3 [18], 65.0 [19]
12 033 467	3.2	1.9 [16]	70 011 19	45.8	47.2 [20], 55.1 [21]
12 070 127	39.2	37.8 [16]	76 501 18	43.8	43.0 [20]
15 601 31	33.6	27.8, 36.8 [17]	78 501 20	29.0	32.8 [17]

TABLE 3

Comparison of calculated and experimental values for size separates of two lunar soils

Particle size (μm)	Weight percent	H_2 found ($\mu g\ g^{-1}$)	Contribution to bulk ($\mu g\ g^{-1}$)	Weight percent	H_2 found ($\mu g\ g^{-1}$)	Contribution to bulk ($\mu g\ g^{-1}$)
	Sample 10084,149			*Sample 15021,2*		
<20	25.78	146.7	37.8	23.02	128.5	29.6
20- 45	18.33	39.7	7.3	22.96	51.1	11.7
45- 75	15.01	24.4	3.7	15.61	22.4	3.5
75- 90	5.01	20.1	1.0	5.37	20.8	1.1
90- 150	12.24	20.2	2.5	13.26	15.5	2.1
150- 250	9.06	11.3	1.0	9.25	8.4	0.8
250- 500	8.73	15.7	1.4	7.23	8.2	0.6
500-1000	5.82	7.2	0.4	3.31	11.0	0.4
	Total H_2 calculated		55.1	Total H_2 calculated		49.8
	H_2 found		54.2	H_2 found		49.6

Administration's Planetary Materials Program. R.H.C. was supported by an NAS/MRC Resident Research Associateship at the Johnson Space Center.

REFERENCES

1 S. Chang, K. Lennon and E.K. Gibson, Jr., Proc. 5th Lunar Sci. Conf., Geochim. Cosmochim. Acta, (1974) 1785.
2 I.S. Tsong and R.B. Liebert, Nucl. Instrum. Methods, 149 (1978) 523.
3 R.E. Hanneman, Proc. Apollo 11 Lunar Sci. Conf., Geochim. Cosmochim. Acta, (1970) 1207.

4 I. Friedman, J.R. O'Neil, J.D. Gleason and K. Hardcastle, Proc. 2nd Lunar Sci. Conf., Geochim. Cosmochim. Acta, (1971) 1407.
5 D.J. DesMarais, J.M. Hayes and W.G. Meinschein, Proc. 5th Lunar Sci. Conf., Geochim. Cosmochim. Acta, (1974) 1811.
6 W.E. Beard and W.D. Guenzi, Soil Sci. Soc. Am. Proc., 40 (1976) 319.
7 G.M. Padawer, E.A. Kamykowski, M.C. Stauber and M.D. D'Agostino, Proc. 5th Lunar Sci. Conf., Geochim. Cosmochim. Acta, (1974) 1919.
8 R.G. Johnson, L.G. Evans and J.I. Trombka, IEEE Trans. Nucl. Sci., 26 (1979) 1574.
9 S. Epstein and H.P. Taylor, Jr., Proc. Apollo 11 Lunar Sci. Conf., Geochim. Cosmochim. Acta, (1970) 1085.
10 F.F. Andrawes and E.K. Gibson, Jr., Anal. Chem., 52 (1980) 846.
11 F.F. Andrawes, T.B. Byers and E.K. Gibson, Jr., Anal. Chem., 53 (1981) 1544.
12 F.F. Andrawes and E.K. Gibson, Jr., Anal. Chem., 50 (1978) 1146.
13 E. Bros and J. Lasa, J. Chromatogr., 174 (1979) 273.
14 F.F. Andrawes, T.B. Byers and E.K. Gibson, Jr., J. Chromatogr., 205 (1981) 419.
15 S. Epstein and H.P. Taylor, Jr., Science, 167 (1970) 533.
16 S. Epstein and H.P. Taylor, Jr., Proc. 2nd Lunar Sci. Conf., Geochim. Cosmochim. Acta, (1971) 1421.
17 L. Merlivat, G. Nief and E. Roth, Proc. 3rd Lunar Sci. Conf., Geochim. Cosmochim. Acta, (1972) 1473.
18 R.H. Becker, Proc. 11th Lunar Planet. Sci. Conf., Geochim. Cosmochim. Acta, (1980) 1743.
19 R.W. Stoenner, R. Davis, Jr., K. Norton and M. Bauer, Proc. 5th Lunar Sci. Conf., Geochim. Cosmochim. Acta, (1974) 2211.
20 C. Petrowski, J.F. Kerridge and I.R. Kaplan, Proc. 5th Lunar Sci. Conf., Geochim. Cosmochim. Acta, (1974) 1939.
21 S. Epstein and H.P. Taylor, Jr., Proc. 6th Lunar Sci. Conf., Geochim. Cosmochim. Acta, (1975) 1771.

Analytica Chimica Acta, 202 (1987) 257–264
Elsevier Science Publishers B.V., Amsterdam — Printed in The Netherlands

Book Reviews

J. Koryta and J. Dvorak, *Principles of Electrochemistry.* Wiley, New York, 1987 (ISBN 0-471-91211-5). xi + 447 pp. Price £49.50.

After a lengthy period when very few books on electrochemistry were written, it is refreshing and timely that a number of excellent books is now available. The present book is a welcome addition to the electrochemical literature and highlights the possible contributions of electrochemistry in many fields of research. The extensive literature citations should be particularly valuable to research workers wishing to enter the field of electrochemistry. This reviewer found the book to become increasingly interesting as the chapters proceeded. The first lengthy chapter concerning solution equilibrium properties is not specifically relevant to electrochemistry. Most of this material could be found in standard text books on physical chemistry. This is not true of the later chapters, which concern transport processes, heterogeneous and homogeneous aspects of electrode processes, the double layer, membrane electrochemistry and bioelectrochemistry. These later chapters are extremely interesting and generally not covered in an up-to-date fashion in other books. The entire book is extremely well referenced and generally well written. Perhaps the omission of the area of digital electronics and the advantages that the computer has provided in electrochemistry is unfortunate. This book is particularly recommended for researchers and teachers who may be interested in applying electrochemical techniques to solve problems in their own discipline. It will also be valued by specialists in electrochemistry.

Alan M. Bond

A. Benninghoven, F.G. Rüdenauer and H.W. Werner, *Secondary Ion Mass Spectrometry (Chemical Analysis, Vol. 86.)* Wiley, New York, 1987 (ISBN 0-471-01056-1). xxxv + 1227 pp. Price £143.00.

Within the range of inorganic mass spectrometric methods, secondary ion mass spectrometry (s.i.m.s.) is one of the most widely used, and most rapidly developing. The fundamental concepts of ion-induced neutrals and positive ions ("kanalstrahlen") were first observed by J.J. Thomson in 1910, but the first significant analytical uses of the methodology appeared after the development of commercial instruments for microscopical analysis in the early 1960s. It was only in the last decade that the method developed into a mature and established analytical technique. From a macroscopic surface analytical tool it developed into a true three-dimensional analytical method of vital importance for the microelectronics industry. From an inorganic method it evolved into

the successful method for organic analysis based on fast atom bombardment (f.a.b.) which is of special significance for the mass spectrometric analysis of labile, high molecular mass compounds. Sputtered neutrals mass spectrometry (s.n.m.s.) is a promising new development for highly accurate analysis. Along with static s.i.m.s., it is now considered as one of the most important tools for the characterization of the outside surface layer of materials. With a finely focused primary beam it allows visualisation and analysis with unsurpassed sub-μm spatial resolution and could become a serious alternative to the electron microprobe and scanning electron microscope.

With the proliferation of literature on the subject it is surprising that this is the first book to be published on the subject. Maybe previous would-be authors were wary of undertaking the tremendously complicated and difficult task of trying to condense the literature on this subject to its essentials. The authors of this monograph (all of them well known experts in the field) responded to the challenge and I can state, right away, that they have produced a marvellous book. It covers both the theoretical aspects and the physical basis of secondary ion emission phenomena resulting from ion–solid interactions (Chapter 2), quantitative elemental analysis (Chapter 3), instrumentation including ion optics (Chapter 4), the practical aspects of the various operational modes (Chapter 5), applications (Chapter 6), and a comparison with other analytical techniques (Chapter 7) and future developments (Chapter 8).

This is a monumental work, and contains nearly 600 illustrations and over 2000 references covering nearly all the essential published information up to 1985. The book will certainly find its place as a reference work in most laboratories using this methodology. The price is high, which takes it out of reach of many individuals, but it is worth every penny spent for anybody with an interest in one of the most important methods for the analysis and characterization of solids.

F. Adams

C.O. Ingamells and Francis F. Pitard, in P.J. Elving, J.D. Winefordner and I.M. Kolthoff (Eds.), *Applied Geochemical Analysis, (Chemical Analysis, Vol. 88.)* Wiley, New York, 1986 (ISBN 0-471-83279-0). ix+733 pp. Price £86.00.

On casual inspection the full scope of this book is not immediately apparent since the Contents page consists of some 10 lines containing only the 7 brief chapter titles. The reader must locate the beginning of each chapter to find the detailed contents specified and as the items are listed under section number, not page numbers, individual topics can be difficult to find. The authors, as befits their background and lifelong experience in the field, take a classical analytical chemist's viewpoint, reminding us, rightly, if a trifle pedantically, that "analysis . . . the opposite of synthesis . . . is the separation of a material

into its constituents" and should not be, but is, confused with determination, the quantification of these constituents. The fact that, as the authors point out, modern instrumental methods almost eliminate the need for prior separations, has tended to perpetuate this confusion.

The first chapter presents an excellent and most useful guide to sampling practice for solid and powdered materials with sufficient theory for most analysts. It provides practical methods for ensuring representative sampling to any prescribed error limits for materials heterogeneous in composition, mineralogy and particle size. Chapter 2, like the curate's egg, is good in parts. The portion dealing with instrumentation is adequate but this book will not be read for its contribution in this field. The remainder of the chapter on equipment for basic analytical chemistry and its use is excellent and the application of the various reagents and dissolution procedures is a detailed mine of practical information.

The best of the book lies in the 3rd Chapter, on classical analysis and its application to a range of individual minerals. Here the detailed knowledge and the authors' unrivalled experience is authoritatively presented. It is supported by Chapter 4 dealing with the determination of the elements with the main emphasis on the separation chemistry. Neither neutron activation analysis nor spark source mass spectrometry are mentioned for the determination of rare earth elements. Surprisingly mercury is only considered in terms of a dithizone colorimetric procedure. In Chapter 5, rapid methods including instrumental methods are considered but in general the latter are reviewed in the state-of-the-art existing a few years ago. The cold vapour a.a.s. procedure for mercury is not given. Chapter 6, Basic Calculation and Recommendations, is a bit of a mixed bag ranging from some basic statistics to instruction in logarithms. While this is cheerful stuff for an ancient reviewer it is unlikely to take any tricks with today's computer whizz-kids. Some useful practical instruction in the construction of sampling programs is presented, but again computerized approaches make these techniques obsolescent.

This is an excellent book for a practical chemist entering this field, for a student engaged in research in a geochemical sphere without local geochemical support, for analysts in laboratories in underdeveloped countries or remote locations and for analysts in general who need the chemical experimental detail revealed here. While few laboratories can afford to neglect the rapid and the instrumental approach to analysis in favour of classical procedures the latter still form the basis of the subject and inform all other approaches. To that extent this book is invaluable. It will not appeal to the 'high-tech' instrumentation graduate or the new generation of computer-friendly push-button analysts, but both would benefit from it.

A.M. Ure

John Gilbert (Ed.), *Analysis of Food Contaminants.* Elsevier Applied Science, London, 1984 (ISBN 0-85334-255-5). xiv+386 pp. Price £44.00.

This book describes in some detail a number of techniques in subject areas which are of importance for the determination of food contaminants, and which have developed significantly in the last few years. The topics are: size exclusion and gel chromatography (Shepherd), immunoassay for veterinary drug residues (Heitzman), headspace GC (Kolb), trace metals (Benton Jones), HPLC and other techniques for mycotoxins (Coker), selected ion monitoring MS (Gilbert), and chemiluminescence monitoring of *N*-nitrosamines (Scanlan). Each chapter contains a great deal of detailed information, much gleaned by personal experience, which together provides a comprehensive account of developments in an increasingly important aspects of food analysis.

John Gilbert (Ed.), *Applications of Mass Spectrometry in Food Science.* Elsevier Applied Science, London, 1987 (ISBN 1-85166-081-X). xxii+440 pp. Price £60.00.

Mass spectrometry (MS) is arguably the most powerful analytical technique available today. In combination with chromatography, pyrolysis techniques or further MS, its usefulness is almost unlimited. The present text is intended to indicate such usefulness in the area of food analysis, for desirable components and contaminants. Articles by various British, Irish and American scientists cover quantitative aspects, GC/MS, LC/MS, negative ion chemical ionization, fast atom bombardment, MS/MS, pyrolysis MS and inorganic MS, with emphasis where possible on applications to foodstuffs. They are intended to exemplify the amazing range of applications of MS in food analysis, an aim in which they succeed admirably. As MS is by no means common in food laboratories, this text should be very influential in bringing to the attention of food scientists the great value and potential of mass spectrometric techniques in the subject area.

A. Townshend

J.E. Willett, *Gas Chromatography.* Analytical Chemistry by Open Learning (ACOL), Wiley, Chichester, 1987 (ISBN 0-471-91332-4). xviii+253 pp. Price £9.95.

On the whole this should prove a useful introduction to gas chromatography for the individual working outside the more conventional formal lecturing and teaching system. The approach is informal, friendly and sympathetic to the level of the reader without being trivial or patronising. The book is clearly based on the practical experience of the author and contains numerous prac-

tical insights and tips. The approach is to try to make the reader think through the setting up of the gas chromatograph and to relate the conditions used to the volatility and polarity of the analytes. These are aspects which are often skimmed over in more advanced texts but are important in establishing a feel for method development. The integrated nature of the ACOL programme means this volume should follow the related *Chromatographic Separations,* which contains much of the background and definitions of chromatography.

Although this book works well at the teaching level, unlike most texts it cannot also serve for future reference. Surprisingly, there is no index to enable the reader to go back and revise specific topics. Little guidance is given to further reading. There is a bibliography but this includes neither Grob, nor Poole and Scheutte, the two prominent recent books in this field, nor any of the *Journal of Chromatography Library* but instead recommends Golay (1960), Ettre and Zlatkis (1967), and Pattinson (1969). This and other aspects of the book suggest a rather old fashioned but still correct approach to GLC, but one which might not reflect the day-to-day practical experience of the technician working in modern industry. Fused silica columns are included but so are the now little used Watson–Biemann and Ryhage separators and SCOT columns.

Roger M. Smith

Joseph J. Breen and Philip E. Robinson (Eds.), *Environmental Applications of Chemometrics.* American Chemical Society, Washington, DC, 1985 (ISBN 0-8412-0945-6). x+286 pp. Price $54.95 (U.S.A. and Canada), $65.95 (elsewhere).

The information technology revolution and the ready availability of sophisticated analytical instrumentation has led to an explosive growth of interest in data manipulation and interpretation. The use of well-defined and statistically valid procedures for handling data is now imperative in environmental science and any contribution to the development of chemometrics as regards environmental applications is to be welcomed. This book consists of 19 chapters representing papers presented at a symposium held at the 188th American Chemical Symposium in Philadelphia in 1984. In common with other volumes in this series the papers have been reproduced in camera-ready form. As different type faces have been used the overall presentation is less than ideal and invites comment as to whether such proceedings are not best published in special issues of refereed journals.

Most of the chapters report how specific environmental problems have proved amenable to treatment using chemometric approaches, e.g., the use of Soft Independent Modelling by Class Analogy (SIMCA) for characterising environmental mixtures of polychlorinated biphenyls. Amongst the techniques used are various pattern recognition approaches, cluster analysis, fuzzy sets, krig-

ing, statistical receptor models, partial least squares, molecular connectivity indices, experimental design, and quality control protocols. The majority of chapters are highly specialised and assume a basic knowledge of chemometrics. Many readers would perhaps value more introduction to the techniques covered and perhaps logically these should be covered in the early chapters. Useful tutorial material, however, is given in Chapters 14, 16, 17 and 18 on customary confidence values, kriging (geostatistics), SIMCA, and quality control protocols, respectively. The editors themselves, with Janet Remmers, contribute an excellent chapter on quality assurance applications of pattern recognition to human monitoring data. The book also includes a useful index.

Les Ebdon

L.R. Treiber (Ed.), *Quantitative Thin-Layer Chromatography and its Industrial Application.* M. Dekker, New York, 1987 (ISBN 0-8247-7597-X). xiv+553 pp. Price $79.75.

This is Volume 36 in the Chromatographic Science series of monographs and is a collection of state-of-the-art reviews within the general area of quantitative TLC by well-known workers from equally well-known and respected laboratories. The first chapter is an interesting introduction of some of the pre-requisites for TLC, namely supplies and materials (Hauck, Jost, Krebs and Eisenbeiss). This is followed by three chapters on quantitative evaluation of chromatograms: the mathematical treatment of light-scattering media (Huf), on computer-assisted TLC (Katic, Prosek and Meja), and on the utility of flame ionisation detectors (Mukherjee). The remaining eight chapters deal with specific applications including long chain phenols (Tyman), steroids and related derivatives (Szepesi), vitamins (Watkins), alkaloids (Horváth), fermentation products and antibiotics (Kreuzig), bioactive materials in plant extracts (Prosek, Katic and Pukl), and polymers (Armstrong). The text emphasises methods that have been extensively tried and tested in industrial laboratories and frequently demonstrates the complementary nature of TLC and HPLC. The book will be useful to beginners in its detailing of practical aspects and to those who need a survey of the chemical and application areas as outlined above.

D. Thorburn Burns

S. Middelhoek and J. Van der Spiegel (Eds.), *Sensors and Actuators: State of the Art of Sensor Research and Development.* Elsevier Sequoia, Lausanne, 1987 (ISBN 0-444-75065-7). vii+425 pp. Price SFr 270.

This is a specially bound version of Volume 10 of the journal *Sensors and*

Actuators, containing 22 invited articles and intended to celebrate the appearance of this volume. A wide range of topics from the whole area of chemical and physical sensors is included, and together they provide an impressive and extremely useful account of the state-of-the-art of sensor theory and technology which will be appreciated by newcomers and seasoned practitioners alike.

L. Pawlowski, G. Alaerts and W.J. Lacy (Eds.), *Chemistry for the Protection of the Environment 1985*. Elsevier, Amsterdam, 1986 (ISBN 0-444-42715-5). xii + 796 pp. Price Dfl 450 ($180.00).

This book is Volume 29 in the "Studies in Environmental Science" series and contains the proceedings of the fifth international conference on "Chemistry for Protection of the Environment", held in Leuven, Belgium on 9–13 September, 1985. There are fifty-seven presentations which deal predominantly with physico-chemical and reductive–oxidative treatment of various wastes. The final chapter is of most interest to analytical chemists, with six papers on advances in environmental analytical chemistry; two on capillary gas chromatography for water analysis, two on atomic absorption methods for heavy metals, one on trace metal speciation and one on a continuous residual chlorine monitor based on an ion-selective electrode. It is an interesting book which demonstrates the multi-disciplinary nature of environmental protection but is mainly of peripheral interest to analytical chemists.

Trends in Analytical Chemistry, Reference Edition, Vol. 5: 1986. Elsevier, Amsterdam, 1986 (ISBN 0-444-42772-4). viii + 291 pp. Price Dfl 295.00.

This volume continues the policy of publishing the definitive articles from the year's issues of TrAC within one cover, thus providing a wide-ranging and timely account of recent developments in analytical science by internationally recognized authorities. Computer information and biotechnology aspects are included, and the book concludes with cumulative author and subject indexes for Vols. 1–5.

D.I. Alani and M. Moo-Young (Eds.), *Perspectives in Biotechnology and Applied Microbiology*. Elsevier, London, 1986 (ISBN 1-85166-055-0). ix + 379 pp. Price £45.00.

This book contains selected papers from an international conference on biotechnology and applied microbiology held at Riyadh, Saudi Arabia on 12–15 November, 1984. There are seven chapters which reflect the main themes of the conference, namely, production of microbial proteins, utilization of microorganisms for the production of chemicals, microbial treatment and utilization of waste, continuous culture, application of biotechnology in plant science,

applied microbiology and the environment, and international cooperation in applied microbiology and biotechnology. As is often the case with conference proceedings there is no subject index. At the very least key words supplied by the contributors could be used for this purpose.

The majority of the contributions, which vary from research papers to review articles, are in the first three categories. None of the material is of direct interest to analytical chemists but the chapter on the production of chemicals using microorganisms gives an indication of how selective analytical reagents may be prepared in the future, e.g., the synthesis of optically active amino acids from cheaply available starting materials with microbial pyridoxal 5′-phosphate enzymes.

E.A. Jenne, E. Rizzarelli, V. Romano and S. Sammartano (Eds.), *Metal Complexes in Solution.* Piccin, Padua, 1986 (ISBN 88-299-0679-4). viii+318 pp. Price Lira 40 000.

This soft-back book contains 20 lectures presented at the International School in Metal Complexes in Solution which was held in Porticello, Palermo, Italy in October 1983. All the articles are concerned with quantitative aspects of the formation of complexes. The topics considered include the analysis of solutions by potentiometry, speciation in natural and polluted waters, and multi-metal multi-ligand equilibria. Complex formation by a wide range of ligands and metals in a variety of solvents is discussed. Although there has been a long delay in publishing this material the book provides useful insight into the measurement and assessment of formation constants of metal complexes.

Analytica Chimica Acta, 202 (1987) 265
Elsevier Science Publishers B.V., Amsterdam — Printed in The Netherlands

Erratum

P. Oggenfuss, W.E. Morf, U. Oesch, D. Ammann, E. Pretsch and W. Simon, Neutral-Carrier-Based Ion-Selective Electrodes

Anal. Chim. Acta, 180 (1986) 299–311.

Reference 9 of this paper should read:

B.C. Pressman and E.J. Harris, Seventh International Congress of Biochemistry, Tokyo, August 19–25, 1967. Abstracts Volume H-79.

Corrigendum

M.S. Stanley and K.L. Busch, Positive Secondary-Ion Mass Spectra and Thin-Layer Chromatography/Mass Spectrometry of Phenothiazine Drugs

Anal. Chim. Acta, 194 (1987) 199–209.

In Table 1, the R_2 group for acepromatine should be $COCH_3$; the R_1 groups for prochloroperazine and trifluoroperazine should be $CH_2CH_2CH_2N$–cyclo–C_4H_8–N–CH_3 and the R_1 groups for ethopropazine and trimeprazine should be $CH_2CH(-CH_3)-N(CH_2CH_3)_2$ and $CH_2CH(-CH_3)CH_2-N(CH_3)_2$, respectively.

The discussion of the mass spectra of these compounds is correct.

ANALYTICA CHIMICA ACTA, VOL. 202 (1987)

AUTHOR INDEX

COPS
(Formerly CHEOPS)

Chemometrical Optimization by Simplex

Authors: P.F.A. van der Wiel, B.G.M. Vandeginste and G. Kateman

A Program offering an intelligent sequential optimization plan for a wide range of applications, e.g.

— optimize the yield of a synthesis
— maximize the output of a production plant
— optimize the separation factors for two compounds in a chromatographic separation
— optimize the composition of a polymer
— optimize the determination of an enzyme in blood plasma
etc.

- Incorporates the modified and supermodified sequential simplex optimization methods
- Optimization can be tailored by the user to meet his requirements
- Optimizations involving variation of up to ten parameters can be carried out
- Organizes optimization procedures efficiently to save both time and money
- Available for the Apple II series and IBM-PC
- Includes tutorial
- Full source code listings
- Clear fully descriptive manual
- US$ 475.00

AVAILABLE FROM:

Elsevier Scientific Software (JIC)
52 Vanderbilt Avenue
New York, NY 10017 USA
Phone: (212) 916 1250
Telex: 420643

or

Elsevier Scientific Software
P.O. Box 330
1000 AH Amsterdam
THE NETHERLANDS
Phone: (020) 5862 828
Telex: 18582

Write to us for further information on our other programs

No shipping charge if paid in advance

ELSEVIER SCIENTIFIC SOFTWARE

Apple is a registered trademark of Apple Computer Inc.
IBM-PC is a registered trademark of IBM

INFORMATION FOR AUTHORS

Detailed "Information for Authors" was published in Vol. 190, No. 2, pp. 375–378. A free reprint is available from the Editors or from:
Elsevier Editorial Services Ltd., Mayfield House, 256 Banbury Road, Oxford OX2 7DH (Great Britain)

Types of contribution. The journal welcomes original research papers, short communications and reviews. Reviews are written by invitation of the editors, who welcome suggestions for subjects. Short communications are usually complete descriptions of limited investigations, and should generally not exceed six printed pages. Preliminary communications of important urgent work can be printed within four months of submission, if the authors are prepared to forgo proofs.

Manuscripts. The preferred language of the journal is English, but French and German manuscripts are also acceptable. For authors whose first language is not English, French or German, linguistic improvement is provided as part of the normal editorial processing. Authors should submit three copies of the manuscript in double-spaced typing on one side of the paper only, with a margin of 4 cm, on pages of uniform size. If any variety of machine copying is used (e.g. xerox), authors should ensure that all copies are easily legible and that the paper used can be written on with both ink and pencil. Authors are advised to retain at least one copy of the manuscript. Manuscripts should be preceded by a sheet of paper carrying (a) the title of the paper, (b) the name and full postal address of the person to whom proofs are to be sent, (c) the number of pages, tables and figures.
Information on the *submission of papers* is given on the inside front cover.

Summary. Research papers and reviews begin with a Summary (50–250 words) which should comprise a brief factual account of the contents of the paper, with emphasis on new information. Short communications and preliminary communications require summaries, which should not exceed 50 words. Uncommon abbreviations, jargon and reference numbers must not be used. The Summary should be suitable for use by abstracting services without rewriting. Papers in French or German require a Résumé or Zusammenfassung preceded by a Title and Summary in English; authors are encouraged to provide translations where necessary.

Introduction. The first paragraphs of the paper should contain an account of the reasons for the work, any essential historical background (as briefly as possible and with key references only) and preliminary experimental work.

Figures. Figures should be prepared in black waterproof drawing ink on drawing or tracing paper of the same size as that on which the manuscript is typed. One original (or sharp glossy print) and two photostat (or other) copies are required. Attention should be given to line thickness, lettering (which should be kept to a minimum) and spacing on axes of graphs, to ensure suitability for reduction during printing. Axes of a graph should be clearly labelled, along the axes, and outside the graph itself.
All figures should be numbered with arabic numerals, and require descriptive legends. Explanatory information should be placed not in the figure, but in the legend, which should be typed on a separate sheet of paper. Simple straight-line graphs are not acceptable, because they can readily be described in the text by means of an equation or a sentence. Claims of linearity should be supported by regression data that include slope, intercept, standard deviations of the slope and intercept, standard error, and the number of data points; correlation coefficients are optional.
Photographs should be glossy prints and be as rich in contrast as possible; colour photographs canot be accepted. In general, line diagrams are more informative and less liable to dating than photographs of equipment, which are therefore not usually acceptable.
Computer outputs for reproduction as figures must be good quality on blank paper, and should preferably be submitted as glossy prints.

Nomenclature, abbreviations and symbols. In general, the recommendations of the International Union of Pure and Applied Chemistry (IUPAC) should be followed, and attention should be given to the recommendations of the Analytical Chemistry Division in the journal *Pure and Applied Chemistry* (see also IUPAC *Compendium of Analytical Nomenclature*, 1978).

References. The references should be collected at the end of the paper, numbered in the order of their appearance in the text (*not* arranged alphabetically), and typed on a separate sheet.
In the list of references the following forms should be adopted.
Journals
1 W. Lund and M. Salberg, Anal. Chim. Acta, 76 (1975) 131.
2 M. McDaniel, A.D. Shendrikar, K.D. Reizneir and P. W. West, Anal. Chem., 48 (1976) 2240.
The title of the journal must be abbreviated as in the Bibliographic Guide for Editors and Authors.
Books
1 D.D. Perrin, Masking and Demasking of Chemical Reactions, Interscience-Wiley, New York, 1970, p. 188.
2 S. Hofmann, in G. Svehla (Ed.), Wilson and Wilson's Comprehensive Analytical Chemistry, Vol. 9, Elsevier, Amsterdam, 1979, p. 89.
Titles of papers are unnecessary. Citations of reports which are not widely available (e.g., reports from government research centres) should be avoided if possible. Authors' initials should not be used in the text, unless real confusion could be caused by their omission. If the reference cited contains three or more names, only the first author's name followed by et al. (e.g., McDaniel et al.) should be used in the text; but the reference list must contain the initials and names of *all* authors.